Republic of Iraq
Ministry of Higher Education and Scientific Research
University of Baghdad
College of Education for Pure Science (Ibn-Al-Haitham)
Department of Chemistry

Synthesis, Characterization, Corrosion and Biological Activity for Some Transition and Non-Transition Metals Mixed Ligand Complexes for Dithiocarbamate With 3-Amino Phenol, 8-Hydroxy Quinoline

A Thesis
Submitted to the Council of College of Education for Pure Science /Ibn al-Haitham ,University of Baghdad in Partial Fulfillment of the Requirements for the Degree of Doctor of Philosophy in Inorganic Chemistry
By

Awf Abdul Rahman Ahmed

B.Sc. in Chemistry, 1991
College of Education (Ibn al-Haitham), University of Baghdad
M.Sc. in Physical Chemistry, 2014
College of Education (Ibn al-Haitham), University of Baghdad

Supervisor

Prof. Dr. Ahmed T. Numan

2018 AD   **1440 AH**

1

بِسْمِ اللَّهِ الرَّحْمَٰنِ الرَّحِيمِ

إِنَّا أَعْطَيْنَاكَ الْكَوْثَرَ ۝ فَصَلِّ لِرَبِّكَ وَانْحَرْ ۝

إِنَّ شَانِئَكَ هُوَ الْأَبْتَرُ ۝

صدق الله العلي العظيم

سورة الكوثر

(القران الكريم)

Certification

I certify that, this thesis was prepared under my supervision at Department of Chemistry, College of Education For Pure Science/ Ibn al-Haitham, University of Baghdad in partial requirements for the Degree of Doctor of Philosophy in Inorganic Chemistry, and this work has never been submitted or published anywhere else.

Signature

<div align="center">

Name: Dr. Ahmed T. Numan, (Supervisor)

Title: Prof.

Address: Department of Chemistry

, College of Education For Pure Science /

Ibn al-Haitham University of Baghdad, Iraq.

Date: /   /2018

</div>

In the view of the available recommendation, I forward this thesis for debate by the Examination Committee.

Signature

Name: Dr. Mohamad J. Al-Jeboori

Title: Prof.

Address: Head of Department of Chemistry, College of Education For Pure Science /Ibn al-Haitham , University of Baghdad, Iraq.

Date: /   /2018

Examination Committee

We, the examination committee, after reading this thesis and examining the student (**Awf Abdul Rahman Ahmed**), in its content, we have found it worthy to be accepted for the degree of Doctor of Philosophy in Inorganic Chemistry with (   )**.**

Signature
Name: Dr. Sajid M. Lateef
(Chairman)
Title: Prof.
Address: College of Education For Pure Science/ Ibn al-Haitham, University of Baghdad , Iraq.

Signature
Name: Dr. Amer J. Jarad

(Member)
Title: Asst. Prof.
Address: College of Education For Pure Science/ Ibn al-Haitham, University of Baghdad , Iraq.
Date: /   /2018

Signature
Name: Dr. Rehab A. Jawad

(Member)
Title: Asst. Prof.
Address: College of Science, Al-Mustansiryah University, Baghdad, Iraq

Signature
Name: Dr. Mohammed Z. Ghdhayeb
(Member)
Title: Asst. Prof.
Address: Faculty of sciences, University of Kufa , Iraq.

Signature
Name: Dr. Raied M. Shakir

(Member)
Title: Asst. Prof.
Address: College of Education For Pure Science/ Ibn al-Haitham, University of Baghdad , Iraq.

Signature
Name: Dr. Ahmed T. Numan
(Supervisor)
Title: Prof.
Address:College of Education For Pure Science / Ibn al-Haitham, University of

Approved for the College Committee of Graduate Studies

Signature
Name: Dr. Hasan Ahmed Hasan
Title: Asst. Prof.
Address: The Dean of College of Education For Pure Science/ Ibn al-Haitham,
Date: /   /2018

4

Acknowledgment

Dedication

To…….. My Father and My Mother

With My love and respect

To…….. All My Brothers and Sisters

With My Special Appreciation

To………My wife and children

With My Sincere Love

To……… All My Friends

Many thanks

Awf

Abstract

This study present with the synthesis and characterization of three new precursors (HDa, HDb and HDi) and three new of dithiocarbamate (DTCs) ligands:-

KL1= potassium (1,5-dimethyl-3-oxo-2-phenyl-2,3-dihydro-1H-pyrazol-4-yl)(5,5-dimethyl-3-oxocyclohex-1-en-1-yl)carbamodithioate.

KL2= potassium benzo[d]thiazol-2-yl(5,5-dimethyl-3-oxocyclohex-1-en-1-yl) carbamodithioate.

KL3=potassium(1H-benzo[d]imidazol-2-yl)(5,5-dimethyl-3-oxocyclohex -1-en-1-yl)carbamodithioate.

Two steps synthetic procedures were used to obtain earlier mentioned ligands and this was based on the preparation of enaminone precursors that reacted with carbon disulphide in presence of KOH to get the ligands (KL1, KL2 and KL3). All the prepared ligands were characterized using 1HNMR, 13CNMR, Mass, FT-IR, UV-Vis spectra, C.H.N.S and TGA. The reaction of the DTCs ligands with some metal ions produce complexes of general formula [M(Ln)2] where n=1,2,3. Where M(II)=(Mn, Co, Ni, Cu, Zn, Pd and Cd) using ethanol as a solvent.

The mixed ligand complexes were also prepared from of dithiocarbamate salts, 8-hydroxyquinoline, 3-aminophenol and metal ion M, where M(II)=(Co, Ni, Zn) using ethanol as a solvent and KOH as a base.

The complexes of the composition [M(Ln)(Q)], [M(Ln)(P)] and characterized by FT-IR, UV-Vis, elemental analysis measurement, C.H.N.S, Conductivity , magnetic susceptibility and TGA.

The value molar conductance measurements of complexes in DMSO solutions, indicating their nonelectrolyte behavior. The data are in agreement of the magnetic moments value of Meff indicating for tetrahedral geometry complexes and square planer geometry about Pd(II) complexes. The biological activity of the ligands and their complexes [M(Ln)2], [M(Ln)(P)] and [M(Ln)(Q)] were studied using inhibition zone method which showed that some of complexes are more active than the ligands.

The inhibition effect of their ligands (KL1,KL2 and KL3) an α-brass corrosion was studied with the concentration of the ligands 10-**3 mol.dm-3 in media of three pH values 2,4 and 7 and 0.6 mol.dm-3 NaCl solution over the room temperature 298K. The study indicated that ligands acts as inhibitor in pH=4 and pH=7, while they acts as accelerator in pH=2.**

List of Contains

List of Tables

List of Figures

Colours, yields, melting points and metal salts quantities of KL^{3}-

List of Schemes

List of Abbreviations

DTCs	Dithiocarbamate
Nu¨	Nucleophile
DMSO	Dimethyl sulfoxide
PPA	Poly Phosphoric Acid
Eq	Equivalent
M.P.	Melting point
MW	Molecular Weight
^{1}H NMR	Proton Nuclear Magnetic Resonance Spectroscopy
^{13}C NMR	Carbon(13) Nuclear Magnetic Resonance Spectroscopy
TMS	Tetra methyl Silane
J	Coupling constant
Hz	Hertz
ppm	Part per million
δ	Chemical shift
EI	Electron Impact Ionization
FT-IR	Fourier Transform Infrared
UV-Vis	Ultraviolet-Visible Spectrophotometry
L.F	Ligand field
C.T	Charge Transfer
λ	Wave length
υ	Wave number
nm	Nanometer
ε_{max}	Molar Absorptivity
TGA	Thermos Gravimetric Analysis
TDA	Derivatives Thermal Analysis
χ	Susceptibility
$χ_{g}$	Mass magnetic susceptibility

χ_M	Molar magnetic susceptibility
X_A	Atomic magnetic susceptibility
B.M	Bohr Magneton
μ_{eff}	Effective magnetic moment
Λm	Molar conductivity
A.A	Atomic absorption
cm	Centimeter
Dec.	Decomposition
No.	Number
g	Gram
M	Metal
L	Ligand
hr	Hour
TLC	Thin Liquid Chromatography
T	Absolute temperature
i_{corr}	Corrosion current density
E_{corr}	Corrosion potential
W.L	Weight loss

Chapter One
Introduction

(1.1) Diketone Compounds

A diketone is a molecule containing two (C=O) groups .Its compounds are associated with metal ions and formation of stable complexes and increased interest in these compounds after using with amines in the preparation of a number of compounds such as bromidien derivatives[1].

(1.1.1) α-Diketone Compounds

One of the branches of diketone compounds that are contained in two adjacent carbonyl groups, (two C=O groups, side-by-side), 2,3-butane dione and benzil ,Fig.(1.1)[2].
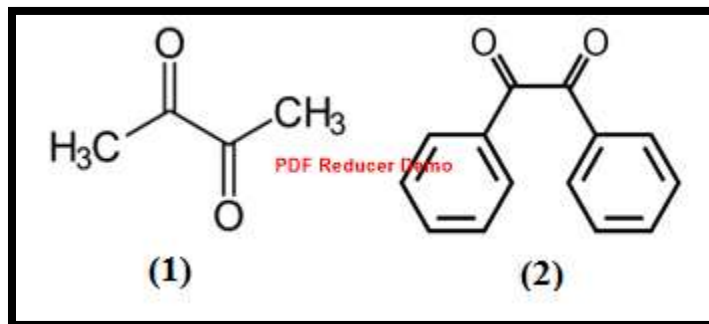
Figure(1.1): The chemical structure of 2,3-butane dione(1) and benzil(2)

(1.1.2) β-Diketone Compounds

β-diketone compounds, whose simplest and the most widely known member is pentane-2,4-dione (informally referred to as acetylacetone), have a number of very interesting and specific properties due to their structure (the presence of two carbonyl groups separated with one carbon atom), pentane-2,4-dione and cyclohexan-1,3-dione, Fig.(1.2). Their crucial feature is keto-enol tautomerism, the presence of the ketone and the enol forms in equilibrium. The equilibrium in the case of β-diketones is strongly shifted towards the enol form due to the formation of the distinct resonance structure as a six-membered ring, Fig.(1.3). Keto-enol equilibrium is affected by a number of other factors with the most important being

solvent polarity and the presence and properties of substituents (both terminal ones and those in the methylene group). The capacity to form stable complexes with most metals is a direct consequence of the occurrence of such compounds in the enol form. Due to the presence of two carbonyl groups, β-diketones are valuable substrates in many chemical synthesis [3,4].
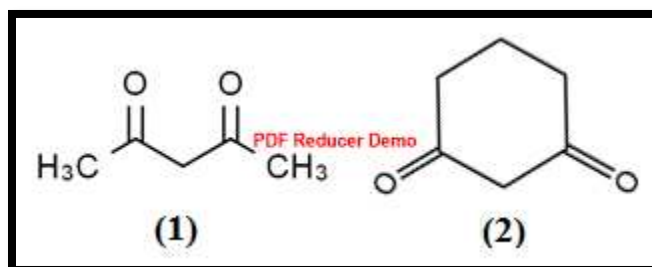
Figure(1.2): The chemical structure of pentane-2,4-dione(1) and cyclohexan-1,3-dione(2)
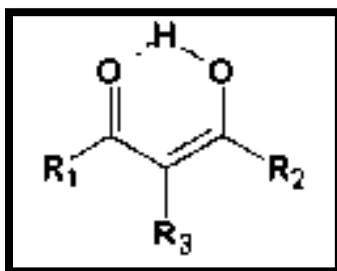
Figure(1.3): Enol-form of the β –diketone with a six membered ring.

(1.1.2.1) Dimedone

Dimedone is an organic compound with molecular formula $C_8H_{12}O_2$. It is useful for synthesis of pharmacutical and heterocyclic compounds. Dimedone has a melting point (148-149)$^{\circ}$C [5]. Chemical and crystal structure is shown in Fig. (1.4).
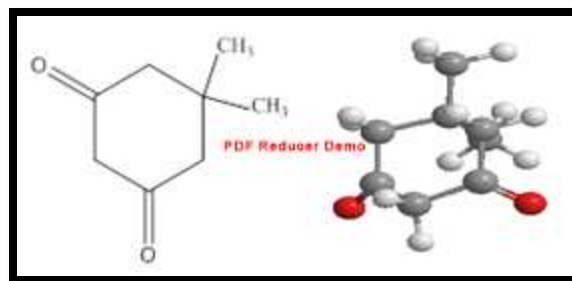
Figure(1.4): The chemical and structure of dimedone

Dimedone is an interesting and versatile motif in most organic transformations. Its white to light yellow crystals have been utilized as substrate in wide range of organic reactions including multi-component transformations. The notability of dimedone is due to the acidic property of its methylene group which is in equilibrium with its tautomeric enol form, Fig.(1.5). This phenomena permit dimedone to be utilized in several kinds of organic reactions eventuated to several organic molecules with potent pharmaceutical exclusivity. The mentioned nature of dimedone in addition with its low toxicity, easily accessibility and handling, moisture stability, and low cost make it interesting for organic chemists[6].
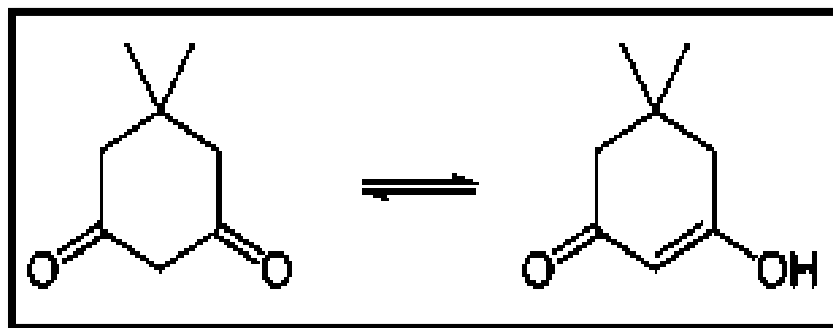
Figure(1.5): General tautomeric enol form

(1.3)Amines

(1.3.1) 4-aminophenazone

The best antiphenazone derivatives is 4-aminophenazone which is used for the protection against oxidative stress as well as prophylactic of some diseases including cancer (breast), and these are important directions in medical

applications , 4-amino phenazone was biologically evaluated, analgesic, anti inflammatory , antimicrobial and anticancer activity have been reported. It is used to relieve pain, congestion, and swelling caused by middle ear inflammation, and used to help remove earwax, and it is also used as a reagent for biochemical reactions producing peroxides or phenols. 4-aminophenazone with molecular formula $C_{11}H_{13}N_3O$ having melting point (105-110)°C,[7-9] , chemical and crystal structure are shown in Fig.(1.6)
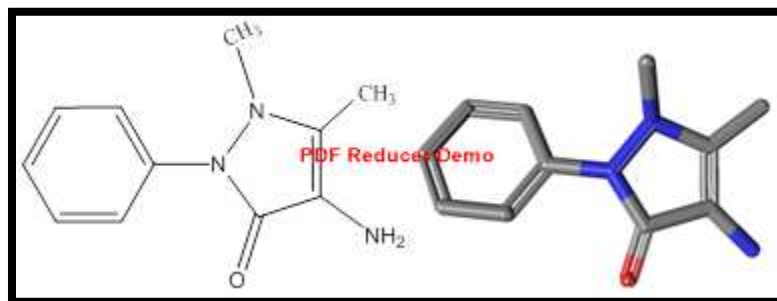
Figure(1.6): The chemical and structure of 4-aminophenazone

(1.3.2) 2-Aminobenzothiazole

Consider one of the important derivatives of aniline. 2-Aminobenzothiazole with molecular formula $C_7H_6N_2S$ and melting point (126-129) °C, chemical and crystal structure are shown in Fig.(1.7).
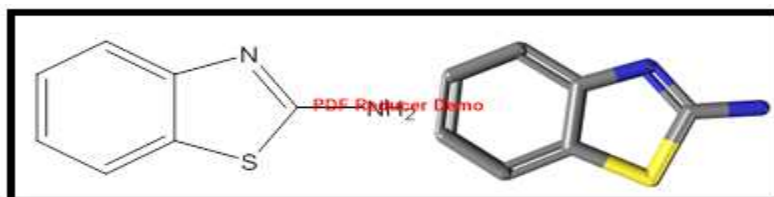
Figure(1.7): The chemical and structure of 2-Aminobenzothiazole

It was used to study adsorption of biologically significant 2-aminobenzothiazole molecules on colloidal silver particles using surface-enhanced raman scattering spectroscopy. It has local anaesthetic action and has numerous applications in human and veterinary medicine , as well as a neutral carrier (ionophore) used to construct a poly (vinyl chloride)-based membrane electrode for determination of

Ce^{3+} ions. 2-Aminobenzothiazole bonds chemically to multi walled carbon nanotubes to produce a sorbent which has been used for separation of Pb(II) from aqueous samples, can find application for making biological activitive agents such as antiviral, antibacterial, anti tuberculous, antbody and antifungal [10-14].

(1.3.3) 2-Aminobenzimidazole

As with 2-aminobenzothiazole the 2-Aminobenzimidazole is considered an aniline derivative as well. It has molecular formula $C_7H_7N_3$ with melting point m.p (226-230)°C .2-Aminobenzoimidazole chemical and crystal structure are shown in Fig.(1.8).
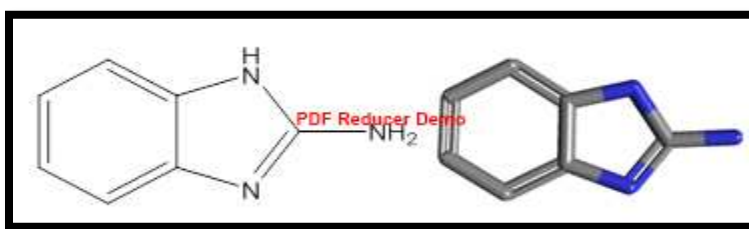
Figure(1.8): The chemical and structure of 2-aminobenzimidazole

2-Aminobenzimidazole was used in the hydrolysis of a choline carbonate. It was also used in the synthesis of imidazo, benzimidazoles, are used in organic synthesis and vermicides or fungicides as they inhibit the action of certain microorganisms. Benzimidazole structure is the nucleus in some drugs such as proton pump inhibitors and anthelmintic agents [15-18].

(1.4) *β*-enaminone

β-enaminone are compounds that bind the amine group through (C=C) to the carbonyl group (C=O),(N-C=C-C=O) as this gives stability to the output and ease of preparation. *β*-enaminon is used in the synthesis of compounds, bioactive substances, pharmaceuticals, anti-tumor, anti-bacterial, anti-epileptic, as well as

other therapeutic properties. It is also used as a medium step (intermediate) in the preparation of many organic compounds [19-25].

(1.4.1) *β*-enaminone compounds

In 2010 Ali reza H. and others synthesis *β*-enaminones with A highly efficient, simple and green procedure. The reaction of aromatic and aliphatic amines with *β*-dicarbonyl compounds using catalytic amount of silica-supported LiHSO₄ (LiHSO$_4$/SiO$_2$) under solvent-free conditions at 80°C,where it obtained a high percentage of output and in short reaction time,[26].The synthesis is outlined in the Scheme(1.1).
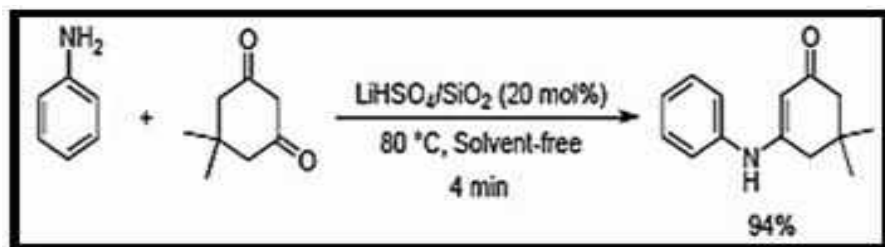
Scheme(1.1): Reaction for the prepartion of β-enaminones

In 2011 Several *β*-enaminones and *β*-enaminoesters have been synthesized by Amiya S. and Devendra D. in high yields from amine and *β*-diketone in the presence of Zeolite (ZSM-5) as a catalyst. This method is applicable to both cyclic and acyclic ketones with aromatic and aliphatic amines,[27].The synthesis is outlined in the Scheme(1.2).
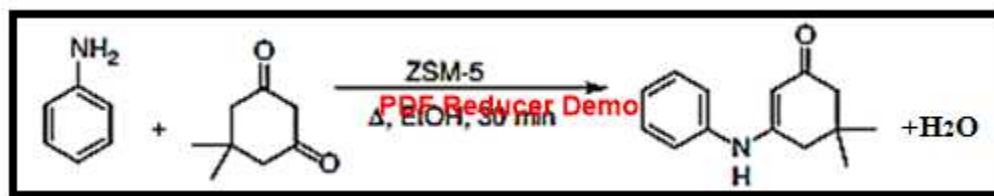
Scheme(1.2): Prepartion of *β*-enaminones using zeolite(ZSM-5) as catalysed

In 2012 Ming Z. and others synthesis of *β*-enaminones and *β*-enaminoesters using a combination of [(PPh₃)AuCl] /AgOTf as catalyst has been developed. The

reaction between 1,3-dicarbonyl compounds and primary amines was carried out under solvent-free conditions with low catalyst loading in good to excellent yields at room temperature[28]. The syntheses are outlined in the Scheme (1.3).
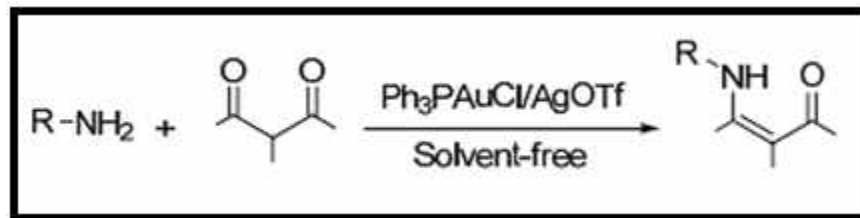
Scheme(1.3): Au(I)/Ag(I) catalyzed enamination of *β*-dicarbonyl compounds

In 2013 Muhammad N. and others synthesized *β*-enaminones under solvent-free reaction conditions using PPA-SiO$_2$ as catalyst. This method affords high selectivity and good tolerance of a variety of different functional groups present on both aromatic and aliphatic amines. In addition, the method is environmentally benign and cost-effective due to absence of solvent and easy work-up,[29].The reaction given in Scheme(1.4).

Scheme(1.4): The reaction conditions using PPA-SiO$_2$ as catalyst

In same year Ramin R. and Mozhdeh S. synthesis of *β*-enaminones using melamine-formaldehyde resin supported (H$^+$) (MFRH) as a mild and inexpensive catalyst in solvent-free media. The present method was performed by combining low cost and readily available amines, 1,3-dicarbonyls and melamine-formaldehyde resin supported (H$^{+)}$ (MFRH) as a catalyst ,Scheme(1.5). This method is applicable to both cyclic and acyclic ketones with aromatic and aliphatic

amines, and provides several advantages such as environmental friendliness, low cost, good yields and simple workup procedure [30].

Scheme(1.5):The condensation reaction between dimedon and 4-chloroaniline

In same year Karimi-Jaberi Z. and Takmilifard Z. developed new and efficient methods for the synthesis of *β*-enaminones in the presence of a catalytic amount of tris(hydrogen sulfato) boron or tri chloro acetic acid as highly efficient catalysts at 120 °C under solvent-free conditions. They concluded that both methods are simple, and provide desired products in good yields and short reaction times. Scheme(1.6),the synthesis of β-enaminones. All products were identified by FT-IR spectral methods[31].
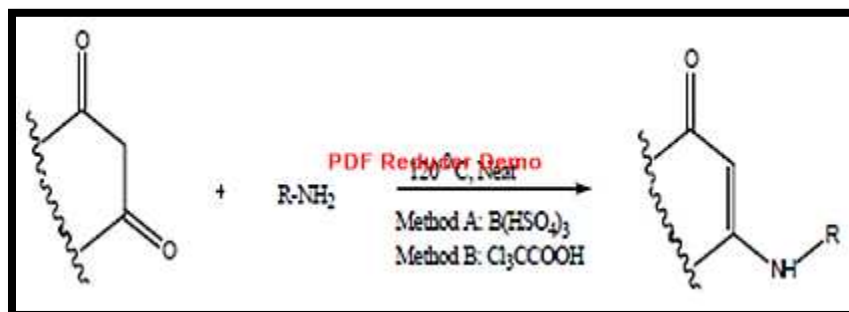
Scheme(1.6): Prepartion of β-enaminones

In 2014 Cheng-Liang F. and others synthesized *β*-enamino ketones under solvent free conditions by the reaction of a set of *β*-dicarbonyl compounds and primary amines with highly stable ferric triflate Fe(OTf)₃ as an efficient catalyst ,Scheme(1.7). The advantage of this method is to shorten the reaction time and the high output, in addition to being of a green synthesis[32].
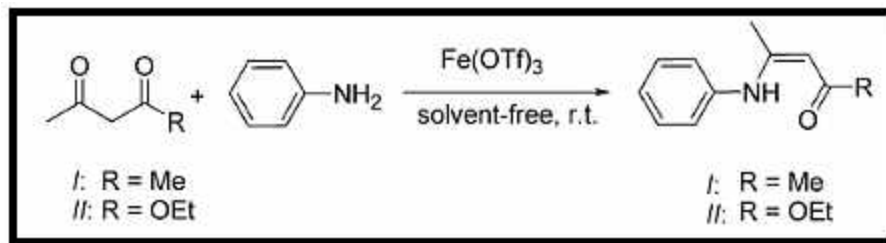
Scheme(1.7): Prepartion of *β*-enamino ketone and esters

In 2015 Sunil U. and others synthesis of *β*-enaminones and *β*-enamino esters by the reaction of amines with various 1, 3-dicarbonyl compounds under catalyst free and solvent free conditions ,Scheme(1.8).This method constitutes a green approach which is a valuable addition to the existing methods for synthesis of these compounds [33].

Scheme(1.8): Prepartion of *β*-enaminones and *β*-enamino esters

In 2017 Arijit S. and others synthesized *β*–enaminanes drivatives by one-pot three component reactions of *β*–nitrostyrenes, aliphatic/ aromatic, amines or alcohols and dimedone\4-hydroxycoumarin and CuO and ZnO NPs as catalyst ,Scheme(1.9) .The reaction yields were moderate to excellent with short reaction time(2-3hrs)[34].
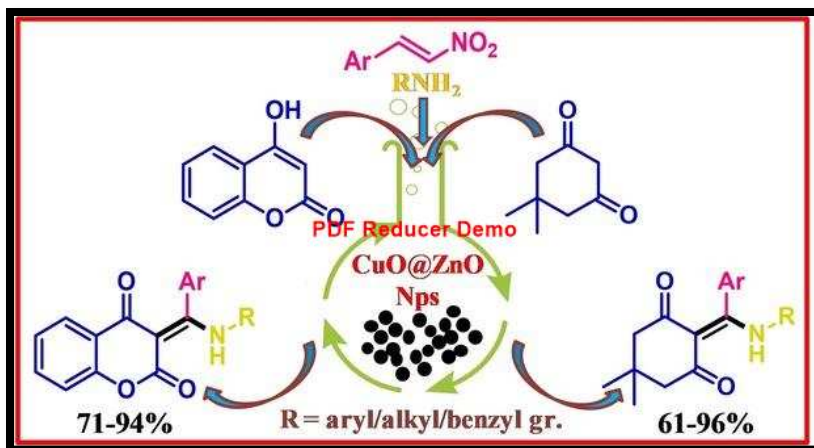
Scheme(1.9): Prepartion of *β*–enaminanes derivatives

In 2017 Dabon L. and others synthesized N-sulfonyl enaminones which are developed. Two different isomers are obtained in a chemocontrolled manner by employing the different properties of Au(I) and Au(III) catalysts. A wide range of substrates afforded moderate to excellent yields and selectivities. These reactions represent the first examples of transition-metal-catalyzed enamine synthesis from sulfonamides and alkynes,[35].The reaction given in Scheme(1.10).
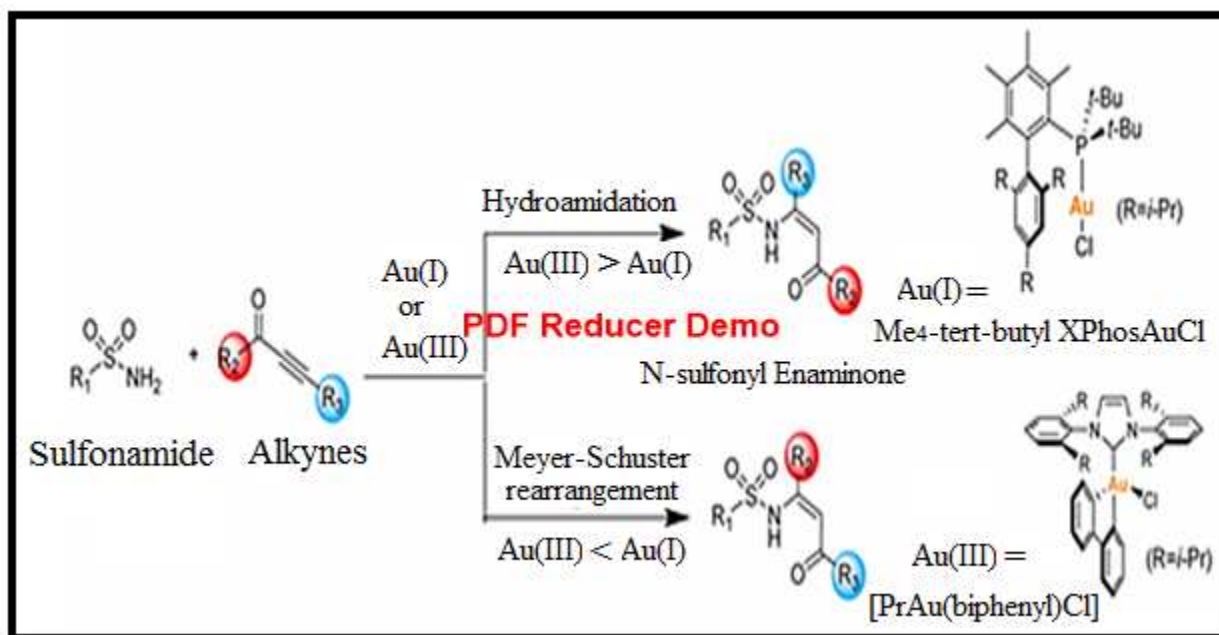
Scheme(1.10): The reaction by Au(I) and Au(III) as catalysts

(1.5) Dithiocarbamate

Dithiocarbamates (DTCs) are a group of small organic molecules,that have an important functional group in organic chemistry.Where the two oxygen atoms of the carbamite group are replaced by two sulpher atoms, so they are considered as an important precursors for a wide range of chemical application such as intermediates in the chemical synthesis of biological active compounds and natural products[36-38]. Also, their applications as sulfur vulcanization agents in rubber manufacturing, and radical chain transfer agents in the reversible addition-fragmentation chain-transfer (RAFT) polymerizations are extensively investigated [39]. Dithiocarbamates are important ligands in metal complexes.Their ability to bind transition metals , including lanthanide, actinide, and representative elements make them useful ligands in both inorganic and bioinorganic chemistry. This is based on the presence of the anionic CS_2^- moiety, that have a range of binding modes; monodentate, bidentate or bridging, upon complexation [40-42]. Due to the large number of ueses of DTCs , it is produced in large quantites estimated at about 35.000 metric tonnes yearly. Finally,it should be noted that the derivatives of DTCs used as fungicides are classified by the Word Health Organization(WHO) as dangerous substances[43].

(1.5.1)Chemistry of dithiocarbamates

Dithiocarbamates, were discovered as a class of chemical compounds in the history of organosulfur chemistry. These are a versatile class of monoanionic 1,1-dithio ligands and as they are easily prepared, a wide range of chemistry has been developed around them. The structure of dithiocarbamate group can be represented by the valence bond formalism as shown below Fig.(1.9). The resonance form (c) i.e. the thioureide form results from the delocalization of nitrogen lone pair. Where

this ion pair is flow from nitrogen to sulfer through a planer,delocalised π–orbital system[44-47].
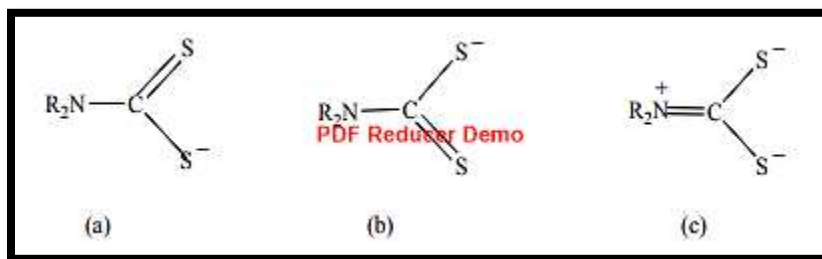
Figure(1.9): Resonance forms of dithiocarbamate complexes

At this state of resonance form(c) has a significant impact on the physical and chemical properties of the dithio compounds. The contribution of the resonance form (c) to the structure of the dithiocarbamate ligands and complexes was offered as a possible explanation for the varying antifungal activities of these compounds. The strong metal binding properties of the dithiocarbamates were recognized early by the virtue of insolubility of the metal salts and the capacity of the molecules to form chelate complexes. Dithiocarbamates can function as unidentate, bidentate chelating as well as bidentate bridging ligands, Fig.(1.10). DTCs and their metal complexes have a specific chemistry and recognize electronic structure, which can be altered upon interaction with other species[48-51].

Figure(1.10): Forms of dithiocarbamate complexes

(1.5.2) Synthesis of dithiocarbamate

There are many methods used to synthesize a range of new type of compounds bearing dithio-moiety, such as ; dithiocarbamate, xanthate, thioxanthate and

dithiophosphate .These compounds come through the reactions which happen between carbon disulphide and a various nucleophiles (Nu), such as nitrogen, oxygen, sulphur and phosphorus, respectively[52,53]. Dithiolates are prepared when nucleophiles (Nu) attack CS_2, Scheme (1.11).The reaction of carbondisulfide and either primary or secondary amines in the presence of alkali base (NaOH or KOH) in the formation of dithiocarbamates,[54,55]. Dithio carbamate salts are one of a range of important compounds. Generally, it is easily prepared, resulting from the reaction Equation(1).The sodium or potassium salts of dithiocarbamates can often be isolated easily, because they are only very poorly soluble in common organic solvents and soluble in water [56-58].

$$R_2NH + CS_2 + MOH \longrightarrow R_2NCS_2M + H_2O \hspace{2cm} (1.1)$$

Where M = K or Na
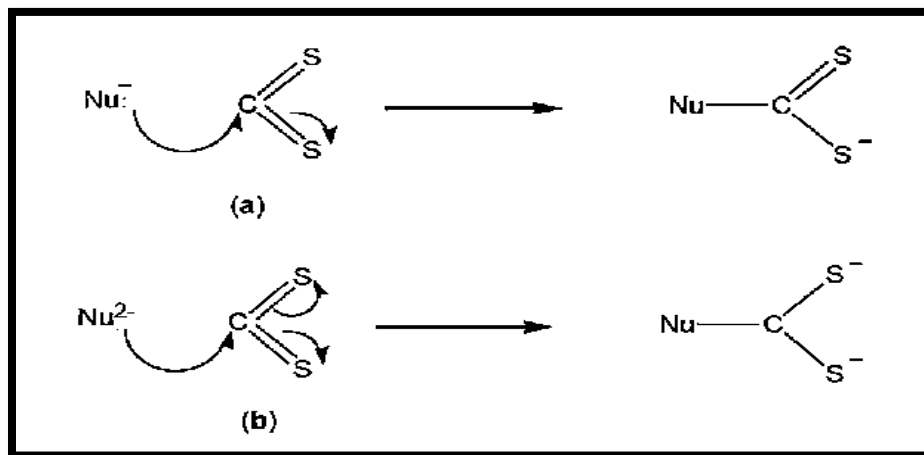
Scheme(1.11): Nucleophiles attack of CS_2

(1.5.3) Binding modes of DTCs

DTCs have the ability to align metals with different modes, and can be explained as follows, Fig.(1.11).

(1) DTCs (ligand) can act as monodentate ligand(B). This mode accures when there is no room for bidentate coordination of the DTCs.

(2) The simple chelating bidentate binding mode, where both S atom can coordinate to the (same or different) metal (A). This mode is approximately 99%.

(3) DTCs can accommodate more than one metal atom acting as a bridging ligand (C-G). The metal can be the same and can be two different metals.

(4) In all of these modes (A-G) it is one of the ion pairs of electrons on S atom which is acting as a further lewis base[59-63].
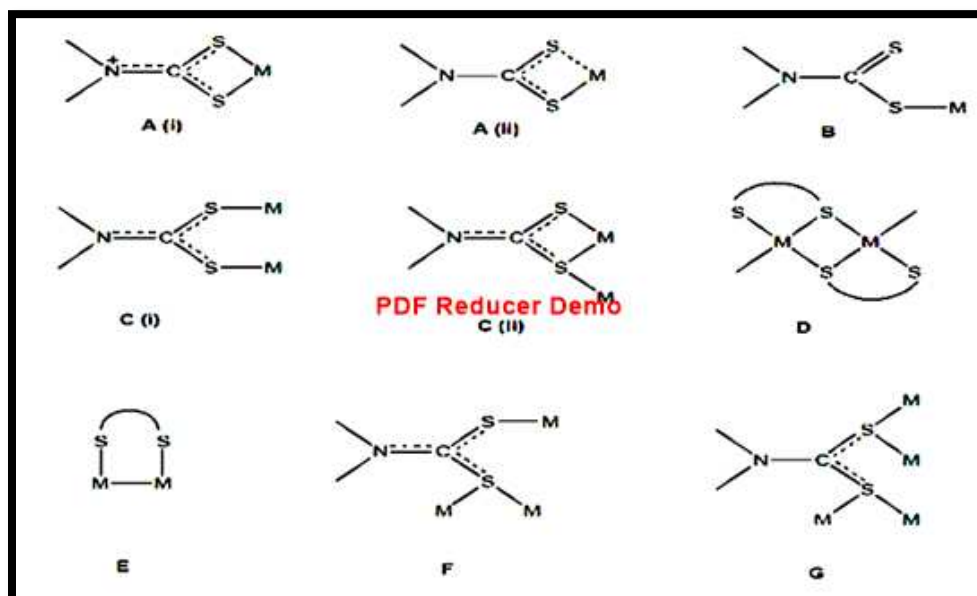
Figure(1.11): dithiocarbamate coordination mode

(1.5.4) Stability of dithiocarbamates

In circles with low pH values, DTCs compounds containing one alkyl group (produced by primary amines) have high stability and, in contrast, are unstable in the basal circles (high pH values), where they are converted into the isothio cyanates. While DTCs compounds containing the two groups of alkyl (produced by secondary amines) are unstable in the acidic circles, where they are decomposed and given CS_2 and secondary amine, Equation (2).

In general, the reason why DTCs compounds have mono alkyl group are more stable than their bialkyl conterparts in the acidic circles is (i) the steric influence of the second alkyl group, which produces a significant increase of strain an the C-N bond. (ii) Increase the electronic density on the nitrogen atom due to the effect of electrons pair located on the sulfer atom, which causes increased stability of ammonium ion formed which affects the polarity of the S-H bond[62-64].

$$R_2NCS_2^{\ominus} \xrightarrow{\ H^{\oplus}\ } R_2NH \ + \ CS_2 \tag{1.2}$$

(1.6) Literatures Servey

Historically DTCs was first prepared in 1850 by Debus, where he developed method for the synthesis of dithiocarbamate acid.Then after a period of time to 1907, the first DTCs complexes were prepared with d-block elements.The name tetramethylthiuram is the famous DTCs derivative commonly known as thiram, was given the method of preparation of a patent in 1934, which is worth mentioning that the DTCs have the ability to form stable compounds with the p-block metals and f-block of lanthanides[57,64,65]. The following literature survey data covering 2 kinds of dithiocarbamate complexes (i) containing only DTCs as a ligand and (ii) the second containing mixed-ligand.

In 2010, Narayanaswamy S. and others [66] synthesized three nickel complexes of DTCs ligand (dbpdtc = benzyl (4-(benzylamino)phenyl) dithiocarbamate), namely [Ni(dbpdtc)$_2$](1), Fig. (1.12) ,[Ni(dbpdtc)(NCS)(PPh$_3$)](2) and [Ni (dbpdtc) (PPh$_3$)$_2$] ClO$_4$(3). The complexes were characterized by FT-IR, electronic spectroscopy and cyclic voltammetry. A single-crystal X-ray structural analysis was carried out for complex and showed that the nickel is in a distorted square planar environment.
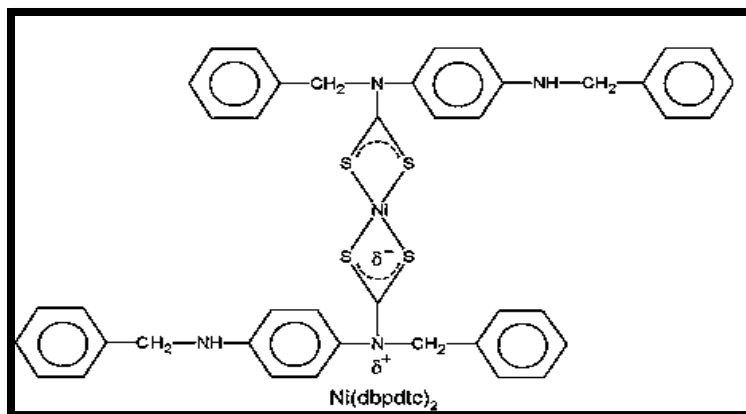
Figure(1.12): Preparation of the complex[Ni(dbpdtc)₂]

In 2011, Zia R. and others [67] synthesized a chain of mononuclear organotin(IV) complexes of the types, R_3SnL {$R = C_4H_9$ (**1**), C_6H_{11} (**2**), CH_3 (**3**) and C_6H_5 (**4**)}, R_2SnClL {$R = C_4H_9$ (**5**), C_2H_5 (**7**) and CH_3 (**9**)} and R_2SnL_2 {$R = C_4H_9$ (**6**), C_2H_5 (**8**) and CH_3(**10**)},Fig.(1.13)where L= 4-(4-methoxyphenyl)piperazine-1-carbodithioate .The ligand-salt and the complexes have been characterized by FT-IR and multinuclear (^{1}H, ^{13}C NMR) spectroscopy and elemental microanalysis (C.H.N.S). Asubsequent antimicrobial study indicates that the compounds are active biologically and may well be the basis for a new class of fungicides.
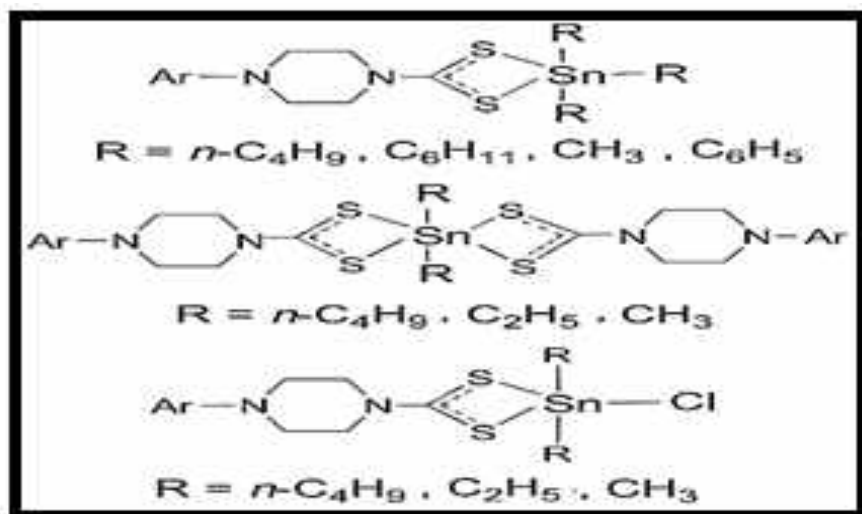
Figure(1.13): Prepartion of organotin(IV) complexes

In 2011, Damian C. and Peter A. [68] synthesized several N-Methyl-N-Phenyl dithiocarbamate complexes [(C$_6$H$_5$)(CH$_3$)NCS$_2$)$_2$M], Fig.(1.14) where M= Zn (II) , Cd(II) and Hg(II).These complexes have been characterized by elemental analysis and spectral studies (FT-IR, ^{1}H,^{13}C-NMR). Thermogravimetric analysis of the complexes show a single weight loss to give MS (M = Zn, Cd, Hg).

Figure(1.14): Prepartion of complexes.

In 2012, Jayaraju A. A.and others [69] developed a new method for the synthesis of a series of novel bidentate DTCs ligand of 2-Amino2-methyl 1-propanol (AMPDTC), [Cu(AMPDTC)$_2$)Cl$_2$] and [Mn(AMPDTC)$_2$Cl$_2$], Fig.(1.15). Two different new complexes have been synthesized of Cu(II) and Mn(II) .The complexes were characterized by Elemental Analysis, FT-IR, ^{1}H NMR , ESR TGA-DTA and anti microbial analysis.

Figure(1.15): Prepartion of complexes [M(AMPDTC)$_2$Cl$_2$]

In 2012, Musthak M. and others [70] synthesized a chain of new bidentate ligands are dithiocarbamates of 4-Aminoantipyrene and 2-aminothiozole (AADTC,

ATDTC), [Au(AADTC)$_2$] and [Ru(ATDTC)$_2$] by new synthetic methods, as the sodium salt, Fig. (1.16). In the reaction of Chloroauric acid and Ruthenium Chloride with AADTC and ATDTC the corresponding complexes were prepared. The complexes was characterized by Elemental Analysis, FT-IR, ESR, ^{1}HNMR and TGA-DTA.

Figure(1.16): Prepartion of complexes [Au(AADTC)$_2$] and [Ru(ATDTC)$_2$]

In 2015, Sajad H. and others [71] synthesized four complexes of Hg(II) with dithiocarbamate as ligand, Bis(N-furfuryl-N-(2-phenylethyl)dithiocarbamato-S,S′)mercury(II)(1),bis((furan-2-yl)methyl(2-(thiophen-2-yl)ethyl)dithiocarbamato -S,S′)mercury(II) (2), bis(N-benzyl-N-(2-(thiophen-2-yl)ethyl)dithiocarbamato-S,S′)mercury(II) (3) and bis(N-furfuryl-N-propyldithiocarbamato-S,S′)mercury(II) (4),Fig.(1.17).The complexes have been characterized by FT-IR and ^{13}C , ^{1}H NMR spectroscopy and X-ray diffraction technique. These complexes show difference in

geometry due to the effect of the N-bound organic moiety of the dithiocarbamate ligand and the crystal packing.
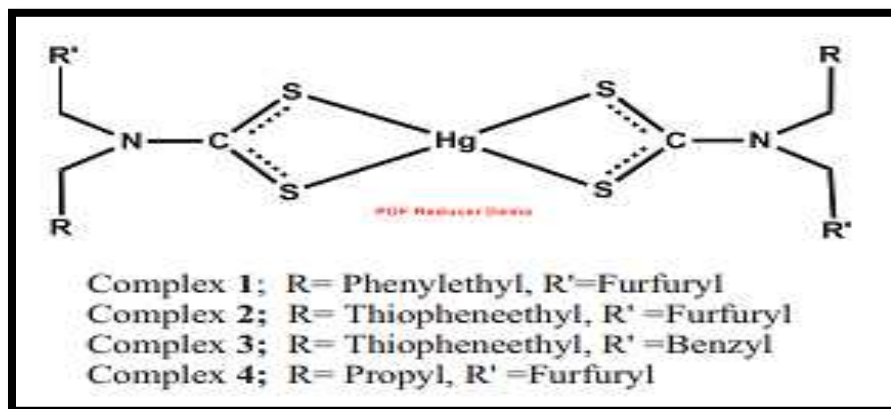
Figure(1.17): Preparation of complexes from (1-4)

In 2015, Chauhan H. and Jaswant C. [72] synthesized Sb(III) complex with chloro bis(N,N-dimethyl dithio carbamato-S,S′) in distilled acetonitrile,Scheme (1.12) .The complex has been characterized by physicochemical [melting point and molecular weight determination, elemental analysis (C.H.N.S), spectral [FT-IR,^{13}C, ^{1}HNMR] studies. The crystal and molecular structure was further confirmed using single crystal X-ray diffraction analysis which features a five-coordinate geometry for Sb(III).

Scheme(1.12): Prepartion of complex.

43
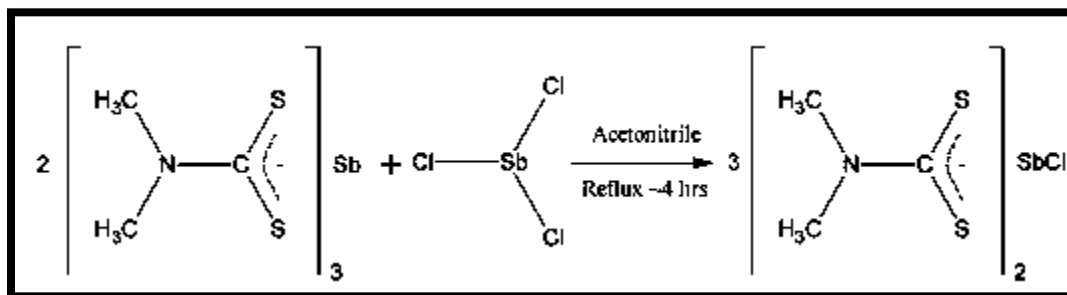
In 2015, Ajit N. and others [73] synthesized five new Sn(IV) dithiocarbamate complexes of the form R_2SnL_2 (R = n-Butane, L = L^1, (4-phenylpiperazine-1-dithiocarbamate), L^2, (N-benzyl-N'-methyl-4-pyridyldithiocarbamate); Ph, L^3, (N-benzyl-N'-methyl-3-pyridyldithiocarbamate) and Ph_3SnL (L = L^4, (N,N'-di(methyl -3-pyridyl dithio carbamate)), L^5,(4-ethoxycarbonylpiperidine-1-dithio carbamate) are derevitives of DTCs. The complexes were characterized by elemental analysis, spectroscopy (FT-IR, UV–Vis., ^{1}H, ^{13}C NMR) and their structures have been investigated by single crystal X-ray crystallography, TGA analysis of two complexes show a double and single step decomposition. These studies suggest distorted octahedral geometry for organotin complexes, Fig.(1.18).
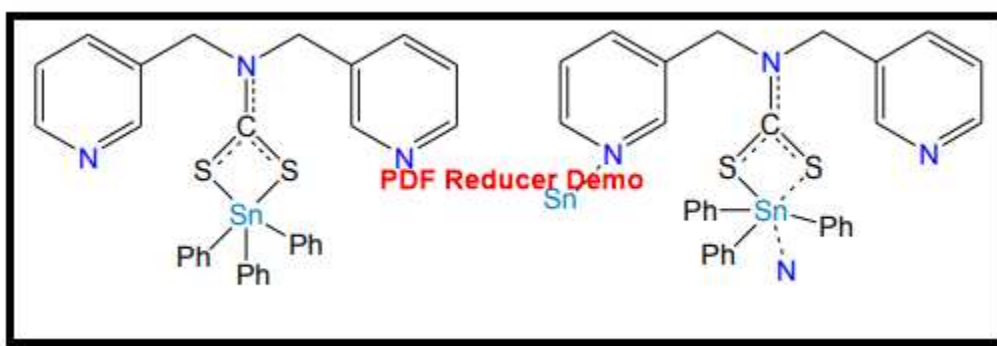
Figure(1.18):The coordination modes for the pyridine functionalized ligand L^4

In 2016, Sathiyaraj E. and others [74] synthesized twelve new Ni(II) complexes of functionalized dithiocarabamates[Ni(S_2CNRR')$_2$](1-6) and [Ni (S_2CNRR') (NCS) (PPh$_3$)](7-12) [whereR=furfuryl;R'=2-hydroxybenzyl (1,7),3-hydroxy benzyl (2,8), 4-hydroxybenzyl (3,9), 4-methoxybenzyl (4,10), 4-fluorobenzyl (5,11), 4-chloro benzyl (6,12)],Fig.(1.19) . These complexes have been characterized by elemental analysis, FT-IR, UV-Vis , ^{13}C , ^{1}H NMR spectroscopy and X-ray crystallography. These measurements of the complexes support the bidentate coordination of dithio carbamate ligands. Electronic spectral studies on complexes indicate square planar geometry around Ni (II) central atom.
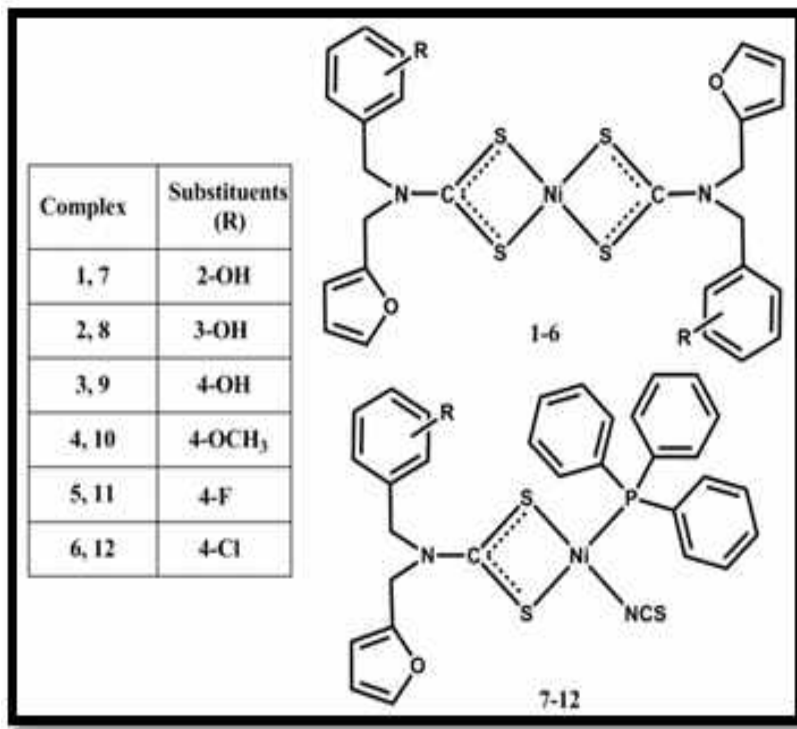
Figure(1.19): Preparation of nickel(II) complexes 1-12

Complex	Substituents (R)
1, 7	2-OH
2, 8	3-OH
3, 9	4-OH
4, 10	4-OCH₃
5, 11	4-F
6, 12	4-Cl

In 2016, Reena Y. and others [75] synthesized three new organic complexes of Sn(IV), [Me$_2$Sn(4-OHPCTDA)$_2$] (1), [n-Bu$_2$Sn(4-OHPCTDA)$_2$] (2) and [Ph$_3$Sn(4-OHPCTDA)] (3) (4-OHPCDTA=4-hydroxypiperidine dithiocarbamate),Fig.(1.20). These complexes have been characterized by elemental analyses, FT-IR, ^{13}C , ^{1}H NMR spectroscopy, thermogravimetric analyses and X-ray crystallography. The X-ray analyses for 1 and 2 indicate bipyramid geometry around Sn(IV) by the two sulfur atoms of the two dithiocarbamate ligands in bidentate fashion while in the case of (3) the monodentate coordination by one sulfur atom of the dithio carbamate ligand imposes distorted tetrahedral geometry around Sn(IV).
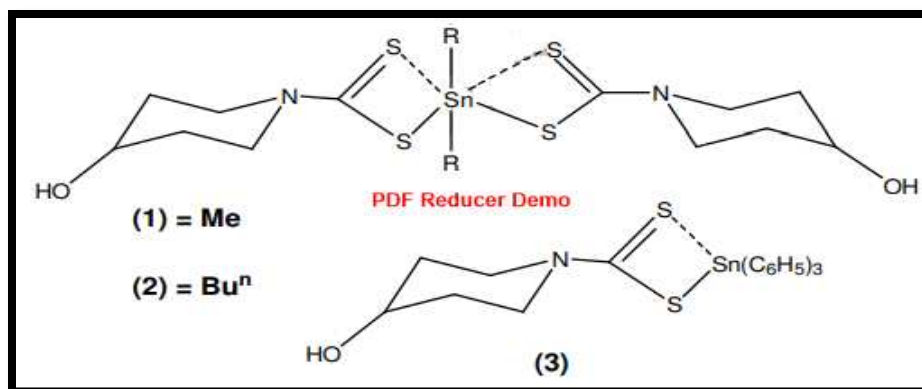
Figure(1.20): Prepartion of the complexes(1),(2) and (3)

In 2016, Imadul S. and others [76] synthesized two square planar Ni(II) and Pd(II) complexes with pyrrolidine dithiocarbamate (PDTC) .These complexes were synthesized by the reaction of Ni(CH$_3$CO$_2$)$_2$.nH$_2$O where n=0,2 and 4 and Pd (CH$_3$CO$_2$)$_2$ with DTCs in 1:2 molar ratio. The complexes were characterized by elemental, physiochemical, and spectroscopic methods. All the spectral data suggest that coordination of the pyrrolidine dithiocarbamate (PDTC) takes place through the two sulphur atoms in a symmetrical bidentate fashion. All the synthesized compounds were screened for their antimicrobial activity against some species of pathogenic bacteria (*Escherichia coli* and *Bacillus cereus*). It has been observed that complexes have higher activity than the free ligand.

In 2017, Ye-Hong D. and others [77] synthesid 12 aromatic hydrocarbon (arene) and cyclo penta dienyl ruthenium (II) dithiocarbamate complexes ,Fig.(1.21).The complexes were characterized by spectroscopic methods. The structures of 3a and 3c have been determined by X-ray crystallography. Their *in vitro* antitumor actions were fated by MTT assay agaiayt 4 lump cells (SKOV-3, HepG-2, A549, as well as PC12) and two murine cells (RAW246.7 and L^6). Notably, the outcomes *in vitro* indicated that the arene Ru(II)

complex 3e (N-methyl piperazine) displayed the highest action and selectivity to cancer HepG-2 cells.
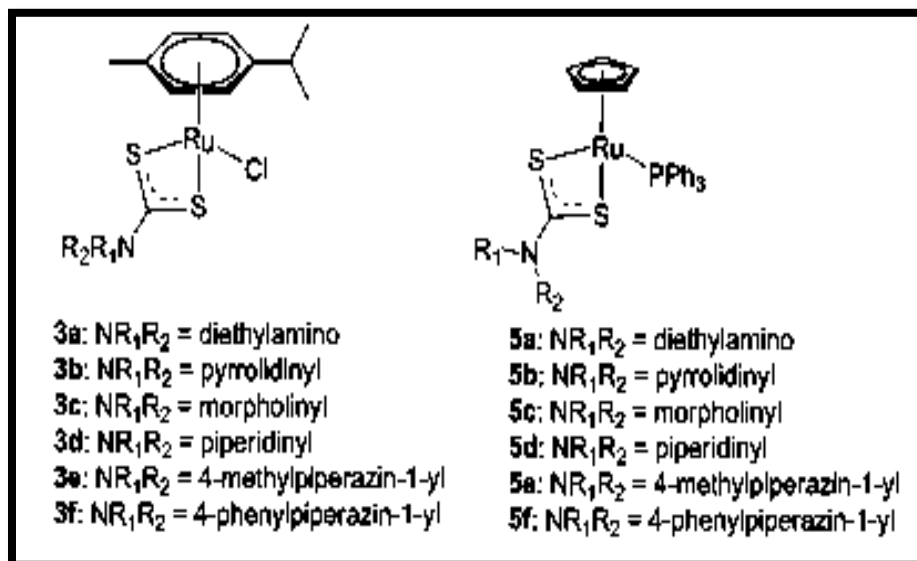
Figure(1.21): Prepartion of ruthenium(II) dithiocarbamate complexes

In 2018, Felicia F. and others [78] synthesized ammonium N-benzyldithio carbamate, they used it to prepare homoleptic(a) Ni(II) bis(N-benzyldithio carbamate) (1) and heteroleptic(b) Ni(II) complexes involving isocyanate (2) and cyanide (3) ions,Scheme(1.13). The complexes were characterized by elemental analysis, FT-IR, and ^{13}C, ^{1}H NMR spectroscopic techniques. Complex 2 was further characterized by single crystal X-ray diffraction analysis. Thermal decomposition profile of the complexes showed decomposition resulting in the formation of nickel sulphides.
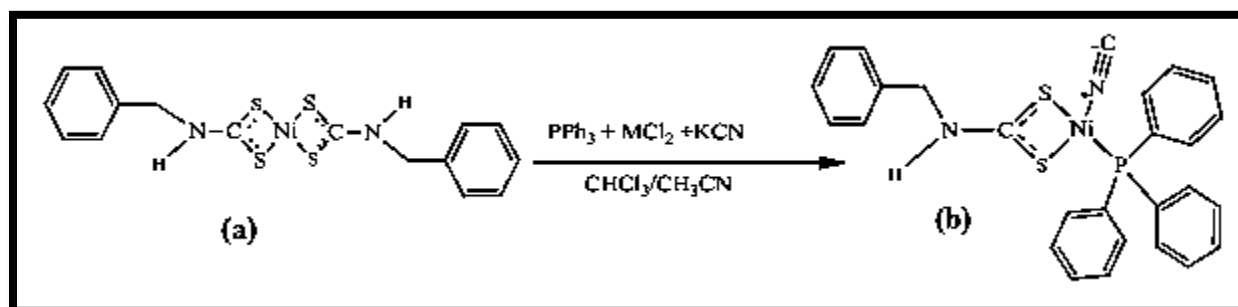
Scheme(1.13): Prepartion of the Ni(II) dithiocarbamate complex.

(1.7) Mix ligands

Mixed-ligand complexes play an important turn in numerous chemical and biological orders like water softening, ion exchange resin, electroplating, dying, antioxidant, photosynthesis in plants, and sweep of undesirable and hurtful metals from living organisms. Considerable of these metals complexes offers good biological activity against pathogenic micro organisms.The mixed ligand complexes are proper for mimicking the turn of metal ions, detoxification mechanism and drug designing. Modren mixed ligand complexes were constantly studied to get biologically live compounds [79-81].

In 2009, Amaal Y. and others synthesized complexes of α -naphthylamine dithiocarbamate of the type [M(α-naph.dtc)2]. Mixed ligands complexes of the type [M(α -naph.dtc)2phen] (phen = 1,10-phenanathroline), M = Fe(II), Co(II), Ni(II), Cu(II) and Zn(II), Fig.(1.22) .The complexes were characterized by elemental analysis (atomic absorption, EDTA titration), infrared, electronic spectra , molar conductances and magnetic moments measurements. The results suggest a tetrahedral for metal ions while Cu^{+2} complex has square planer structure and the hexa coordinated complexes have octahedral structure [82].
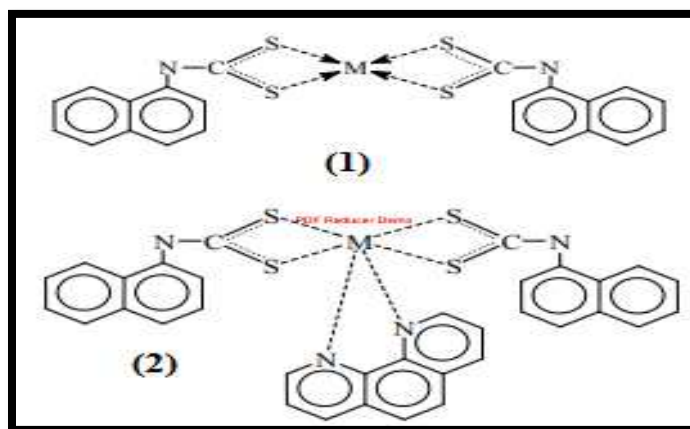
Figure(1.22): The structure for complexes (1) and (2)

In 2012, Jassim M. and others synthesized Co(II) , Ni(II), Cu(II) Zn(II) and Cd(II) metal complexes of new imidazol dithiocarbamate of type [M(imid.dtc)2],Fig.(1.23) and mixed ligands complexes of the type [M(imid.dtc)$_2$ .phen](phen=1,10-phenanthroline) .The complexes were characterized by elemental analysis (atomic absorption) infrared , electronic spectra , molar conductivity measurements and magnetic measurements . It has been found that the imidazol dithiocarbamate behaves as a monodentate ligand in all complexes. The suggested geometry of the four coordinate complexes, appear to be square planer, while octahedral are expected for mixed ligunds [83].
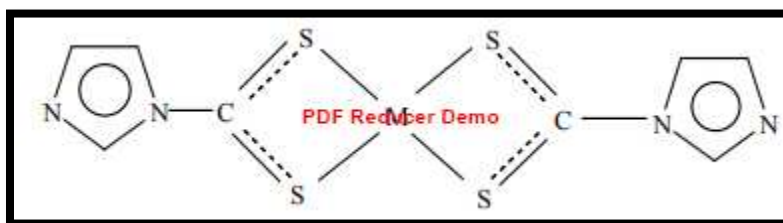
Figure(1.23): The proposed structural formula of the metal complexes

In 2013, Zdenek T. and others synthesized, characterized a mix–ligand Ni(II) DTCs complex have the formula [Ni(bpdtc)(PPh$_3$)$_2$]ClO$_4$·PPh$_3$,Fig.(1.24) by (elemental analysis, UV–Vis, FT-IR and ^{1}HNMR spectroscopy and molar conductivity measurements) and its X-ray structure was determined. The complexes have square-planar geometry [84].
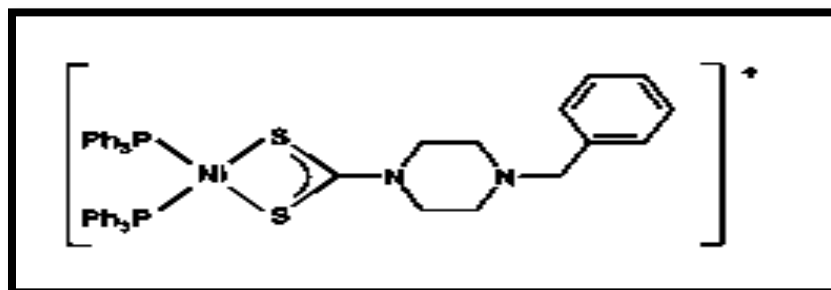
Figure(1.24): The structure of the complex

In 2016, Prakasam B. and others reported the synthesis of isobidentate coordination of dithiocarbamate ligand derived from the reaction a mixture of 1-(diphenylmethyl)piperazine and CS_2 in ethanol as solvent. Palladium (II) complexes were prepared by reaction of the salt of the ligand with Palladium chloride to synthesize three new mixed ligand complexes of palladium(II) dithiocarbamates; [Pd(4-dpmpzdtc)(PPh$_3$)(SCN)](1),[Pd(4-dpmpzdtc)(PPh$_3$)Cl] (2) and [Pd (bzbudtc) (PPh$_3$)Cl] (3), (where, 4-dpmpzdtc = 4-(diphenylmethyl) piperazine carbodithioato anion, bzbudtc = N-benzyl-N-butyldithiocarbamato anion and PPh$_3$ =triphenyl phosphine) have been synthesized from their respective parent dithiocarbamates by ligand exchange reactions. Analytical techniques revealed the formation of square planar geometry for 1-3 about metal centre, Fig.(1.25) exhibits that [85].
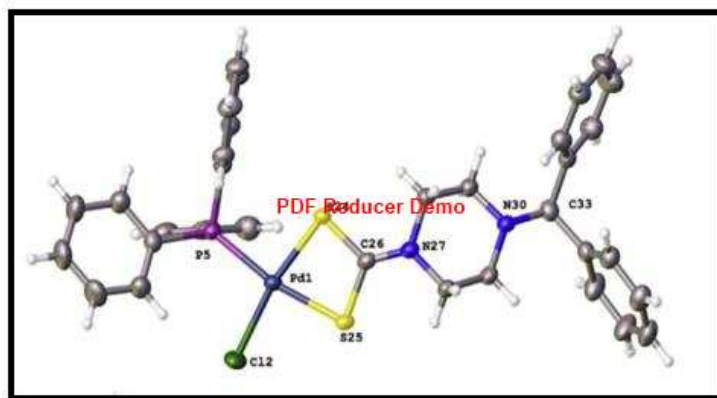
Figure(1.25): Molecular conformation with complex

(1.7.1) 3-Aminophenol

3-Amino phenol (P) is an organic compound with molecular formula C_6H_7NO. It is an amphoteric molecule and a reducing agent useful for the synthesis of dyes and heterocyclic compounds [86,87]. Fig.(1.26) shows the chemical and crystal structure of 3-amino phenol.
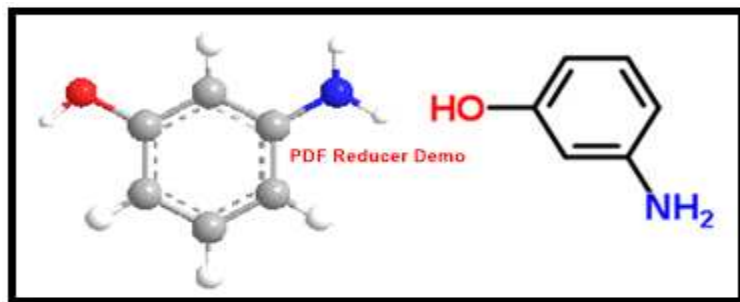
Figure(1.26): The chemical structure of 3-aminophenol

(1.7.2) 8-Hydroxy Quinoline

8-Hydroxy quinoline (Q) is an organic compound with molecular formula C_9H_7NO. It is a conjugated order and in the same time, a bifunctional hydrogen bonding molecule, which in protic solvents jointly acts as an H donor at the O-H group and as an H acceptor at the N atom[88]. The O-H and aza groups may be also concerned in a keto-enol tautomeric equilibrium. On account of a too short distance between the OH group and the ring N atom,the intramolecular and intermolecular hydrogen bonding induce the presence of many conformers of (Q) in different environments. Fig.(1.27) shows chemical structure and two conformers named, a (with intra molecular hydrogen bonding) and b (with inter-molecular hydrogen bonding). The tautomeric from of (Q), assumed to be present in polar solvents, is presented in c [89-93].
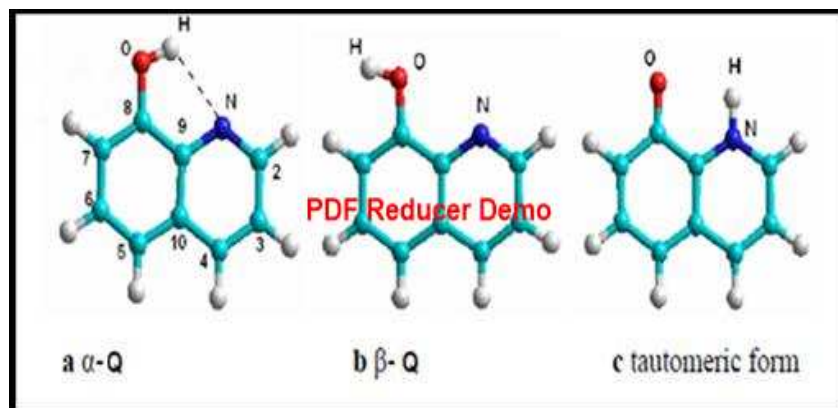
Figure(1.27): Chemical structure of 8-Hydroxyquinolines

51

(1.8) Applications and uses of dithiocarbamates

Special interest in the research of metal dithiocarbamates was recusant due to the striking constitutional features presented by this group of compounds and also due to their potential biological action and practical enforcements in the fields of rubber technology and agriculture [94]. They have different applications acting as lofty pressure lubricants in industry, fungicides and pesticides, and also as gun in vulcanization. Dithiocarbamates applied in the process of vulcanization of rubber compounds form a class of ultra-guns of the treating process [95]. Disulfiram or $(CH_3CH_2)_4N_2C_2S_4$, Fig.(1.28), which is a dithiocarbamate was first synthesized in 1881 and used to gun the vulcanization of rubber. It was only in the 1930s that disulfiram develop a medicinal use as a scabiescide and subsequently, as a vermicide for it was venomais to lower animal forms due to its ability to chelate Cu; an essential motif of the respiratory string of these organisms.[94]
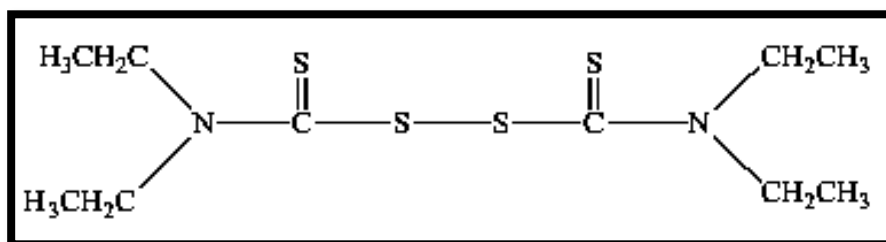
Figure(1.28): The chemical structure of Disulfiram

Disulfiram and other DTCs have been reported to offer a historic potential in the treating of human cancers[96,97]. Au(III) complexes with DTCs ligands, DMDT = N,Ndimethyldithiocarbamate and ESDT = ethylsarcosinedithiocarbamate are reported to have antitumor action. These DTCs have eminent chemotherapeutic list in terms of growing bioavailability, higher cytotoxicity and lowerest side effects than cisplatin which is one of the most openly ysed anticancer drug[94].

DTCs and two different alternative analogues of this compound were evaluated for adverse effect. These compounds were examined for their *in vitro* inhibitory

action on the growth of Candida races and it was observed that $NaS_2CN(C_2H_5)_2$ and $NaS_2CN(CH_3)_2$ generated inhibitory hassling to amphotericin-B, a drug clinically used to address candidiasis. The *in vivo* effects of these DTCs were also emboldening with N-methyl-D-glucaminedithiocarbamate being the most effective. The synthetic use of DTCs moiety ($M-S_2CNR_2$) is due to the inclusion of a set of organic substituents (R) in the firm ligand [98].

Finally, DTCs and its complexes are important in the field of agriculture where they are used in the production of antibodies to various types of fungal diseases affecting plants, which are used in the protection and storage of plants and the most famous are Thirm, Metirem,Zineb and propineb[99-102].

(1.9)Aim of the work

DTCs-based complexes have been the focus of many researches. Their fabrication and design attract the attention of workers due to their potential applications in many fields such as analytical chemistry, industry, catalysis, biological, sensing, biomimetic and agriculture. Therefore, the preparation of there compounds requires fall characterisation to the chemical structure of the species. The aim of this work could be summarised as follows:

1- Synthesis and characterization of three new precursors(β-enaminone compound) , HDa, HDb and HDi, and used in preparing new ligands.

2- Synthesis and characterization of three new dithiocarbamate ligands by using of precursors.The synthetic route is based on multiple organic synthesis steps.

3- Synthesise and characterization of metal complexes and mixed ligand complexes of these ligands (KL^1 , KL^2 and KL^3) separately with some metal ions: Mn(II) ,Co(II), Ni(II), Cu(II), Zn(II), Cd(II) and Pd(II) and suggest the geometric shapes.

4- Study the possible structures and the stereochemistry of the prepared compounds.

5- Study the viability of the prepared ligands in habiting the corrosion of α–brass alloy.

6- Study the bacterial activity of the prepared ligands and their complexes towards gram positive and gram negative bacteria.

Chapter Two
Experimental

(2.1) Chemicals

All common laboratory chemicals and reagents and their suppliers are listed in Table (2.1) and have been used without further purification.

Table (2.1): Chemicals used in this work and their suppliers.

No.	Materials	Formula	Company source of supply	Purity %
1	Acetone	C_3H_6O	RieDel-DeHaen	≥ 99.8
2	2-Amino benzimidazole	$C_7H_7N_3$	HIMEDIA	99
3	4-Amino Phenazone	$C_{11}H_{13}N_3O$	BDH	99
4	2-Amino phenol	$C_7H_6N_2S$	BDH	99
5	Benzene	C_6H_6	BDH	99.9
6	Cobalt (II) chloride hexahydrate	$CoCl_2.6H_2O$	Merck	99
7	Copper (II) chloride dehydrate	$CuCl_2.2H_2O$	BDH	98
8	Cadmium (II)chloride dehydrate	$CdCl_2.2H_2O$	BDH	98
9	Carbon disulphide	CS_2	Sigma-Aldrich	≥ 99.9
10	Dimedone	$C_8H_{12}O_2$	BDH	99
11	Dimethyl sulfoxide	$(CH_3)_2SO$	BDH	≥ 99.9
12	Ethanol	C_2H_5OH	Merck	99
13	Glacial acetic acid	CH_3COOH	BDH	99.5
14	Hydrochloric acid	HCl	Thomas baker (37N)	-
15	8-Hydroxy quinoline	C_9H_7NO	BDH	99
16	Manganis(II)chloride tetrahydrate	$MnCl_2.4H_2O$	BDH	98
17	Nickel (II) chloride hexahydrate	$NiCl_2.6H_2O$	BDH	98
18	Potassium hydroxide (solid)	KOH	Fluka	99
19	Palladium(II)chloride	$PdCl_2$	BDH	98
20	Sodium chloride	NaCl	Hopkins	99.5
21	Zinc (II) chloride	$ZnCl_2$	BDH	98

(2.2) Physical measurements

The following techniques were used to characterise precursors, ligands and their complexes.

(2.2.1) Melting points

Melting points of compounds were obtained on an Electro-thermal Stuart SMP10 at Central Service Laboratory/ College of Education For Pure Science/ Ibn al-Haitham, University of Baghdad.

(2.2.2) FTIR spectra

Infrared spectra were obtained using KBr discs by a (SIDCO, England FT-IR 600) in the range 4000-400 cm^{-1}, at Central Service Laboratory/ College of Education for Pure Science (Ibn Al-Haitham), University of Baghdad and via CsI discs in the range 400-200 cm^{-1} on Shimadzu 8400s FT-IR recorded at College of Science, University of Baghdad.

(2.2.3) Electronic spectra

Electronic spectra were measured from 200-1100 nm for 10^{-3} M solutions in DMSO at 25 ℃ with (UV-Vis) spectrophotometer type (Shimadzu 1800), using quartz cell of 1.0 cm length. The measurements were obtained at Central Service Laboratory/ College of Education For Pure Science /Ibn al-Haitham, University of Baghdad.

(2.2.4) Metal analysis

Metal content for complexes were measured using a Shimadzu flame atomic absorption spectrophotometer (A.A) 680G in Ibn Sina Company, Ministry of Industry Baghdad, Iraq.

(2.2.5) Elemental microanalysis

Elemental analyses (C.H.N.S) for ligands and their metal complexes were carried out on an (Euro EA 3000) at Central Service Laboratory/College of Education For Pure Science /Ibn al-Haitham, University of Baghdad.

(2.2.6) Chloride content

Potentiometric titration method was used to determine chloride content for complexes using a 686-titro processor-665 Dosimat-Metrohm Swiss in Ibn Sina Company, Ministry of Industry, Baghdad, Iraq.

(2.2.7) Conductivity measurements

Electrical conductivity measurements of the complexes were made with DMSO solutions at 25 ℃ using a (PW9526 meter) at College of Education For Pure Science/ Ibn al-Haitham, University of Baghdad.

(2.2.8) Mass spectra

Mass spectra for ligands were obtained by Electron Impact (EI) mass spectroscopy. The spectra were recorded at University of Tehran, Islamic Republic of Iran**.**

(2.2.9) ^{1}H-, ^{13}C- Nuclear magnetic resonance (NMR)

^{1}H-, ^{13}C-NMR spectra for some selected precursors, ligands were acquired in suitable deuterated solvents using TMS as an internal standard for ^{1}HNMR analysis. Chemical shifts are reported in ppm downfield from tetramethylsilane (TMS), at 298 K. Coupling constants (J) are reported in Hertz (Hz). Standard abbreviations indicating multiplicity were used as follows: m= multiplet, t= triplet, d= doublet, s= singlet. The samples were recorded at University of Tehran, Islamic Republic of Iran.

(2.2.10) Magnetic moment measurement

Magnetic moments at 303.8K were determined with a magnetic susceptibility balance (Sherwood Scientific). Samples were recorded at College of Sciences, Al-Mustansiriyah University.

(2.2.11) Thermal gravimetric analysis

Thermo gravimetric analysis was carried out using a STA PT-1000 Linseis company /Germany. The measurement was conducted under atmosphere of argon gas at a heating rate 10 ˚C/min. Samples were recorded at College of Education For Pure Science / Ibn al-Haitham, University of Baghdad.

(2.2.12) Corrosion test

The evaluation test of ligands as an inhibitor were performed using M Lab 200 potentiostat /galvanostst was obtained from Bank Electronik-Intelligent Controls GmbH with maximum CE voltage of ± 14 V and maximum current per channel ± 200 mA.The tests were recorded at College of Education For Pure Science / Ibn al-Haitham), University of Baghdad.

(2.2.13) Bacterial activity

The evaluation of ligands and their metal complexes against two bacterial species *(Staphylococcus aurous and Escherichia coli)* were performed using agar-well diffusion . In this method, the wells were dug in the media with the help of a sterile metallic borer with centres at least 6 mm. Recommended concentration (100 μL) of the test sample 1 mg/mL in DMSO was introduced in the respective wells. The plates were incubated immediately at 37°C for 24 h. Activity was evaluated by measuring the diameter of inhibition zones (mm). The activity of determined samples was at College of Science, University of Baghdad.

(2.3) Abbreviation of precursors

Table (2.2) shows the suggested abbreviation, structures and nomenclature of the synthesised precursors used to prepare ligands.

Table (2.2): Structure and nomenclature of synthesised precursors.

abbreviation	precursors
HDa	
	4-((5,5-dimethyl-3-oxocyclohex-1-en-1-yl)amino)-1,5-dimethyl -2-phenyl-1,2-dihydro-3*H*-pyrazol-3-one
HDb	
	3-(benzo[*d*]thiazol-2-ylamino)-5,5-dimethylcyclohex-2-en-1-one
HDi	
	3-((1*H*-benzo[*d*]imidazol-2-yl)amino)-5,5-dimethyl cyclohex-2-en-1-one
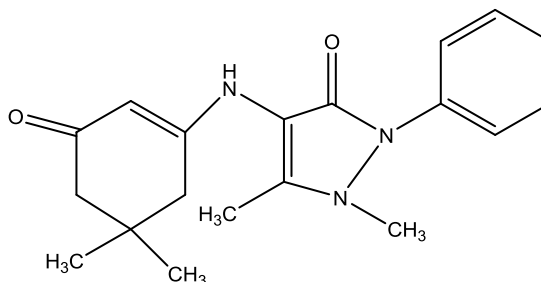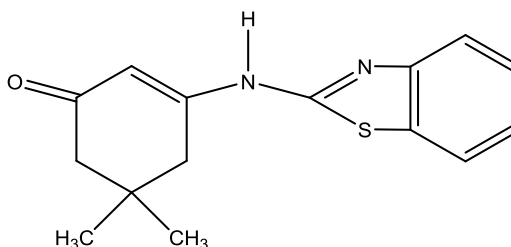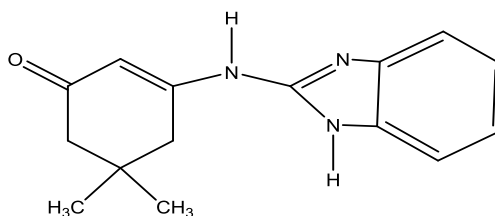
(2.4) Abbreviation of ligands

Table(2.3) describes the suggested abbreviation, structures and nomenclature of synthesised ligands.

Table (2.3): Structure and nomenclature of ligands (KL^1, KL^2 and KL^3).

(2.5) Synthesis of new precursors and ligands

In this work, the preparations of free ligands were achieved *via* several synthetic routes and as follows [103,104] .

(2.5.1) Synthesis of precursor(HDa)

abbreviation	ligands
KL[1]	
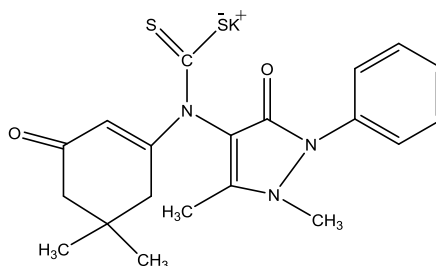
potassium (1,5-dimethyl-3-oxo-2-phenyl-2,3-dihydro-1*H*-pyrazol-4-yl)(5,5-dimethyl-3-oxocyclohex-1-en-1-yl)carbamodithioate

| KL[2] | |

potassium benzo[*d*]thiazol-2-yl(5,5-dimethyl-3-oxocyclohex-1-en-1-yl) carbamodithioate

| KL[3] | |
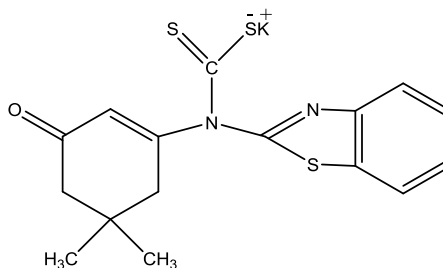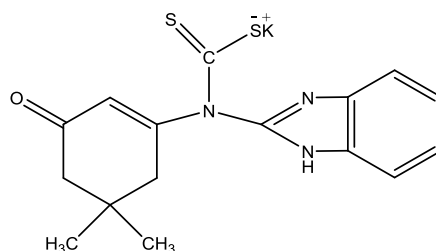
potassium (1*H*-benzo[*d*]imidazol-2-yl)(5,5-dimethyl-3-oxocyclohex-1 -en-1-yl)carbamodithioate

Dimedone (1g, 7.13 mmole) was grinded together with 4-aminophenazone (1.44g , 7.10 mmole) ,then adding (25ml) of benzene. The mixture was allowed to

continuous stirring until complete dissolution and formation of yellow light colour solution. To the solution (3-4) drops of glacial acetic acid was added, then resulting solution was refluxed for (9) hrs until the dark yellow precipitate was observed, the reaction was monitored by TLC. The reaction mixture was allowed to cool to room temperature, a dark yellow product was isolated by filtration and washed several times with benzene and dried to give a yellow precipitate. Weight (1.25 g), yield (53.92 %), m.p (220-222)°C, Scheme(3.1).

(2.5.1.1) Synthesis of precursors (HDb) and (HDi)

A same method to that mentioned in preparation of precursor (HDa), was used to prepare other amine precursors with dimedone. Table (2.4) shows some physical properties of the prepared precursors.

Table (2.4): Colours, yields and weights of precursors (HDb) and (HDi).

Compound	starting material	Colour	Weight (g)	m.p (°C)	Yield (%)
Precursor (HDb)	2-aminobenzothiozole	yellow	1.09	78	56.09
Precursor (HDi)	2-aminobenzimidazole	Pale yellow	1.10	90	60.04

(2.5.2) Synthesis of the ligands

New ligands were prepared according to standard methods used in the synthesis of dithiocarbamte compounds [103,104].

(2.5.2.1) Synthesis of potassium (1,5-dimethyl-3-oxo-2-phenyl-2,3-dihydro-1H-pyrazol-4-yl)(5,5-dimethyl-3-oxocyclohex-1-en-1-yl)carbamodithioate (KL[1])

To a solution of (HDa) (0.10 g, 0.30mmol) in 10 mL of ethanol, was added an excess of KOH (0.07 g, 1.25 mmol) dissolved in ethanol (2mL). The mixture was allowed to stir in an ice bath, and then a solution of carbon disulfide (0.07 g, 0.92mmol) was added drop wise with stirring. The mixture was allowed to stir at

0 °C for 2 h, during which the formation of the potassium dithiocarbamate salt was obtained as a yellow solid, m.p= (176-178) °C. Yield: (0.11)g, (81.5%).

(2.5.2.2) Synthesis of (KL^2) and (KL^3) Ligands

The method used was similar to that for KL^1,but with other precursors HDb, HDi using carbon disulphide and KOH. Table (2.5) shows some physical properties of the prepared ligands, Scheme(3.3).

Table (2.5): Colours, yields, melting points, weight of the ligands (KL^2 and KL^3).

Free ligand	Weight of precursor(g)	weight of thr ligand (g)	Yield (%)	Colour	m.p. °C
KL^2	0.10	0.113	79.3	Light orange	85 -87
KL^3	0.10	0.144	71.18	yellow	110 -112

(2.6) Abbreviation of the suggested complexes

Table (2.6) describes the suggested abbreviation, structures and ionic metals types.

Table (2.6): Proposed structures of complexes.

ligands   complexes

KL^1

M(II)= Mn, Co, Ni, Cu, Zn and Cd

KL^2

KL^3

M(II)= Mn, Co, Ni, Cu, Zn and Cd

M(II)= Mn, Co, Ni, Cu, Zn and Cd
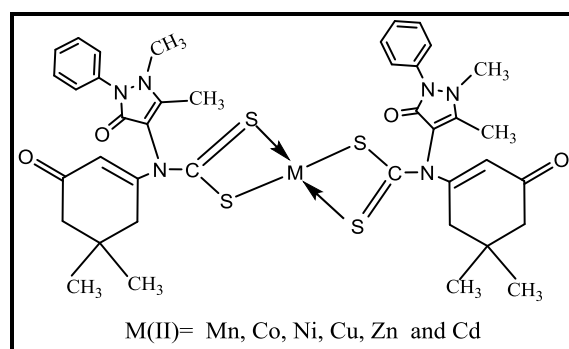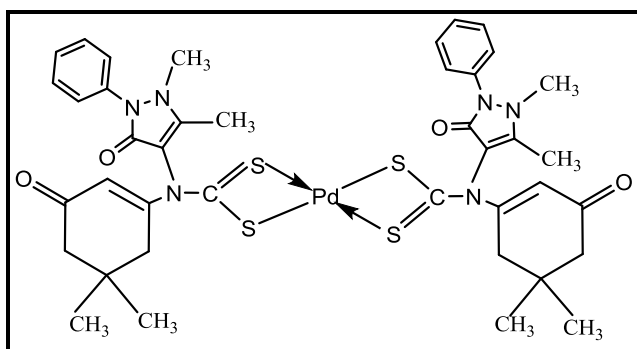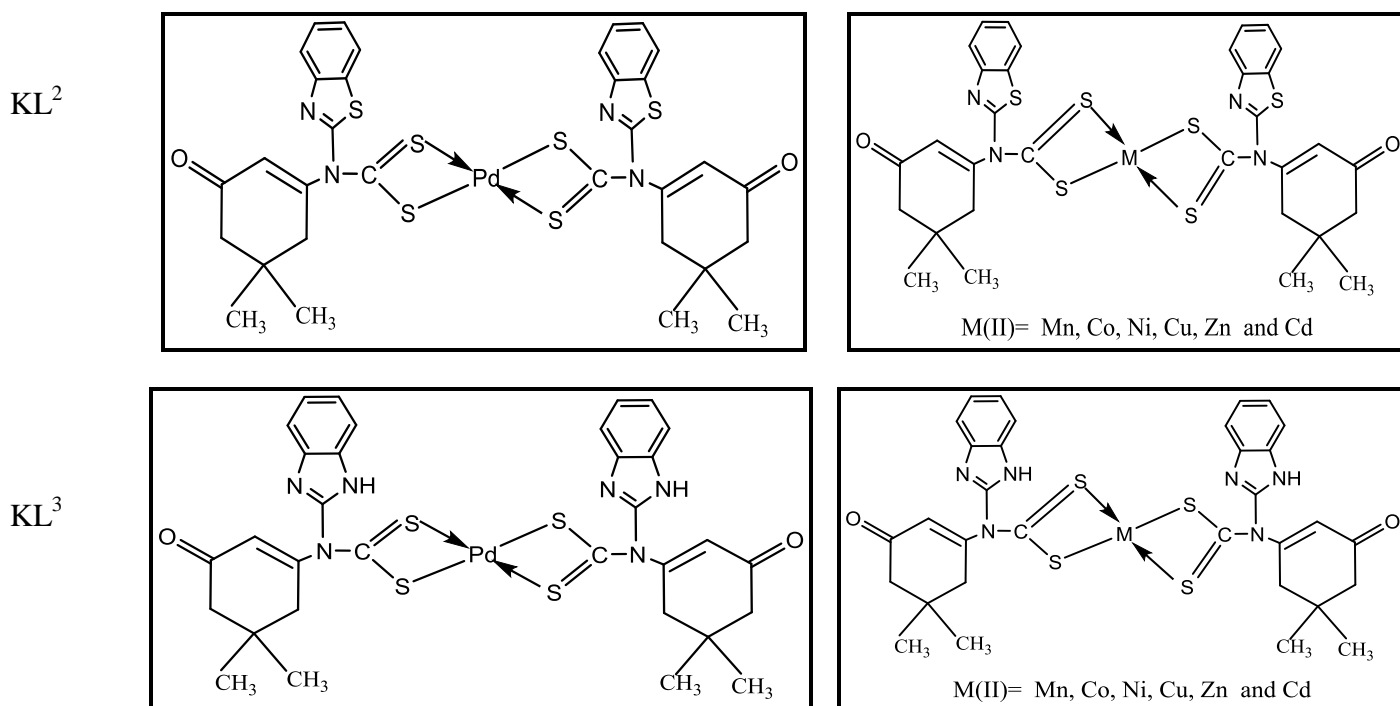
(2.7)Synthesis of KL^1 complexes

(2.7.1) Synthesis of [Cu(L^1)$_2$]

A solution of (0.034g,0.2mmol) CuCl$_2$.2H$_2$O in (3ml) ethanol was added to solution of (0.177g,0.4mmol)(KL^1) in (10ml) ethanol. The mixture was reflexed for 3 hrs, the green yellow solid was collected by filtration, washed with (1:1) mixture of water: ethanol, crystallized from ethanol. Then with diethylether and dried at room temperature to give a green yellow precipitate. Weight (0.0735), yield (79%) ,m.p (300)°C, Scheme(3.4).

(2.7.1.1) Synthesis of [Mn(L^1)$_2$], [Co(L^1)$_2$], [Ni(L^1)$_2$], [Zn(L^1)$_2$], [Cd(L^1)$_2$] and ,[pd(L^1)$_2$] complexes

A similar method to that for [Cu(L^1)$_n$] complex was used to prepare other KL^1 complexes with [Mn^{+2} ,Co^{+2}, Ni^{+2}, Zn^{+2}, Cd^{+2} and pd^{+2}] ions. Table (2.7) shows some physical properties of the prepared complexes.

(2.7.1. 2) Synthesis of KL^2 and KL^3 complexes

A similar method to that mentioned in preparation of $[Cu(L^1)_n]$ complex was used to prepare other KL^2 and KL^3 complexes with $[Mn^{+2}, Co^{+2}, Ni^{+2}, Zn^{+2}, Cd^{+2}$ and $pd^{+2}]$. Tables((2.8) – (2.9)) represent selected physical properties and weight of metal salts and the yield of the prepared complexes.

Table(2.7):Colours, yields, melting points and metal salts quantities of KL^1-complexes.

Metal ion	Weight of ligand(g)	Weight of metal salt(g)	Weight of complex(g)	Yield (%)	Colour	m.p. ºC
Mn^{II}	0.104	0.02	0.0556	76.68	Green	300[*]
Co^{II}	0.104	0.02	0.0679	81.16	Brown	298[*]
Ni^{II}	0.175	0.03	0.0710	66.98	Olive green	350[*]
Cu^{II}	0.177	0.03	0.0735	79.00	Green yellow	300[*]
Zn^{II}	0.1592	0.025	0.0653	76.28	Light yellow	270[*]
pd^{II}	0.104	0.02	0.0534	75.87	Brown	300[*]
Cd^{II}	0.104	0.02	0.358	63.89	Light yellow	255[*]

*= Decomposition

Table (2.8):Colours , yields, melting points and metal salts quantities of KL^2-complexes.

Metal ion	Weight of ligand(g)	Weight of metal salt(g)	Weight of complex(g)	Yield (%)	Colour	m.p. ºC
Mn^{II}	0.1	0.016	0.0503	78.55	Light brown	138
Co^{II}	0.1	0.017	0.0513	77.48	green	130
Ni^{II}	0.1	0.017	0.0527	79.96	Green	285[*]
Cu^{II}	0.1	0.02	0.0421	87.16	Light green	170
Zn^{II}	0.1	0.017	0.0504	78.82	Light yellow	300[*]
pd^{II}	0.1	0.02	0.0468	81.87	Light brown	250[*]
Cd^{II}	0.1	0.02	0.0479	83.30	Light yellow	180

*= Decomposition

Table (2.9): Colours, yields, melting points and metal salts quantities of KL³-complexes.

Metal ion	Weight of ligand(g)	Weight of metal salt(g)	Weight of complex(g)	Yield (%)	Colour	m.p. ºC
Mn^{II}	0.1	0.017	0.0371	71.07	Light brown	220*
Co^{II}	0.1	0.018	0.0385	71.16	Green	150-152
Ni^{II}	0.1	0.018	0.0401	73.98	Green	250*
Cu^{II}	0.1	0.023	0.0392	73.54	Green yellow	158-160
Zn^{II}	0.1	0.018	0.0394	75.19	Light yellow	265*
pd^{II}	0.1	0.024	0.0480	81.08	Brown	259*
Cd^{II}	0.1	0.025	0.0478	79.00	Light yellow	180-182

*= Decomposition

(2.8) Synthesis of the mixed-ligand(KL¹) and 3-aminophenol(P) complexes with some metal ions [M(L¹)(P)] [105]

(2.8.1) Synthesis of [Co(L¹)(P)] complex

The metal solution of $CoCl_2.6H_2O$ (0.06 g, 0.46 mmole) in (10) ml ethanol was stirred for (10) minutes. The ligand solution KL¹ (0.2 g, 0.45 m mole) in (10) ml ethanol after adjusted to pH= 9 using few drops of KOH solution was added to the solution. Finally a solution of 3-amino phenol (0.05 g, 0.46 mmole) in (10) ml ethanol (with few drops of KOH solution) was also added to the above metal solution. The resulting mixture was heated under reflux for (2) hrs. Then the mixture was filtered and the precipitate was washed with an excess of ethanol and dried at room temperature during (24) hrs. A dark green solid was obtained. Weight (0.1850g), yield (71.38%), m.p (> 300°C) dec., Scheme(3.5).

(2.8.2) Synthesis of [Ni(L^1)(P)], [Zn(L^1)(P)] complexes

The method used to prepare the complexes of (Ni^{II}) and (Zn^{II}) ions was a similar method to that mentioned in preparation of [Co] complex in paragraph(2.8.1).

(2.8.3) Synthesis of the mixed-ligand[KL^2], [KL^3] and 3-aminophenol complexes with some metal ions [M(L^2)(P)] , [M(L^3)(P)]

The method used to prepare the complexes of (Co^{II}) ,(Ni^{II}) and (Zn^{II}) ions was a similar method to that mentioned in paragraph (2.8.1).Table(2.10) shows the physical properties of the complexes and their reactant quantity.

Table(2.10): Some physical properties of the prepared mixed-ligand complexes [M(L^n)(P)] and their reactant quantity.

Empirical formula	Color	m.p. °C	Wt of metal chloride salt (g)	Wt of product (g)	Yield %
[Co(L^1)(P)]	Green	> 300*	0.06	0.1850	71.38
[Ni(L^1)(P)]	Pale green	> 240*	0.06	0.1720	66.39
[Zn(L^1)(P)]	Off white	> 300*	0.06	0.1901	72.48
[Co(L^2)(P)]	Dark green	285*	0.06	0.1790	67.04
[Ni(L^2)(P)]	Pale green	250*	0.06	0.1681	62. 92
[Zn(L^2)(P)]	Off white	215	0.06	0.1882	69.62
[Co(L^3)(P)]	Dark green	> 300*	0.06	0.1810	66.94
[Ni(L^3)(P)]	Pale green	> 300*	0.06	0.1754	64.75
[Zn(L^3)(P)]	Off white	> 300*	0.06	0.1653	60.24

*= Decomposition   n=1,2,3

(2.9) Synthesis of the mixed-ligand (KL^1) and 8-hydroxyquinoline (Q) complexes with some metal ions [M(L^1)(Q)]

(2.9.1) Synthesis of [Co(L^1)(Q)] complex

The metal solution of CoCl$_2$.6H$_2$O (0.06g, 0.46 mmole) in (10) ml ethanol was stirred for (10) minutes. The ligand solution KL^1 (0.2 g, 0.45 m mole in (10) ml

ethanol after adjusted to pH=9 using few drops of KOH solution was added to the solution. Finally a solution of 8-hydroxyquinoline (0.066g, 0.45 mmole) in (10) ml ethanol(with few drops of KOH solution) was also added to the above metal solution. The resulting mixture was heated under reflux for (2) hrs. Then the mixture was filtered and the precipitate was washed with an excess of ethanol and dried at room temperature during (24) hrs. A solid was obtained. Weight (0.1920g), yield (65.45%), m.p (> 300°C) dec.

(2.9.2) Synthesis of [Ni(L^1)(Q)], [Zn(L^1)(Q)] complexes

The method used to prepare the complexes of (Ni^{II}), (Zn^{II}) ions was a similar method to that mentioned in preparation of [Co] complex in paragraph (2.9.1). Scheme(3.6) .

(2.9.3) Synthesis of the mixed-ligand [KL^2] , [KL^3]and 8-hydroxy quinolone(Q)complexes with some metal ions [M(L^2)(Q)],[M(L^3)(Q)]

The method used to prepare the complexes of (Co^{II}),(Ni^{II}) and (Zn^{II}) ions was a similar method to that mentioned in paragraph (2.9.1). Table (2.11) shows the physical properties of the complexes and their reactant quantity.

Table(2.11): Some physical properties of the prepared mixed-ligand complexes [M(L^n)(Q)] and their reactant quantity.

Empirical formula	Color	m.p. ºC	Wt of metal chloride salt (g)	Wt of product (g)	Yield %
[Co(L^1)(Q)]	Dark green	> 300[*]	0.06	0.1920	69.81
[Ni(L^1)(Q)]	Light green	> 300[*]	0.06	0.1804	65.45
[Zn(L^1)(Q)]	Off white	> 285[*]	0.06	0.1891	68.02
[Co(L^2)(Q)]	Dark green	>250[*]	0.06	0.1752	61.28
[Ni(L^2)(Q)]	Light green	195-197	0.06	0.1815	63. 50
[Zn(L^2)(Q)]	Off white	> 235[*]	0.06	0.1663	57.48

[Co(L^3)(Q)]	Dark green	> 300*	0.06	0.1785	61.57
[Ni(L^3)(Q)]	Green	> 300*	0.06	0.1686	58.18
[Zn(L^3)(Q)]	Off white	> 300*	0.06	0.1711	58.53

*= Decomposition   n=1,2,3

Chapter Three
Results
&
Discussion

(3.1) Results and discussion

(3.1.1)Synthesis and characterisation of the precursors

In this study three of dithiocarbamate ligands have been reported. The synthesis of the ligands was based on using of amines, which were synthesised in two steps, included preparation of precursors from the reaction of demedone with 4-aminophenazone or 2-aminobenzothiozole or 2-aminobenzimidazole using benzene as a solvent according to the general bath shown in Scheme (3.1). The proposed mechanism of this reaction is shown in Scheme (3.2)[103,105].
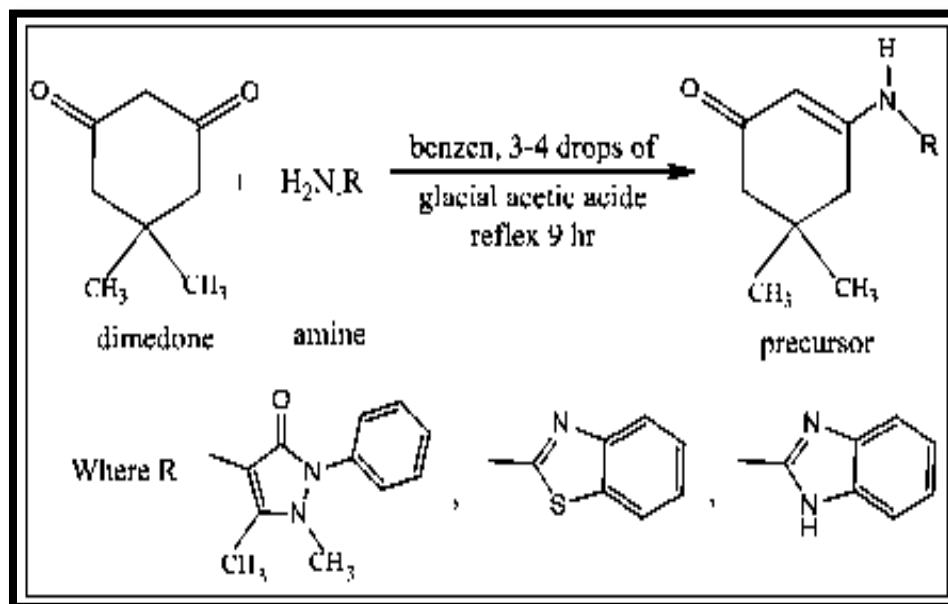
Scheme (3.1): Synthesis bath of the precursors.
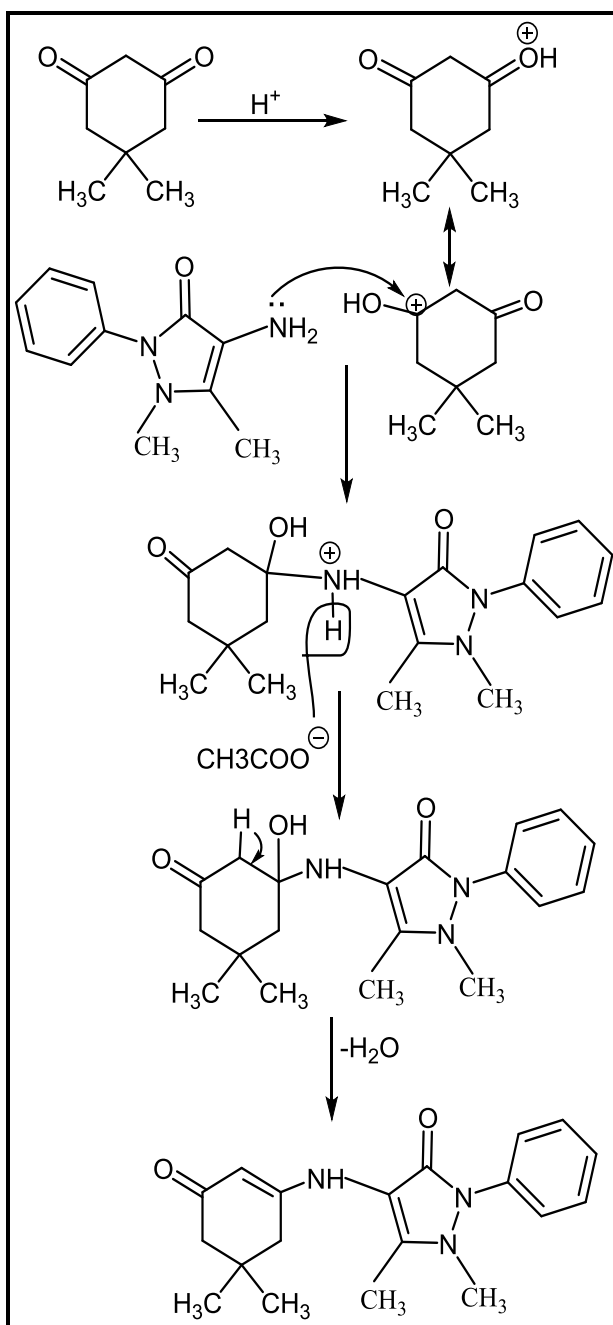
Scheme(3.2):A proposed mechanism of the synthesis of precursor [HDa].

(3.1.2) Synthesis and characterisation of the ligands.

The three dithiocarbamate ligands; KL^1 , KL^2 and KL^3 ,Scheme (3.3) are synthesised by mixing the precursor and carbondisulfide in the presence of (KOH) in ethanol as a solvent. The formation of ligands was to allow us to conduct full characterisation for the ligands. The ligands were characterised by elemental

analysis Table(3.1),Thermal analysis, FTIR, UV-Vis, mass spectra and ^{1}H,^{13}C-NMR spectroscopy. The solubility of the ligands in different solvents is summarised in Table(3.2).
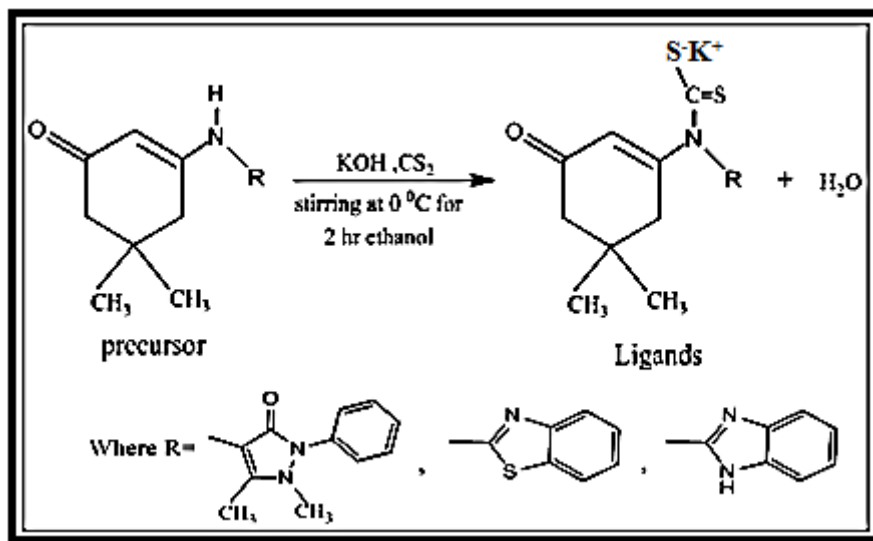
Scheme (3.3): Synthesis bath for ligands KL^{1} , KL^{2} and KL^{3}.

Table (3.1): Elemental analysis data and some physical properties for ligands.

Compound	Empirical Formula	M.W	Yield(%)	Colour	Microanalysis found, (calc)%			
					C	H	N	S
KL^{1}	C$_{20}$H$_{22}$KN$_{3}$O$_{2}$S$_{2}$	439.63	81.5	Yellow	54.01 (54.64)	5.10 (5.04)	9.99 (9.56)	14.38 (14.58)
KL^{2}	C$_{16}$H$_{15}$ KN$_{2}$OS$_{3}$	386.59	79.3	Light orange	49.48 (49.71)	4.02 (3.91)	7.92 (7.25)	24.49 (24.88)
KL^{3}	C$_{16}$H$_{16}$KN$_{3}$OS$_{3}$	369.54	71.18	Yellow	51.90 (52.00)	4.32 (4.36)	11.51 (11.37)	17.38 (17.35)

(calc) = Calculated

Table (3.2): Solubility of ligands in different solvents.

Compound	H$_{2}$O	MeOH	EtOH	DMF	DMSO	CCl$_{4}$
KL^{1}	+	÷	÷	+	+	-
KL^{2}	+	÷	÷	+	+	-
KL^{3}	+	÷	÷	+	+	-

(÷) sparingly, (+) soluble, (-) insoluble

(3.1.3) Synthesis and characterisation of the complexes.

The complexes were synthesised by; (i) the reaction of ligands with metal ion; Mn^{II}, Co^{II}, Ni^{II}, Cu^{II}, Zn^{II} , Pd^{II} and Cd^{II} ,by using the ethanol as a solvent, scheme(3-4). Complexes were isolated in moderate yield. The complexes were characterised by FTIR, UV-Vis, magnetic susceptibility, molar conductance and elemental analysis. The elemental analysis data and some physical properties for complexes are shown in Tables ((3.3)-(3.5)).The complexes were soluble in DMSO, the solubility of the complexes in different solvents is shown in Tables ((3.6)-(3.8)).
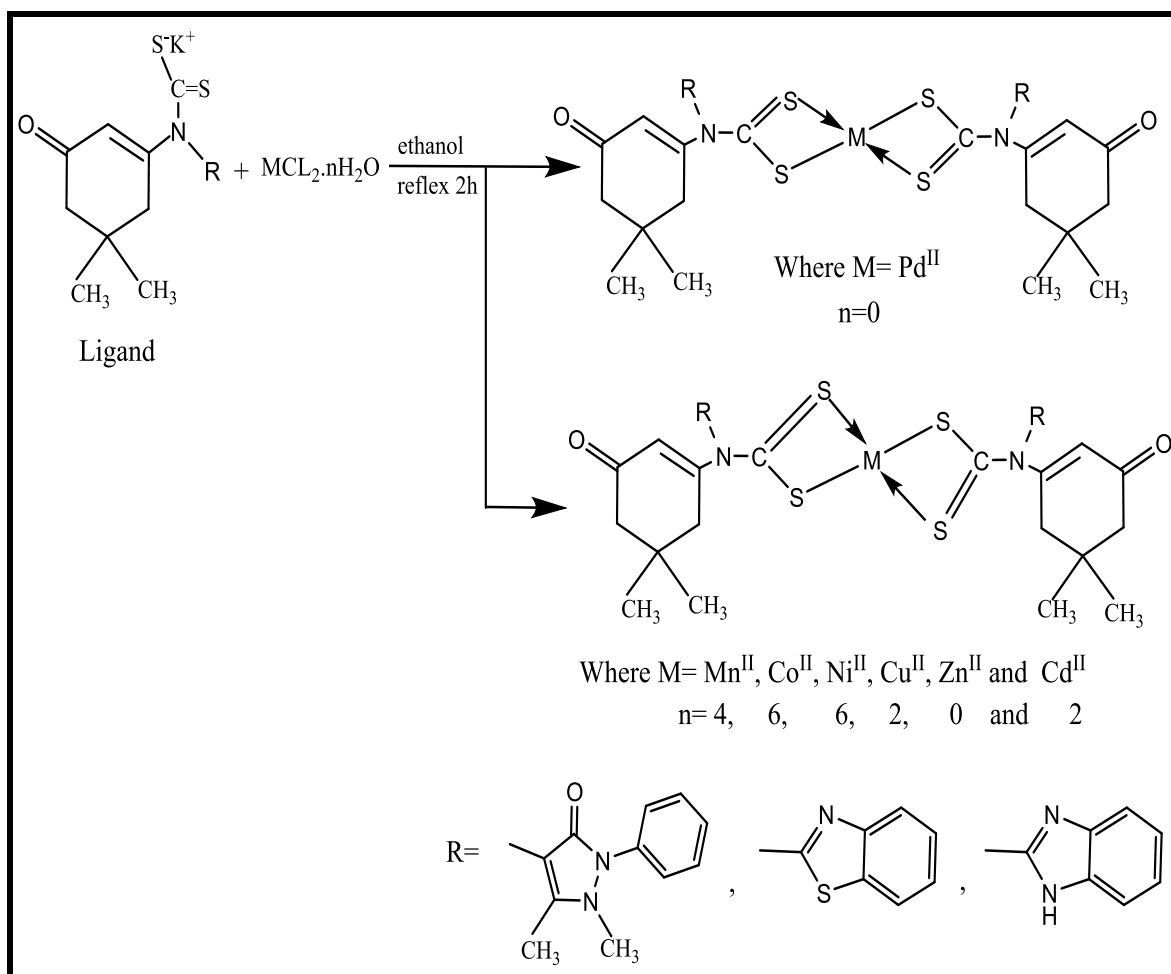
Scheme (3.4): Synthesis bath of complexes.

Table (3.3): Elemental analysis data and some physical properties for (KL^1) and its complexes.

Compound	Empirical formula	M.W g / mol	Yield %	M.P° C	colour	Microanalysis found, (calc.) %					
						Metal%	C	H	N	S	Cl
[Mn(L^1)$_2$]	C$_{40}$H$_{44}$N$_6$O$_4$S$_4$Mn	858.19	76.68	300*	green	6.21 (6.40)	55.77 (55.93)	5.01 (5.12)	10.06 (9.78)	14.72 (14.91)	Nil
[Co(L^1)$_2$]	C$_{40}$H$_{44}$N$_6$O$_4$S$_4$Co	862.19	81.16	298*	brown	6.66 (6.83)	55.51 (55.67)	5.00 (5.10)	9.95 (9.74)	14.73 (14.84)	Nil
[Ni(L^1)$_2$]	C$_{40}$H$_{44}$N$_6$O$_4$S$_4$ Ni	861.95	66.98	350*	Olive Green	6.11 (6.81)	55,48 (55.68)	4.98 (5.10)	9.95 (9.74)	14.61 (14.85)	Nil
[Cu(L^1)$_2$]	C$_{40}$H$_{44}$N$_6$O$_4$S$_4$Cu	866.80	79.00	300*	Green yellow	7.01 (7.33)	55.21 (55.37)	4.72 (5.07)	10.00 (9.69)	14.22 (14.76)	Nil
[Zn(L^1)$_2$]	C$_{40}$H$_{44}$N$_6$O$_4$S$_4$Zn	868.65	76.28	270*	Light yellow	7.31 (7.52)	55.10 (55.25)	4.88 (5.06)	9.89 (9.67)	14.15 (14.73)	Nil
[Pd(L^1)$_2$]	C$_{40}$H$_{44}$N$_6$O$_4$S$_4$Pd	909.68	75.87	300*	brown	11.35 (11.69)	52.55 (52.76)	4.66 (4.83)	9.56 (9.23)	13.90 (14.07)	Nil
[Cd(L^1)$_2$]	C$_{40}$H$_{44}$N$_6$O$_4$S$_4$Cd	915.67	63.89	255*	Light yellow	12.01 (12.69)	52.30 (52.42)	4.20 (4.80)	9.49 (9.17)	13.14 (13.97)	Nil

Table (3.4): Elemental analysis data and some physical properties for (KL^2) and its complexes.

Compound	Empirical formula	M.W g / mol	Yield %	M. P °C	colour	Microanalysis found, (calc.) %					
						Metal%	C	H	N	S	Cl
[Mn(L^2)$_2$]	C$_{32}$H$_{30}$N$_4$O$_2$S$_6$Mn	752.11	78.55	138	Light brown	7.11 (7.30)	50.91 (51.05)	3.72 (3.98)	7.89 (7.44)	24.91 (25.52)	Nil
[Co(L^2)$_2$]	C$_{32}$H$_{30}$N$_4$O$_2$S$_6$Co	756.11	77.48	130	Blue green	7.25 (7.79)	50.55 (50.78)	3.61 (3.96)	7.91 (7.40)	25.00 (25.39)	Nil
[Ni(L^2)$_2$]	C$_{32}$H$_{30}$N$_4$O$_2$S$_6$Ni	755.87	79.96	285*	green	7.29 (7.76)	50.39 (50.80)	3.63 (3.96)	7.89 (7.40)	25.13 (25.40)	Nil
[Cu(L^2)$_2$]	C$_{32}$H$_{30}$N$_4$O$_2$S$_6$Cu	760.72	87.16	170	Light green	7.98 (8.35)	50.19 (50.47)	3.55 (3.94)	7.76 (7.36)	24.89 (25.23)	Nil
[Zn(L^2)$_2$]	C$_{32}$H$_{30}$N$_4$O$_2$S$_6$Zn	762.57	78.82	300*	Light yellow	8.21 (8.57)	50.00 (50.35)	3.50 (3.93)	7.77 (7.34)	24.93 (25.17)	Nil
[Pd(L^2)$_2$]	C$_{32}$H$_{30}$N$_4$O$_2$S$_6$Pd	803.60	81.87	250*	Light brown	13.01 (13.24)	47.50 (47.78)	3.25 (3.73)	7.20 (6.96)	24.25 (24.63)	Nil
[Cd(L^2)$_2$]	C$_{32}$H$_{30}$N$_4$O$_2$S$_6$Cd	809.59	83.30	180	Light yellow	13.15 (13.88)	47.11 (47.43)	3.37 (3.70)	7.31 (6.91)	23.15 (23.71)	Nil

Table (3.5): Elemental analysis data and some physical properties for (KL³)

and its complexes.

Compound	Empirical formula	M.W g / mol	Yield %	M.P °C	colour	Microanalysis found, (calc.) %					
						Metal%	C	H	N	S	Cl
[Mn(L³)₂]	C₃₂H₃₂N₆O₂S₄Mn	718.01	71.07	220*	Light brown	7.44 (7.65)	53.20 (53.48)	4.13 (4.45)	11.91 (11.69)	17.55 (17.82)	Nil
[Co(L³)₂]	C₃₂H₃₂N₆O₂S₄Co	722.01	71.16	150-152	green	7.90 (8.16)	53.02 (53.18)	4.15 (4.43)	11.98 (11.63)	17.40 (17.72)	Nil
[Ni(L³)₂]	C₃₂H₃₂N₆O₂S₄Ni	721.77	73.98	250*	green	8.00 (8.13)	50.89 (51.07)	4.11 (4.43)	11.90 (11.63)	17.38 (17.73)	Nil
[Cu(L³)₂]	C₃₂H₃₂N₆O₂S₄Cu	726.62	73.54	158-160	Green yellow	8.33 (8.74)	52.20 (52.84)	4.25 (4.40)	11.81 (11.56)	17.26 (17.61)	Nil
[Zn(L³)₂]	C₃₂H₃₂N₆O₂S₄Zn	728.47	75.19	265*	Light yellow	8.60 (8.97)	52.50 (52.71)	4.22 (4.39)	11.88 (11.53)	17.11 (17.57)	Nil
[Pd(L³)₂]	C₃₂H₃₂N₆O₂S₄Pd	769.50	81.08	259*	brown	13.59 (13.83)	49.77 (49.90)	3.69 (4.15)	11.20 (10.91)	16.48 (16.63)	Nil
[Cd(L³)₂]	C₃₂H₃₂N₆O₂S₄Cd	775.49	79.00	180-182	Light yellow	14.11 (14.49)	49.17 (49.51)	3.89 (4.12)	11.07 (10.83)	16.31 (16.50)	Nil

(calc.) = Calculated   * = Decomposition

Table (3.6): The solubility of KL¹ complexes in different solvents.

Compound	H₂O	MeOH	EtOH	CH₂Cl₂	CHCl₃	DMF	DMSO
[Mn(L¹)₂]	-	-	-	-	-	+	+
[Co(L¹)₂]	-	-	-	-	-	+	+
[Ni(L¹)₂]	-	÷	÷	÷	÷	+	+
[Cu(L¹)₂]	-	-	-	-	-	+	+
[Zn(L¹)₂]	-	÷	÷	-	-	+	+
[Pd(L¹)₂]	-	-	-	-	-	+	+
[Cd(L¹)₂]	-	-	-	-	-	+	+

Table (3.7): The solubility of KL² complexes in different solvents.

Compound	H₂O	MeOH	EtOH	CH₂Cl₂	CHCl₃	DMF	DMSO
[Mn(L²)₂]	-	÷	÷	-	-	+	+
[Co(L²)₂]	-	-	-	-	-	+	+
[Ni(L²)₂]	-	-	-	-	-	+	+
[Cu(L²)₂]	-	-	-	÷	-	+	+
[Zn(L²)₂]	-	-	-	÷	-	+	+
[Pd(L²)₂]	-	-	-	÷	-	+	+
[Cd(L²)₂]	-	-	-	÷	-	+	+

Table (3.8): The solubility of KL^3 complexes in different solvents.

Compound	H$_2$O	MeOH	EtOH	CH$_2$Cl$_2$	CHCl$_3$	DMF	DMSO
[Mn(L^3)$_2$]	-	÷	-	+	÷	+	+
[Co(L^3)$_2$]	-	÷	÷	÷	÷	+	+
[Ni(L^3)$_2$]	-	÷	-	-	÷	+	+
[Cu(L^3)$_2$]	-	-	-	-	-	+	+
[Zn(L^3)$_2$]	-	÷	÷	÷	÷	+	+
[Pd(L^3)$_2$]	-	-	-	÷	-	+	+
[Cd(L^3)$_2$]	-	-	-	÷	÷	+	+

(÷) sparingly, (+) soluble, (-)insoluble

(3.1.4) Characterization of the mixeded-ligand complexes.

(3.1.4.1) Characterization of the mixed-ligand [KL^1] and 3-amino phenol complexes with some selective metal ions [(M(L^1)(P)].

All complexes were prepared by a similar method shown in Scheme (3.5). The complexes were prepared from the reaction of the ligand and 3-amino phenol with metal chloride salt in (1:1:1) mole ratio at reflux in ethanol, as a solvent, potassium hydroxide was used as a base and pure complexes were formed. All the complexes of KL^2 , KL^3 ligands were prepared by a similar methods. Table (3.9) shows the solubility of the complexes in different solvents. The metals analysis of the complexes is in good agreement with the calculated values, Table(3.10). Spectroscopic methods (FT-IR, UV-Vis) along with chloride contents, melting point, molar conductance and magnetic susceptibility measurements, were used to characterize the complexes.
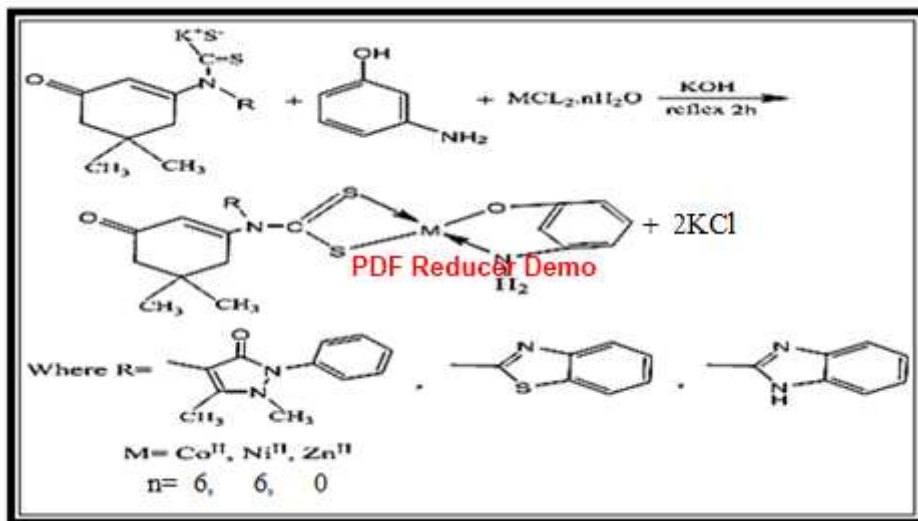
Scheme (3.5): Synthesis bath of mixed-ligand complexes [M(L^n)(P)], n=1,2,3.

Table(3.9): Solubility of the complexes [M(L^n)(P)] in different solvents.

Compound	H$_2$O	MeOH	EtOH	CH$_2$Cl$_2$	CHCl$_3$	DMF	DMSO
[Co(L^1)(P)]	_	+	÷	+	÷	+	+
[Ni(L^1)(P)]	_	_	_	÷	÷	÷	+
[Zn(L^1)(P)]	_	+	÷	÷	+	+	+
[Co(L^2)(P)]	_	÷	_	+	÷	+	+
[Ni(L^2)(P)]	_	+	+	÷	+	+	+
[Zn(L^2)(P)]	_	÷	_	÷	÷	÷	+
[Co(L^3)(P)]	_	+	÷	+	÷	+	+
[Ni(L^3)(P)]	-	_	_	÷	÷	÷	+
[Zn(L^3)(P)]	-	÷	_	_	+	÷	+

(÷) sparingly, (+) soluble, (-)insoluble

Table(3.10): Analytical data of complexes [M(L^n)(P)], where n=1,2,3.

Compound	Microanalysis found, (calc)%					
	Metal	C	H	N	S	Cl
[Co(L^1)(P)]	9.18 (10.36)	54.22 (54.56)	4.70 (4.92)	9.97 (9.84)	11.01 (11.25)	Nil
[Ni(L^1)(P)]	9.11 (10.32)	54.39 (54.88)	4.71 (4.93)	10.01 (9.85)	11.07 (11.26)	Nil
[Zn(L^1)(P)]	10.51 (11.36)	53.98 (54.24)	4.59 (4.88)	9.99 (9.73)	10.90 (11.12)	Nil
[Co(L^2)(P)]	9.21 (10.25)	50.94 (51.19)	3.88 (4.07)	8.77 (8.14)	18.20 (18.61)	Nil
[Ni(L^2)(P)]	9.09 (10.22)	51.00 (51.22)	3.90 (4.07)	8.83 (8.15)	18.25 (18.63)	Nil
[Zn(L^2)(P)]	10.50 (11.30)	50.20 (50.56)	3.78 (4.02)	8.34 (8.04)	18.00 (18.38)	Nil

78

$[Co(L^3)(P)]$	10.78 (11.81)	52.70 (52.94)	4.19 (4.41)	11.75 (11.23)	12.29 (12.83)	Nil
$[Ni(L^3)(P)]$	10.40 (11.77)	52.76 (52.97)	4.21 (4.41)	11.80 (11.24)	12.33 (12.84)	Nil
$[Zn(L^3)(P)]$	11.35 (12.94)	52.01 (52.27)	4.12 (4.35)	11.55 (11.08)	12.35 (12.67)	Nil

* = Decomposition

(3.1.4.2) Characterization of the mixed-ligand [KL^1] and 8-hydroxy quinoline complexes with some selective metal ions [M(L^1)(Q)].

All complexes were prepared by a similar method shown in Scheme (3.6) . The complexes were prepared from the reaction of the ligand KL^1 and 8-hydroxyquinoline with metal chloride salt in (1:1:1) mole ratio at reflux in ethanol, as a solvent, potassium hydroxide was used as a base and pure complexes were formed. All the complexes of KL^2 and KL^3 ligands were prepared by a similar methods. Table (3.11) shows the solubility of the complexes in different solvents. The metals analysis of the complexes is in good agreement with the calculated values, Table (3.12). Spectroscopic methods (FT-IR, UV-Vis) along with chloride contents, melting point, molar conductance and magnetic susceptibility measurements, were used to characterize the complexes.
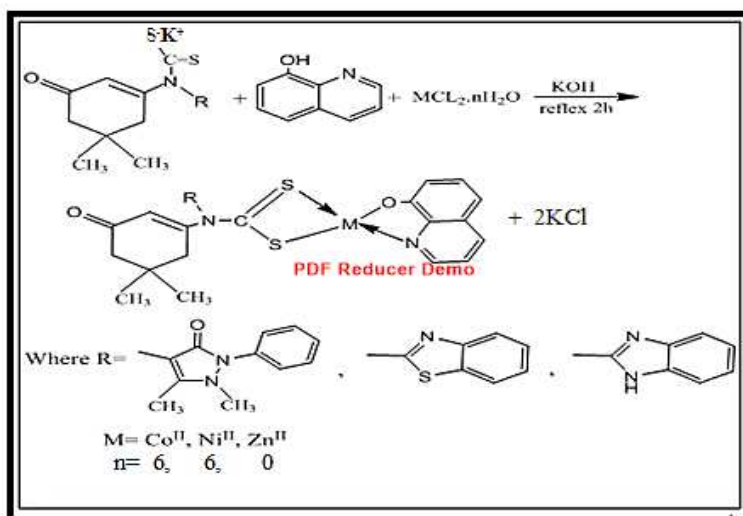
Scheme (3.6): Synthesis bath of mixed ligand complexes [M(L^n)(Q)], n=1,2,3.

79

Table(3.11): Solubility of the complexes[M(L^n)(Q)] in different solvents.

Compound	H$_2$O	MeOH	EtOH	CH$_2$Cl$_2$	CHCl$_3$	DMF	DMSO
[Co(L^1)(Q)]	_	+	÷	÷	÷	+	+
[Ni(L^1)(Q)]	_	+	÷	_	÷	+	+
[Zn(L^1)(Q)]	_	÷	+	÷	÷	+	+
[Co(L^2)(Q)]	_	÷	÷	_	÷	+	+
[Ni(L^2)(Q)]	_	÷	+	÷	÷	+	+
[Zn(L^2)(Q)]	_	÷	+	÷	÷	+	+
[Co(L^3)(Q)]	_	+	+	÷	÷	+	+
[Ni(L^3)(Q)]	_	÷	÷		+	+	+
[Zn(L^3)(Q)]		÷	÷	÷	+	+	+

(÷) sparingly, (+) soluble, (-)insoluble

Table(3.12): Analytical data of complexes [M(L^n)(Q)] where n=1,2,3.

Compound	Microanalysis found, (calc)%					
	Metal	C	H	N	S	Cl
[Co(L^1)(Q)]	8.69 (9.74)	57.31 (57.54)	4.44 (4.63)	9.59 (9.26)	10.41 (10.74)	Nil
[Ni(L^1)(Q)]	8.60 (9.71)	57.40 (57.57)	4.47 (4.63)	9.70 (9.26)	10.19 (10.58)	Nil
[Zn(L^1)(Q)]	9.19 (10.69)	56.11 (56.69)	4.33 (4.58)	9.81 (9.16)	10.11 (10.47)	Nil
[Co(L^2)(Q)]	9.75 (10.68)	54.05 (54.37)	3.69 (3.80)	8.17 (7.61)	17.12 (17.40)	Nil
[Ni(L^2)(Q)]	9.00 (10.06)	54.13 (54.40)	3.75 (3.81)	8.25 (7.62)	17.19 (17.41)	Nil
[Zn(L^2)(Q)]	10.36 (11.71)	52.44 (53.74)	3.51 (3.76)	8.20 (7.52)	16.91 (17.19)	Nil
[Co(L^3)(Q)]	10.20 (11.02)	59.91 (56.11)	3.90 (4.11)	10.99 (10.47)	11.60 (11.97)	Nil
[Ni(L^3)(Q)]	10.01 (10.98)	56.00 (56.13)	3.90 (4.12)	11.11 (10.48)	11.73 (11.98)	Nil
[Zn(L^3)(Q)]	11.87 (12.12)	55.23 (55.64)	3.82 (4.08)	10.97 (10.38)	11.49 (11.87)	Nil

* = Decomposition

(3.2) Nuclear Magnetic Resonance(NMR) spectral

(3.2.1) ^{1}H-NMR spectrum for the precursor [HDa]

The ^{1}H-NMR spectrum of [HDa] is shown in Fig.(3.1), the spectrum showed the singlet signal at (δ=8.02 ppm) is assigned to (NH) proton of enamine group[106], where this signal suffered a disappearance compared to the spectrum of the ligand KL^1. The multiple chemical shifts at range (δ=7.52-7.32 ppm)are assigned to protons of aromatic rings [107]. The signal at chemical shift (δ=5.21

ppm) is assigned to the proton of the $(C_5\text{-H})$ for the aliphatic ring[108]. The chemical shift at (δ=2.13, 3.09 ppm) refers to the $(C_{10}\text{-H}, C_{11}\text{-H})$ proton of methyl groups respectively [109]. The chemical shift at (δ=2.5) is assigned to DMSO solvent. The chemical shift at (δ=2.34) is assigned to the $(C_3\text{-H}$ and $C_7\text{-H})$ protons of the CH_2 groups[110]. The singlet chemical shift at (δ=1.01-0.99 ppm) is assigned to the $(C_1\text{-H})$ protons of methyl groups[111]. The results are summarized in Table (3.13).

Table(3.13): ^{1}H-NMR data for Precursor [HDa] measured in DMSO-d^6 and chemical shift in ppm (δ)

Compound	Functional groups	δ (ppm)
[HDa]	N-H [enamine group]	(8.02) (1H, s)
	Ar-H (C_{12},C_{13},C_{14})	(7.52-7.32) (4H, m)
	C_5 for C_2H group	(5.21) (1H, s)
	C_{10} for CH_3 group	(2.13) (3H, s)
	C_{11} for CH_3 group	(3.09) (3H, s)
	C_3,C_7 for CH_2 groups	(2.34) (4H, s)
	C_1 for CH_3 groups	(1.01-0.99) (6H, s)

s=single ,m=multiple
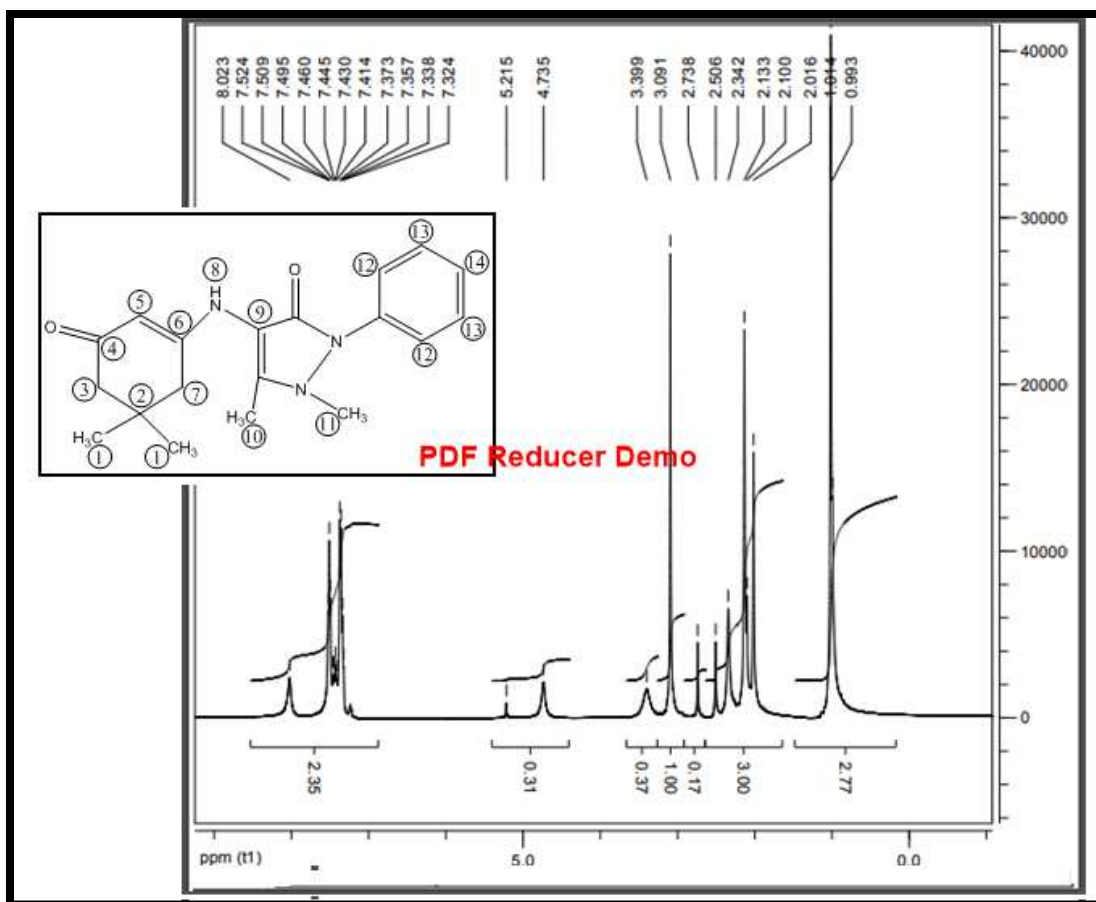
Figure (3.1): ^{1}H-NMR spectrum for the precursor [HDa] in DMSO-d^6

(3.2.2) ^{1}H-NMR spectral for the ligands KL^1, KL^2 and KL^3

(3.2.2.1) ^{1}H-NMR spectrum for the ligand KL^1

The ^{1}H-NMR spectrum for the ligand KL^1 in Figure (3.2) shows the following characteristic chemical shift (DMSO-d^6 as a solvent): The spectrum exhibited singlet signal at (δ =0.96 ppm) is assigned to the (C$_1$) six protons of two methyl groups [112].The chemical shift at range (δ =2.09 -1.12 ppm) is assigned to the (C$_3$and C$_7$)protons of the CH$_2$ groups [113]. The signal at chemical shift (δ =4.20 ppm) is assigned to the proton of (C$_5$) [114],while the multiple chemical shifts at (δ =7.47-7.29 ppm) range are referred to the protons of the (C$_{12}$,C$_{13}$ and C$_{14}$)[115] . Finally the signals at (3.05 and 3.31 ppm) are assigned to the protons of

82

(C_{10} and C_{11}) respectively. The NMR spectral data of ligand was reported in literatures [116,117-120].The results in Table (3.14).

Table(3.14): ^{1}H-NMR data for ligand KL^1 measured in DMSO-d^6

Compound	Functional groups	δ (ppm)
KL^1	C_{12}, C_{13}, C_{14} for C-H (aromatic group)	7.47-7.29 (5H, m)
	C_5 for C_2H group	4.16-4.20 (1H, m)
	C_{10} for CH_3 group	3.05 (3H, s)
	C_{11} for CH_3 group	3.31 (3H, s)
	C_3, C_7 for CH_2 groups	1.12-2.09 (4H)
	C_1 for CH_3 groups	0.96-1.12 (6H, s)

s=single ,m=multiple

Figure (3.2): ^{1}H-NMR spectrum of ligand KL^1 in DMSO-d^6

(3.2.2.2) ^{1}H-NMR spectrum for the ligand KL^2

The ^{1}H-NMR spectrum for the ligand KL^2 in Figure (3.3) shows the following characteristic chemical shift (DMSO-d^6 as a solvent): The multiple chemical shifts at (δ =7.64-7.16 ppm) range are referred to protons of (C$_{12}$, C$_{13}$, C$_{14}$ and C$_{15}$) for aromatic rings. The signal at chemical shift (δ =4.41 ppm) is assigned to the proton of (C$_5$), while the signal at chemical shift at (δ =4.20 ppm) is assigned to the (C$_3$ and C$_7$) protons of the CH$_2$ groups. Finally the signal at chemical shift (δ =1.14-0.91 ppm) is assigned to the (C$_1$) protons of two methyl groups. The NMR spectral data of ligand was reported in literatures [112-120].The results are in Table (3.15).

Table(3.15): ^{1}H-NMR data for ligand KL^2 measured in DMSO-d^6

Compound	Functional groups	δ (ppm)
KL^2	C$_{12}$, C$_{13}$, C$_{14}$ for C-H (aromatic group)	7.64-7.16 (4H, m)
	C$_5$ for C$_2$H group	4.41 (1H, s)
	C$_3$, C$_7$ for CH$_2$ groups	4.20 (4H, m)
	C$_1$ for CH$_3$ groups	1.14-0.91 (6H, s)

s=single ,m=multiple

84
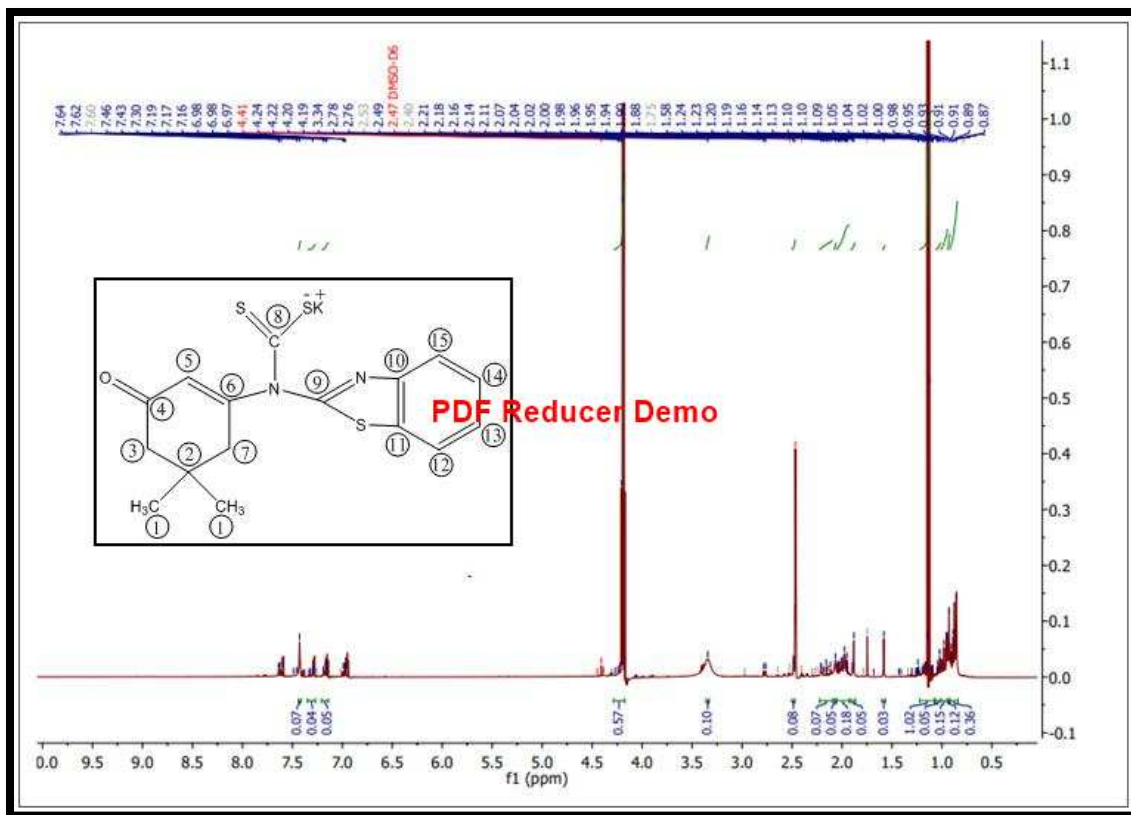
Figure (3.3): ^{1}H-NMR spectrum of ligand KL^2 in DMSO-d^6

(3.2.2.3) ^{1}H-NMR spectrum for the ligand KL^3

The ^{1}H-NMR spectrum for the ligand KL^3 in Figure (3.4) shows the following characteristic chemical shift (DMSO-d^6 as a solvent): The spectrum exhibited singlet signal at (δ =6.34 ppm) for proton of N-H group. The chemical shifts at range (δ =7.89-6.76 ppm) are referred to the protons of the (C_{12} and C_{13}) for aromatic group. The signal at chemical shift (δ =4.74 ppm) is assigned to the proton of (C_5) ,while the signal at chemical shift at (δ = 2.11, 2.78 ppm) is assigned to the (C_3 and C_7) protons of the CH$_2$ groups. Finally the signal at chemical shift (δ=1.01 ppm) which assigned to (C_1) protons of two methyl groups. The NMR spectral data of ligand was reported in literatures [112-120].The results in Table (3.16).

Table(3.16): ^{1}H-NMR data for ligand KL^3 measured in DMSO-d^6

Compound	Functional groups	δ (ppm)
KL^3	Proton N-H group	6.34 (1H,s)
	C$_{12}$, C$_{13}$ for C-H (aromatic group)	7.89-6.76 (4H, s)
	C$_5$ for C$_2$H group	4.74 (1H, s)
	C$_3$, C$_7$ for CH$_2$ groups	2.11, 2.78 (4H, m)
	C$_1$ for CH$_3$ groups	1.14 (6H, s)

s=single ,m=multiple
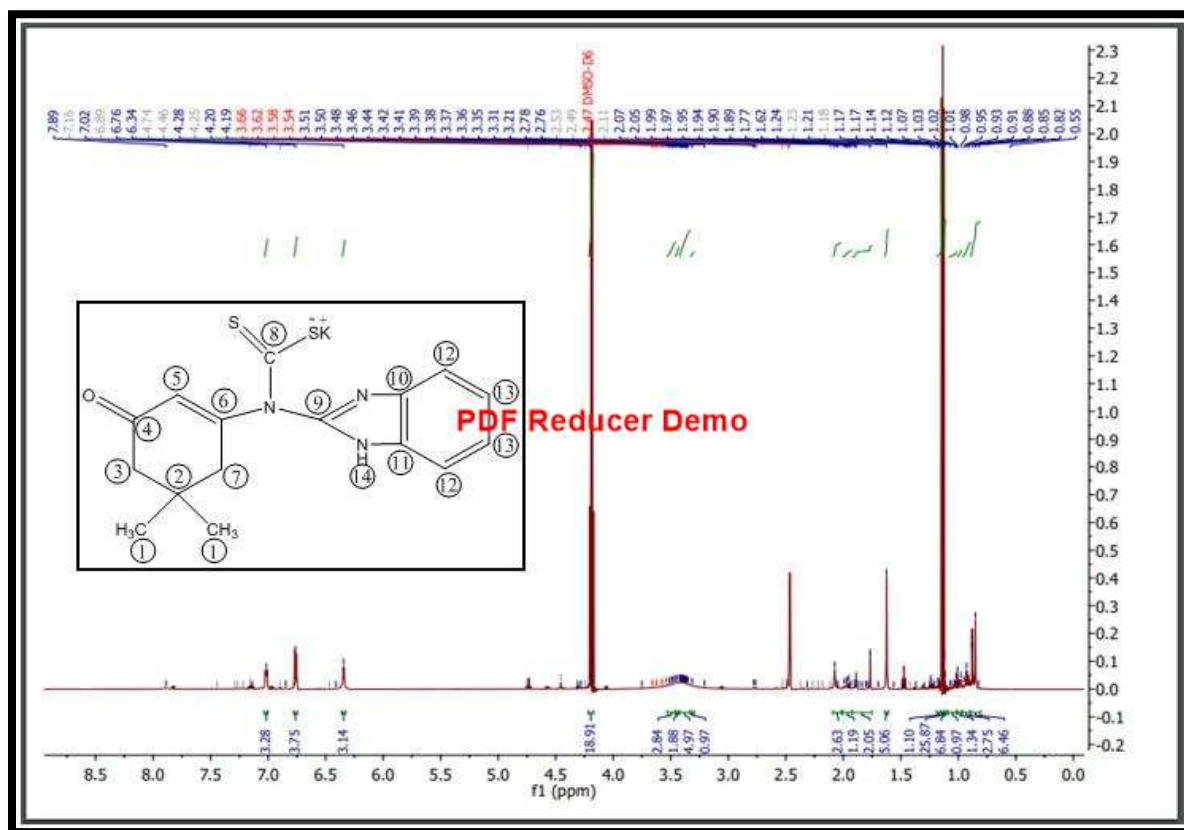
Figure (3.4): ^{1}H-NMR spectrum of ligand KL^3 in DMSO-d^6

(3.2.3) ^{13}C-NMR spectrum for the Precursor [HDa]

The ^{13}C-NMR spectrum of [HDa], Fig.(3.5) in DMSO-d^6 solvent shows the carbonyl group (C=O)$_{di.}$ for aliphatic ring observed at (δ=195.33 ppm)[121]. The carbonyl group (C=O)$_{ami.}$ for aromatic ring observed around (δ=162.3 ppm)[122].

86

The chemical shift at (δ=153.42 ppm) to C_6 for (C_6-NH) group[123]. The chemical shifts at (δ=135.60 ppm) are assigned to (C_{10}, C_{14}) for aromatic ring[124]. The chemical shift at (δ=129.74-129.53 ppm) to C_{16} for (C_2H) group[125].The other results are summarized in Table (3.17).

Table(3.17): ^{13}C-NMR data for precursor [HDa] measured in DMSO-d^6 and chemical shift in ppm (δ)

Compound	Functional groups	δ (ppm)
[HDa]	$C=O_{dim}$ group	195.33
	$C=O_{ami}$ group	162.33
	C_6-NH group	153.42
	C_{10},C_{14} for aromatic ring	135.60
	C_{16} for aromatic ring	129.74-129.53
	C_{17} for aromatic ring	127.01
	C_{15} for aromatic ring	124.45
	C_9 for aromatic ring	122.46
	C_5 for C_2H group	108.41
	C_3,C_7 for CH_2 groups	50.91,40.63
	C_{12} for methyl group	36.43
	C_2 for dimedone ring	33.11
	C_1 for methyl groups	15.05
	C_{11} for methyl group	11.05
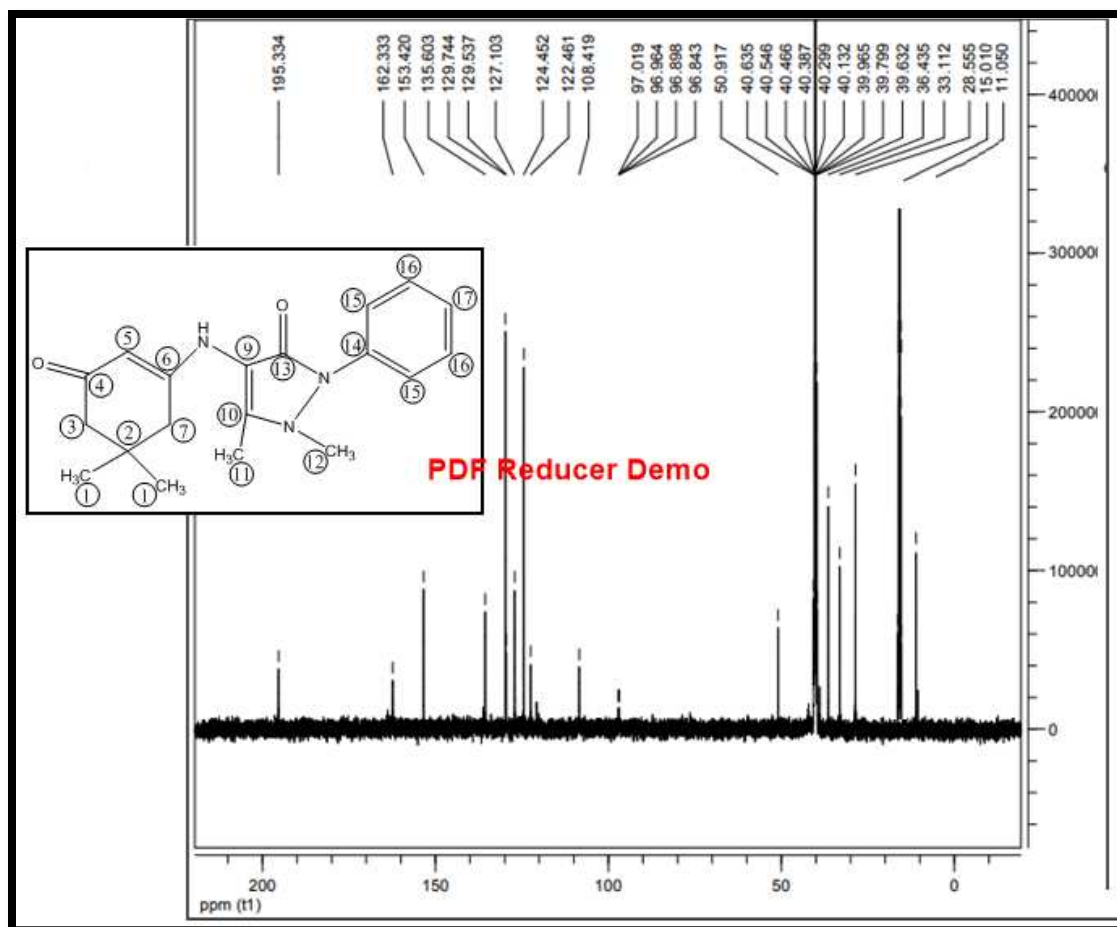
Figure (3.5): ^{13}C-NMR spectrum for the precursor [HDa] in DMSO-d^6

(3.2.4) ^{13}C-NMR spectral for the ligands KL^1 , KL^2 and KL^3

(3.2.4.1) ^{13}C-NMR spectrum for the ligand KL^1

The ^{13}C-NMR spectrum, Figure (3.6) in DMSO-d^6 solvent shows a numbers of signals attributed to ligand KL^1, explained as following: The formation of the ligand has been revealed by detecting signal at (δ=191.6 ppm), which can be attributed to carbon atom (C$_8$) for S=C-S of dithiocarbamate group[126]. The carbon atoms (C$_4$ and C$_{13}$) resonated with the chemical shifts at (δ= 195.25 ppm and 160.01 ppm) respectively. Signals at (δ=153.34, 135.50 ppm) assigned to (C$_6$ and C$_{10}$,C$_{14}$) respectively. Also the resonances at (δ=124.38, 127.02 and 129.66

88

ppm) attribute to (C_{15}, C_{16} and C_{17}), respectively. The carbon atoms (C_9 and C_5) resonated with the chemical shift at (δ = 117.5 and 66.56 ppm). The carbon atoms 1,2,3,7,11 and 12 resonated with the chemical shifts at (δ = 15.04, 33.01, 50.84, 50.84, 10.98 and 36.37 ppm) respectively[127-129]. The results are summarized in Table (3.18). The FTIR, ^{1}H-NMR and ^{13}C-NMR spectra confirmed the chemical structure of a new ligand KL^1.

Table(3.18): ^{13}C-NMR data for ligand KL[1] measured in DMSO-d[6]

Compound	Functional groups	δ (ppm)
KL[1]	C_4 for C=O group (dimedone)	195.25
	C_8 for S=C-S of dithiocarbamate group	191.5
	C_{13} for C=O group	160.1
	C_6 for aromatic ring	153.34
	C_{10}, C_{14} for aromatic ring	135.50
	C_{17} for aromatic ring	129.66
	C_{16} for aromatic ring	127.02
	C_{15} for aromatic ring	124.38
	C_9 for aromatic ring	117.5
	C_5 for aromatic ring	66.56
	C_3,C_7 for CH_2 group	50.84
	C_{12} for methyl group	36.37
	C_2 for dimedone ring	33.01
	C_1 for methyl groups	15.04
	C_{11} for methyl group	10.98
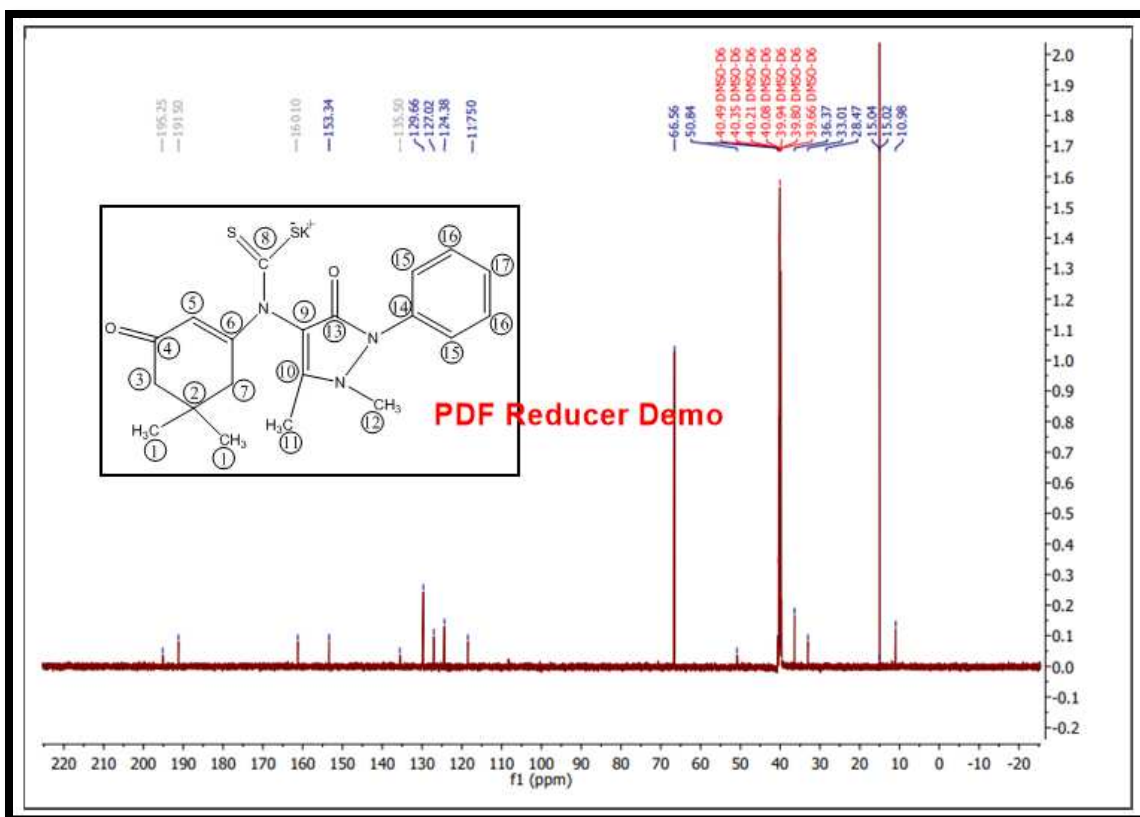
Figure (3.6):[13]**C-NMR spectrum of ligand KL**[1] **in DMSO-d**[6]

(3.2.4.2) ^{13}C-NMR spectrum for the ligand KL[2]

The ^{13}C-NMR spectrum of a ligand KL[2], Figure (3.7) in DMSO-d[6] solvent shows that the chemical shift at (δ= 191.6 ppm) attributed to carbon atom (C_8) for S=C-S of dithiocarbamate group [130]. The carbon atoms (C_6, C_{10}) resonated with the chemical shifts at (δ= 153.32 ppm). The carbon atoms ($C_{11}, C_{12}, C_{13}, C_{14}$ and C_{15}) resonated with the chemical shift at (δ =131.44 ,121.30, 112.37,125.91 and118.25 ppm) respectively. The chemical shift at (δ= 39.65-40.60 ppm) attributed to DMSO [128,131-132]. The results are summarized in Table (3.19). The FTIR, ^{1}H-NMR and ^{13}C-NMR spectra confirmed the chemical structure of a new ligand KL[2].

90

Table(3.19): ^{13}C-NMR data for ligand KL^2 measured in DMSO-d^6

Compound	Functional groups	δ (ppm)
KL^2	C$_4$ for C=O group(dimedone)	194.31
	C$_8$ for S=C-S of dithiocarbamate group	191.61
	C$_9$ for N-C=N group	160.11-166.00
	C$_6$,C$_{10}$ for aromatic ring	153.32
	C$_{11}$ for aromatic ring	131.44
	C$_{14}$ for aromatic ring	125.91
	C$_{13}$ for aromatic ring	121.37
	C$_{12}$ for aromatic ring	121.3
	C$_{15}$ for aromatic ring	118.25
	C$_5$ for aromatic ring	66.54
	C$_3$,C$_7$ for CH$_2$ group	40.60
	C$_2$ for dimedone ring	31.37
	C$_1$ for methyl groups	15.04
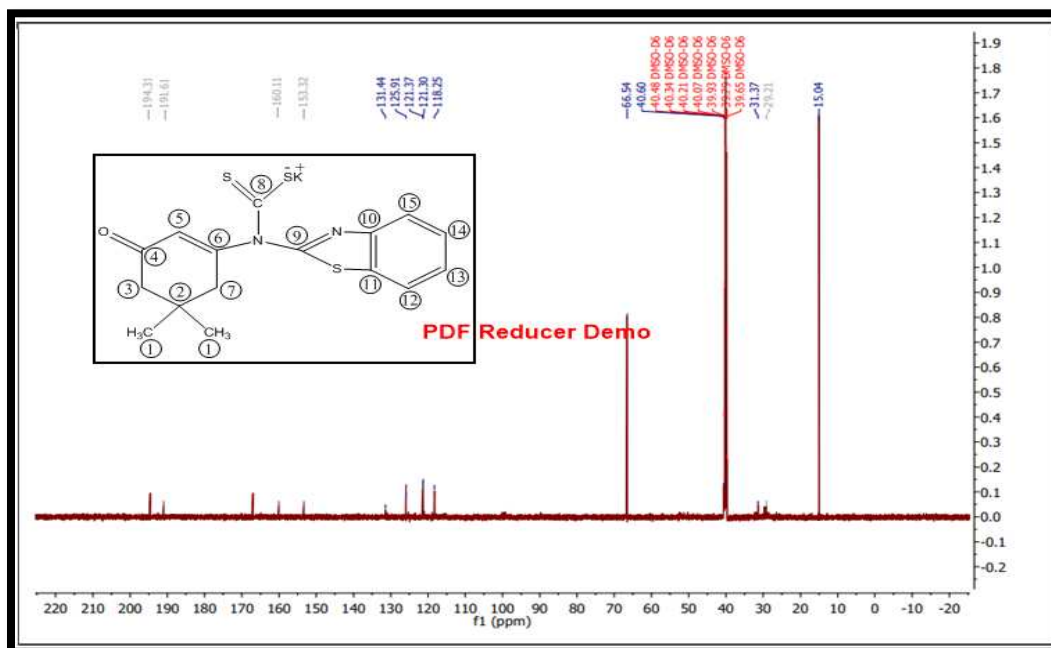
Figure (3.7): ^{13}C-NMR spectrum of ligand KL^2 in DMSO-d^6

91

(3.2.4.3) ^{13}C-NMR spectrum for the ligand KL^3

The ^{13}C-NMR spectrum of a ligand KL^3, Figure (3.8) in DMSO-d^6 solvent shows that the chemical shift at (δ= 191.15 ppm) attributed to carbon atom (C$_8$) for S=C-S of dithiocarbamate group [130]. The carbon atoms (C$_6$, C$_5$) of α,β-unsaturated part resonated with the chemical shifts at (δ= 156.58,66.59 ppm) respectively. The carbon atoms (C$_{10}$,C$_{11}$ and C$_{12}$) resonated with the chemical shift at (δ =120.73 ,116.17 and 119.18 ppm) respectively . The chemical shift at (δ= 39.63-40.59 ppm) attributed to DMSO [133,134]. The results are summarized in Table (3.20). The FTIR, ^{1}H-NMR and ^{13}C-NMR spectra confirmed the chemical structure of a new ligand KL^3.

Table(3.20): ^{13}C-NMR data for ligand KL^3 measured in DMSO-d^6

Compound	Functional groups	δ (ppm)
KL^3	C$_4$ for C=O group	195.25
	C$_8$ for S=C-S of dithio group	191.15
	C$_6$ for dimedone part	156.58
	C$_9$ for N-C=N group	150.31
	C$_{10}$ for aromatic ring	120.73
	C$_{12}$ for aromatic ring	119.18
	C$_{11}$ for aromatic ring	116.17
	C$_5$ for dimedone part	66.59
	C$_3$,C$_7$ for CH$_2$ group	56.54
	C$_2$ for dimedone ring	32.44
	C$_1$ for methyl group	15.03
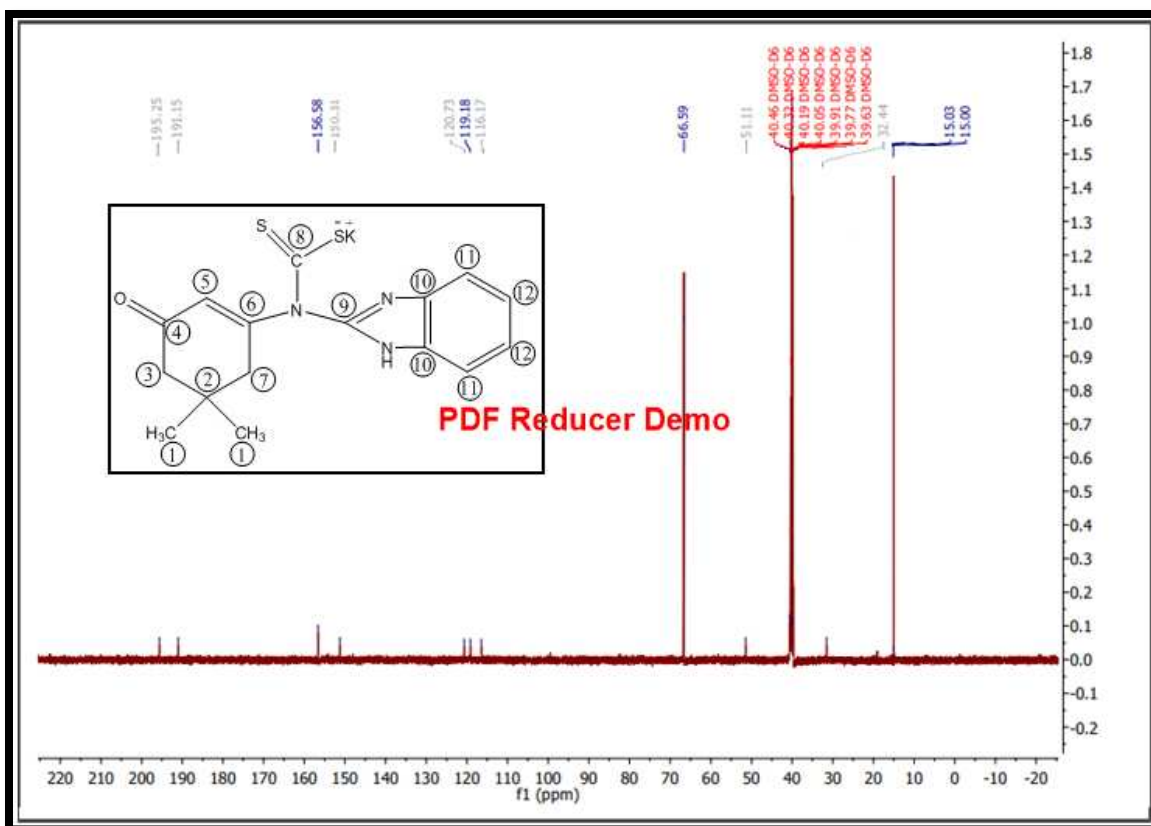
Figure (3.8): ^{13}C-NMR spectrum of ligand KL^3 in DMSO-d^6

(3.2.5) Mass spectral of free ligands (KL^1, KL^2 and KL^3)

(3.2.5.1) Mass spectrum of free ligand KL^1

The electro impact EI(-) mass spectrum of ligand KL^1 is presented in Figure (3.9). The spectrum reveals successive fragments related to ligand structure with the appropriate isotope distribution pattern. The molecular ion peak for the ligand is observed at m/z = 438.30 (M-H)$^+$ (3%) for $[C_{16}H_{21}KN_3O_2S_2^-H]^+$; requires=439.63. Other fragments and their relative abundance and fragmentation pattern are shown in Table(3.21).
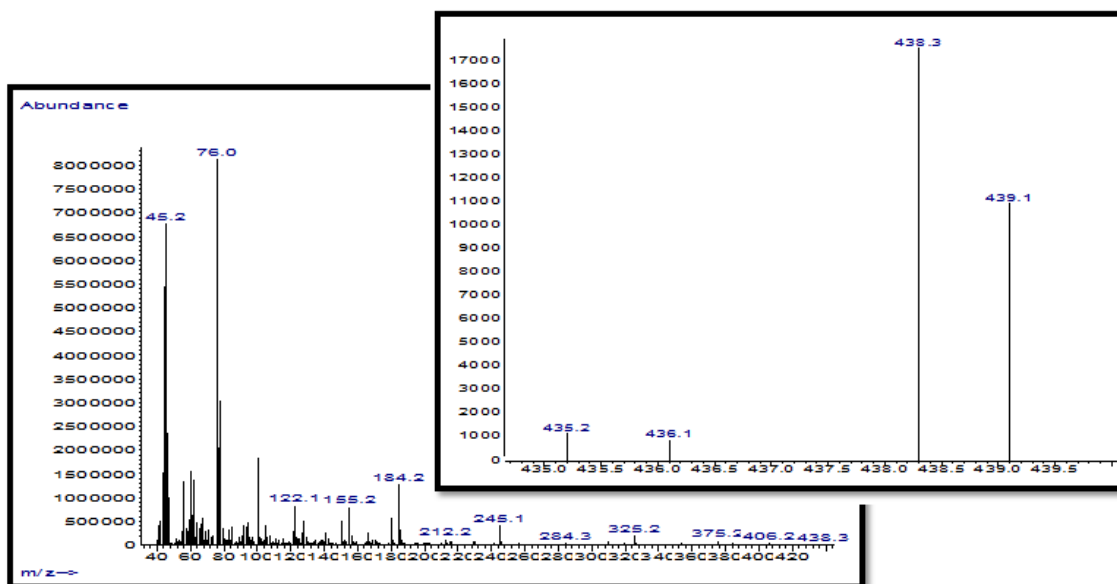
Figure (3.9): EI mass spectrum of KL^1.

Table(3.21): EI-Mass data of the ligand KL^1

Fragment	Mass/charge (m/z)	Relative abundance
$[M-H]^+ = [C_{20}H_{22}KN_3O_2S_2-H]^{+\cdot}$	438.3	3%
$[C_{20}H_{21}KN_3O_2S]^{+\cdot}$	406.2	3%
$[C_{19}H_{19}NO_2S]^{+\cdot}$	325.2	4%
$[C_{13}H_{11}NO_2S]^{+\cdot}$	245.1	6%
$[C_{12}H_8S]^{+\cdot}$	184.2	12%
$[C_6H_5NO_2S]^{+\cdot}$	155.2	10%
$[C_6H_4NO_2]^{+\cdot}$	122.1	10%
$[CSO_2]^{+\cdot}$	76.0	100%
$[CSH]^{+\cdot}$	45.2	70%

(3.2.5.2) Mass spectrum of free ligand KL^2

The electro impact EI mass spectrum of ligand KL^2 is presented in Figure(3.10). The spectrum reveals successive fragments related to ligand structure

with the appropriate isotope distribution pattern. The molecular ion peak for the ligand is observed at m/z =386.3 $(M)^+$ (3%) for $[C_{16}H_{15}KN_2OS_3]^+$; requires =386.59. other fragments and their relative abundance and fragmentation pattern are shown in Table(3.22).
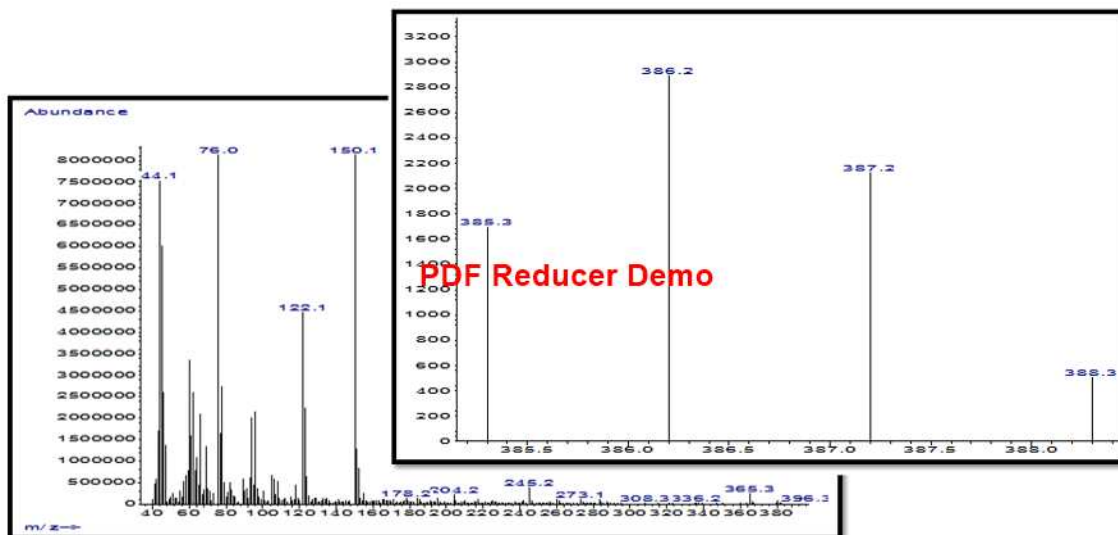
Figure(3.10): EI mass spectrum of KL^2

Table(3.22): EI-Mass data of the ligand KL^2

Fragment	Mass/charge (m/z)	Relative abundance
$[C_{16}H_{15}KN_2OS_3]^{+\cdot}$	386.3	3%
$[C_{16}H_{10}KN_2S_3]^{+\cdot}$	365.3	4.5%
$[C_{13}H_{15}KNOS_3]^{+\cdot}$	336.2	3%
$[C_{13}H_{11}NS_2]^{+\cdot}$	245.2	4.5%
$[C_{10}H_{14}O]^{+\cdot}$	150.1	100%
$[C_8H_{10}O]^{+\cdot}$	122.1	52%
$[CS_2]^{+\cdot}$	76.0	100%
$[CS]^{+\cdot}$	44.1	90%

(3.2.5.3) Mass spectrum of free ligand KL^3

     The electro impact EI mass spectrum of ligand KL^3 is presented in Figure (3.11). The spectrum reveals successive fragments related to ligand structure with the appropriate isotope distribution pattern. The molecular ion peak for the ligand is observed at m/z =369.3 (M)$^+$ (3%) for [C$_{16}$H$_{16}$KN$_3$OS$_3$]$^+$; requires =369.54. other fragments and their relative abundance and fragmentation pattern are shown in Table(3.23).
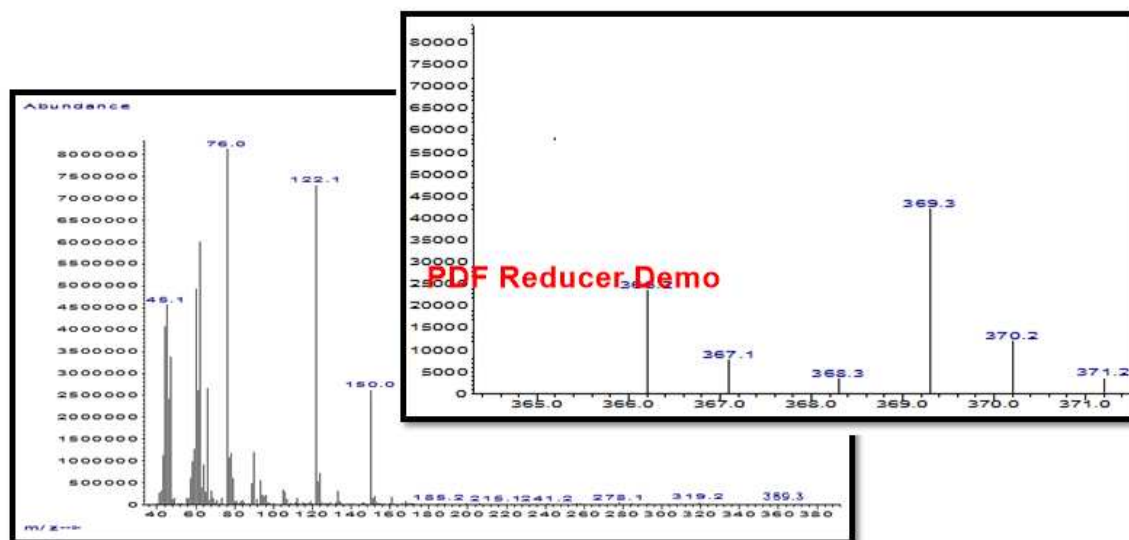
Figure(3.11): EI mass spectrum of KL^3.

Table(3.23): EI-Mass data of the ligand KL^3

Fragment	Mass/charge (m/z)	Relative abundance
[C$_{16}$H$_{16}$KN$_3$OS$_2$]$^{+\cdot}$	369.3	3%
[C$_{13}$H$_{16}$KN$_2$OS$_2$]$^{+\cdot}$	319.2	3%
[C$_8$H$_6$OS]$^{+\cdot}$	150.0	40%
[C$_8$H$_{10}$O]$^{+\cdot}$	122.1	85%
[CS$_2$]$^{+\cdot}$	76.0	100%
[CSH]$^{+\cdot}$	45.1	50%

(3.2.6) FT-IR Spectral data for compounds.

(3.2.6.1) FT-IR Spectral data for the Precursors HDa, HDb and HDi.

The FT-IR spectra for the precursors HDa, HDb and HDi, Fig.(3.12), Fig.(3.13) and Fig.(3.14), display bands at 3222 cm^{-1} ,3284 cm^{-1} and 3141 cm^{-1} respectively are due to υ(N-H) stretching vibration [135]. The assignments of characteristic bands of the precursors are summarized in Table(3.24).
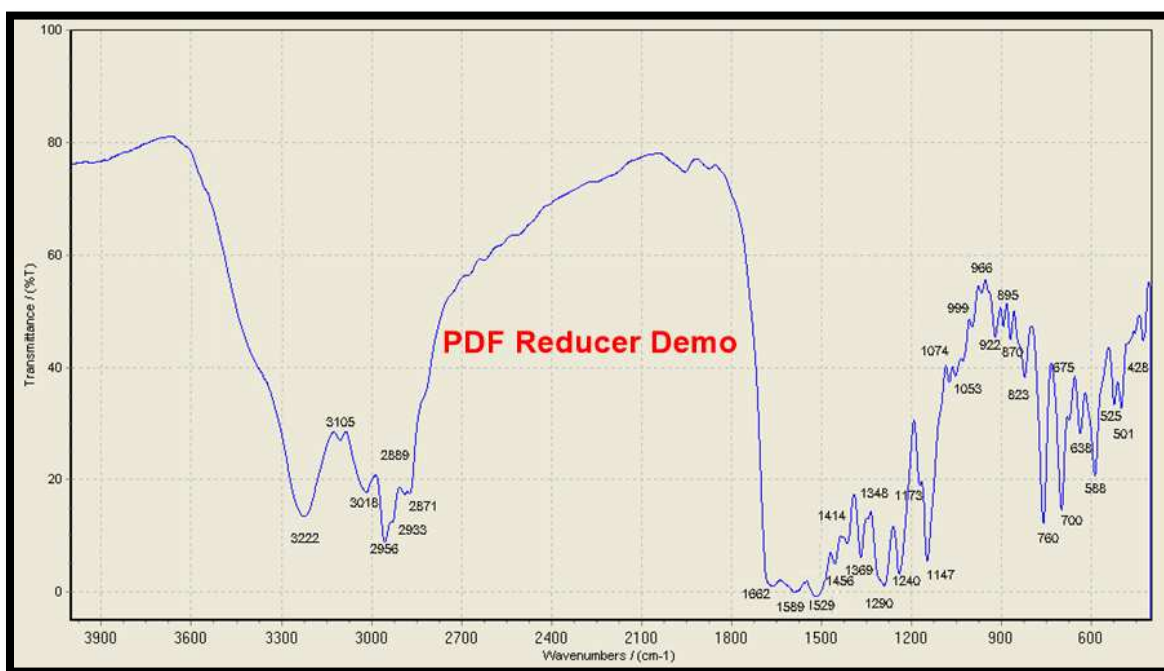
Figure(3.12): FT-IR spectrum of precursor(HDa).
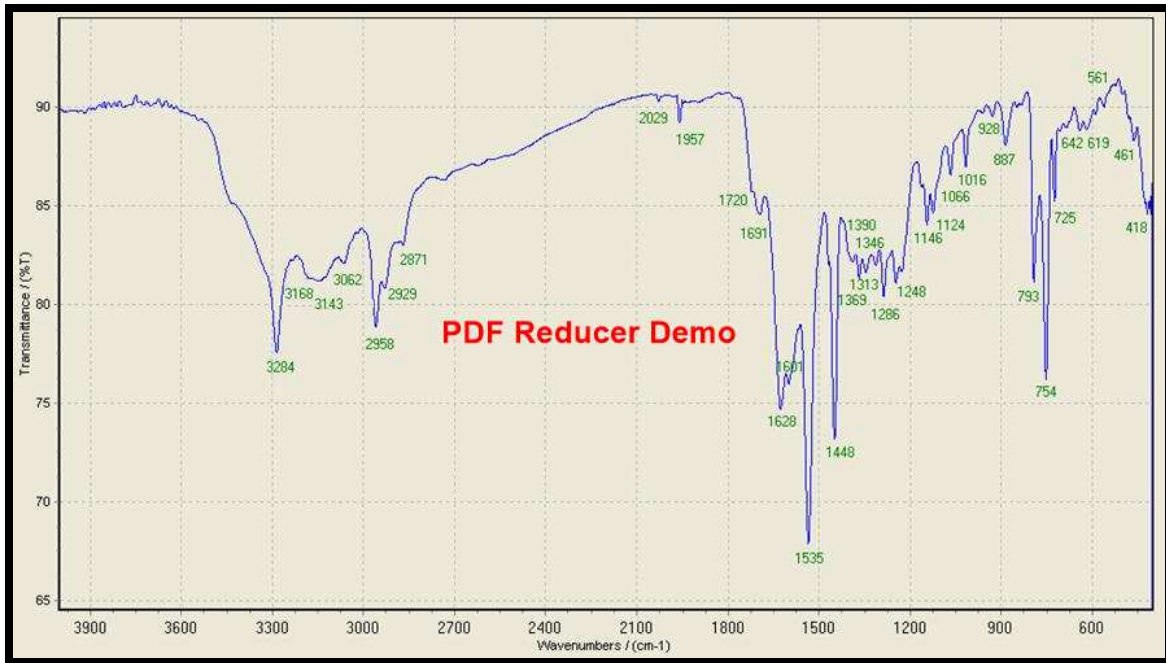
Figure(3.13): FT-IR spectrum of precursor (HDb).
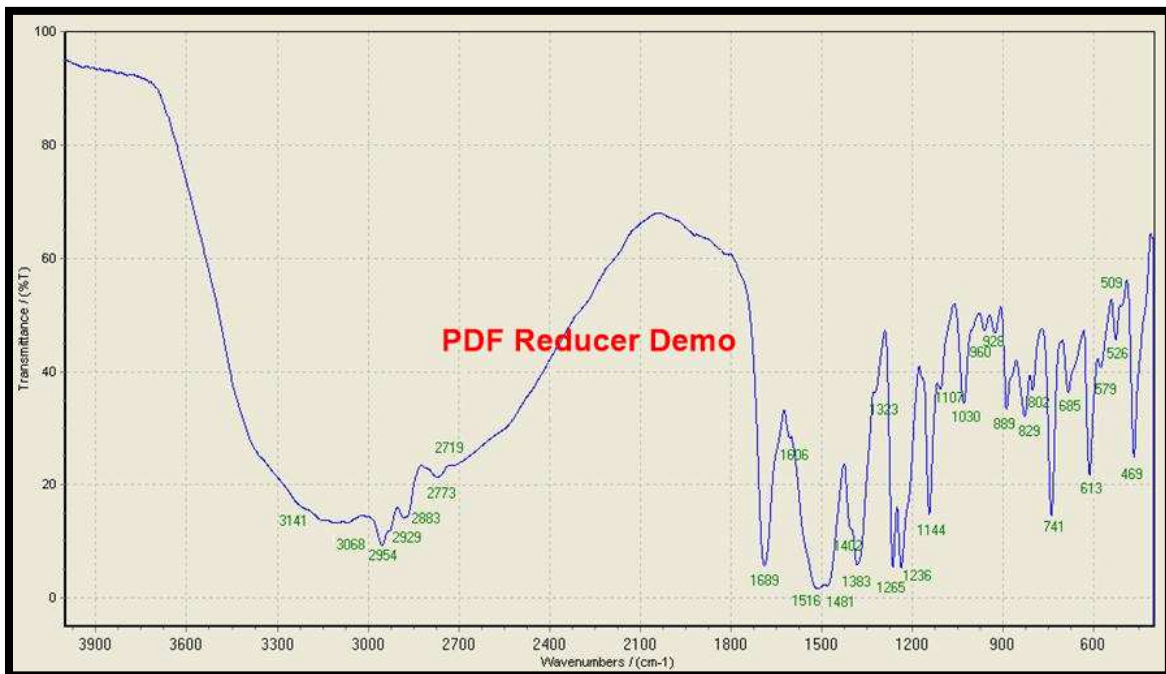
Figure(3.14): FT-IR spectrum of precursor (HDi).
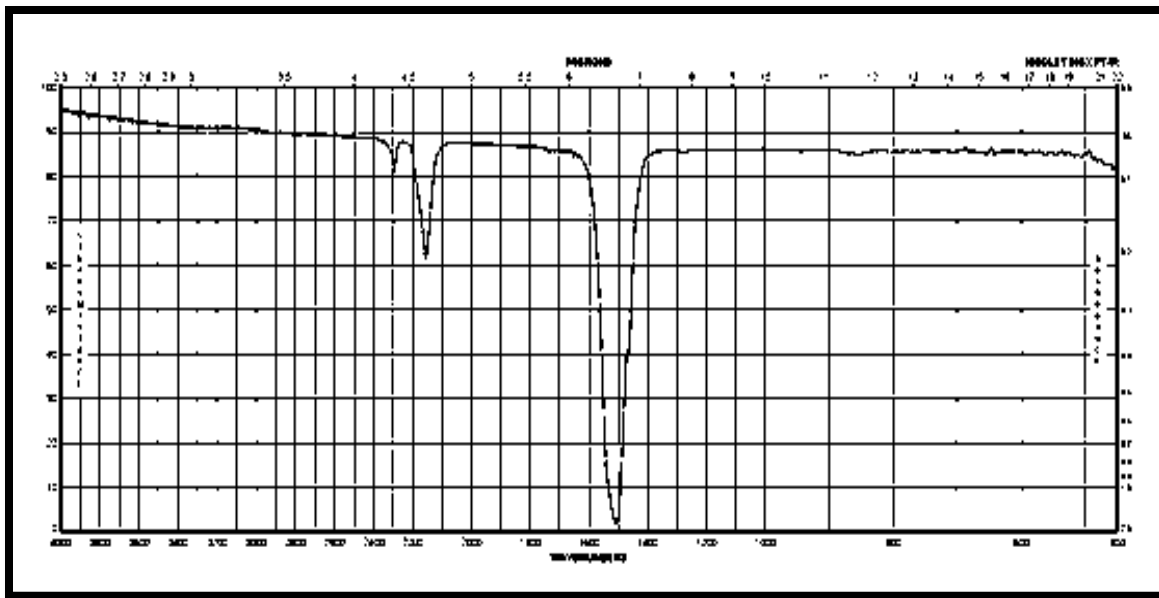
Figure(3.15): FT-IR bands of carbon disulphide.

Table (3.24): FT-IR spectral data (wave number) cm^{-1} of precursors (HDa), (HDb) and (HDi).

Compound (Precursors)	ν(NH) amine	ν_{ar} (C-H)	ν_{ali} (C-H)	ν(C=O) keto	ν (C=N)	ν_{ar}(C=C)
(HDa)	3222	3105	3018-2956	1589	1662	1529
(HDb)	3284	3062	2958	1535	1628	1448
(HDi)	3141	3068	2954	1516	1689	1481

(3.2.6.2) FT-IR Spectral data for ligands KL^{1}-KL^{3}.

The FT-IR spectra of the dithiocarbamate compounds showed characteristic bands that confirmed the formation of ligands.

(3.2.6.2.1) FT-IR Spectrum of KL^{1}

The FT-IR spectrum of [potassium (1,5-dimethyl-3-oxo-2-phenyl-2,3-dihydro-1H-pyrazol-4-yl)(5,5-dimethyl-3-oxocyclohex-1-en-1-yl) carbamo dithioate] (KL^{1}), Fig.(3.16), is compared with the FT-IR spectra of the precursor(HDa), Fig.(3.12), and carbon disulphide, Fig.(3.15).The spectrum of KL^{1}

shows no band around 3222cm^{-1} could be related to $\nu(NH)_{amine}$ stretching, compared with that observed in the precursor(HDa) spectrum. The new band at 1493 cm^{-1} can be attributed to $\nu(C-N)$ stretching of (N-CS$_2$) moiety [136]. The spectrum reveals two new bands at 1003 and 945 cm^{-1} that attributed to $\nu_{as}(CS_2)$ and $\nu_s(CS_2)$, respectively [137]. Band observed at 1653 and 1585 cm^{-1} is related to $\nu(C=O)$ groups and band observed at 1529cm^{-1} was assigned to $\nu_{ar}(C=C)$ mode of aromatic system [138]. The assignments of characteristic bands are summarised in Table (3.25).

(3.2.6.2.2) FT-IR spectra of ligands KL^2 and KL^3

The FT-IR spectra for ligands KL^2, KL^3 are shown in Fig.(3.17), Fig.(3.18) respectively. These spectra show bands similar to that of KL^1 and same reasoning could be used to interpret the spectra. The assignments bands of ligands are summarized in Table (3.25).
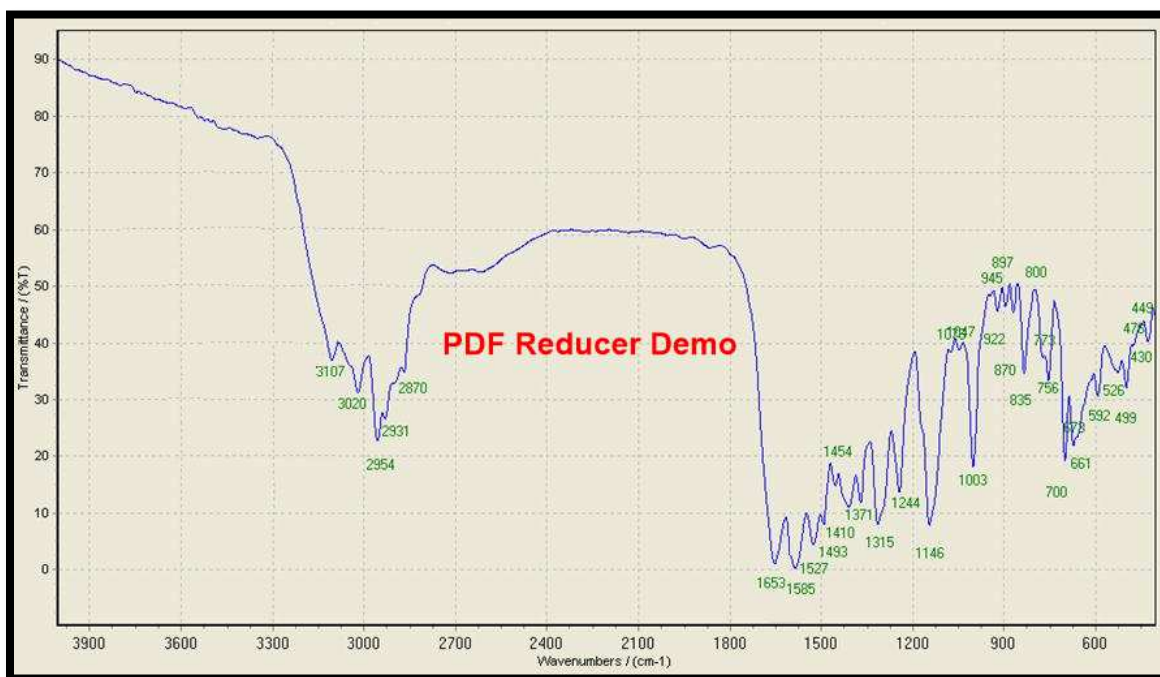
Figure(3.16): FT-IR spectrum of KL^1.
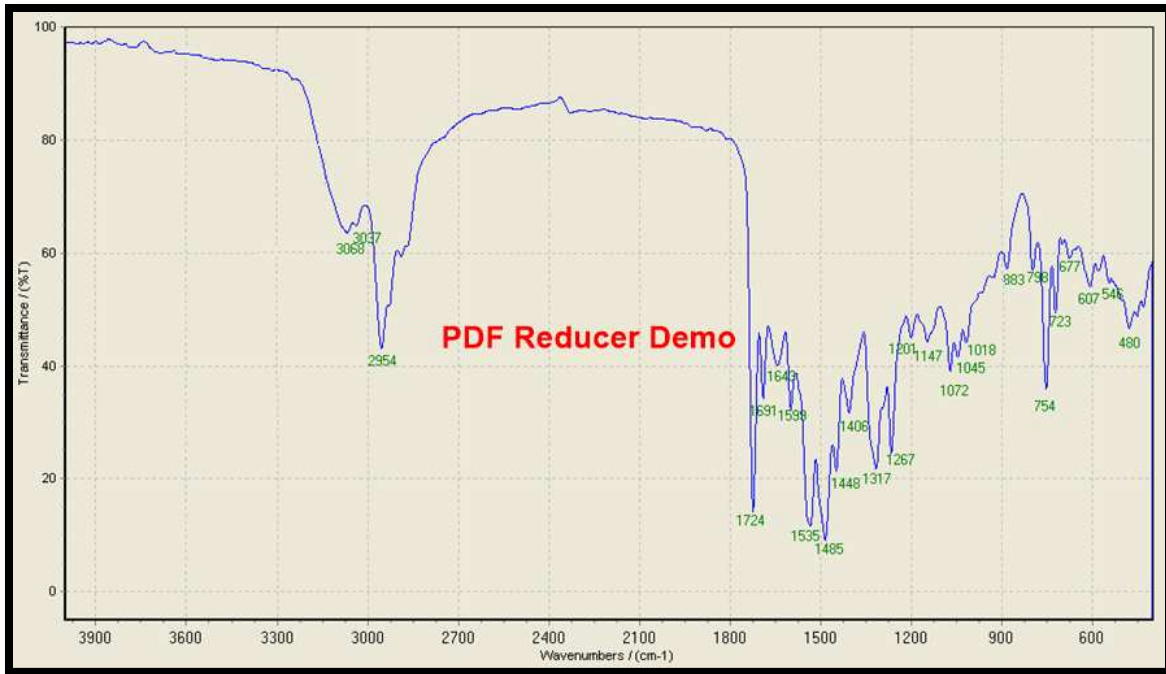
Figure(3.17): FT-IR spectrum of KL^2.
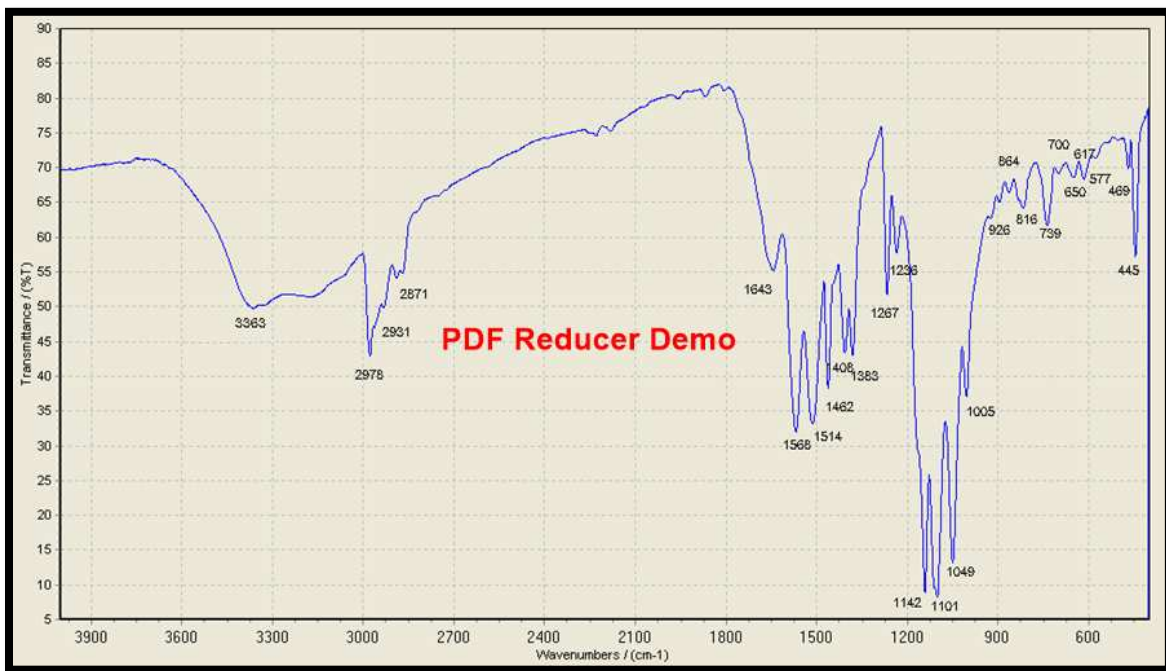
Figure(3.18): FT-IR spectrum of KL^3.

101

Table (3.25): FT-IR spectral data (wave number) cm^{-1} for ligands.

Compound (Ligands)	ν (N-H)	ν_{ar} (C-H)	ν_{ali} (C-H)	ν(C=O) keto	ν_{ar}(C=C) amin	ν(N-CS$_2$)	ν(C- N)	ν_{as}(CS$_2$) ν_s(CS$_2$)
KL1	-	3107	3020-2954	1585 ,1653	1527	1493	1146	1003 ,945
KL^2	-	3068	2954	1724	1535	1485	1147	1072 ,1018
KL^3	3363	3150	2978	1643	1514	1462	1142	1049 ,1005

(3.2.7) FT-IR spectral data for the complexes

The infrared spectra of dithiocarbamate metal complexes gave evidence for the formation of the complexes and confirm the proposed coordination mode of (CS$_2$) and the proposed structure of complexes. There are three important and useful regions in the spectra of dithiocarbamat complexes should be checked at; (1383–1504, 885–1192 and 362–397)cm^{-1}. The 1383–1504cm^{-1} region is concerned with the stretching of the (C-N) of (NCS$_2^{-}$) moiety. The band present around 1500cm^1 is expected as arising from a polar structure such as ($^+$N=CSS$^-$). The increasing electron donating character in alkyl group would stabilize this structure and increase the ν(CS$_2$) wave number [139]. The second region around 885–1192cm^{-1} is associated with the C-S stretching frequency. The third important region in the range (325– 450)cm^{-1}, refers to ν(M-S) resulting from coordination, the latter band is absent in the free ligands [140].

(3.2.7.1) FT-IR spectral data for [Mn(L^1)$_2$], [Co(L^1)$_2$], [Ni(L^1)$_2$], [Cu(L^1)$_2$] , [Zn(L^1)$_2$], [Pd(L^1)$_2$] and [Cd(L^1)$_2$].

(3.2.7.1.1) FT-IR spectrum for [Mn(L^1)$_2$]

The FT-IR spectra of KL^1 and its metal complexes are shown in Fig. ((3.19)-(3.25)). The FT-IR spectrum of [Mn(L^1)$_2$], Fig.(3.19), exhibits bands revealed complex formation. Band observed at 1662cm^{-1} can be attributed to ν(C=O)

102

group. Band observed at 1587cm^{-1} is assigned to v_{ar}(C=C) mode of aromatic system. The spectrum displays band at 1456cm^{-1}, which is related to v(N-CS$_2$) mode [136]. This suggests an increase in the v(N-C) double bond character as a result of the delocalisation of electrons towards the metal centre upon coordination to the dithiocarbamate ligand [137]. Bands appeared at (1053 and 1003)cm^{-1} attributed to asymmetric v_{as}(CS$_2$) and symmetric v_s(CS$_2$) of the CS$_2$ group respectively, which confirmed an bidentate chelation mode of the ligand to the metal ion [141,142]. Band related to v_{ar}(C-H) aromatic [138], was detected at (3248)cm^{-1} .At lower frequency complexes [Mn(L^1)$_2$], Fig.(3.19) and [Cu(L^1)$_2$], Fig.(3.22) exhibited two bands at 362, 324 and 351, 331 cm^{-1}, respectively that are assigned to the v(M-S) vibrational mode, and supporting the bidentate chelation mode of the ligand [142]. The FT-IR spectra for [Co(L^1)$_2$], [Ni(L^1)$_2$], [Cu(L^1)$_2$], [Zn(L^1)$_2$] ,[Pd(L^1)$_2$] and [Cd(L^1)$_2$] complexes, Fig.((3.20)-(3.25)), show similar trend to that of the [Mn(L^1)$_2$] complex and same reasoning could be used to interpret the spectra. The structurally important FT-IR absorption bands of the prepared complexes are summarised in Table (3.26).
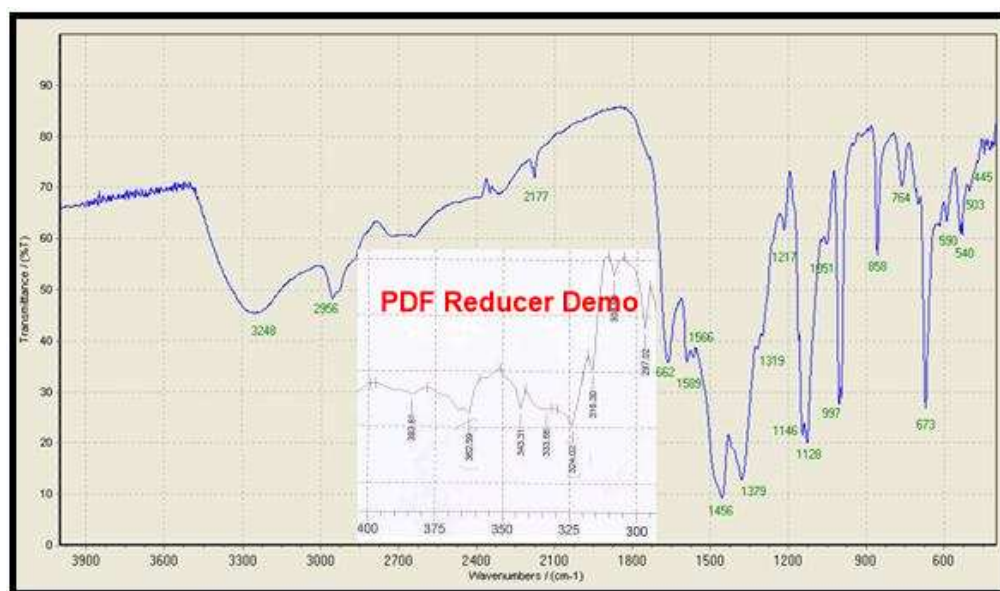
Figure(3.19): FT-IR spectrum of [Mn(L^1)$_2$] complex.
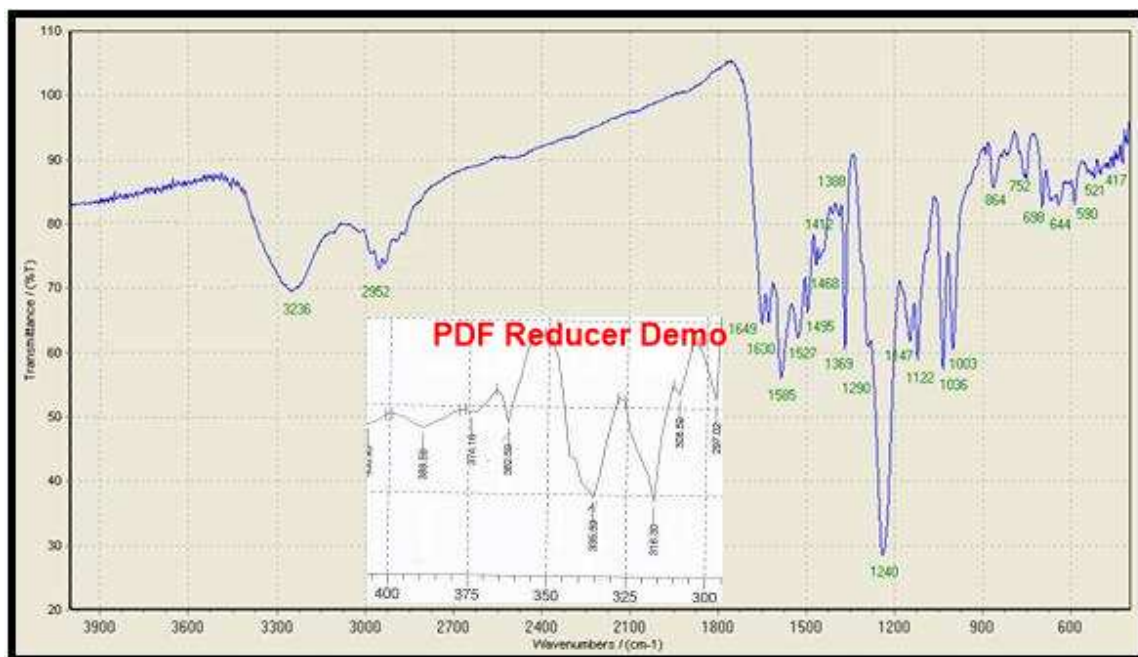
Figure(3.20): FT-IR spectrum of [Co(L^1)$_2$] complex.
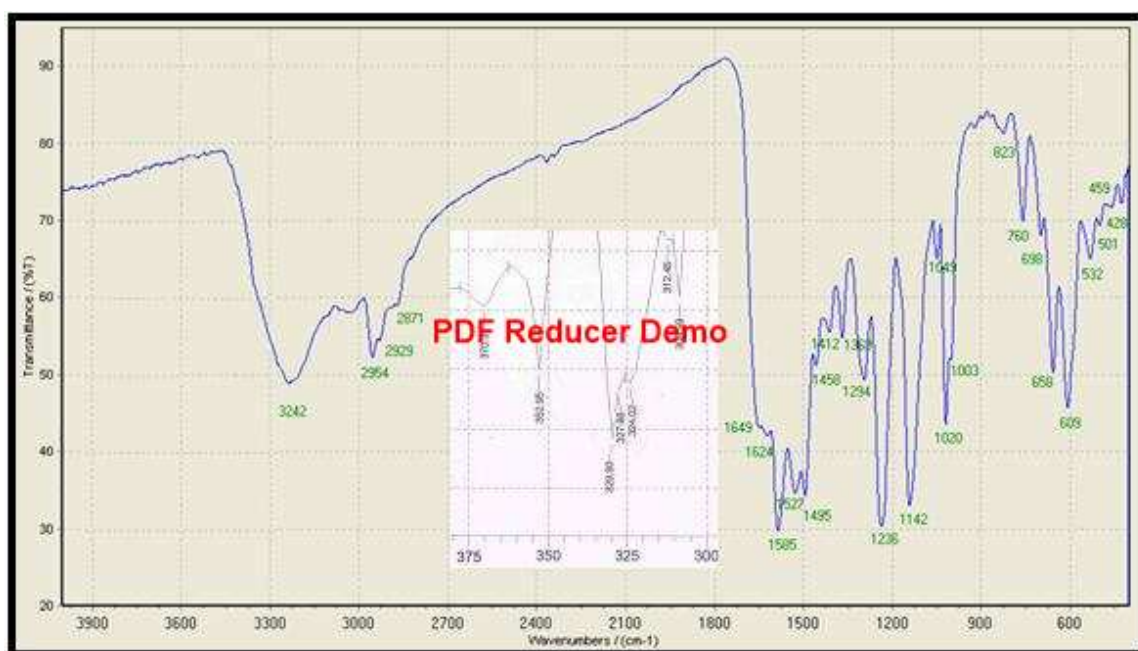
Figure(3.21): FT-IR spectrum of [Ni(L^1)$_2$] complex.
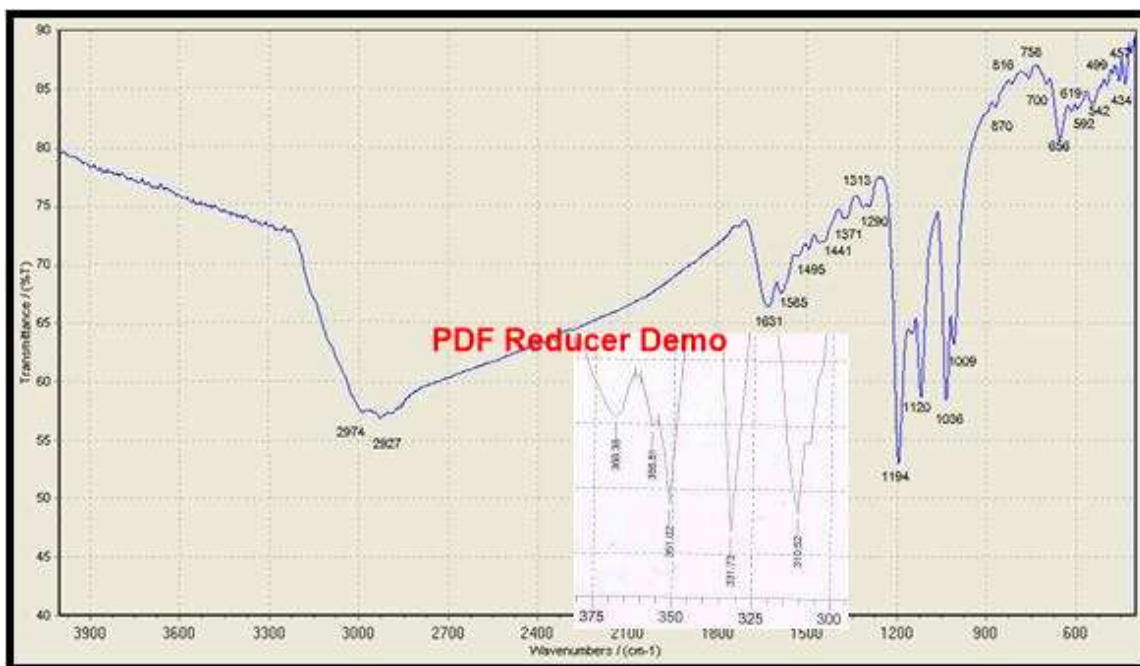
Figure(3.22): FT-IR spectrum of [Cu(L^1)$_2$] complex.
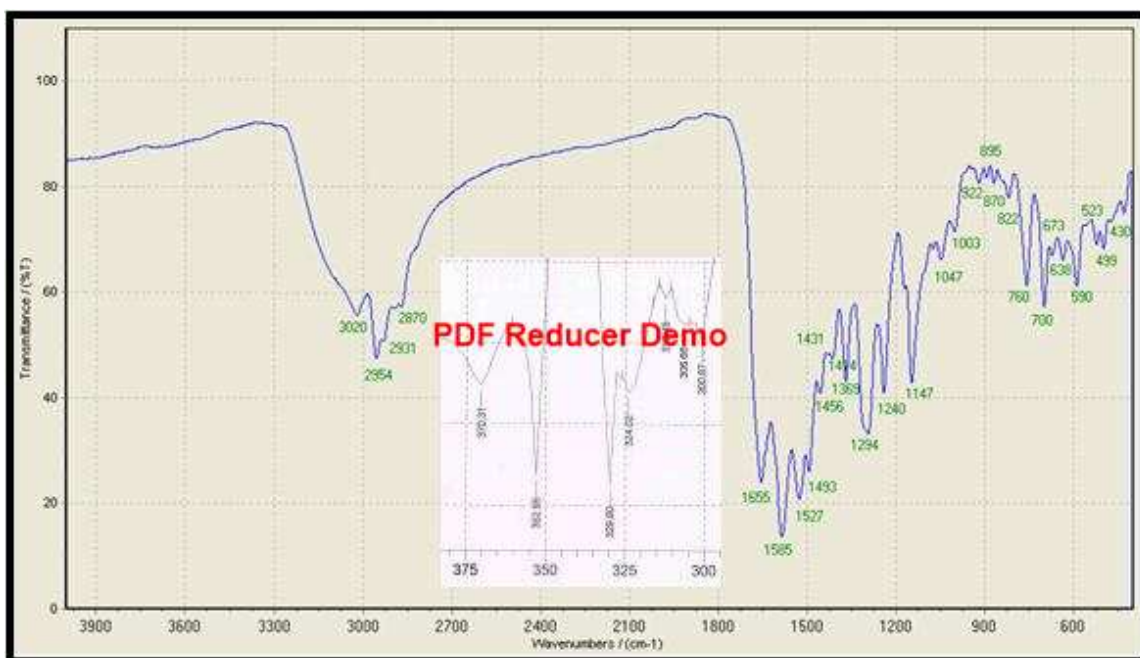
Figure(3.23): FT-IR spectrum of [Zn(L^1)$_2$] complex.
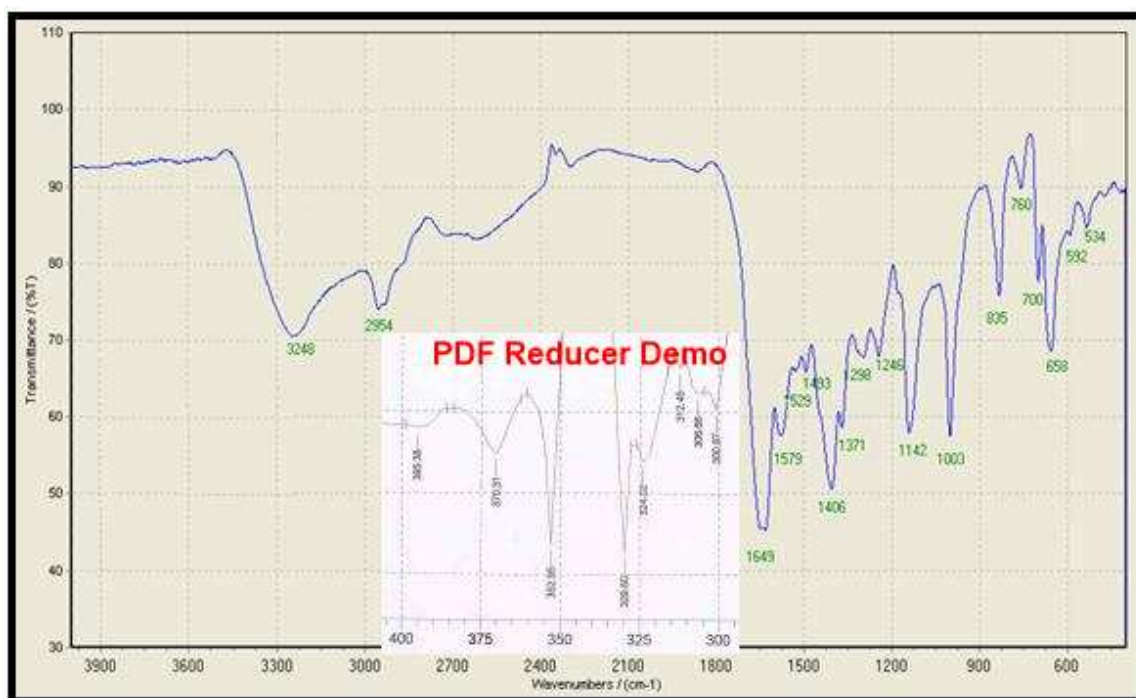
Figure(3.24): FT-IR spectrum of [Pd(L^1)$_2$] complex.
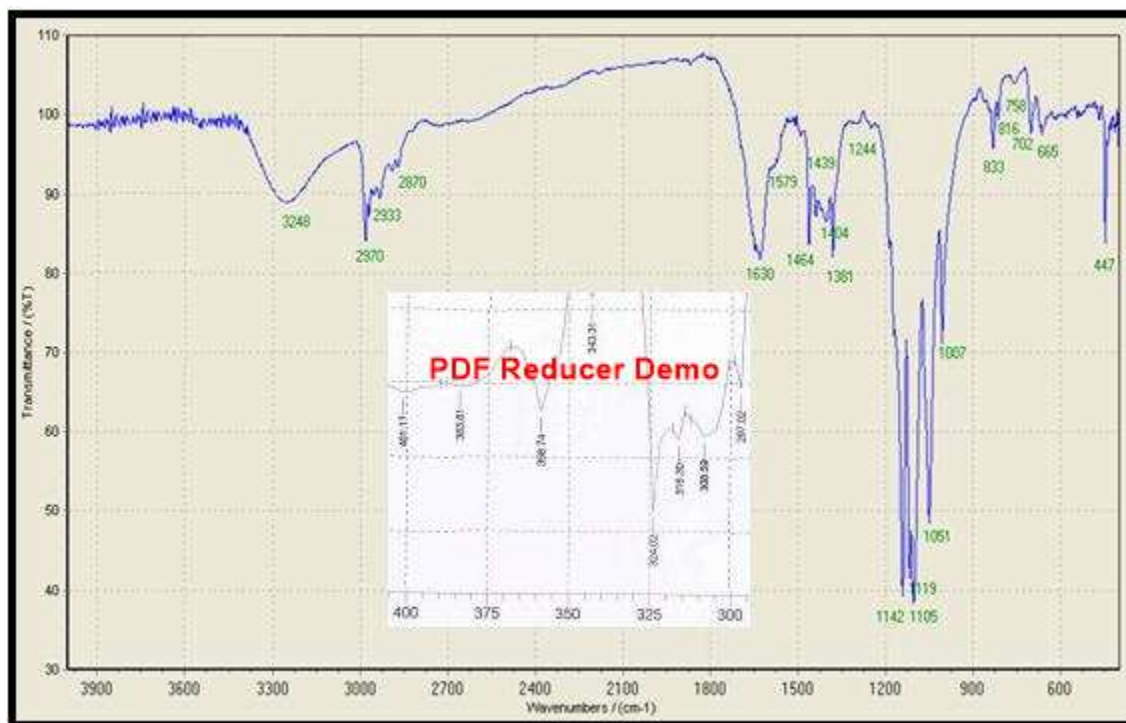
Figure(3.25): FT-IR spectrum of [Cd(L^1)$_2$] complex.

Table(3.26): FT-IR spectral data (wave number)cm^{-1} of KL^1 and its complexes.

Compound	$\nu_{aro.}$ (C-H)	$\nu_{alph.}$ (C-H)	$\nu_{ket,amin}$ (C=O)	$\nu_{vin.}$ (C=C)	ν (N-CS$_2$)	ν (C-N)	ν (C-S)$_{sy.}$ ν (C-S)$_{asy.}$	ν (M-S)
KL^1	3107(w)	3020-2954(m)	1585(w) 1653	1527(w)	1493(w)	1244(s)	1003(w) 945(s)	-
[Mn(L^1)$_2$]	3248(w)	2956(m)	1583(w)	1566(s)	1456(s)	1217(w	1053(m) 1003(s)	362(w), 324(w)
[Co(L^1)$_2$]	3236(w)	2958(m)	1649(w)	1585(w)	1495(w)	1238(s)	1036(w) 1003(s)	362(w), 335(w)
[Ni(L^1)$_2$]	3242(w)	2954(m)	1649(w)	1556(w)	1495(w)	1236(s)	1020(s) 1003(w)	352(w), 324(w)
[Cu(L^1)$_2$]	2974(w)	2927(w)	1585(w) 1631	1533(w)	1495(w)	1194(s)	1036(s) 1009(m)	351(w), 331(w)
[Zn(L^1)$_2$]	3020(w)	2954(m)	1585(w) 1655	1527(w)	1493(w)	1240(s)	1047(w) 1003(w)	352(w), 324(w)
[Pd(L^1)$_2$]	3248(w)	2954(m)	1579(w) 1649	1493(w)	1406(w)	1142(s)	1049(w) 1003(s)	381(w), 335(w)
[Cd(L^1)$_2$]	3248(w)	2978(m)	1579(w) 1630	1491(w)	1460(s)	1142(s)	1051(m) 1005(s)	358(w), 324(w)

(3.2.7.2) FT-IR spectral data for of [Mn(L^2)$_2$] [Co(L^2)$_2$], [Ni(L^2)$_2$], [Cu(L^2)$_2$], [Zn(L^2)$_2$] , [Pd(L^2)$_2$] and [Cd(L^2)$_2$] complexes.

(3.2.7.2.1) FT-IR spectrum for [Co(L^2)$_2$].

The FTIR spectrum of [Co(L^2)$_2$], Fig.(3.27), exhibits bands related to the ligand with the appropriate shift due to complex formation. The Band observed at 1714 cm^{-1}, can be attributed to the bending band for ν_{ket}(C=O). The spectrum displays band at 1452 cm^{-1}, which is related to ν(N-CS$_2$) mode, compared with that detected in the ligand at 1448 cm^{-1}, indicating an increase of the carbon-nitrogen double bond character that is caused by electron delocalization towards metal centre upon coordination [136]. The spectrum showed asymmetric ν(CS$_2$) and symmetric ν(CS$_2$) bands which appear at (1066 and 930) cm^{-1}, respectively . At lower frequency complexes [Co(L^2)$_2$] Fig.(3.27) and [Zn(L^2)]$_2$ Fig.(3.30) exhibited

two bands at (364, 333) and (343, 331) cm^{-1}, respectively that are assigned to the ν(M-S) vibrational mode, and supporting the bidentate chelation mode of the ligand [143]. The FT-IR spectra for [Mn(L^2)$_2$], [Ni(L^2)$_2$], [Cu(L^2)$_2$] ,[Zn(L^2)$_2$], [Pd(L^2)$_2$] and [Cd(L^2)$_2$] complexes, Fig.((3.26),(3.28)-(3.32)) show similar trend to that of the [Co(L^2)$_2$] complex and same reasoning could be used to interpret the spectra. The structurally important FT-IR absorption bands of the prepared complexes are summarised in Table(3.27).
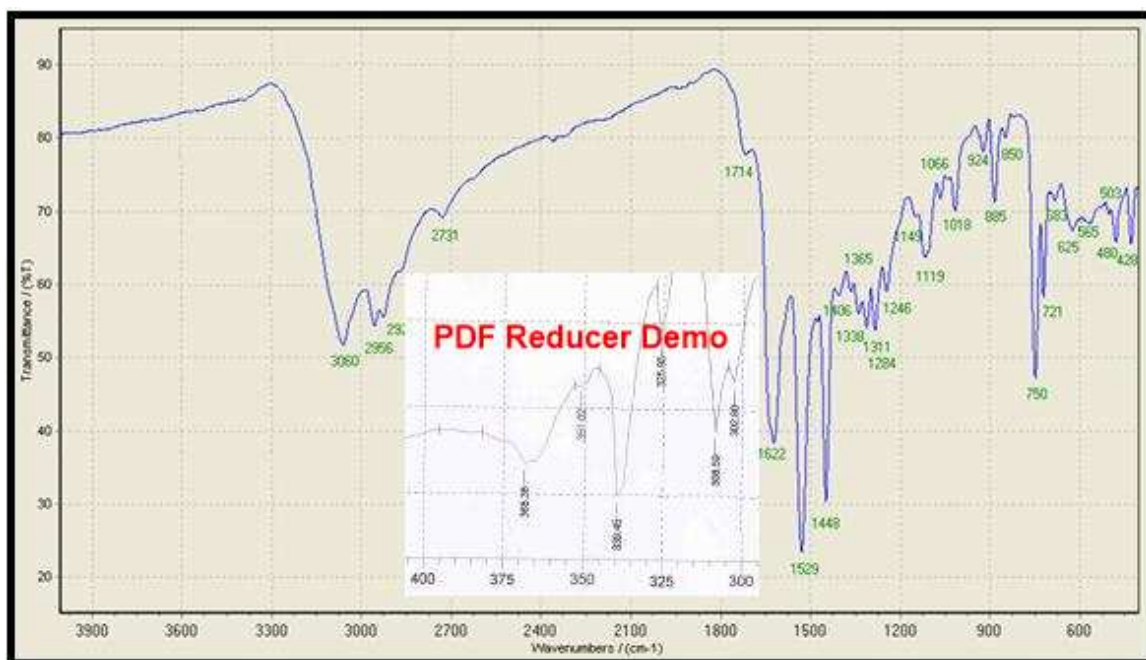
Figure(3.26): FTIR spectrum of [Mn(L^2)$_2$] complex.
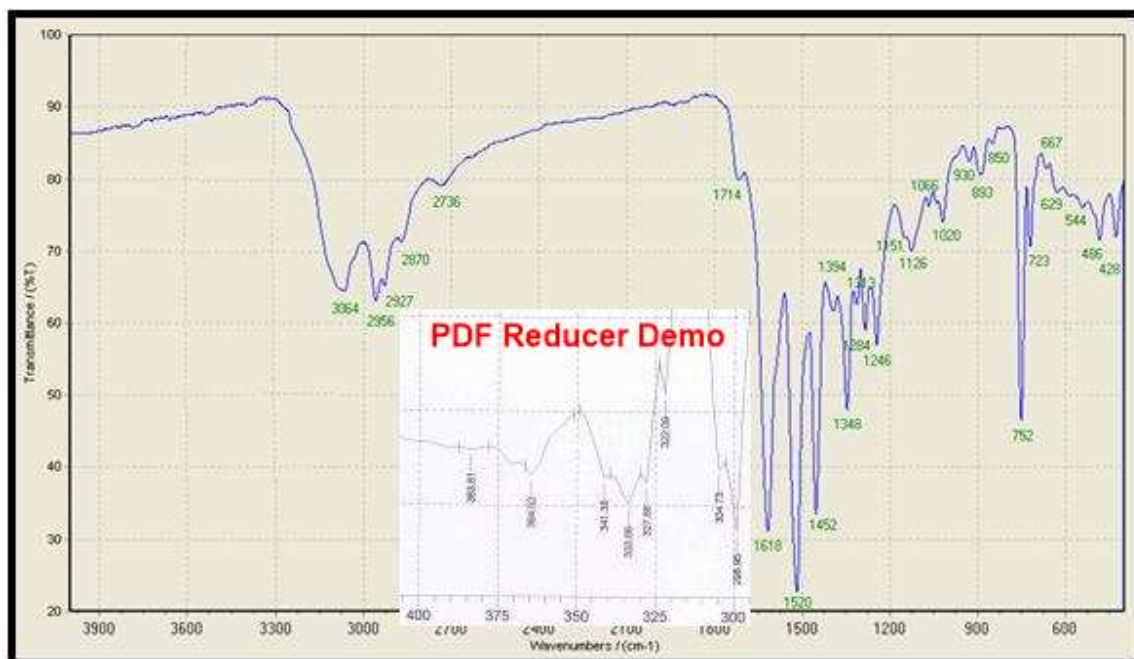
Figure(3.27): FT-IR spectrum of [Co(L^2)$_2$] complex.
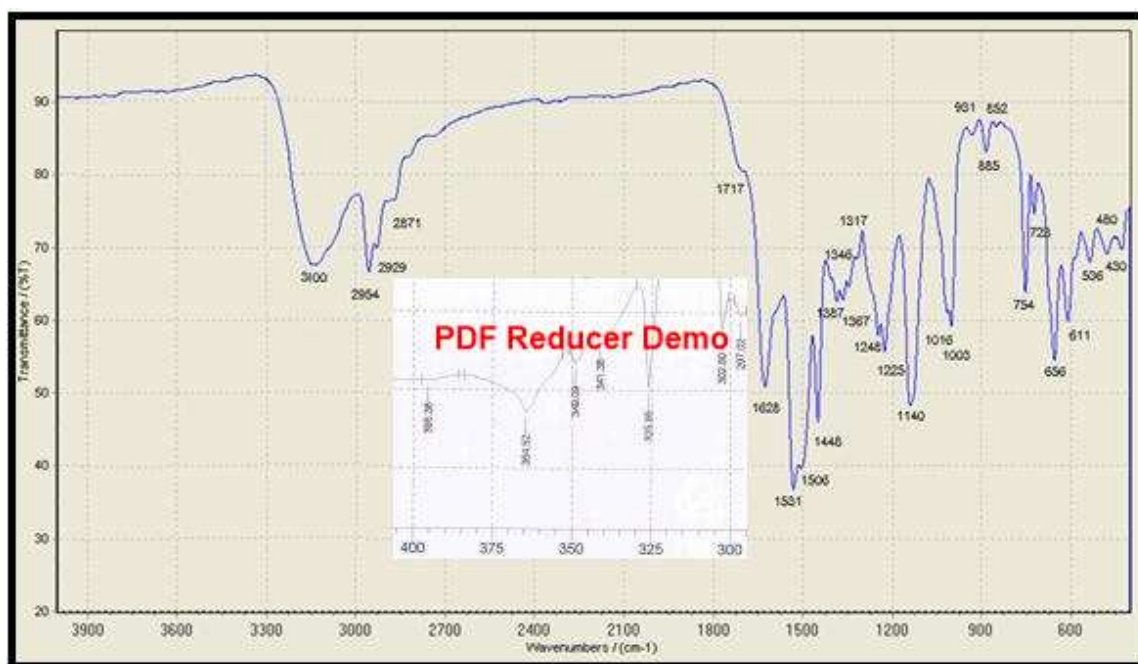
Figure(3.28): FT-IR spectrum of [Ni(L^2)$_2$] complex.
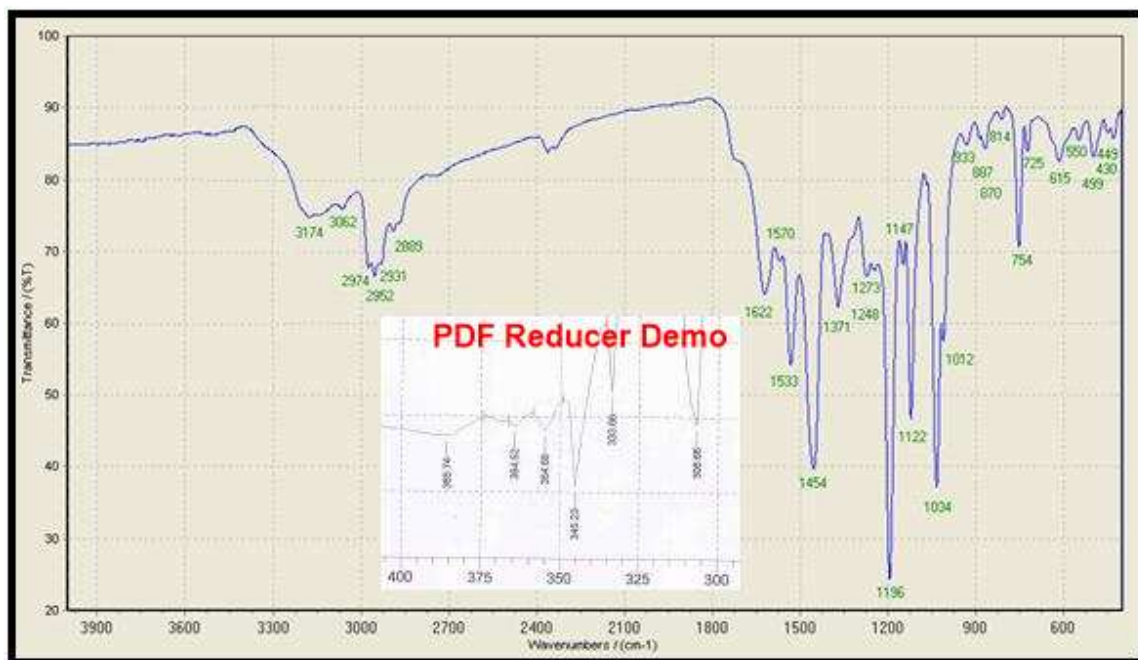
Figure(3.29): FT-IR spectrum of [Cu(L^2)$_2$] complex.
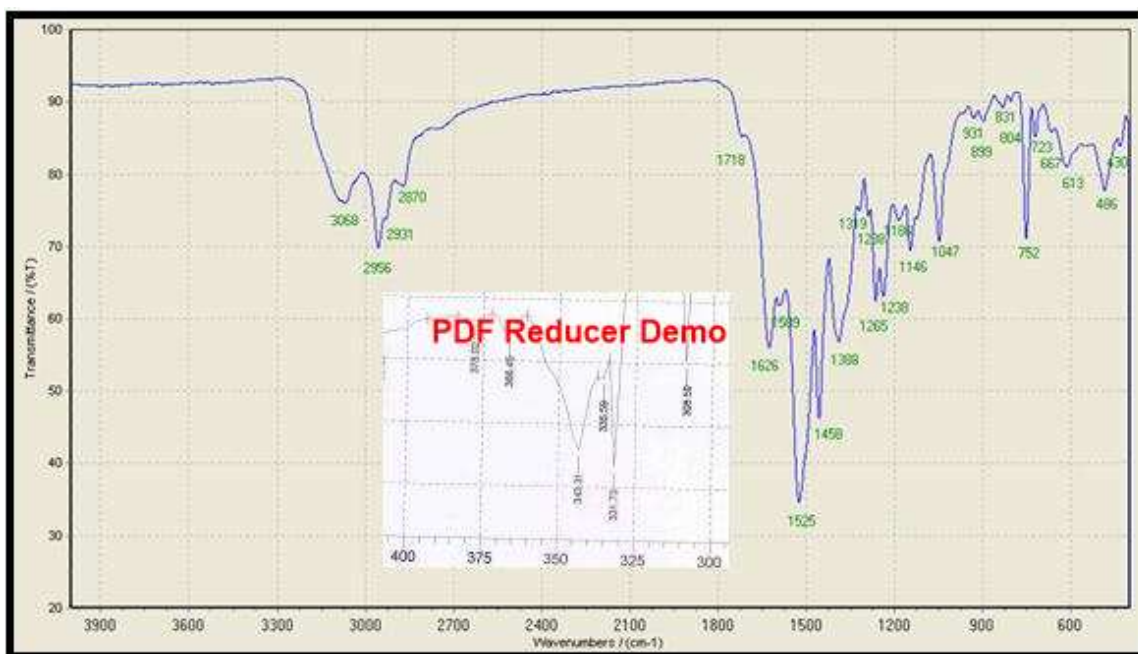
Figure(3.30): FT-IR spectrum of [Zn(L^2)$_2$] complex.

110
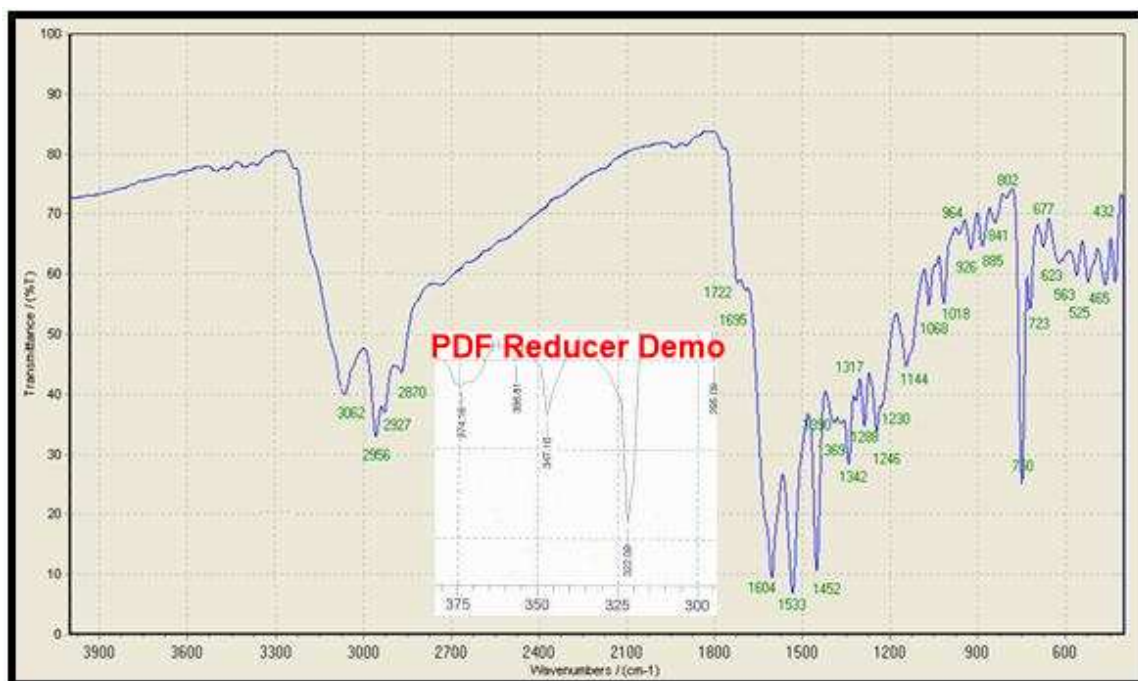
Figure(3.31): FT-IR spectrum of [Pd(L^2)$_2$] complex.
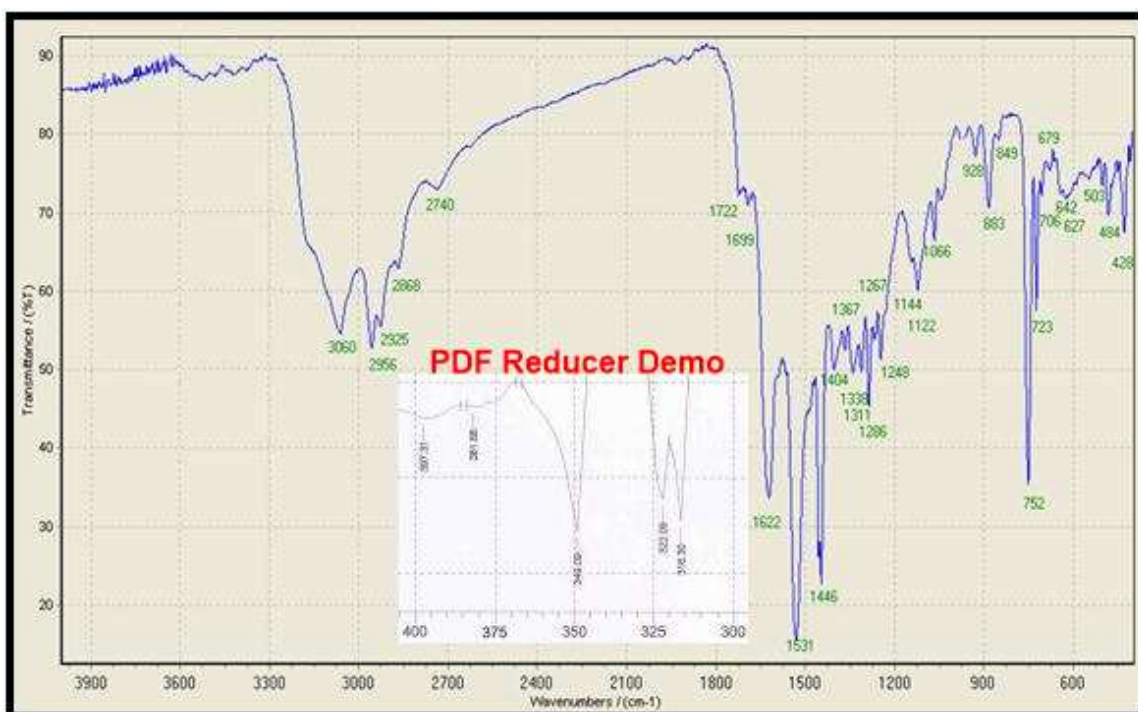
Figure(3.32): FT-IR spectrum of [Cd(L^2)$_2$] complex.

111

Compound	$\nu_{aro.}$ (C-H)	$\nu_{alph.}$ (C-H)	ν_{ket} (C=O)	$\nu_{vin.}$ (C=C)	ν (N-CS$_2$)	ν (C-N)	ν (C-S)$_{sy.}$ ν (C-S)$_{asy.}$	ν (M-S)
KL^2	3068(w)	2954(m)	1724(w)	1535(w)	1448(w)	1147(s)	1072(w) 1018	-
[Mn(L^2)$_2$]	3060(w)	2956(m)	1714(w)	1529(s)	1448(s)	1149(w)	1119(s) 1018(m)	368(w) ,339(w)
[Co(L^2)$_2$]	3064(w)	2956(m)	1714(w)	1520(w)	1452(w)	1151(s)	1066(w) 930(s)	364(w) ,333(w)
[Ni(L^2)$_2$]	3100(w)	2954(m)	1720(w)	1531(w)	1448(w)	1141(s)	1016(s) 1003(w)	364(w) ,325(w)
[Cu(L^2)$_2$]	3062(w)	2952(w)	1710(w)	1533(w)	1454(w)	1196(w)	1034(s) 1012(m)	354(w) ,333(w)
[Zn(L^2)$_2$]	3068(w)	2956(m)	1718(w)	1525(w)	1458(w)	1146(s)	1047(w) 931(w)	343(w) ,331(w)
[Pd(L^2)$_2$]	3062(w)	2956(m)	1722(w)	1533(w)	1452(w)	1144(s)	1068(w) 1018(s)	347(w) ,322(w)
[Cd(L^2)$_2$]	3060(w)	2956(m)	1722(w)	1531(w)	1446(s)	1144(s)	1066(m) 1043(s)	349(w) ,322(w)

(3.2.7.3) FT-IR spectral data for of [Mn(L^3)$_2$] [Co(L^3)$_2$], [Ni(L^3)$_2$], [Cu(L^3)$_2$], [Zn(L^3)$_2$] , [Pd(L^3)$_2$] and [Cd(L^3)$_2$] complexes.

(3.2.7.3.1) FT-IR spectrum for [Ni(L^3)$_2$].

The FT-IR spectrum of [Ni(L^3)$_2$], Fig.(3.35), exhibits bands related to the ligand with the appropriate shift due to complex formation. The ν(N-H) stretching for the all complexes has been detected around 3359-3435 cm^{-1}, compared with that found at 3363cm^{-1} in the spectrum of ligand. The bands observed at (1643 and 1564) cm^{-1}, can be attributed to the bending band for δ(N-H) and ν_{ar}(C=C). The spectrum displays band at 1491cm^1, which is related to ν(N-CS$_2$) mode, compared with that detected in the ligand at 1462cm^{-1}, indicating an increase of the carbon-

nitrogen double bond character that is caused by electron delocalization towards metal centre upon coordination[136]. The spectrum showed asymmetric $v(CS_2)$ and symmetric $v(CS_2)$ bands which appear at (1018 and 920) cm^{-1}, respectively . At lower frequency complexes [Ni(L^3)$_2$],Fig.(3.35) and [Zn(L^3)]$_2$, Fig.(3.37) exhibited two bands at (364, 331 and 366, 331)cm^{-1}, respectively that are assigned to the v(M-S) vibrational mode, and supporting the bidentate chelation mode of the ligand [143]. The FT-IR spectra for [Mn(L^3)$_2$], [Co(L^3)$_2$], [Cu(L^3)$_2$] ,[Zn(L^3)$_2$], [Pd(L^3)$_2$] and [Cd(L^3)$_2$] complexes, Fig.((3.33),(3.34), (3.36-3.39) show similar trend to that of the [Ni(L^3)$_2$] complex and same reasoning could be used to interpret the spectra. The structurally important FTIR absorption bands of the prepared complexes are summarised in Table (3.28).
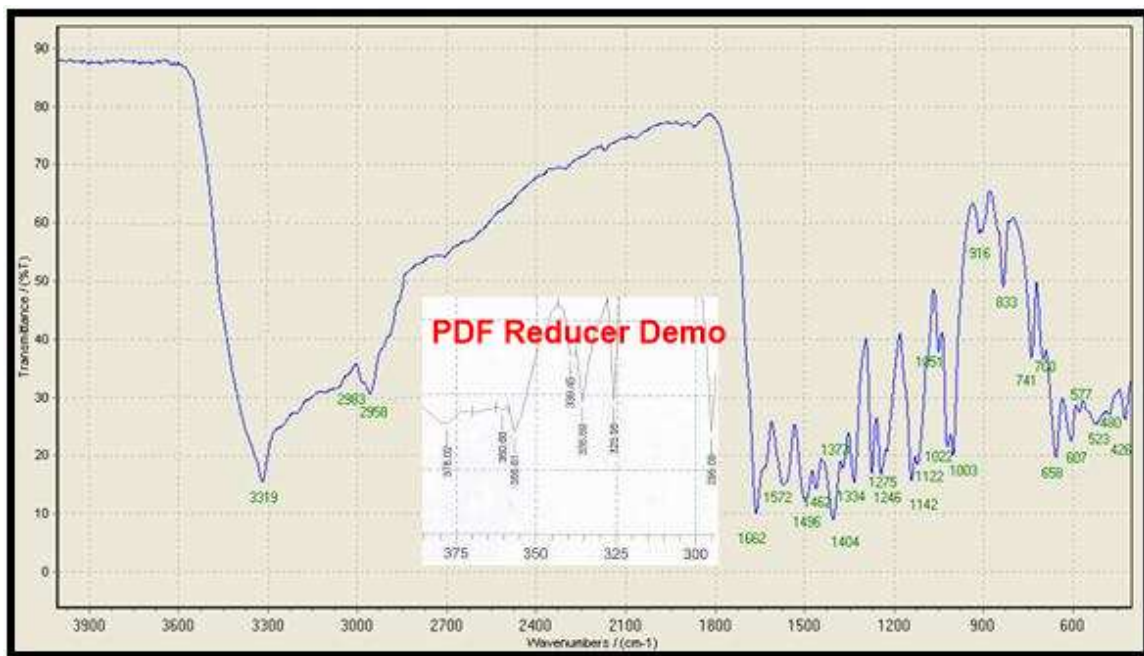
Figure(3.33): FT-IR spectrum of [Mn(L^3)$_2$] complex.
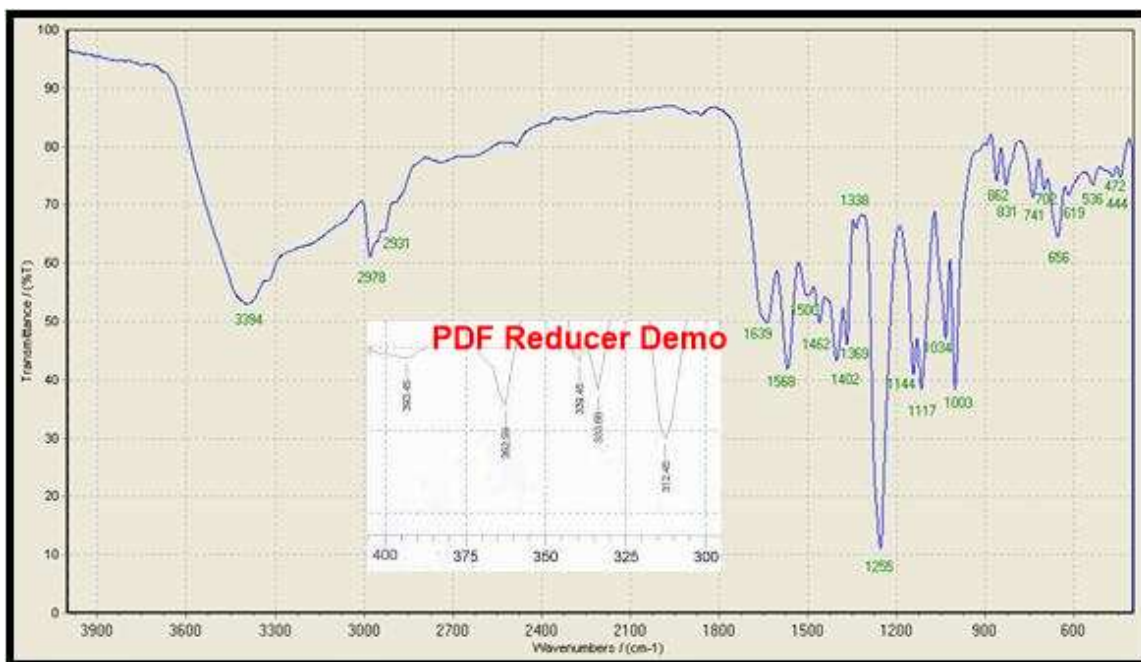
Figure(3.34): FT-IR spectrum of [Co(L^3)$_2$] complex.
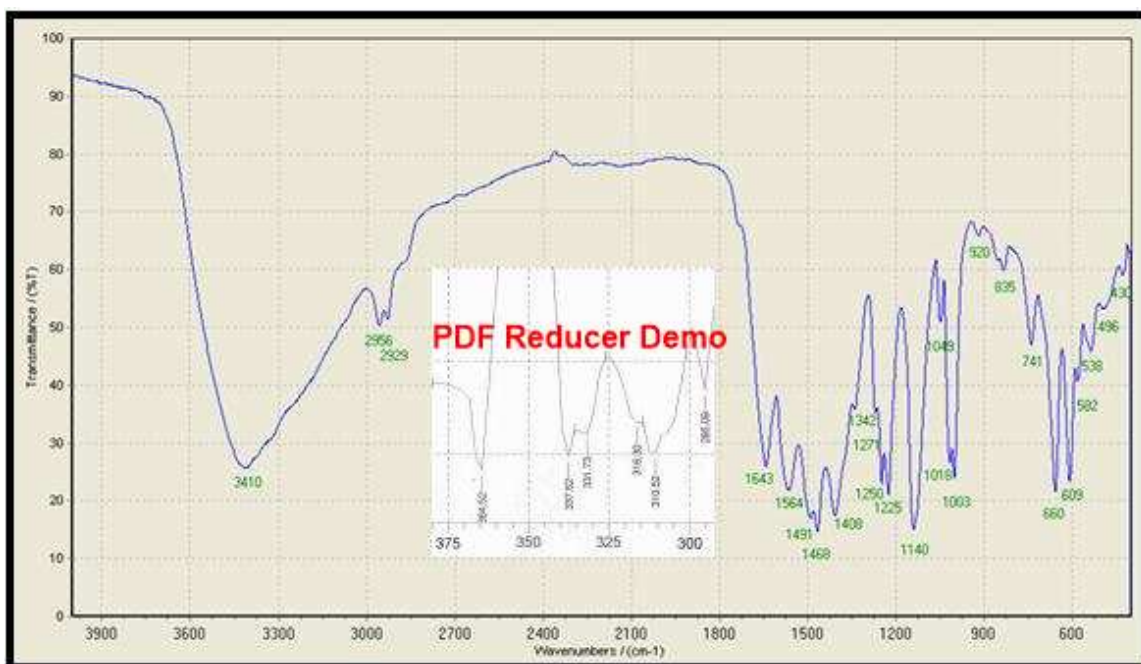
Figure(3.35): FT-IR spectrum of [Ni(L^3)$_2$] complex.
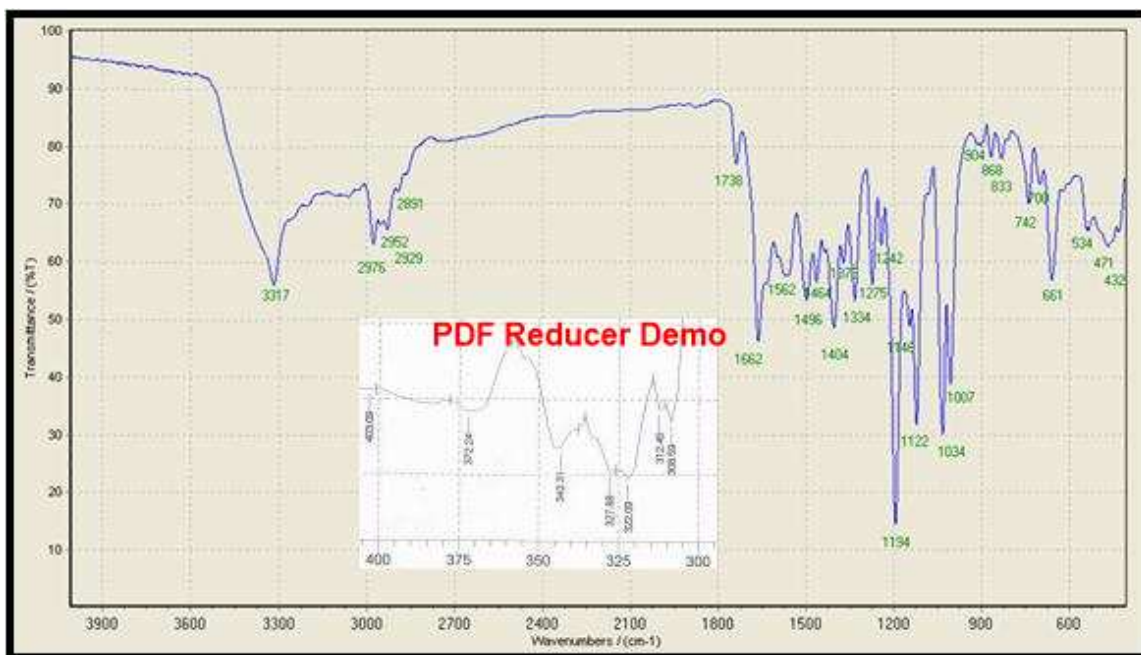
Figure(3.36): FT-IR spectrum of [Cu(L³)₂] complex.
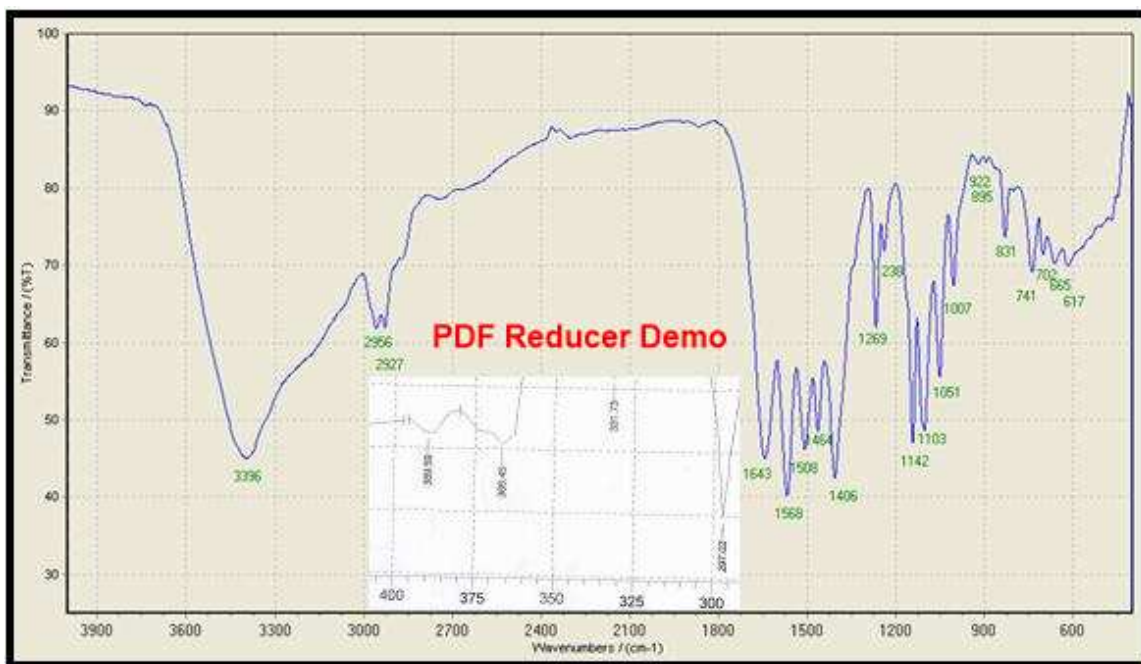
Figure(3.37): FT-IR spectrum of [Zn(L³)₂] complex.
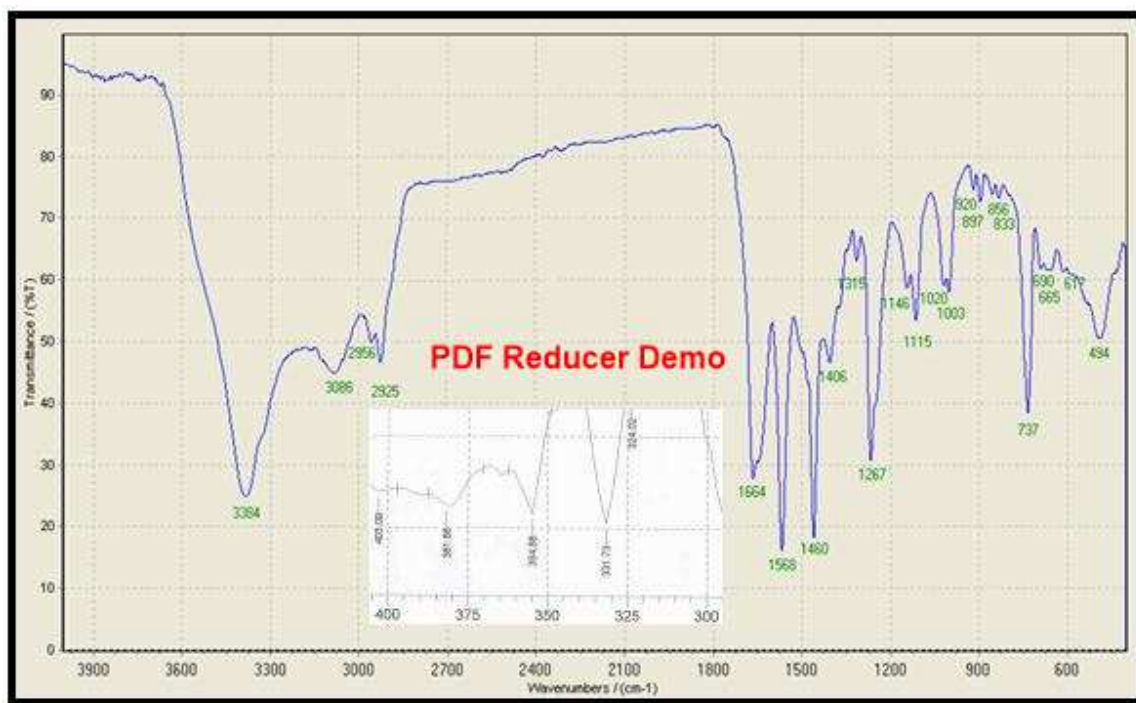
Figure(3.38): FT-IR spectrum of [Pd(L^3)$_2$] complex.
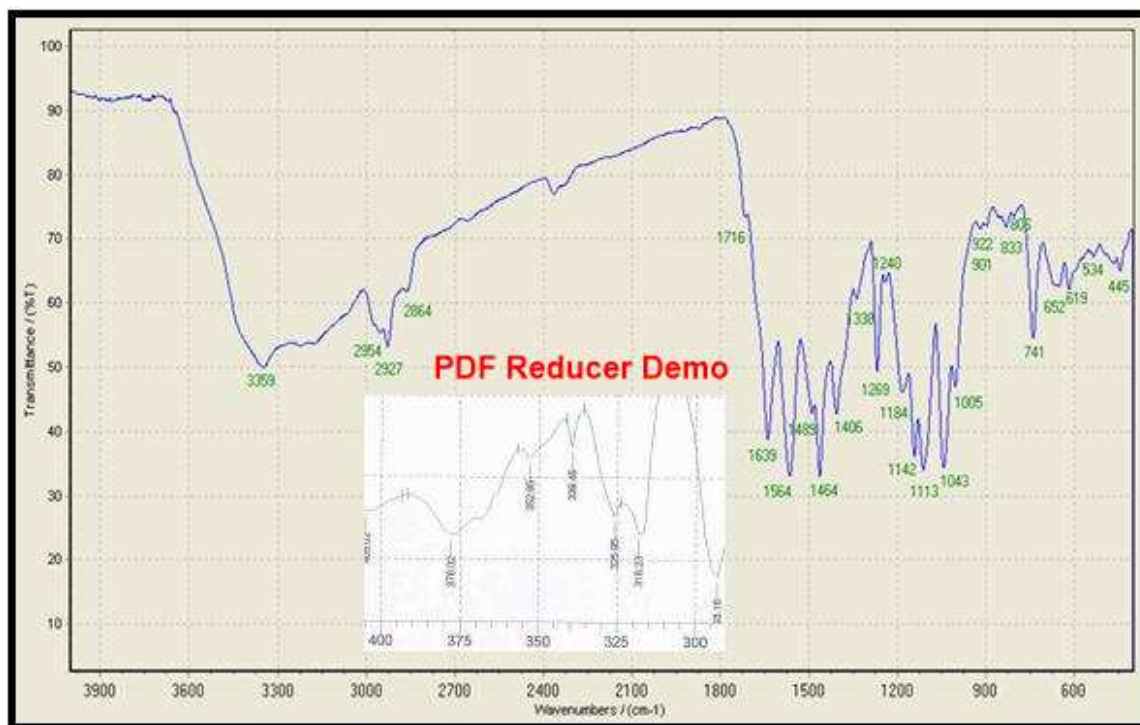
Figure(3.39): FT-IR spectrum of [Cd(L^3)$_2$] complex.

Table(3.28):FT-IR spectral data (wave number)cm^{-1} of KL^3 and its complexes.

Compound	ν (N-H)	$\nu_{alph.}$ (C-H)	ν (C=O)	ν (N-H)	$\nu_{vin.}$ (C=C)	ν (N-CS$_2$).	ν (C-N)	ν (C-S)$_{sy.}$ ν (C-S)$_{asy.}$	ν (M-S)
KL^3	3363(m)	2998-2875	1645(w)	1643(w)	1568(w)	1462(w)	1142(s)	1049-1005(w)	-
[Mn(L^3)$_2$]	3400(m)	2958(w)	-	1662(w)	1572(s)	1496(s)	1142(w)	1051(m)-1003(s)	295(w) ,235(w)
[Co(L^3)$_2$]	3394(m)	2978(w)	-	1639(w)	1568(w)	1500(w)	1144(s)	1034(w)-1003(s)	333(w) ,312(w)
[Ni(L^3)$_2$]	3410(m)	2956(w)	-	1643(w)	1564(w)	1491(w)	1140(s)	1018(s)-1003(w)	364(w) ,331(w)
[Cu(L^3)$_2$]	3435(w)	2976(w)	1738(w)	1662(w)	1562(w)	1496(w)	1194(w)	1034(s)-1007(m)	343(w) ,322(w)
[Zn(L^3)$_2$]	3396(m)	2956(w)	-	1643(w)	1568(w)	1508(w)	1142(s)	1051(w)-1007(w)	366(w) ,331(w)
[Pd(L^3)$_2$]	3384(m)	2956(w)	1664(w)	1664(w)	1568(w)	1460(w)	1146(s)	1020(w)-1003(s)	354(w) ,331
[Cd(L^3)$_2$]	3359(m)	2954(w)	1716(w)	1639(w)	1564(w)	1464(s)	1142(s)	1043(m)-1005(s)	318(w) ,293

(3.2.8) FT-IR Spectral data for the mixed ligand complexes:-

(3.2.8.1) FT-IR Spectrum data for 3-aminophenol (P).

The spectrum of the 3-amino phenol [144], Fig.(3.40) displays one band at 3419 cm^{-1} is due to υ(OH) stretching vibration. The two bands at (3359 and 3296) cm^{-1} are due to υ_{as}(NH$_2$) and υ_s(NH$_2$) stretching vibration respectively . On the other hand the spectrum displayed band at 3026 cm^{-1} is due to υ(C-H) aromatic stretching vibration. The band at 1599 cm^{-1} was assigned to the δ (N-H) bending vibration[145-147]. The characteristic bands are summarized in Table(3.29).
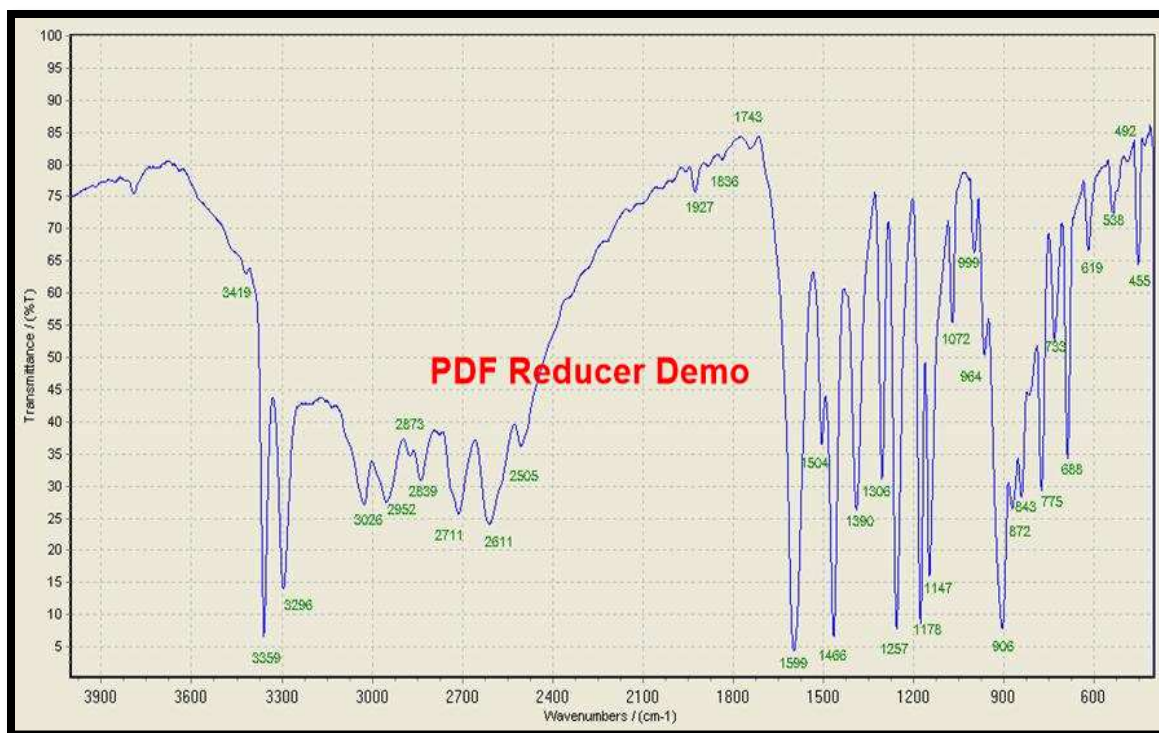
Figure(3.40) FT-IR spectrum of 3-amino phenol (P)

(3.2.8.1.2) FT-IR of [Co(L^1)(P)],[Ni(L^1)(P)] and [Zn(L^1)(P)] complexes.

The assignment of the characteristic bands FT-IR spectrum for the ligand KL^1 are summarized in Table(3.25) Fig.(3.16), the FT-IR spectra for complexes [Co(L^1)(P)],[Ni(L^1)(P)] and [Zn(L^1)(P)] are shown in Fig.(3.41), (3.42) and (3.43) respectively. The assignment of the characteristic bands are summarized in Table(3.29). The FT-IR spectrum for the 3-aminophenol (P) which exhibits band at 3419 cm^{-1} is due to the υ(O-H) group, on complexation the band υ(O-H) of the 3-amino phenol has been disappeared for complexes [Co(L^1)(P)],[Ni(L^1)(P)] and [Zn(L^1)(P)], showing that the coordination is through the oxygen atom of hydroxyl group. Also the FT-IR spectrum for the 3-amino phenol which exhibits bands at (3359 and 3296) cm^{-1} are due to the υ_{as}(NH$_2$) and υ_{s}(NH$_2$) groups stretching vibration, these bands have been shifted to lower frequency ((3217,3057),(3221,3024) and (3219,3057)) cm^{-1} for complexes

118

[Co(L^1)(P)],[Ni(L^1)(P)] and [Zn(L^1)(P)] respectively[149], showing that the coordination is through the nitrogen atom of amine group and that the coordination is through the oxygen atom of hydroxyl group. This reduced shift can be explained to the delocalization of the metal electron density in to the ligand π-system [150,151] (HOMO→LUMO) ,(where HOMO: Highest Occupied Molecular Orbital , LUMO: Lowest Unoccupied Molecular Orbital). The new bands at (609, 526) ,(530,499) and (532,501) cm^{-1} were assigned to υ(M-N) for compounds [Co(L^1)(P)] ,[Ni(L^1)(P)] and [Zn(L^1)(P)] respectively[137], indicating that to the nitrogen of (NH$_2$) group of 3-amino phenol are involved in coordination with metal ions. Finally the new bands at ((453),(455,426) and (457,426)) cm^{-1} were assigned to the υ(M-O) for complexes [Co(L^1)(P)], [Ni(L^1)(P)] and [Zn(L^1)(P)] respectively[152], indicating that the oxygen of hydroxyl group of 3-amino phenol are   involved in coordination with metal ions.

 (3.2.8.1.3) FT-IR of [Co(L^2)(P)] ,[Ni(L^2)(P)], [Zn(L^2)(P)], [Co(L^3)(P)], [Ni(L^3)(P)] and [Zn(L^3)(P)] complexes.

The assignment of the characteristic bands FT-IR spectra for these complexes are summarized in Table(3.29), The FT-IR spectra for complexes are shown in Fig.(3.44)-(3.49).
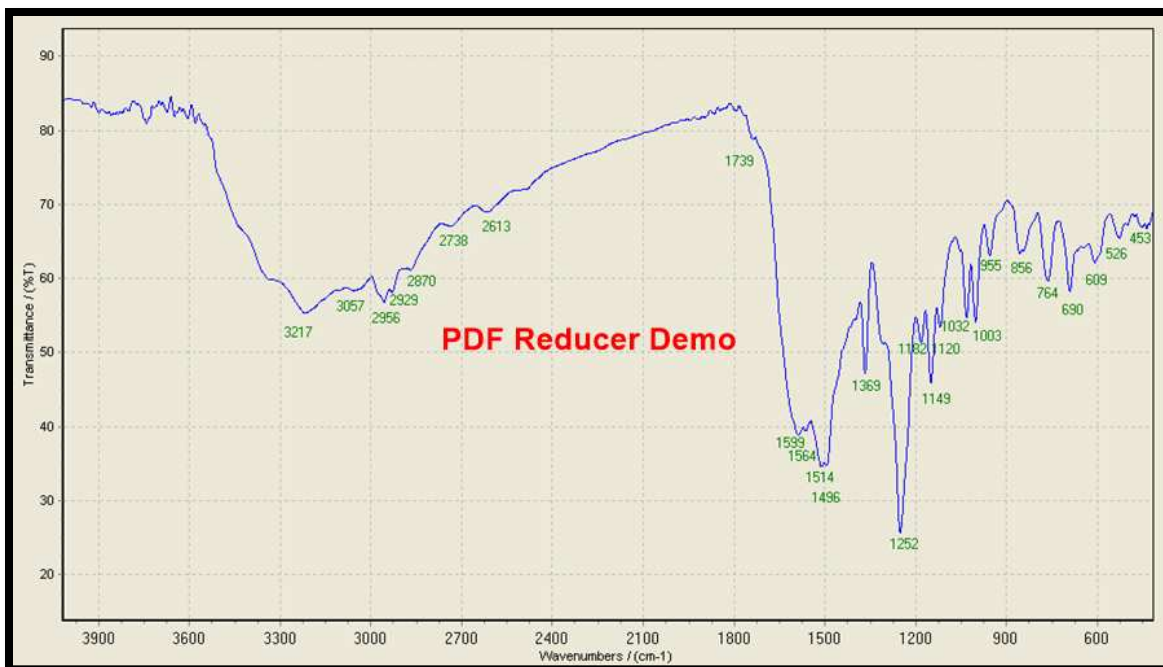
Figure(3.41): FT-IR spectrum of [Co(L^1)(P)] complex.
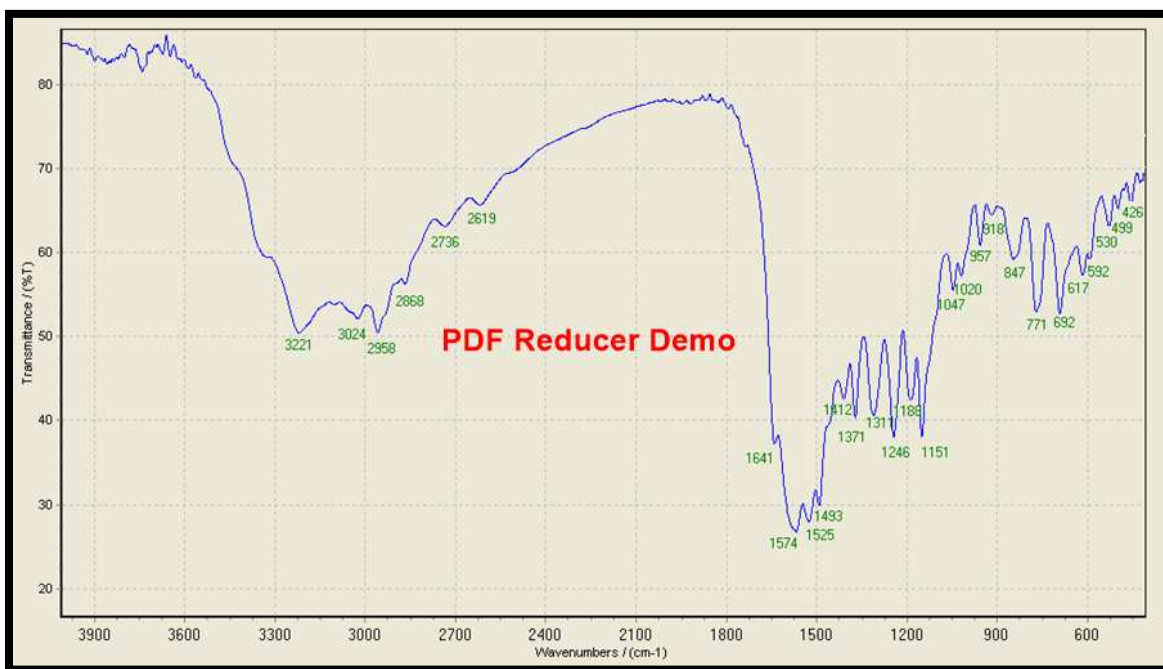
Figure(3.42): FT-IR spectrum of [Ni(L^1)(P)] complex.
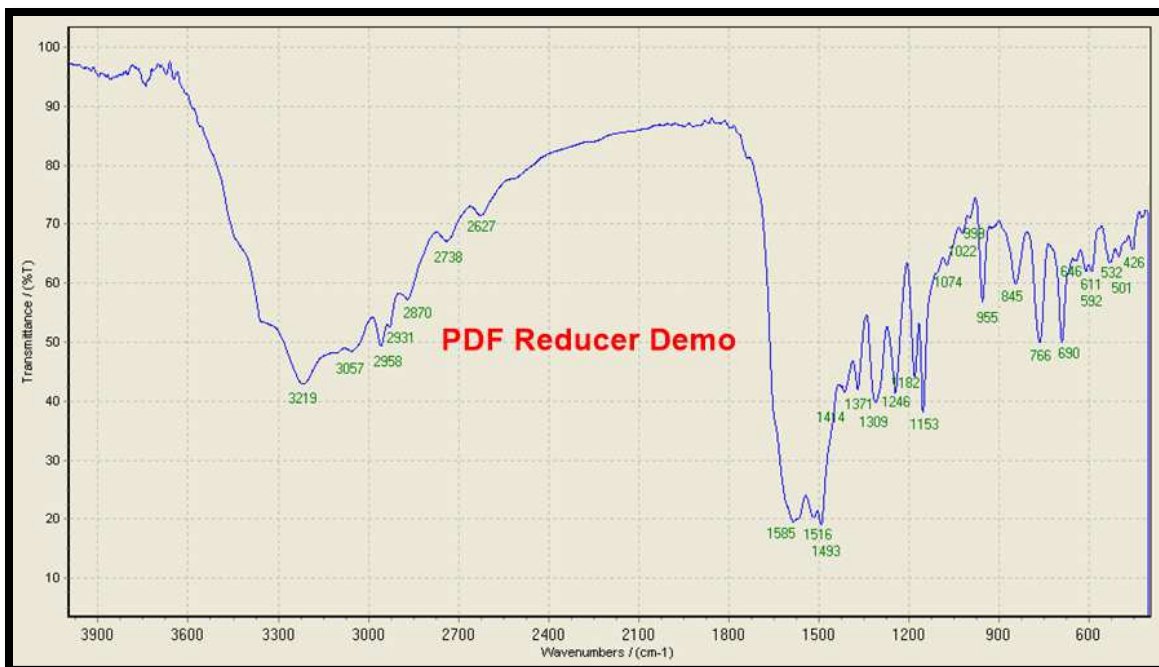
Figure(3.43): FT-IR spectrum of [Zn(L^1)(P)] complex.
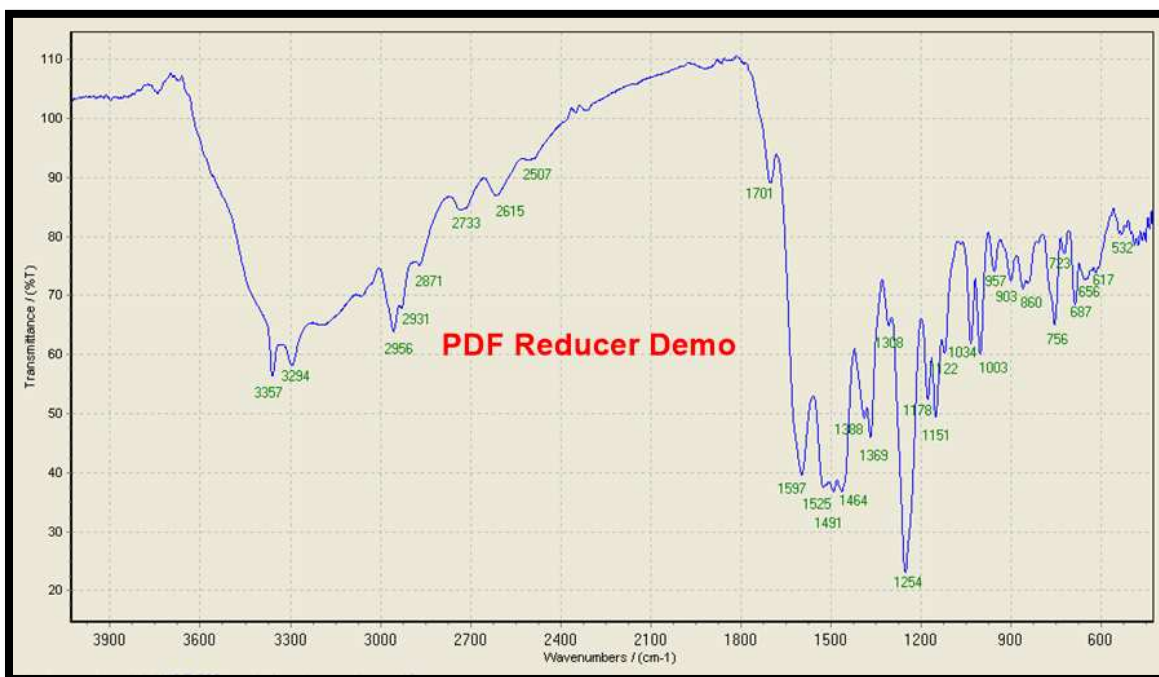
Figure(3.44): FT-IR spectrum of [Co(L^2)(P)] complex.
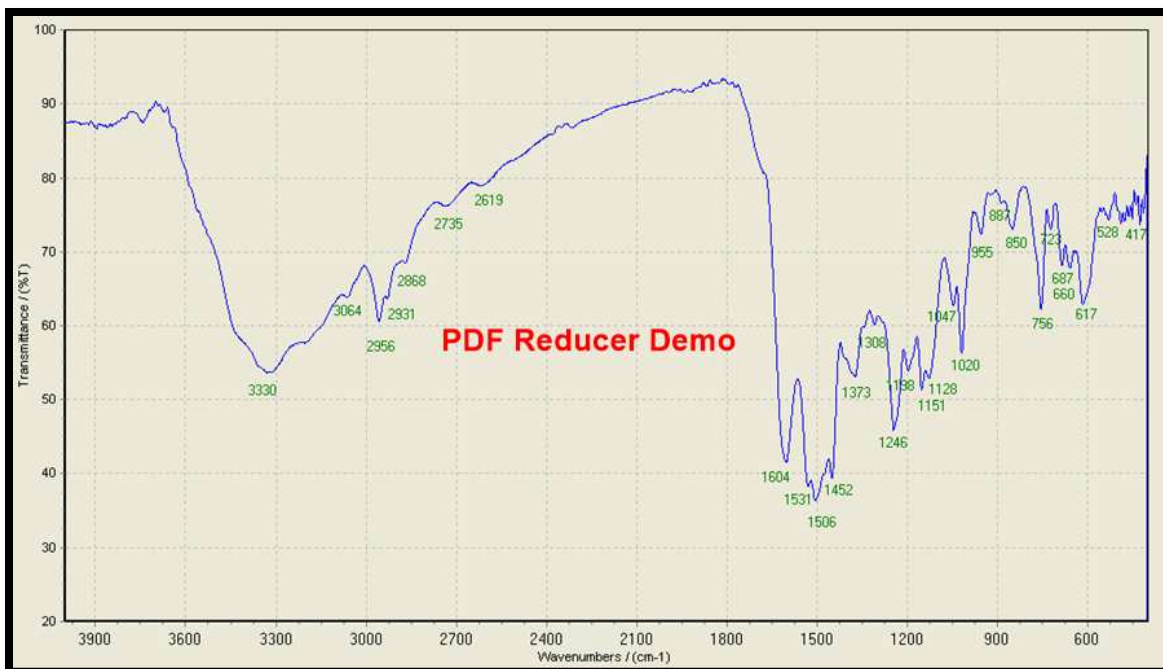
Figure(3.45): FT-IR spectrum of [Ni(L^2)(P)] complex.
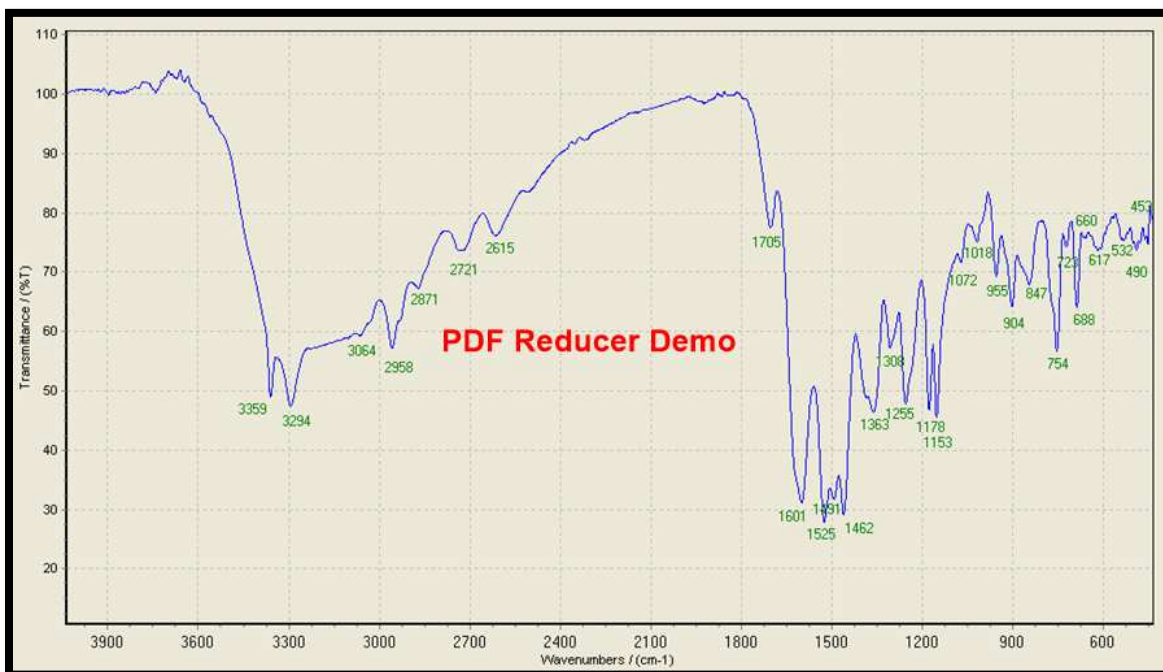
Figure(3.46): FT-IR spectrum of [Zn(L^2)(P)] complex.
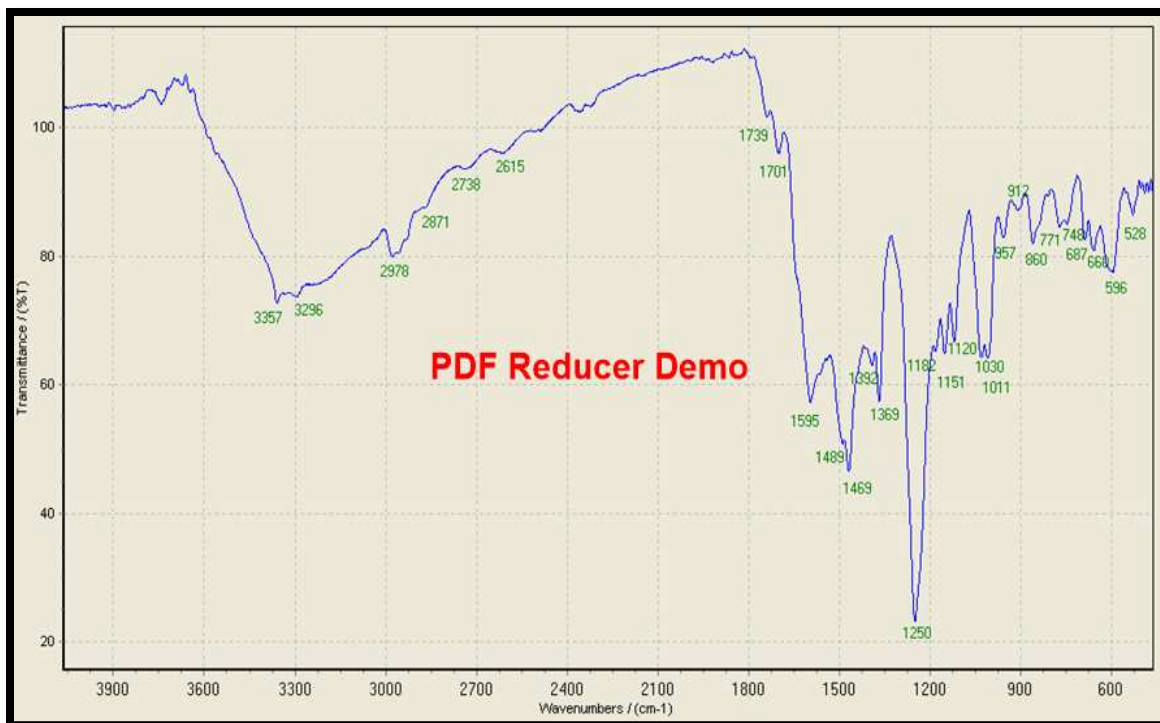
Figure(3.47): FT-IR spectrum of [Co(L^3)(P)] complex.
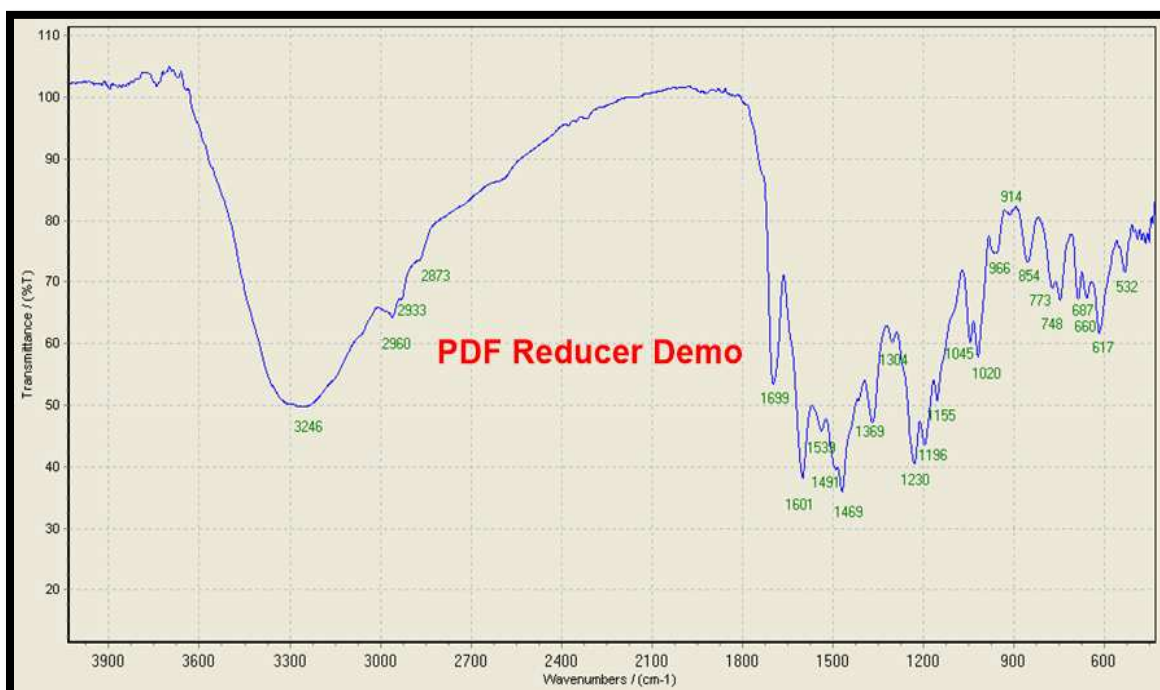
Figure(3.48): FT-IR spectrum of [Ni(L^3)(P)] complex.
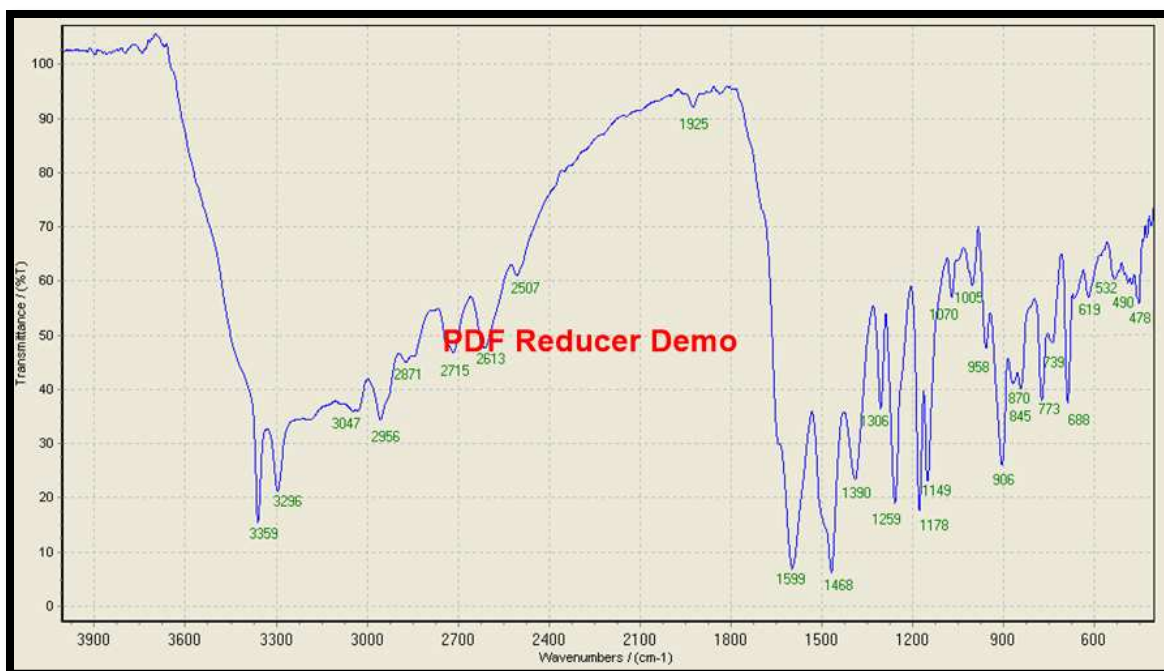
Figure(3.49): FT-IR spectrum of [Zn(L^3)(P)] complex.

Table(3.29): FT-IR spectral data (wave number)cm^{-1} of the mixed-ligand complexes [M(L^n)(P)] (where n=1,2,3)with some metal ions.

Compound	v (O-H)	v_{as}(NH$_2$) v_{sy}(NH$_2$)	v (C-H) armo. v (C-H)$_{vin.}$	v (C-H) alph	v (C=C)$_{armo.}$ v (C=C)$_{vin}$	v (C-N) v (C-O)	v (M-N)	v (M-O)
(P)	3419(w)	3359(w) 3296(m)	3026(w)	2952(m) 2873(m)	1504(m)	1306(m) 1257(w)	-	-
[Co(L^1)(P)]	-	3217(m)	3057(w)	2956(w) 2870(m)	1496(w) 1514(m)	1252(w) 1182(m)	609(w) 526(m)	453(w)
[Ni(L^1)(P)]	-	3221(m)	3024(w)	2958(w) 2870(m)	1493(s) 1525(m)	1246(w) 1188(w)	530(w) 499(w)	455(w) 426(m)
[Zn(L^1)(P)]	-	3219(m)	3057(w)	2958(w) 2870(m)	1493(s) 1516(m)	1246(m) 1182(w)	532(m) 501(w)	457(w) 426(m)
[Co(L^2)(P)]	-	3357(m) 3294(m)	-	2956(w) 2871(m)	1491(w) 1525(m)	1254(w) 1178(m)	532(m)	450(w)
[Ni(L^2)(P)]	-	3330(m)	3064(w)	2956(w) 2868(w)	1452(w) 1506(w)	1246(w) 1198(w)	528(w)	417(m)

124

[Zn(L²)(P)]	-	3359(m) 3294(w)	3064(w)	2958(w) 2871(m)	1491(s) 1525(w)	1255(w) 1178(m)	532(w)	490(w) 453(w)
[Co(L³)(P)]	-	3357(w) 3296(w)	-	2978(w) 2871(w)	1469(m) 1489(w)	1250(w) 1182(m)	596(m)	528(w)
[Ni(L³)(P)]	-	3246(m)	-	2960(m) 2873(w)	1469(m) 1491(w)	1230(m) 1196(m)	532(w)	450(m)
[Zn(L³)(P)]	-	3359(w) 3296(m)	3047(w)	2956(w) 2871(m)	1468(s)	1259(w) 1178(m)	532(w) 490(m)	478(w)

(3.2.8.2) FT-IR spectrum for 8-hydroxyquinoline (Q).

The spectrum of the 8-hydroxyquinoline , Fig.(3.50) displays a band at 3159 cm^{-1} is due to υ(OH) stretching vibration. The band at 3047 cm^{-1} is due to υ(C-H) aromatic stretching vibration. The band at 1576 cm^{-1} was assigned to the υ(C=N) stretching vibration. On the other hand the spectrum displayed band 1504 cm^{-1} is due to the υ(C=C) aromatic stretching vibration [153-158]. The characteristic bands are summarized in Table (3.30)`` .
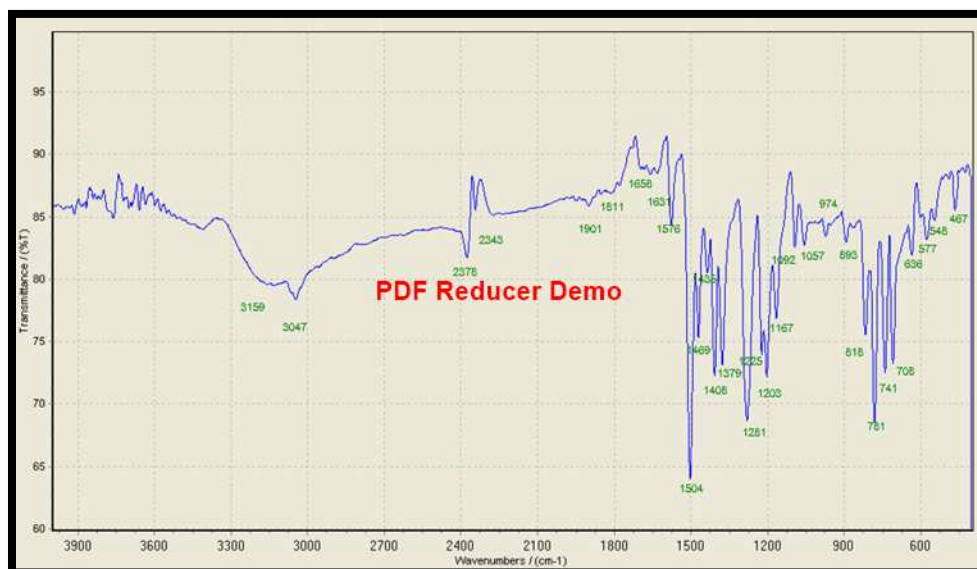
Figure(3.50) FT-IR spectrum of 8-hydroxyquinoline (Q)

(3.2.8.2.1) FT-IR of [Co(L[1])(Q)],[Ni(L[1])(Q)] and [Zn(L[1])(Q)] complexes.

The assignment of the characteristic bands FT-IR spectrum for the ligand KL[1] are summarized in Table(3.25) Fig.(3.16), the FT-IR spectra for complexes [Co(L[1])(Q)],[Ni(L[1])(Q)] and [Zn(L[1])(Q)] are shown in Fig.(3.51), (3.52) and (3.53) respectively. The assignment of the characteristic bands are summarized in Table(3.30). The FT-IR spectrum for the 8-hydroxy quinoline, which exhibits band at 3159 cm^{-1} is due to the υ(O-H) group stretching vibration, on complexation these bands have been disappeared for complexes [Co(L[1])(Q)],[Ni(L[1])(Q)] and [Zn(L[1])(Q)], showing that the coordination is through the oxygen atom of the phenoxy group. The band at 1576 cm^{-1} for υ(C=N) of 8-hydroxyquinoline, this band has been shifted to higher frequency ((1581),(1581) and (1579)) cm^{-1} for complexes [Co(L[1]) (Q)] ,[Ni(L[1])(Q)] and [Zn(L[1])(Q)] respectively[159], showing that the coordination is through the nitrogen atom of (C=N) group. This shifting can be explained to the delocalization of the metal electron density in to the ligand π-system[150,151] (HOMO→LUMO),(where HOMO: Highest Occupied Molecular Orbital, LUMO: Lowest Unoccupied Molecular Orbital). The new bands at ((526,503),(550,523) and (563,505)) cm^{-1} were assigned to υ(M-N) for complexes [Co(L[1])(Q)] ,[Ni(L[1])(Q)] and [Zn(L[1]) (Q)], indicating that to the nitrogen of ligands are involved in coordination with metal ions. The new bands at ((447),(498) and (447)) cm^{-1} were assigned to υ(M-O) for complexes [Co(L[1])(Q)],[Ni(L[1])(Q)] and [Zn(L[1])(Q)] [137] respectively, indicating that the oxygen of hydroxyl group of 8-hydroxyquinoline are involved in coordination with metal ions.

(3.2.8.2.2) FT-IR of [Co(L^2)(Q)] ,[Ni(L^2)(Q)], [Zn(L^2)(Q)], [Co(L^3)(Q)], [Ni(L^3)(Q)] and [Zn(L^3)(Q)] complexes.

The assignment of the characteristic bands FT-IR spectra for these complexes are summarized in Table(3.30), The FT-IR spectra for complexes are shown in Fig.(3.54)-(3.59).
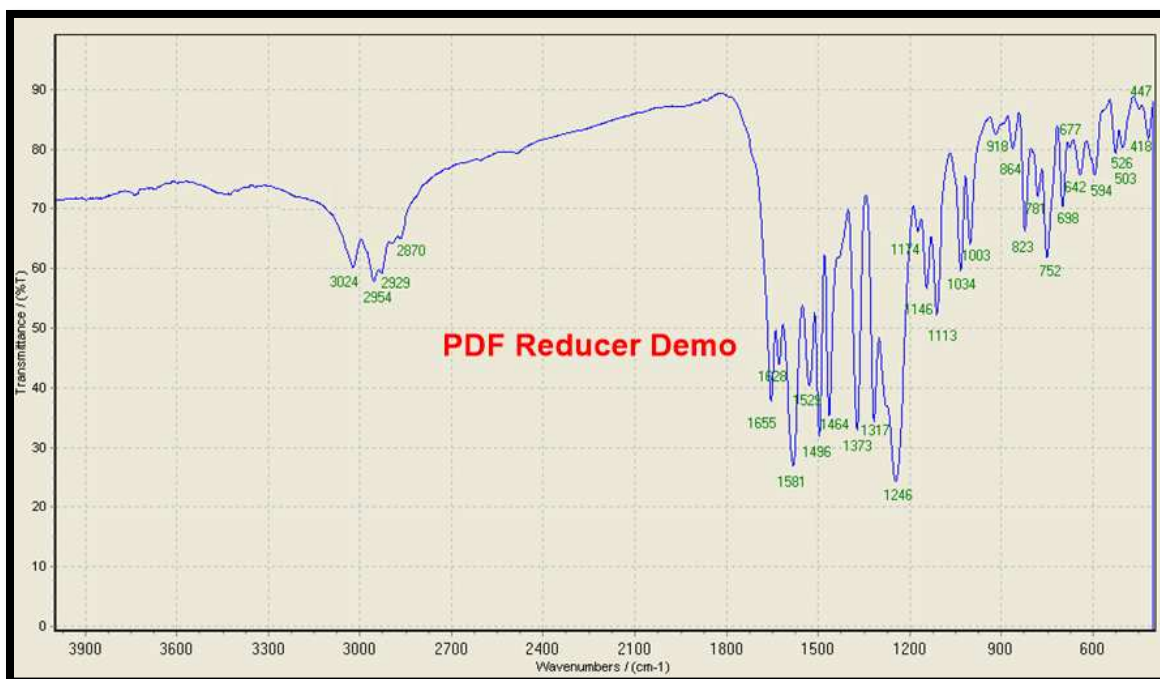
Figure(3.51): FT-IR spectrum of [Co(L^1)(Q)] complex.
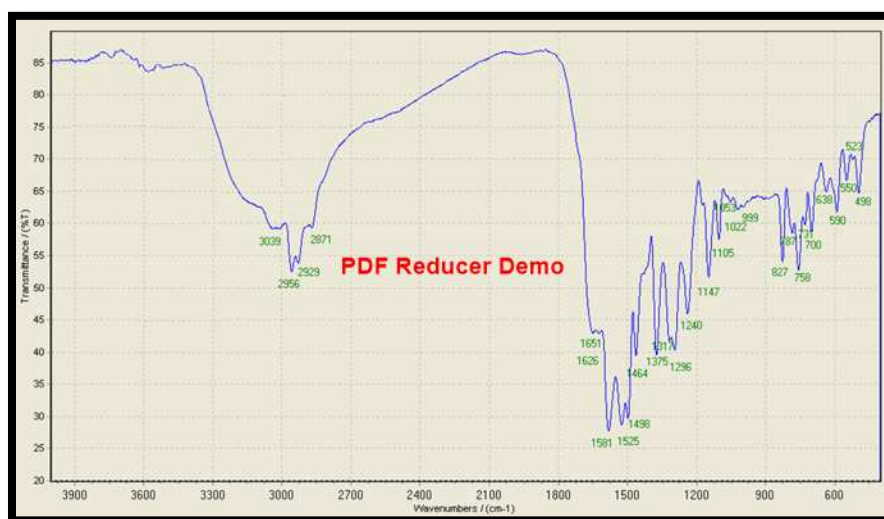
Figure(3.52): FT-IR spectrum of [Ni(L^1)(Q)] complex.

127
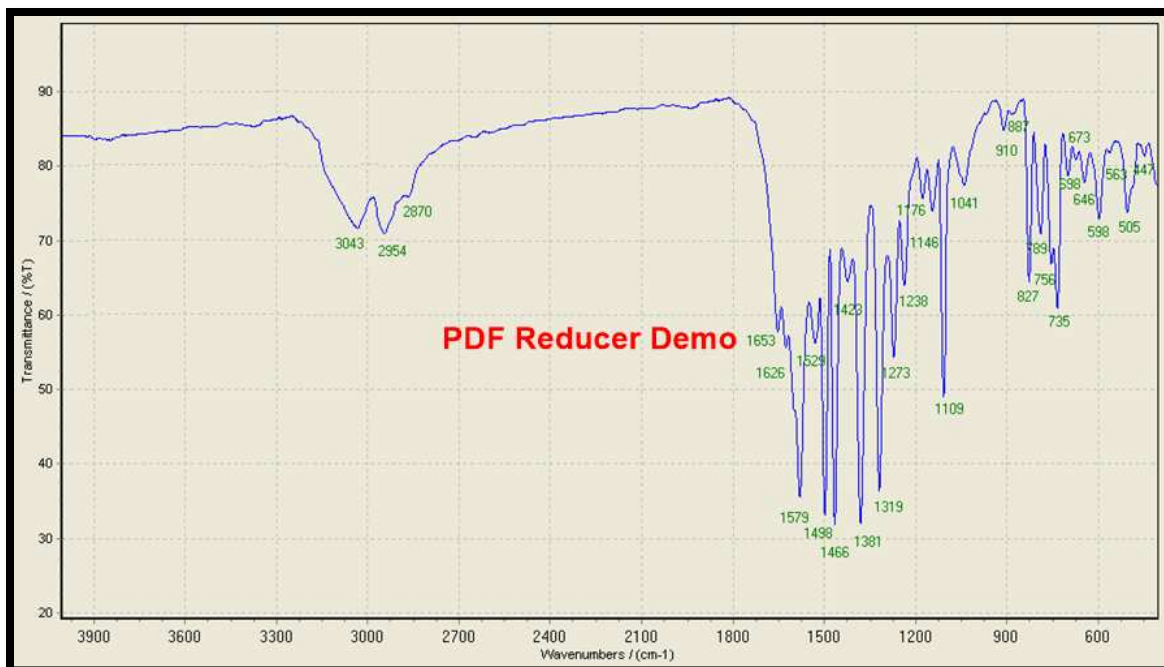
Figure(3.53): FT-IR spectrum of [Zn(L^1)(Q)] complex.
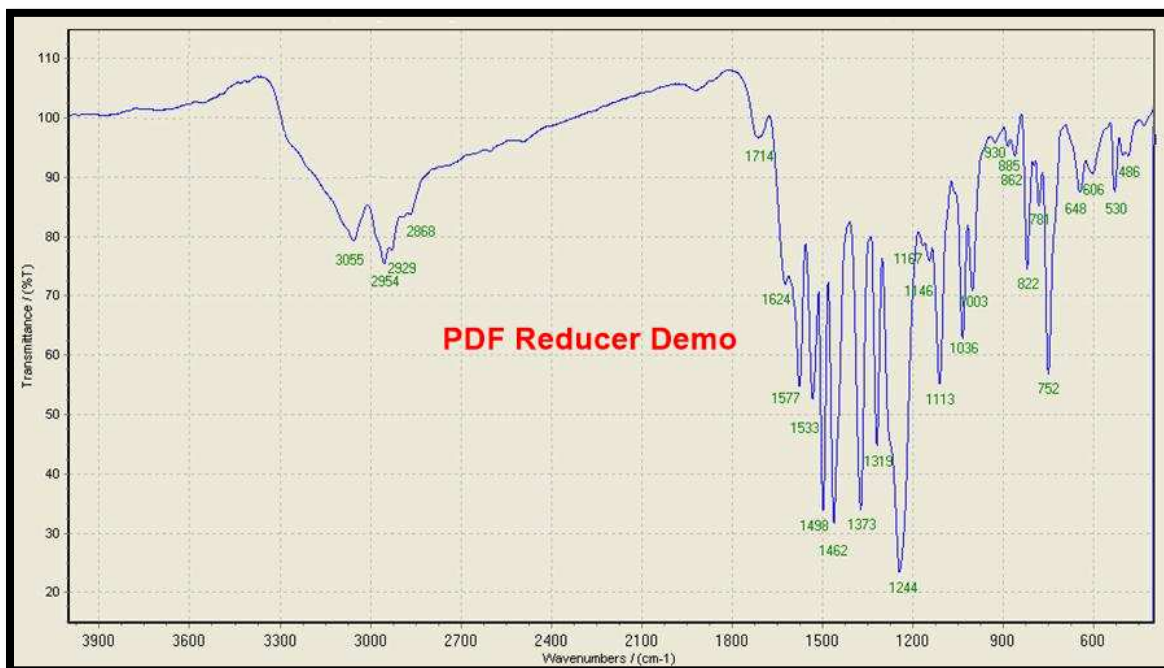
Figure(3.54): FT-IR spectrum of [Co(L^2)(Q)] complex.

128
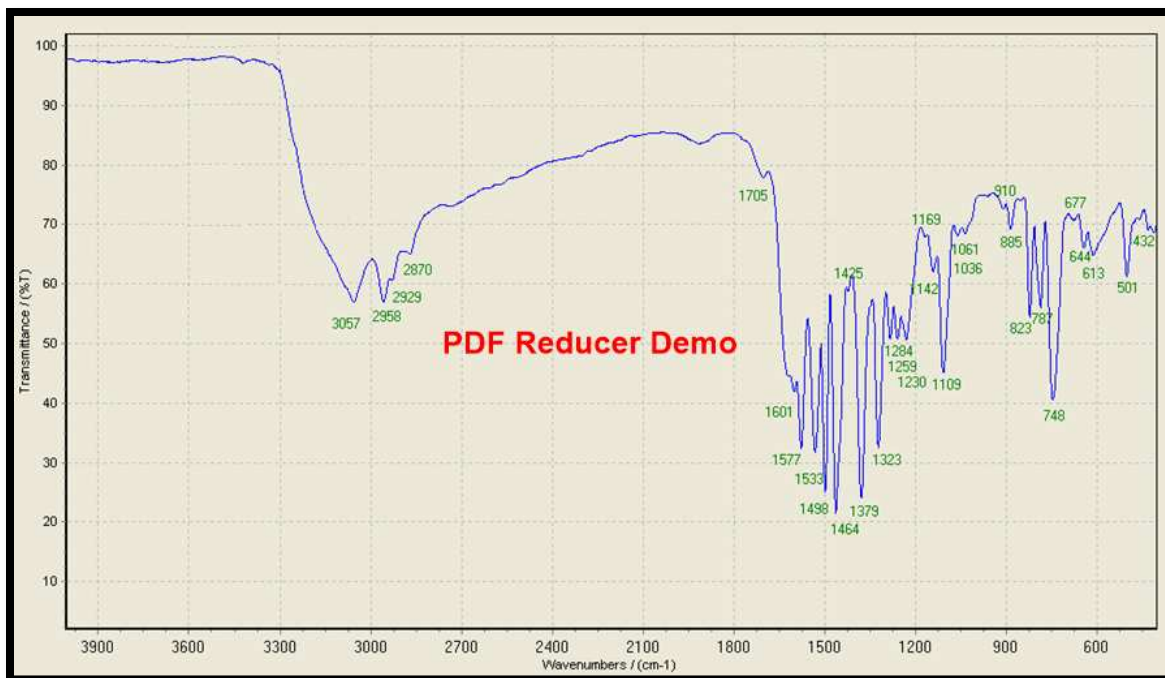
Figure(3.55): FT-IR spectrum of [Ni(L^2)(Q)] complex.
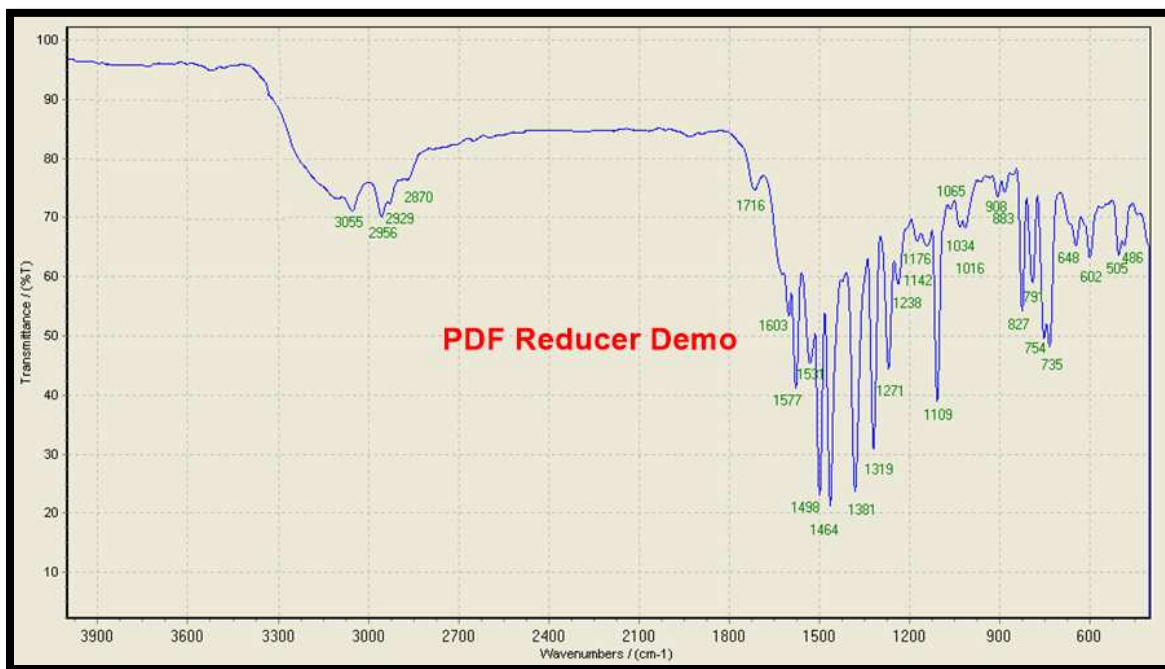
Figure(3.56): FT-IR spectrum of [Zn(L^2)(Q)] complex.

129
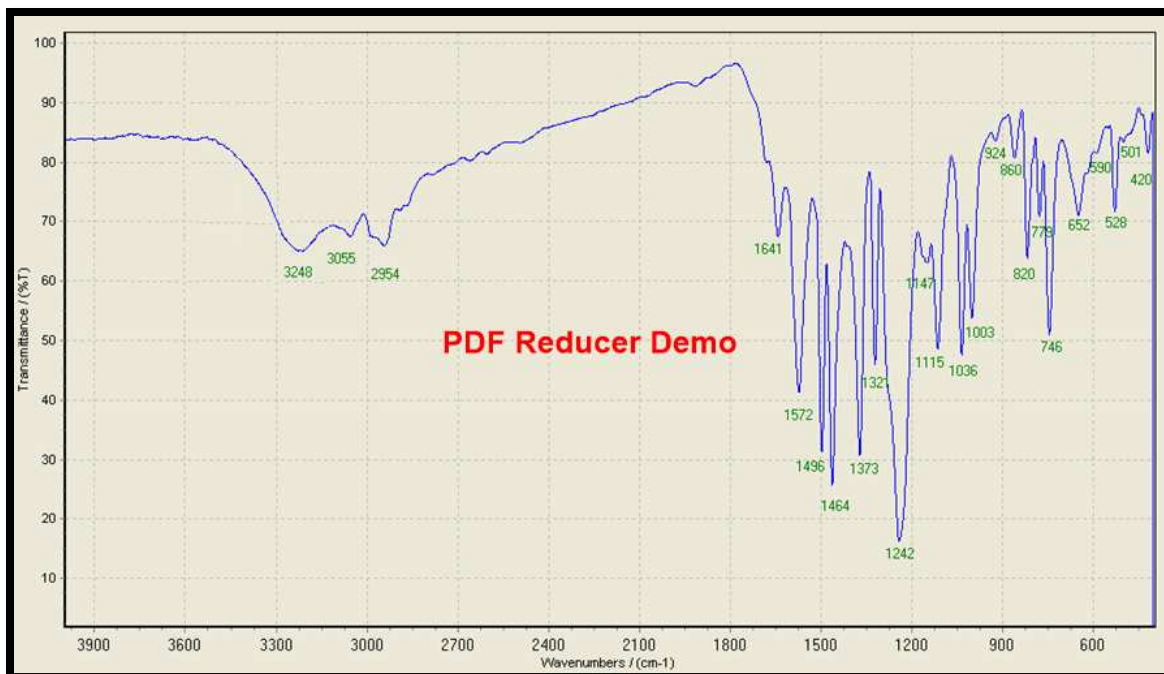
Figure(3.57): FT-IR spectrum of [Co(L^3)(Q)] complex.
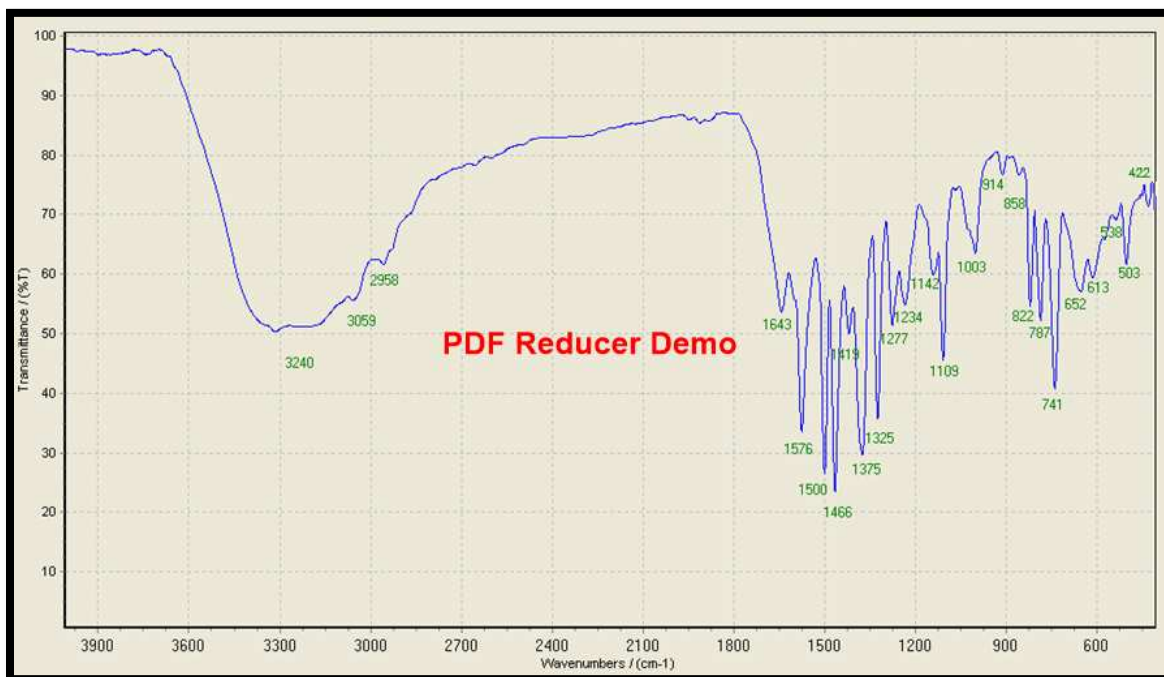
Figure(3.58): FT-IR spectrum of [Ni(L^3)(Q)] complex.

130
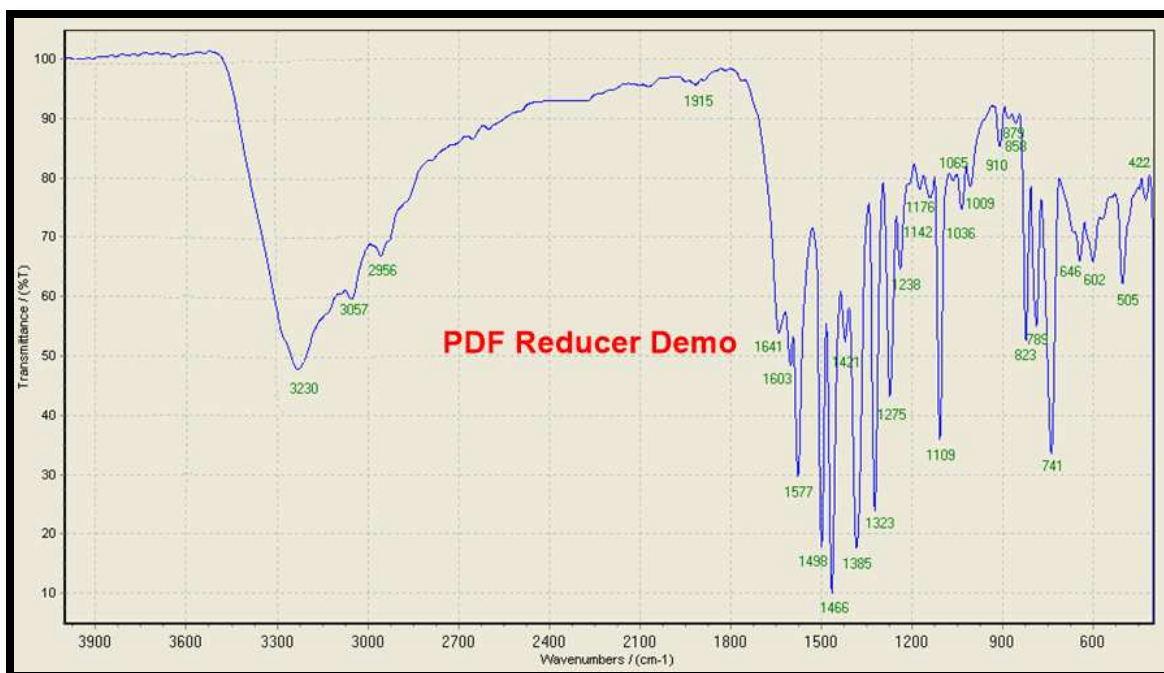
Figure(3.59): FT-IR spectrum of [Zn(L^3)(Q)] complex.

Table(3.30): FT-IR spectral data (wave number) cm^{-1} of the Mix Ligand complexes ML^{n}Q (where n=1,2,3)with some metal ions.

Compound	v(O-H) v(N-H)	v (C-H)$_{armo.}$ v (C-H)$_{vin.}$	v (C-H)$_{alph}$	v (C=C)$_{armo.}$ v (C=C)$_{vin}$	v (C=N)	v (C-N) v (C-O)	v (M-N)	v (M-O)
(Q)	3159(m)	3047(w)	-	1504(w)	1576(w)	- 1281(w)	-	-
[Co(L^1)(Q)]	- -	3024(m)	2954(w) 2870(m)	1464(w) 1496(w)	1581(m)	1246(w)	526(w) 503(m)	447(m)
[Ni(L^1)(Q)]	- -	3039(w)	2956(w) 2871(m)	1464(w) 1498(m)	1581(m)	1296(m) 1240(w)	550(w) 523(m)	498(w)
[Zn(L^1)(Q)]	- -	3043(m)	2954(w) 2870(m)	1466(w) 1498(m)	1579(m)	1273(w) 1238(m)	563(w) 505(m)	447(m)
[Co(L^2)(Q)]	- -	3055(m)	2954(w) 2868(m)	1462(w) 1498(m)	1577(w)	1244(w)	530(w)	486(m)
[Ni(L^2)(Q)]	- -	3057(m)	2958(w) 2870(m)	1464(w) 1498(m)	1577(w)	1284(w) 1259(m)	501(w)	432(w)

131

[Zn(L2)(Q)]	- -	3055(w)	2956(w) 2870(m)	1464(w) 1498(m)	1577(m)	1271(w) 1238(m)	505(m)	486(w)
[Co(L3)(Q)]	- 3248	3055(m)	2954(w)	1464(w) 1496(m)	1572(w)	1242(w)	528(w) 501(m)	420(m)
[Ni(L3)(Q)]	- 3240	3059(w)	2958(w)	1466(w) 1500(m)	1576(m)	1277(m) 1234(w)	538(w) 503(m)	422(w)
[Zn(L3)(Q)]	- 3230	3057(w)	2956(w)	1466(w) 1498(m)	1577(w)	1275(m) 1238(w)	505(m)	422(m)

$[Co(L^1)(Q)]$	301 378 599	33222 26455 16694	3857 3820 159	Intra Ligand C.T $^4A_{2(F)} \rightarrow {}^4T_{1(P)}$	Tetrahedral
$[Ni(L^1)(Q)]$	305 401 875	32786 24937 11428	3979 1912 197	Intra Ligand C.T $^3T_1 \rightarrow {}^3T_{1(P)}$	Tetrahedral
$[Zn(L^1)(Q)]$	218 278 400	45871 35971 25000	2048 3876 2633	Intra Ligand Intra Ligand C.T	Tetrahedral
$[Co(L^2)(Q)]$	297 407 610	33670 24570 16393	3457 3962 440	Intra Ligand C.T $^4A_{2(F)} \rightarrow {}^4T_{1(P)}$	Tetrahedral
$[Ni(L^2)(Q)]$	290 342 404 801	34482 29239 24752 12484	3911 2891 2543 51	Intra Ligand Intra Ligand C.T $^3T_1 \rightarrow {}^3T_{1(P)}$	Tetrahedral
$[Zn(L^2)(Q)]$	294 339 398	34013 29498 25125	3830 2539 2545	Intra Ligand Intra Ligand C.T	Tetrahedral
$[Co(L^3)(Q)]$	321 429 608	31152 23310 16447	3716 3870 463	Intra Ligand C.T $^4A_{2(F)} \rightarrow {}^4T_{1(P)}$	Tetrahedral
$[Ni(L^3)(Q)]$	293 341 407 800	34129 29325 24570 12500	3844 3483 3319 16	Intra Ligand Intra Ligand C.T $^3T_{1(F)} \rightarrow {}^3T_{1(P)}$	Tetrahedral
$[Zn(L^3)(Q)]$	274 339 399	36496 29498 25062	3508 2559 2882	Intra Ligand Intra Ligand C.T	Tetrahedral

3.3) UV-Vis Spectral of ligands and their complexes

(3.3.1) UV-Vis spectral data of ligands (KL^1, KL^2 and KL^3)

(3.3.1.1) UV-Vis spectrum of ligand KL^1

The UV-Vis spectrum of ligand KL^1 in DMSO solution is shown in Fig. (3.60). The spectrum reveals two absorption peaks at (239 nm =41841 cm^{-1} ; ε_{max}= 3037 molar^{-1} cm^{-1}) and (310 nm =32258 cm^{-1}; ε_{max}= 2304 molar^{-1} cm^{-1}) which assigned to ($\pi\rightarrow\pi^*$) and ($\pi\rightarrow\pi^*$)transitions, respectively [160-162] , Table (3.31).
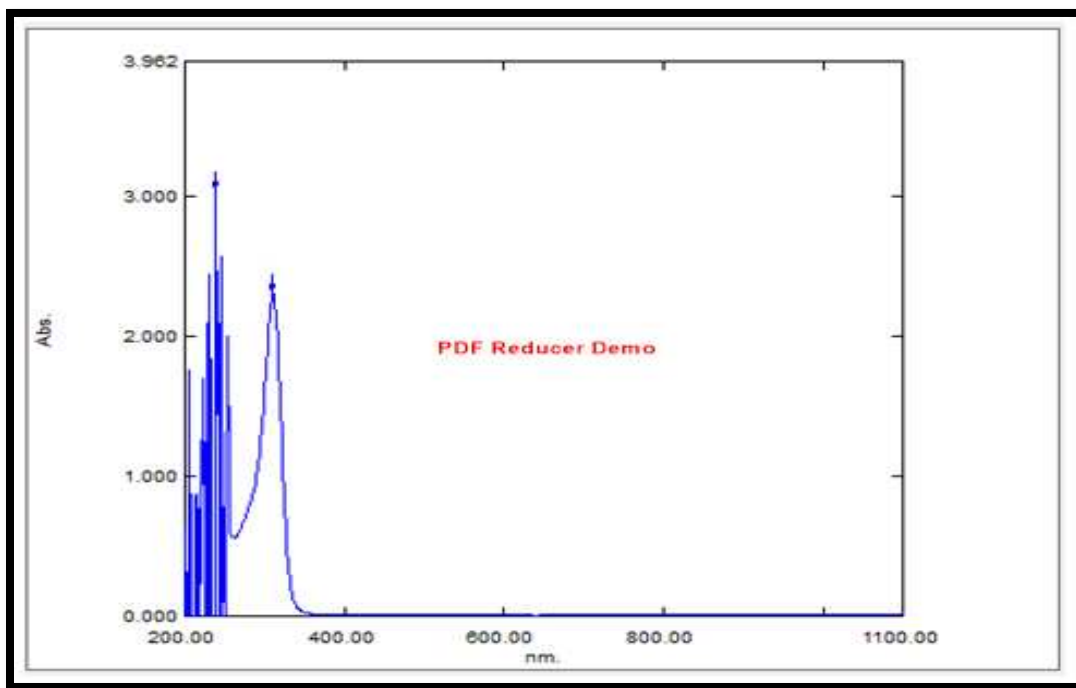
Figure (3.60): Electronic spectrum of ligand KL^1 in DMSO solution.

(3.3.1.2) UV-Vis spectrum of ligand KL^2

The UV-Vis spectrum of ligand KL^2 in DMSO, Fig.(3.61), shows two absorption peaks at (269 nm =37174 cm^{-1}; ε_{max}= 2285 molar^{-1} cm^{-1}) and (375 nm =26666 cm^{-1}; ε_{max}= 56 molar^{-1} cm^{-1}) assigned to ($\pi \rightarrow \pi^*$)and (n $\rightarrow \pi^*$)transitions, respectively [160-162] ,Table (3.31).
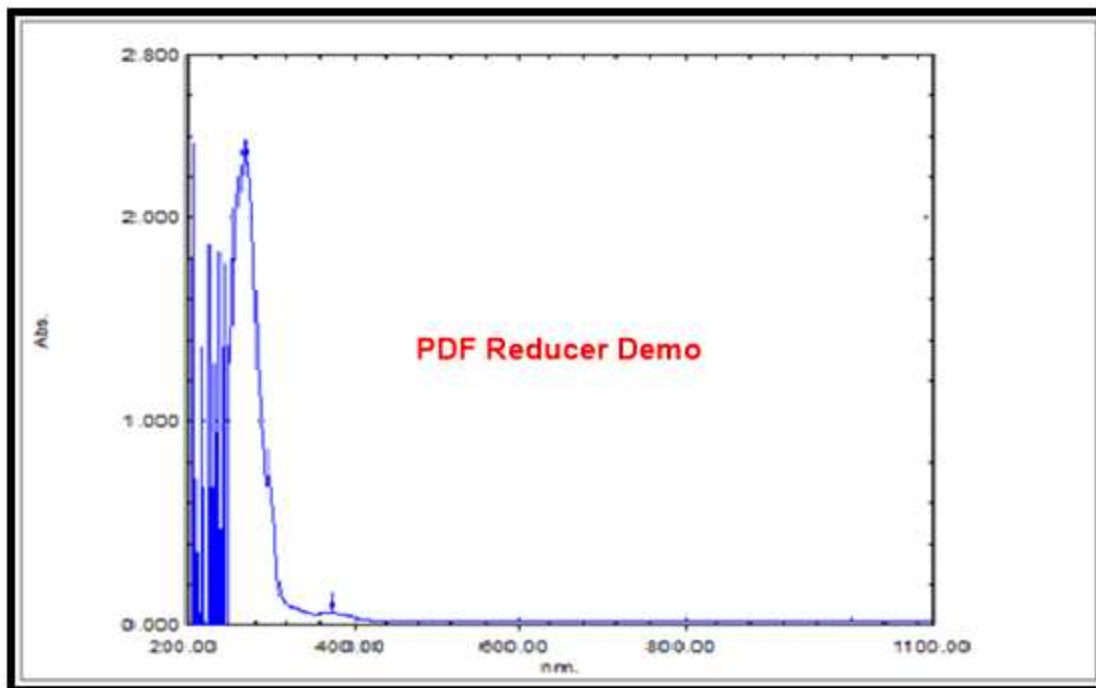
Figure (3.61): Electronic spectrum of ligand KL^2 in DMSO solution.

(3.3.1.3) UV-Vis spectrum of ligand KL^3

The UV-Vis spectrum of ligand KL^3 in DMSO is presented in Fig. (3.62). The spectrum shows two absorption peaks at (264 nm = 37878 cm^{-1}; ε_{max}= 3276 molar^{-1} cm^{-1}) and (299 nm =33444 cm^{-1}; ε_{max}= 3917 molar^{-1} cm^{-1}) assigned to ($\pi \rightarrow \pi^*$) and ($\pi \rightarrow \pi^*$) transitions, respectively [160-162], Table (3.31).
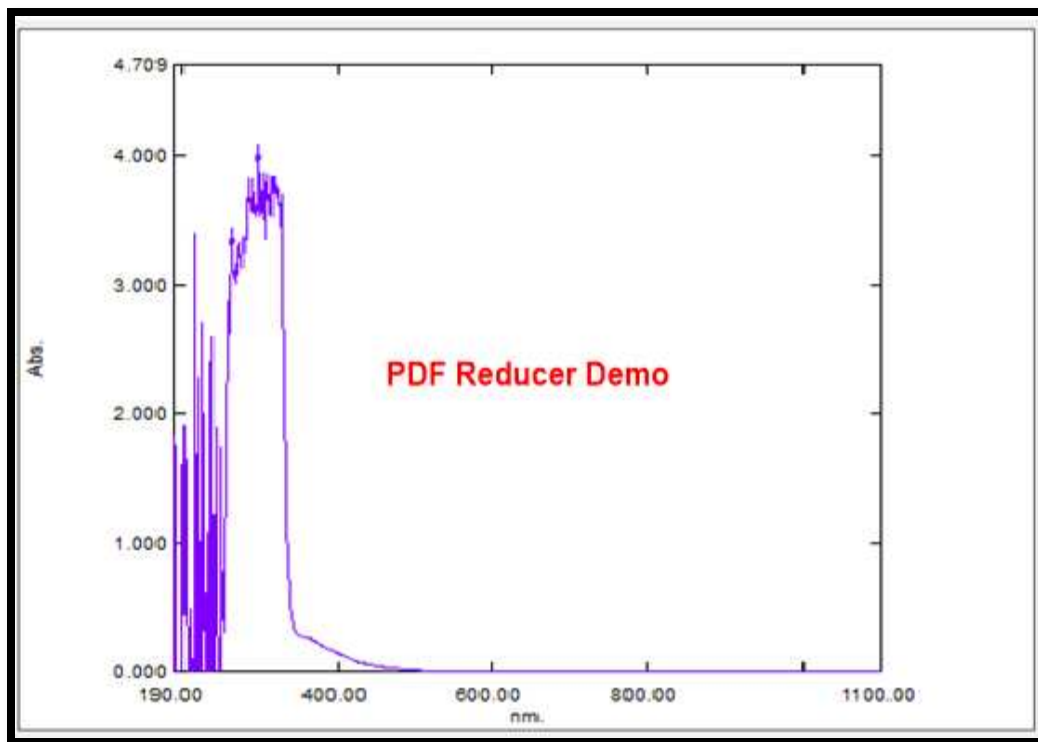
Figure (3.62): Electronic spectrum of ligand KL^3 in DMSO solution.

Table (3.31): Electronic spectral data for the ligands KL^1, KL^2 and KL^3 in DMSO solutions.

Compound	Wave length λ_{nm}	Wave number (cm^{-1})	ε_{max} $(moler^{-1}.cm^{-1})$	Assignment
KL^1	239 310	41841 32258	3037 2304	$\pi \rightarrow \pi^*$ $\pi \rightarrow \pi^*$
KL^2	269 375	37174 26666	2285 56	$\pi \rightarrow \pi^*$ $n \rightarrow \pi^*$
KL^3	264 299	37878 33444	3276 3917	$\pi \rightarrow \pi^*$ $\pi \rightarrow \pi^*$

(3.3.2) UV-Vis Spectral data for complexes

135

(3.3.2.1) UV-Vis Spectral data for $[Mn(L^1)_2]$, $[Co(L^1)_2]$, $[Ni(L^1)_2]$, $[Cu(L^1)_2]$, $[Zn(L^1)_2]$, $[Pd(L^1)_2]$ and $[Cd(L^1)]_2$ for the ligand KL^1 complexes.

The electronic spectra for the complexes of KL^1 exhibited various extents of shift of peaks related to the intra ligand $(\pi \rightarrow \pi^*)$ and $(n \rightarrow \pi^*)$ transition, Table(3.32). Peaks in the range of (398-450) nm related to the charge transfer transitions (C.T), were observed in the spectra of the Mn^{II}, Co^{II}, Ni^{II}, Cu^{II}, Zn^{II}, Pd^{II} and Cd^{II} complexes, Fig.((3.63)-(3.69)) [160-162].

The spectrum of the Mn^{II}-complex showed peak in the (d-d) region at 617 nm which assigned to $^6A_1 \rightarrow {}^4T_{1(G)}$ transition, indicating tetrahedral geometry about Mn ion [142,163].

The Co^{II} complex displays additional peak in the (d-d) region at 813 nm due to $^4A_{2\ (F)} \rightarrow {}^4T_{1\ (P)}$ transition. This spectrum is characteristic for Co^{II}-complex with tetrahedral geometry around Co ion [143,163-165].

The spectrum of the Ni^{II}-complex showed a peak in the (d-d) region at 981 nm assigned to $^3T_1 \rightarrow {}^3T_{1\ (P)}$ transition, indicating tetrahedral geometry about Ni ion [143,164].

The spectrum of the Cu-complex showed a peak in the (d-d) region at 475 nm attributed to d-d transition type $^2B_{1g} \rightarrow {}^2E_g$, confirming square planer geometry about Cu ion [166].

The electronic spectra of the $[Zn(L^1)_2]$ and $[Cd(L^1)_2]$ complexes exhibited peaks at ((250, 299) and (223, 307)) nm, which were assigned to the intra-ligand field and other two peaks at (398 and 400) nm which were assigned to charge transfer transitions, indicating tetrahedral geometry about Zn and Cd ion [161,162,167].

The spectrum of the Pd^{II}-complex showed two peaks in the (d-d) region at 890 and 995 nm assigned to $^1A_1g \rightarrow {}^1A_2g$ and $^1A_1g \rightarrow {}^1B_1g$,respectively, indicating square planar geometry about Pd ion [168,169].
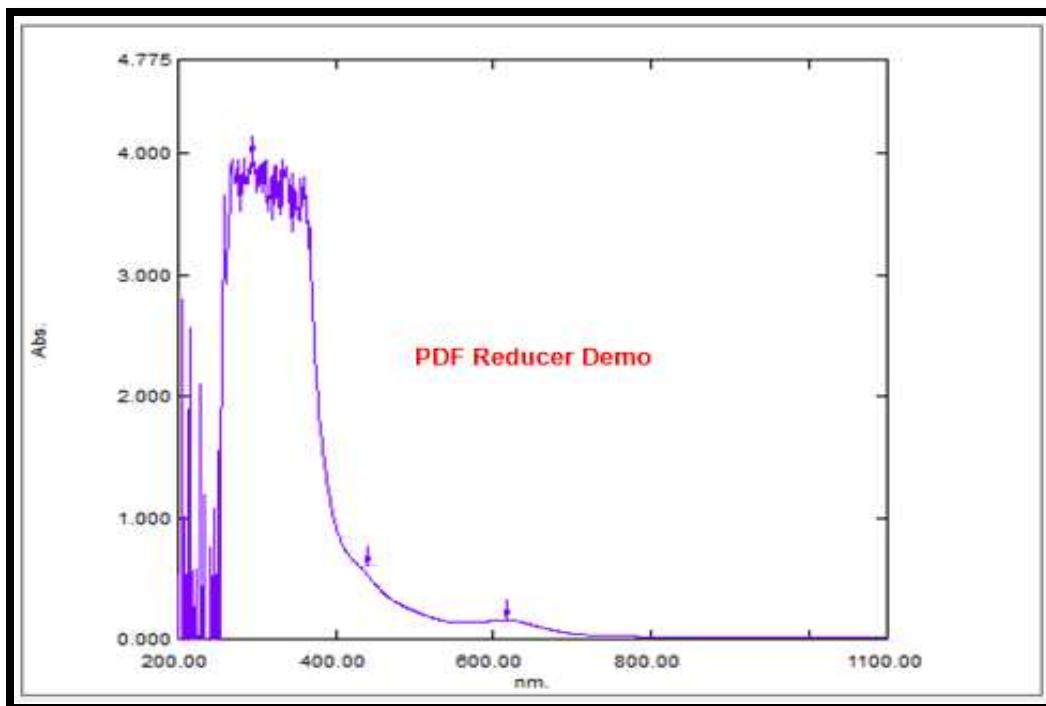
Figure (3.63): Electronic spectrum of [Mn(L^1)$_2$]complex in DMSO solution.
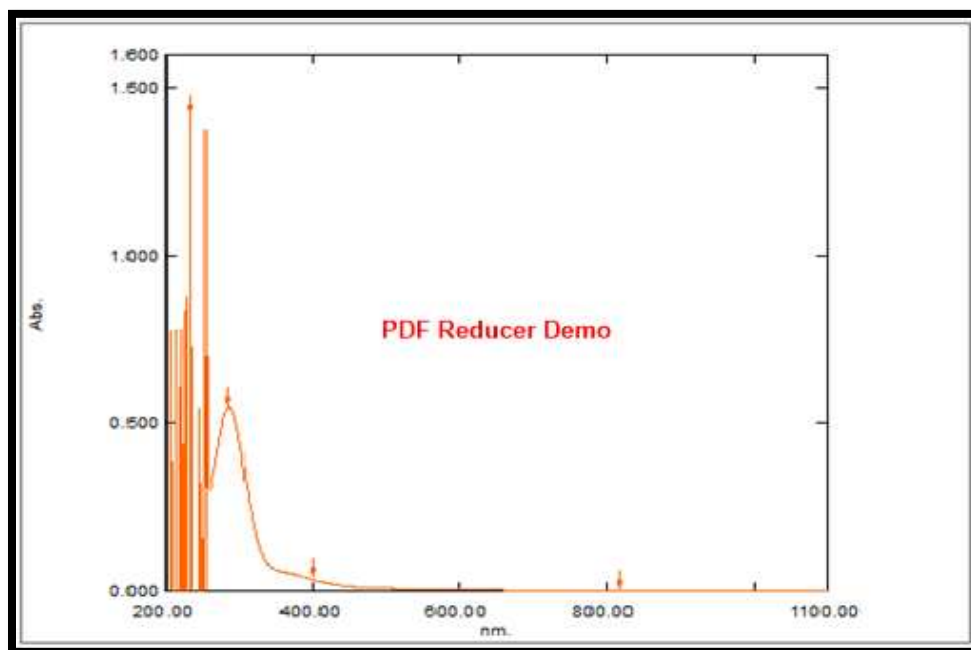
Figure (3.64): Electronic spectrum of [Co (L^1)$_2$]complex in DMSO solution.
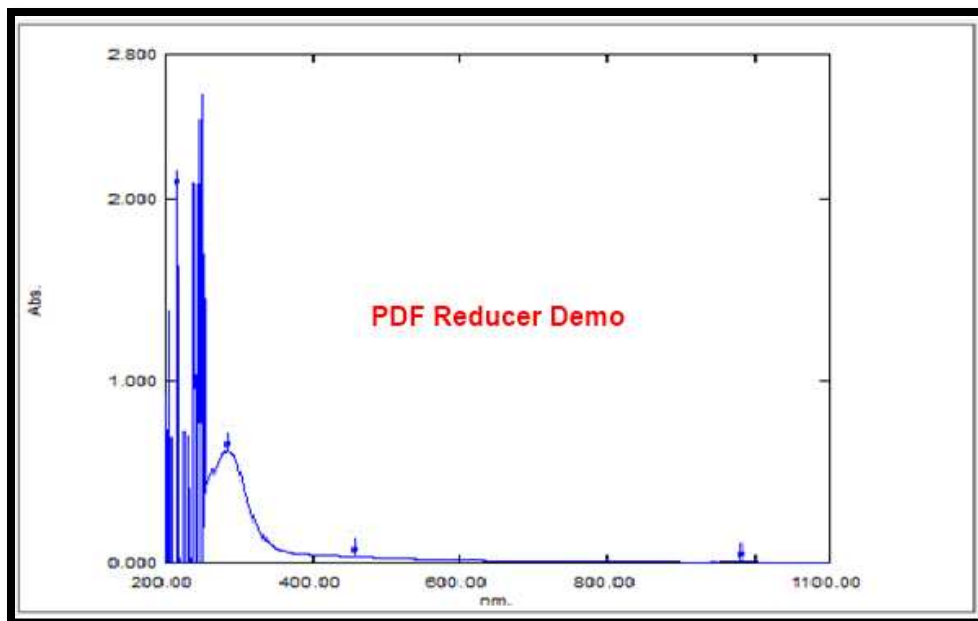
Figure (4.65): Electronic spectrum of [Ni(L^1)$_2$]complex in DMSO solution.
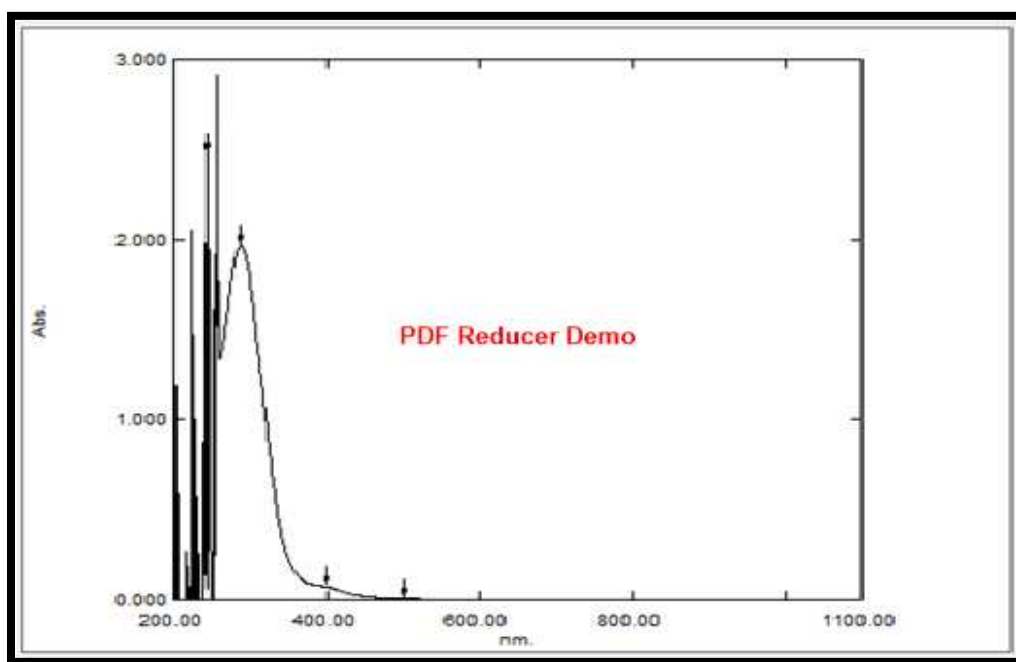
Figure (3.66): Electronic spectrum of [Cu(L^1)$_2$]complex in DMSO solution.
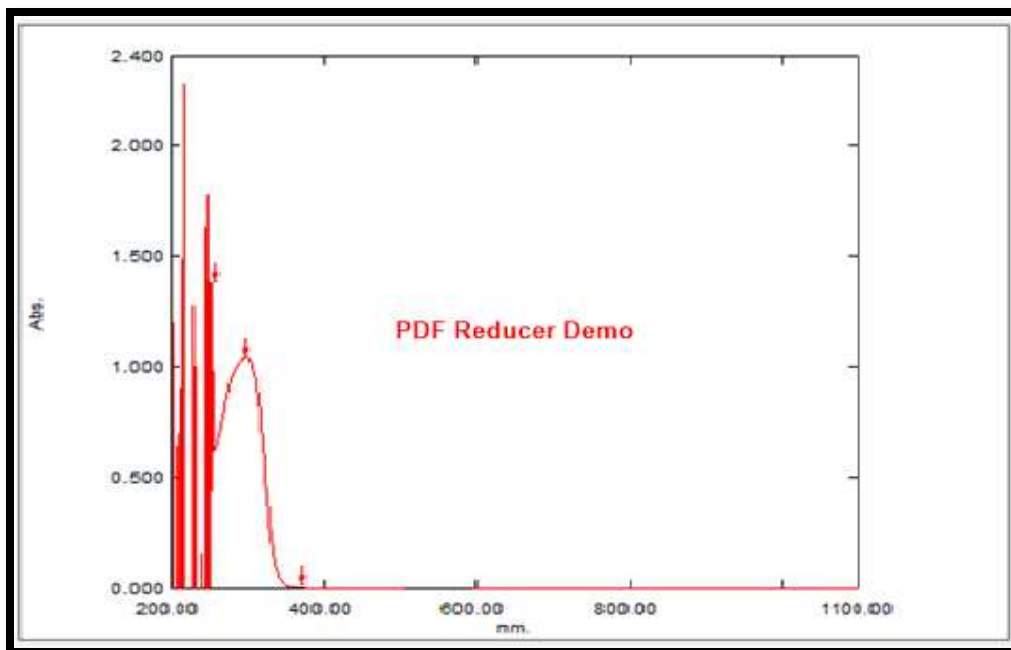
Figure (3.67): Electronic spectrum of [Zn(L^1)$_2$]complex in DMSO solution.
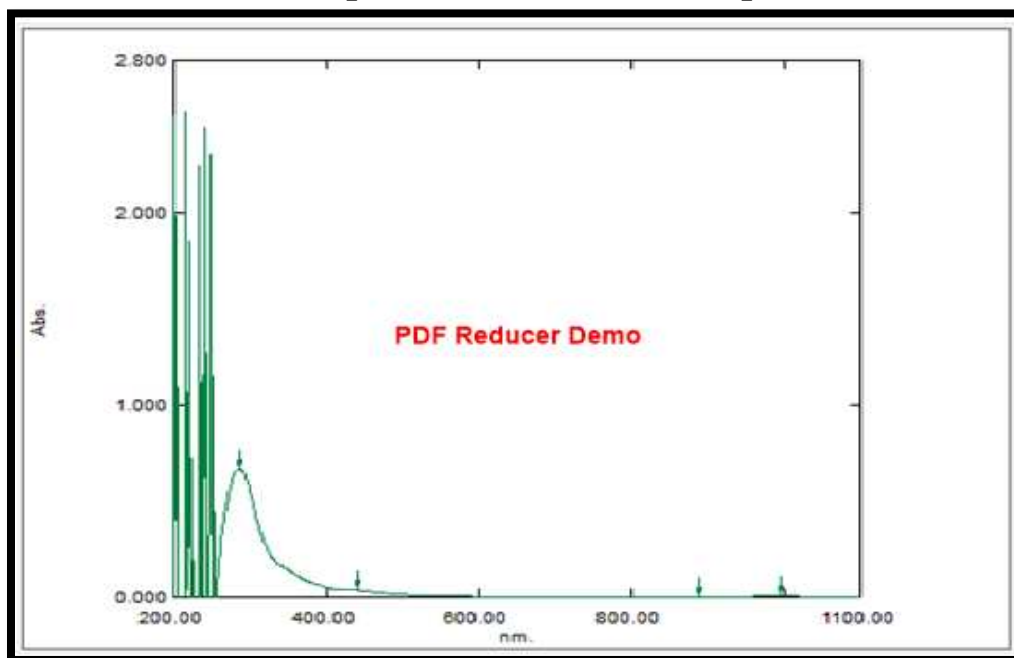
Figure (3.68): Electronic spectrum of [Pd(L^1)$_2$]complex in DMSO solution.
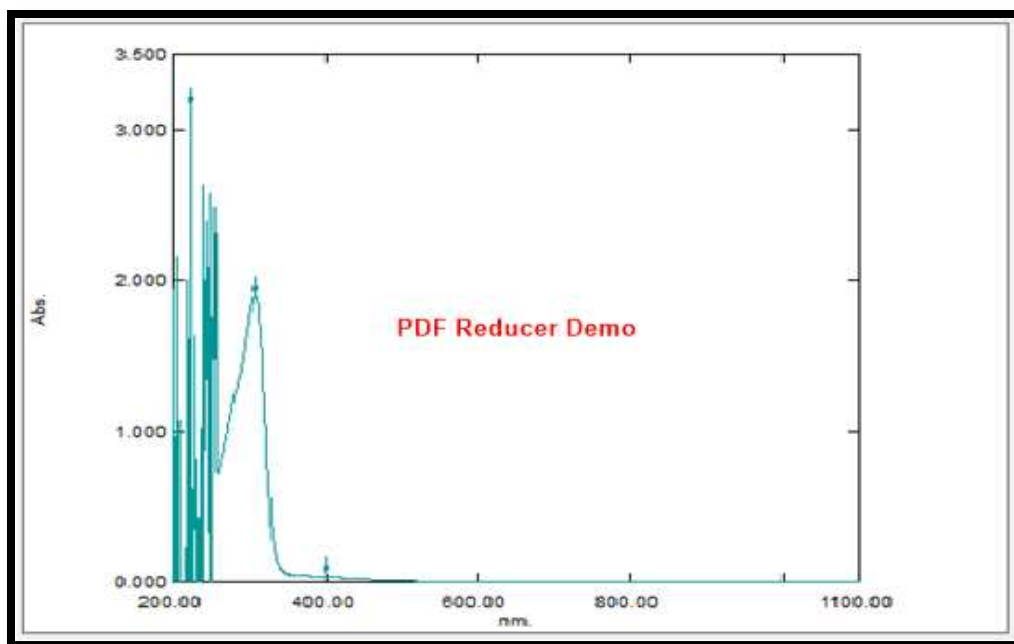
Figure (3.69): Electronic spectrum of [Cd(L^1)$_2$]complex in DMSO solution.

Table (3.32): UV-Vis spectral data of KL^1 complexes in DMSO solutions.

Compound	Wave length λ_{nm}	Wave number(cm^{-1})		ε_{max} (moler^{-1}.cm^{-1})		Assignment	Suggested geometry
KL^1	239 310	41841	32258	3037	2304	$\pi \rightarrow \pi^*$ n $\rightarrow \pi^*$	-
[Mn(L^1)$_2$]	295 435 617	33898 22988 16207		3977 550 155		Intra Ligand C.T $^6A_1$ $\rightarrow ^4T_{1(G)}$	Tetrahedral
[Co(L^1)$_2$]	234 285 400 813	42735 35089 25000 12300		1421 547 98 57		Intra Ligand Intra Ligand C.T $^4A_2 \rightarrow ^4T_{1(P)}$	Tetrahedral
[Ni(L^1)$_2$]	216 283 450 981	46296 35335 22222 10204		2061 613 100 50		Intra Ligand Intra Ligand C.T $^3T_{1(f)} \rightarrow ^3T_{1\ (P)}$	Tetrahedral
[Cu(L^1)$_2$]	242 287 400 475	41322 34842 25000 21052		2482 1967 98 110		Intra Ligand Intra Ligand C.T $^2B_{1g} \rightarrow ^2E_g$	Square planar
[Zn(L^1)$_2$]	250 299 398	40000 33444 25125		1415 1041 50		Intra Ligand Intra Ligand C.T	Tetrahedral

140

[Pd(L^1)$_2$]	286 450	34965	22222	669	100	Intra Ligand C.T ^{1}A$_{1g}\rightarrow$^{1}A$_{2g}$ ^{1}A$_{1g}\rightarrow$^{1}B$_{1g}$	Square planar
	890 995	11235	10050	10	70		
[Cd(L^1)$_2$]	223 307	44573	32573	3151	1900	Intra Ligand Intra Ligand C.T	Tetrahedral
	400	25000		98			

(3.3.2.2) UV-Vis Spectral data for [Mn(L^2)$_2$], [Co(L^2)$_2$], [Ni(L^2)$_2$)], [Cu(L^2)$_2$],[Zn(L^2)$_2$] ,[Pd(L^2)$_2$] and [Cd(L^2)$_2$] for the ligand KL^2 complexes.

The electronic spectra of the KL^2 complexes exhibited various extents of shift of the peaks related to the intra ligand $(\pi\rightarrow\pi^*)$, $(n\rightarrow\pi^*)$ and charge transfer (C.T) transitions, Table (3.33). Peaks in the range of (317-460) nm that were related to the charge transfer transition (C.T) were observed in the spectra of the Mn^{II}, Co^{II}, Ni^{II}, Cu^{II}, Zn^{II}, Pd^{II} and Cd^{II} complexes, Fig.((3.70)-(3.76)) [161,162,170].

The Mn^{II}-complex spectrum displays a peaks at 520 nm were assigned to ^{6}A$_1\rightarrow$ ^{4}T$_{1(G)}$ transitions, indicating tetrahedral geometry about Mn ion [142,163].

The Co^{II}-complex shows additional peaks in the d-d region at 677nm may due to ^{4}A$_{2(F)}\rightarrow$ ^{4}T$_{1\ (p)}$ transitions. These peak was characteristic for tetrahedral structure around Co ion [142,164,170].

The Ni^{II}-complex exhibits peaks in the d-d region at 1009 nm and 1089 nm assigned to ^{3}T$_{1\ (F)}\rightarrow$ ^{3}T$_{1(P)}$ and ^{3}T$_{1\ (F)}\rightarrow$ ^{3}A$_{2(F)}$ transitions respectively, indicating tetrahedral geometry about Ni ion [143,164].

Band in the Cu spectrum at 420 nm attributed to d-d transition type ^{2}B$_{1g}\rightarrow$ ^{2}E$_g$ transition confirming square planar geometry about Cu ion [166].

The electronic spectra of the [Zn(L^2)$_2$] and [Cd(L^2)$_2$] complexes exhibited peaks at ((270, 269,370) and (395, 400)) nm, which were assigned to the intra ligand $(\pi\rightarrow\pi^*)$, $(n\rightarrow\pi^*)$ and charge transfer transitions, respectively [161,162,167]. The

Pd^{II} - complex shows addition at peaks in the (d-d) region at (420) nm may due to $^1A_1g \rightarrow {}^1B_1g$ transitions, indicating square planar geometry about Pd ion [168,169].
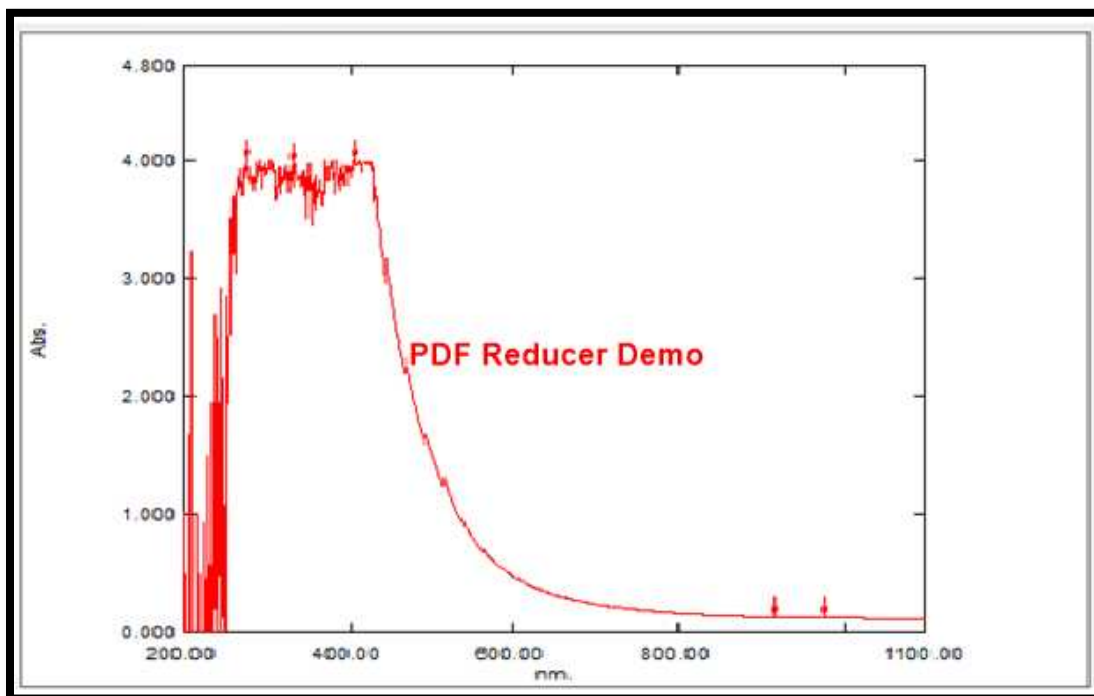
Figure(3.70):Electronic spectrum of [Mn(L^2)$_2$]complex in DMSO solution.
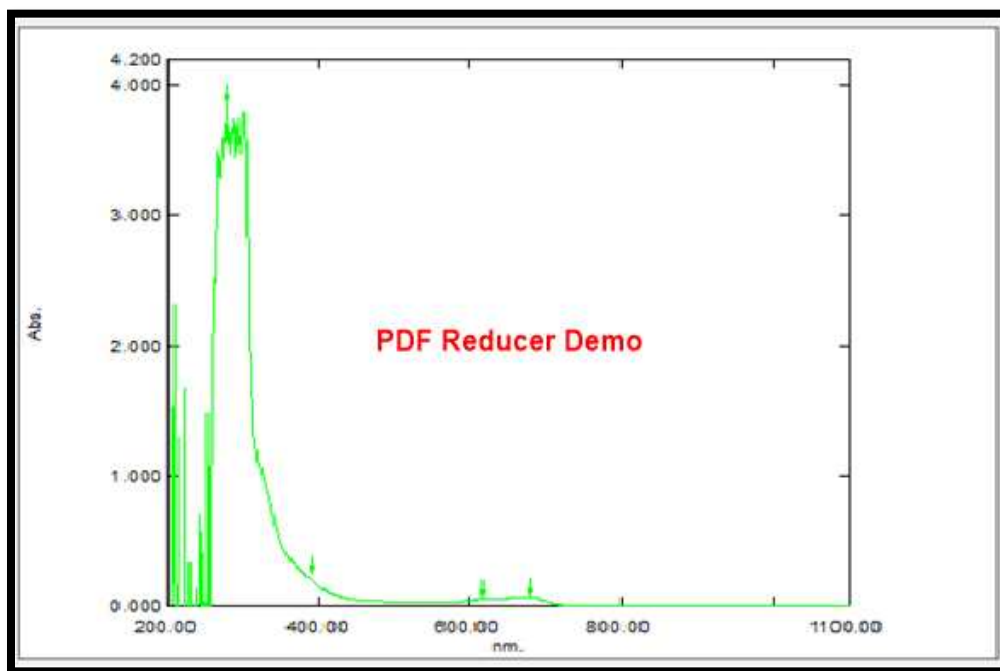
Figure(3.71):Electronic spectrum of [Co(L^2)$_2$] complex in DMSO solution.
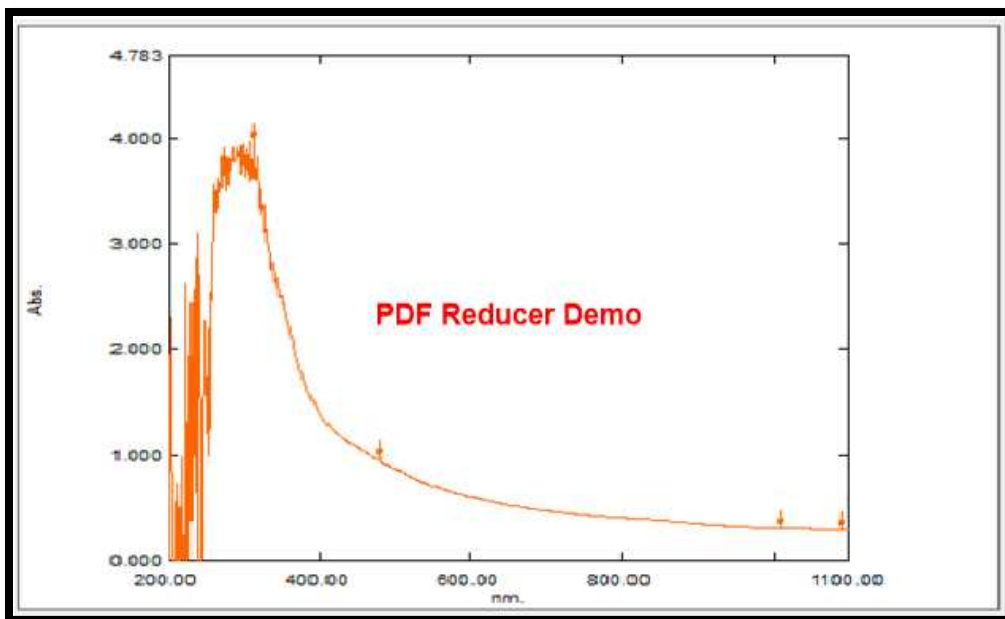
Figure(3.72):Electronic spectrum of [Ni(L^2)$_2$] complex in DMSO solution.
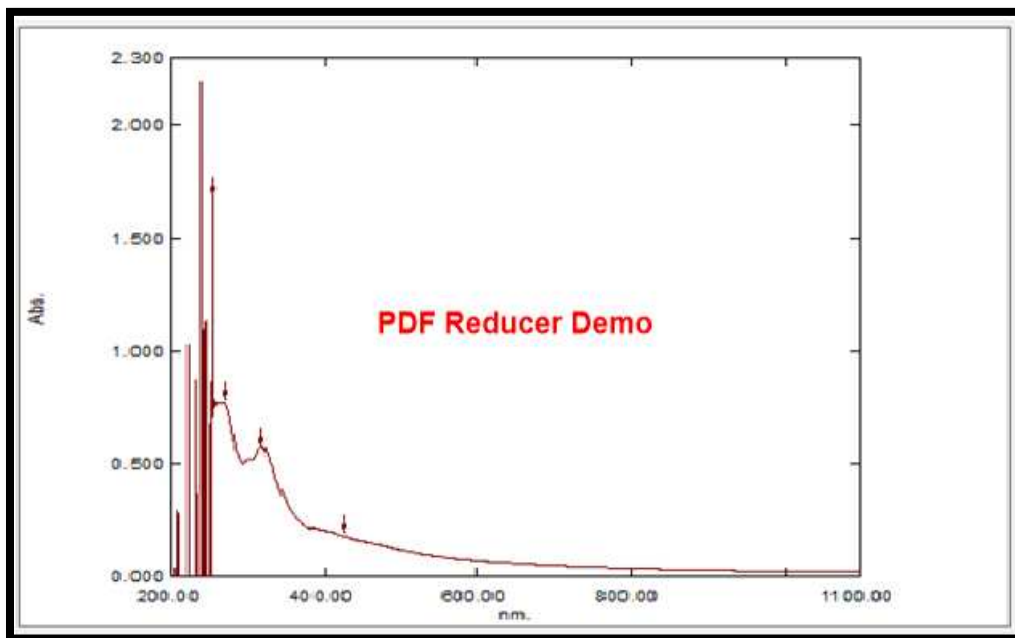
Figure(3.73):Electronic spectrum of [Cu(L^2)$_2$] complex in DMSO solution.
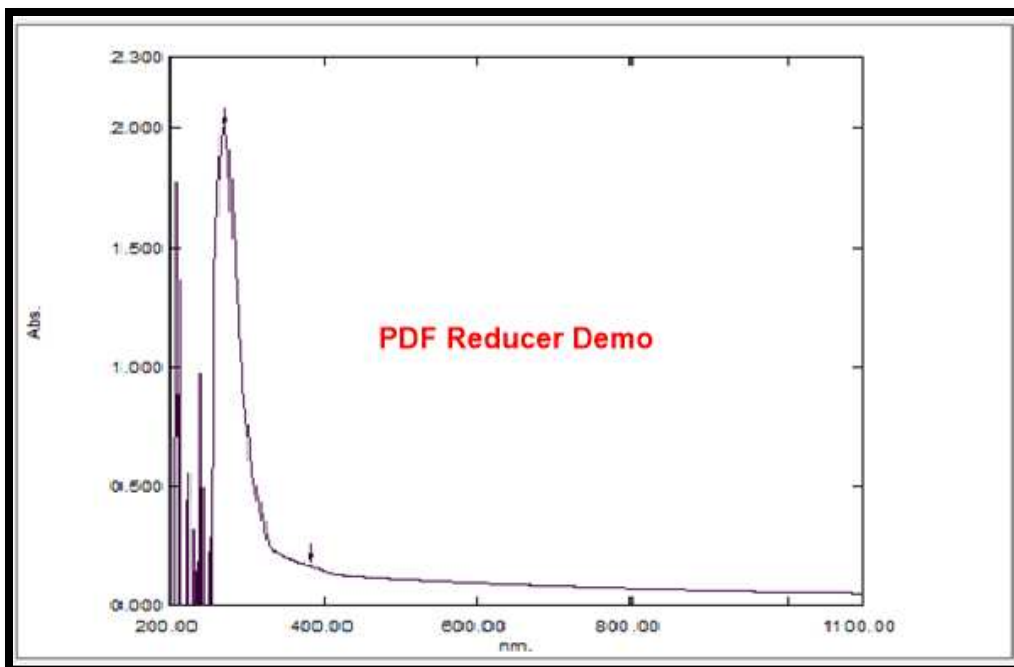
Figure(3.74): Electronic spectrum of [Zn(L^2)$_2$] complex in DMSO solution.
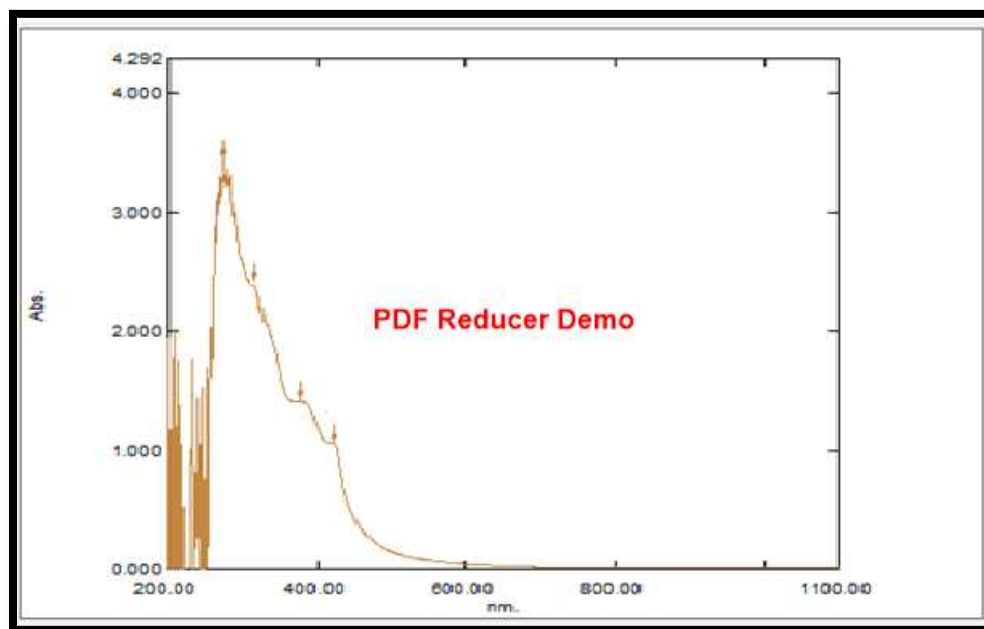
Figure(3.75):Electronic spectrum of [Pd(L^2)$_2$] complex in DMSO solution.

144
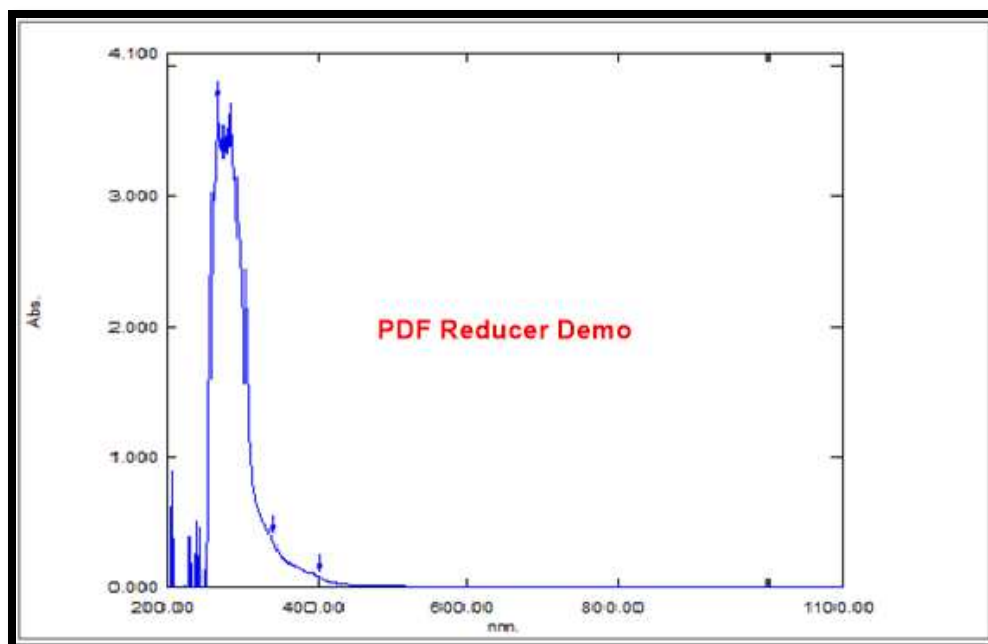
Figure(3.76):Electronic spectrum of [Cd(L^2)$_2$] complex in DMSO solution.

Table (3.33): UV-Vis spectral data of KL^2 complexes in DMSO solutions.

Compound	Wave length λ_{nm}	Wave number(cm^{-1})		ε_{max} (moler^{-1}.cm^{-1})		Assignment	Suggested geometry
KL^2	269 375	371748	26666	2285	56	$\pi \to \pi^*$ n $\to \pi^*$	-
[Mn(L^2)$_2$]	275 333 406 520	36363 24630	30030 19230	4000 3998	3974 125	Intra Ligand Intra Ligand C.T ^{6}A$_1$ $\to ^4$T$_{1(G)}$	Tetrahedral
[Co(L^2)$_2$]	275 397 677	36363 14771	25188	3856 66	235	Intra Ligand C.T ^{4}A$_{2(F)} \to ^4$T$_{1(F)}$	Tetrahedral
[Ni(L^2)$_2$]	311 460 1009 *1089*	32154 9910	21739 9182	3968 306	1129 294	Intra Ligand C.T ^{3}T$_{1(F)} \to ^3$T$_{1(P)}$ ^{3}T$_{1(F)} \to ^3$A$_{2(F)}$	Tetrahedral
[Cu(L^2)$_2$]	255 260 317 420	39215 31545	38460 23809	1684 572	750 216	Intra Ligand Intra Ligand C.T ^{2}B$_{1g}$ $\to ^2$E$_g$	Square planar

145

$[Zn(L^2)_2]$	270 395	37037	25316	2001	152	Intra Ligand C.T	Tetrahedral
$[Pd(L^2)_2]$	273 300 378 420	36630 26455	33333 23809	3451 1416	2401 1063	Intra Ligand Intra Ligand C.T $^1A_1g \rightarrow ^1B_1g$	Square planar
$[Cd(L^2)_2]$	269 370 400	37174 25000	27027	3737 113	400	Intra Ligand Intra Ligand C.T	Tetrahedral

(3.3.2.3)UV-Vis Spectral data for $[Mn(L^3)_2]$, $[Co(L^3)_2]$, $[Ni(L^3)_2]$, $[Cu(L^3)_2]$, $[Zn(L^3)_2]$], $[Pd(L^3)_2]$ and $[Cd(L^3)_2]$ for the ligand KL^3 complexes.

The electronic spectra of the KL^3 complexes exhibited various extents shift of bands related to the intra ligand $(\pi \rightarrow \pi^*)$ and $(n \rightarrow \pi^*)$ transitions ,Table (3.34). Peaks in the range of 309-495 nm that related to the charge transfer transitions (C.T), were observed in the spectra of the Mn^{II}, Co^{II}, Ni^{II}, Cu^{II}, Zn^{II}, Pd^{II} and Cd^{II} complexes Fig.((3.77)-(3.83)) [161,162,170].

The Mn^{II}-complex displays additional band in the (d-d) region at (605)nm, due to $^6A_1 \rightarrow ^4T_{1(G)}$ that characteristic for tetrahedral geometry around Mn ion [142,163].

The Co^{II}-complex displays additional peaks in the (d-d) region at (500 and 618)nm assigned to $^4A_{2(F)} \rightarrow ^4T_{1(P)}$,$^4A_{2(F)} \rightarrow ^4T_{1(F)}$.These peaks are characteristic for tetrahedral geometry in Co(II)-complexes [142,164,170].

The Ni^{II}-complex showed (d-d) peak at 1049 nm assigned to $^3T_1 \rightarrow ^3T_{1 (P)}$, which confirms tetrahedral geometry about Ni ion [143,164].

The spectrum of Cu^{II}-complex displays peak at 1049 nm attributed to (d-d) transition type $^2T_2 \rightarrow ^2E$, that confirm tetrahedral geometry about Cu ion[166].

The electronic spectrum of Zn^{II}-complex exhibited peaks at ((259,289) and (309, 385)) nm, which were assigned to the intra- ligand field and charge transfer transitions, respectively[161,162,167].

Cd^{II}-complex shows three peaks at (285,311 and 365) nm which were assigned to the intra ligand $(\pi \rightarrow \pi^*)$,$(n \rightarrow \pi^*)$and charge transfer transitions, respectively, both of Zn^{II} and Cd^{II} complexes have a tetrahedral geometry about Zn, Cd ions[161,162,167].

Finally Pd^{II}-complex shows additional peak in the (d-d) region at 400 nm which assigned to$^1A_1g \rightarrow {}^1Eg$ transition, which confirms square planer geometry about Pd ion [168,169].
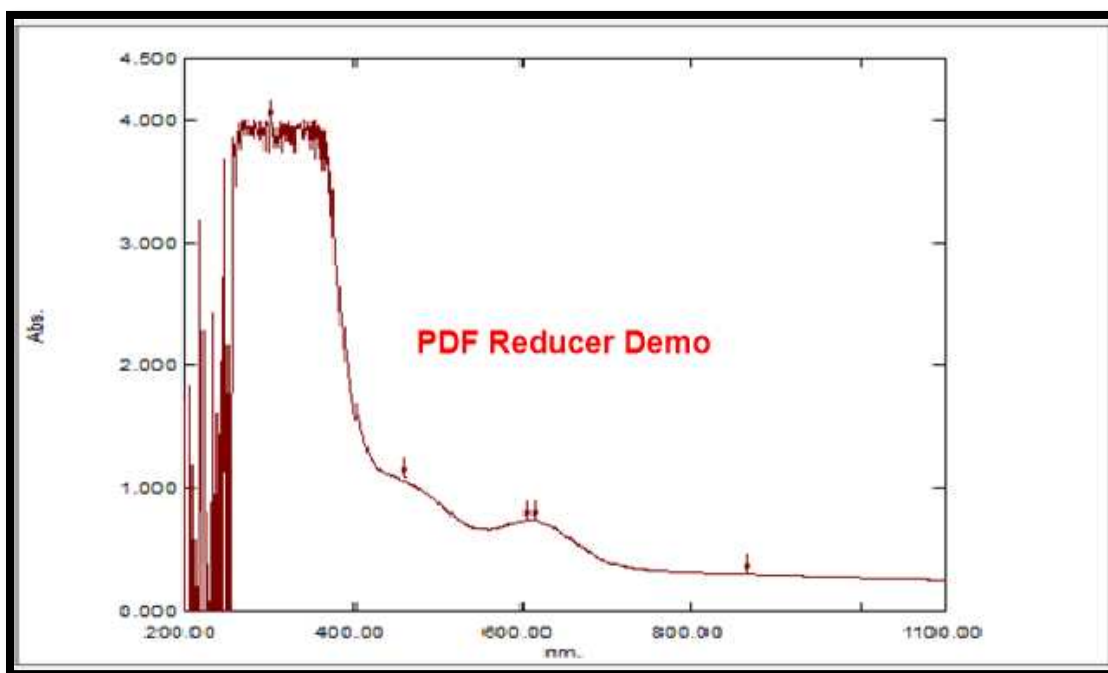
Figure(3.77):Electronic spectrum of $[Mn(L^3)_2]$complex in DMSO solution.
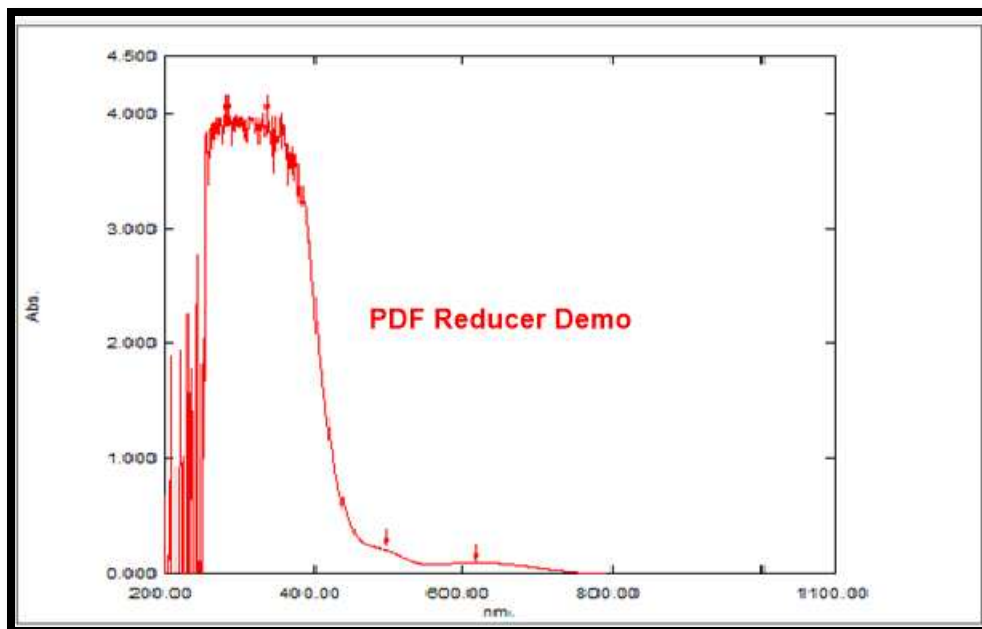
Figure(3.78):Electronic spectrum of [Co(L³)₂] complex in DMSO solution.
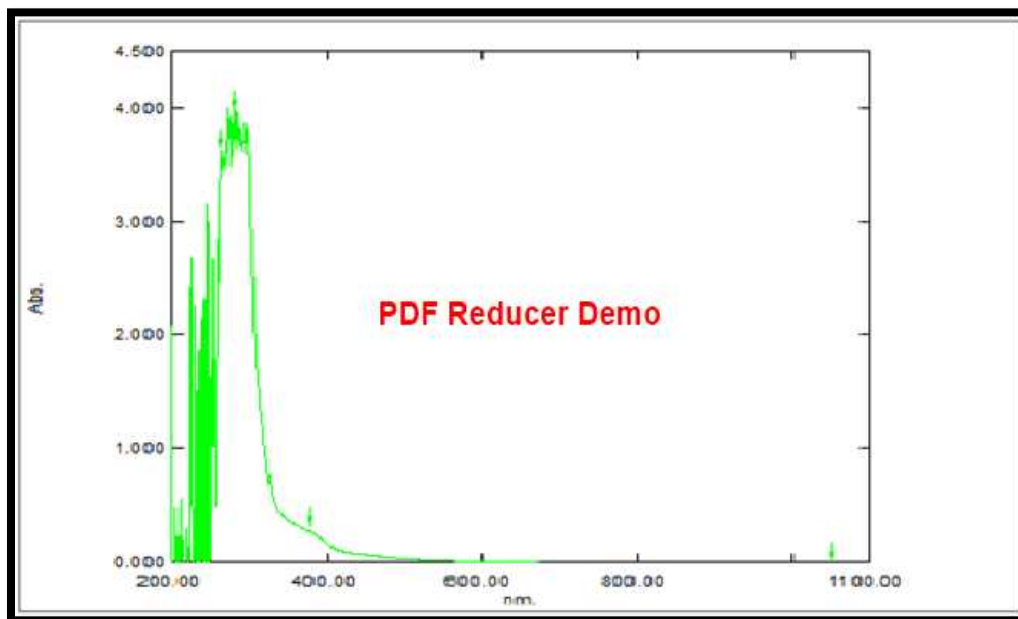
Figure(3.79): Electronic spectrum of [Ni(L³)₂] complex in DMSO solution.
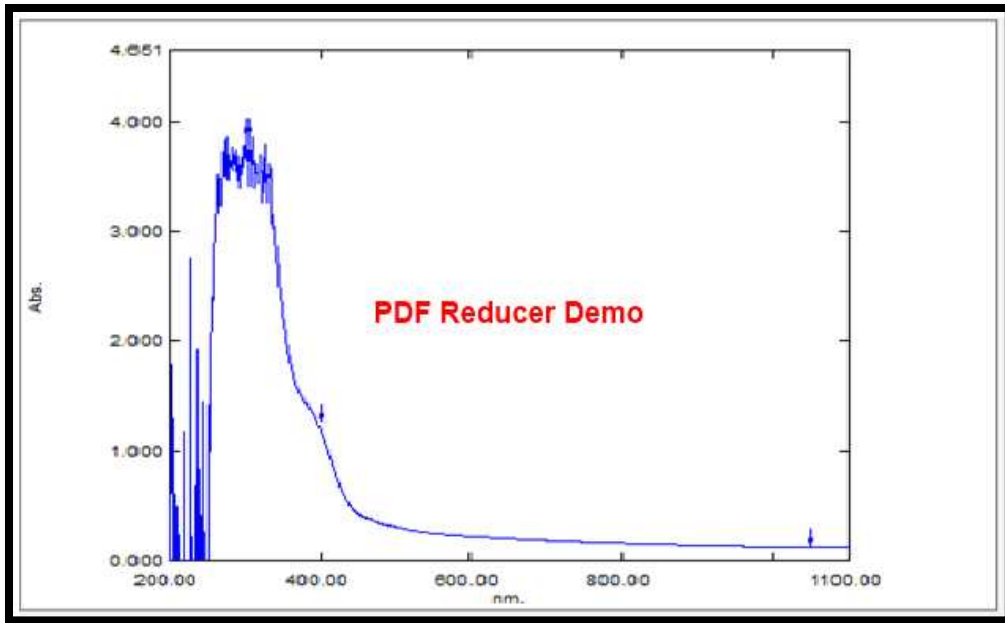
Figure(3.80):Electronic spectrum of [Cu(L³)₂] complex in DMSO solution.
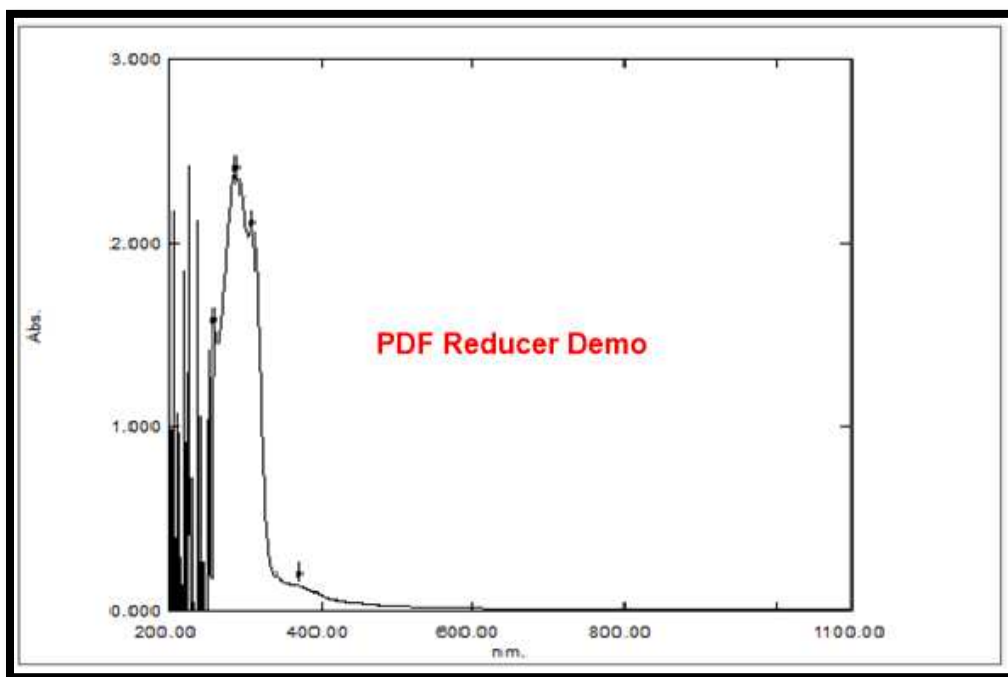
Figure(3.81):Electronic spectrum of [Zn(L³)₂] complex in DMSO solution.
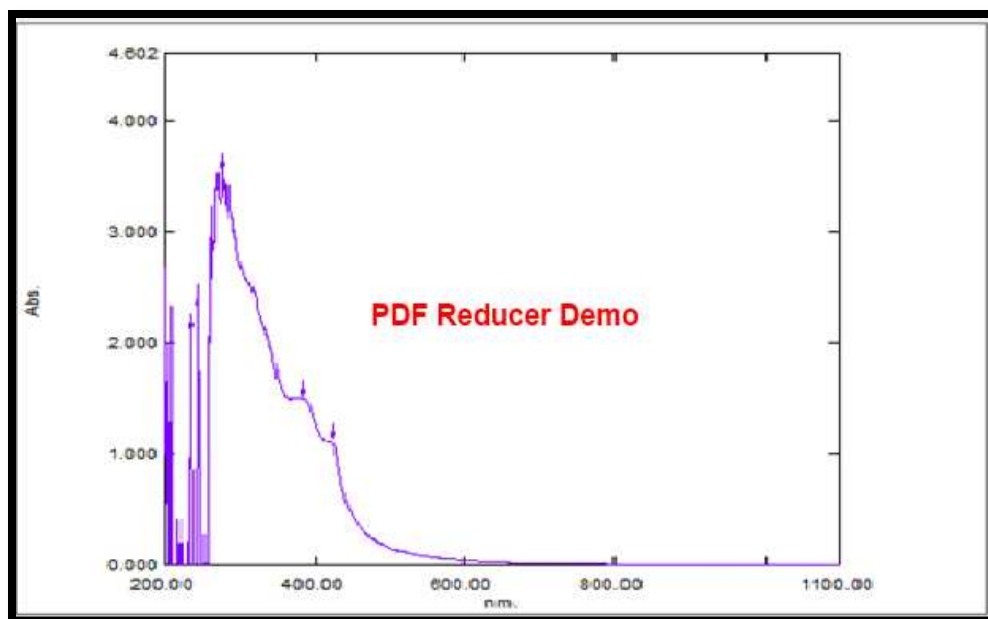
Figure(3.82):Electronic spectrum of [Pd(L^3)$_2$] complex in DMSO solution.
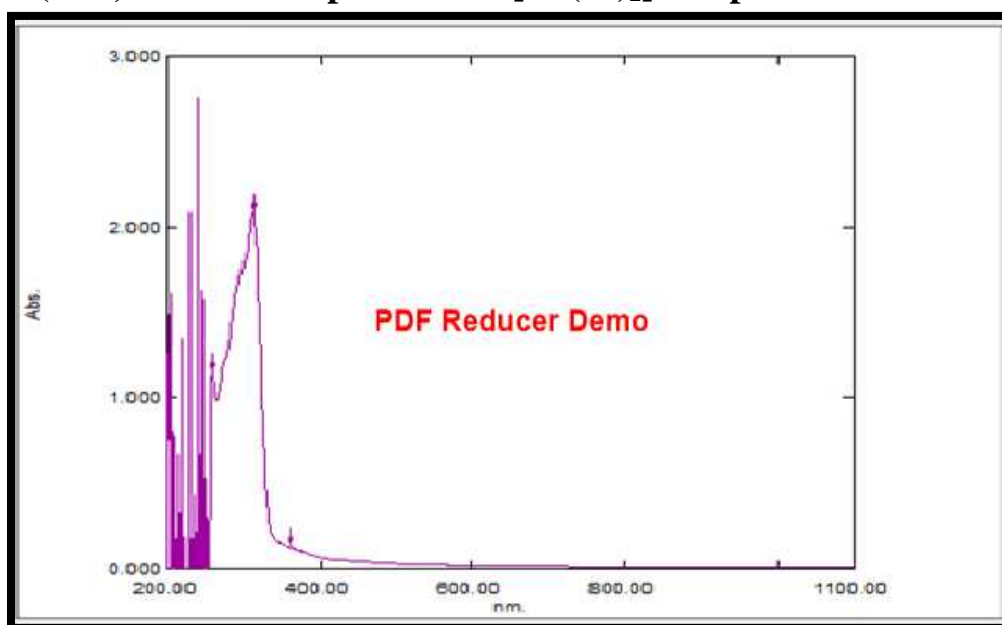
Figure(3.83):Electronic spectrum of [Cd(L^3)$_2$] complex in DMSO solution.

Table (3.34): UV-Vis spectral data of KL^3 complexes in DMSO solutions.

Compound	Wave length λ_{nm}	Wave number(cm^{-1})		ε_{max} (moler^{-1}.cm^{-1})		Assignment	Suggested geometry
KL^3	264 299	37878	33444	3276	3917	$\pi \to \pi^*$ n $\to \pi^*$	-

150

Compound	Wave length λ_{nm}	Wave number (cm^{-1})		ε_{max} (moler^{-1}.cm^{-1})		Assignment	Geometry
[Mn(L^3)$_2$]	302 495 605	33112 16528	20202	4000 734	1000	Intra Ligand C.T $^6A_1 \rightarrow {}^4A_1$	Tetrahedral
[Co(L^3)$_2$]	285 338 500 618	35087 20000	29585 16181	3997 200	4000 96	Intra Ligand C.T $^4A_{2(F)} \rightarrow {}^4T_{1(P)}$ $^4A_{2(F)} \rightarrow {}^4T_{1(F)}$	Tetrahedral
[Ni(L^3)$_2$]	254 279 387 1049	39370 25839	35842 9532	3612 295	3984 185	Intra Ligand Intra Ligand C.T $^3T_1 \rightarrow {}^3T_{1\,(P)}$	Tetrahedral
[Cu(L^3)$_2$]	303 400 1049	33003 9532	25000	3864 123	1200	Intra Ligand C.T $^2T_2 \rightarrow {}^2E$	Tetrahedral
[Zn(L^3)$_2$]	259 289 309 385	38610 32362	34602 25974	1535 2071	2369 200	Intra Ligand Intra Ligand C.T C.T	Tetrahedral
[Pd(L^3)$_2$]	233 276 380 425	42918 26315	36231 23529	2091 1512	3538 1125	Intra Ligand Intra Ligand C.T $^1A_1g \rightarrow {}^1Eg$	Square planar
[Cd(L^3)$_2$]	258 311 365	38759 27397	32154	1154 150	2089	Intra Ligand Intra Ligand C.T	Tetrahedral

(3.3.3) (UV-Vis) spectra of Mixed-Ligands and their complexes.

(3.3.3.1)(UV-Vis) spectrum for the 3-aminophenol (P)

The (UV-Vis) spectrum for the ligand (P), Fig.(3.84) exhibits two absorption peaks, at (262 nm =38167 cm^{-1} ; ε_{max} =2418 molar^{-1} cm^{-1}) and (293nm =34129 cm^{-1}; ε_{max}= 3223 molar^{-1} cm^{-1}) which were assigned to ($\pi \rightarrow \pi^*$) and ($\pi \rightarrow \pi^*$) transition respectively [171] ,Table (3.35).

Table(3.35): Electronic spectral data of the ligand(P).

Compound	Wave length λ_{nm}	Wave number(cm^{-1})	ε_{max} (moler^{-1}.cm^{-1})	Assignment
(P)	262	38167	2418	$\pi \rightarrow \pi^*$
	293	34129	3223	$\pi \rightarrow \pi^*$
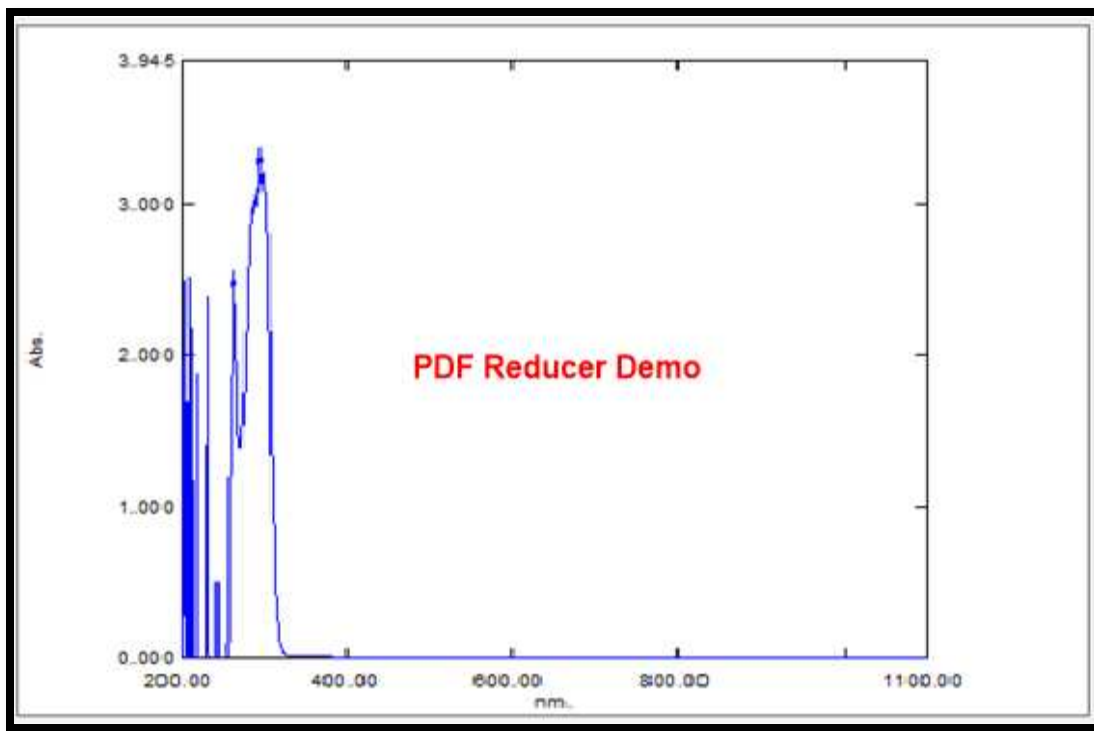
Figure(3.84) Electronic spectrum of the ligand(P).

(3.3.3.2) (UV-Vis) spectrum for the 8-hydroxyquinoline (Q)

The (UV-Vis) spectrum for the ligand (Q), Fig.(3.85) exhibits two absorption peaks, at (260 nm=38461cm^{-1}; ε_{max}=2020 molar^{-1}cm^{-1}) and (310 nm =32258 cm^{-1};ε_{max}= 3248 molar^{-1}cm^{-1}) which were assigned to ($\pi \rightarrow \pi^*$) and (n$\rightarrow \pi^*$) transition respectively[172],Table (3.36).

Table(3.36): Electronic spectral data of the ligand(Q).

Compound	Wave length λ_{nm}	Wave number (cm^{-1})	$\varepsilon_{max}(moler^{-1}.cm^{-1})$	Assignment
(Q)	260	38461	2020	$\pi \rightarrow \pi^*$
	310	32258	3248	$\pi \rightarrow \pi^*$
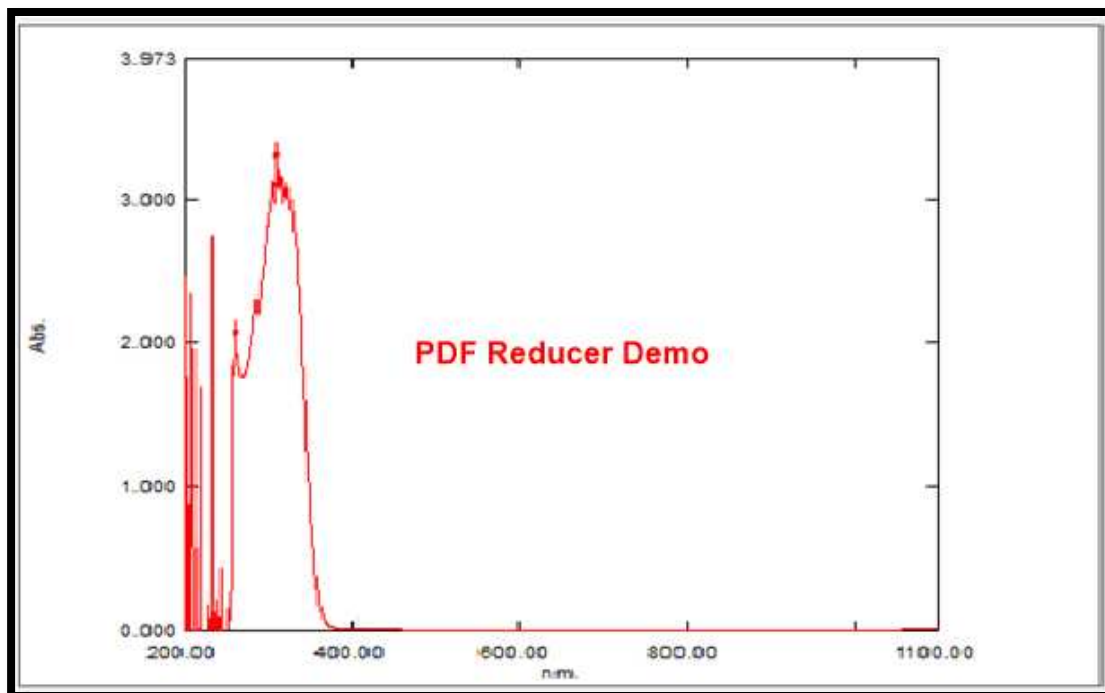
(3.85) Electronic spectrum of the ligand(Q).

(3.3.4) (UV-Vis) Spectra of mixed–ligand complexes.

(3.3.4.1)(UV-Vis)Spectra of [Co(L^1)(P)], [Ni(L^1)(P)],[Zn(L^1)(P)], [Co(L^2)(P)], [Ni(L^2)(P)],[Zn(L^2)(P)], [Co(L^3)(P)], [Ni(L^3)(P)] and [Zn(L^3)(P)] for mixed-ligand complexes.

All the results obtained from the mixed-ligand complexes were listed in Table(3.37).the (UV-Vis) spectrum of [Co(L^1)(P)] complex , exhibits five peaks Fig.(3.86), the first and second absorption peaks at (242nm = 41322 cm$^-$^{1} ;ε_{max}=1862 molar^{-1}cm^{-1}) and (295 nm =33898 cm^{-1} ;ε_{max}=3941 molar^{-1}cm^{-1}) are due to the intra ligand .These peaks were shifted in comparison with the spectrum of the free ligands .The third peak at (358 nm =27932 cm^{-1} ;ε_{max}=2740 molar^{-1}cm^{-1}) is due to the charge transfer transition, while the four at (615nm =16260 cm$^-$^{1} ;ε_{max}= 120 molar^{-1}cm^{-1}) which can be assigned to the(d-d) electronic transition

153

type $^4A_{2(F)} \rightarrow {}^4T_{1(P)}$, suggested a distorted tetrahedral structure around the (Co^{II}) ion [173].

The (UV-Vis) spectrum of [Ni(L^1)(P)] complex, exhibits five peaks Fig. (3.87), the first and second peaks at (303 nm =33003cm^{-1} ;ε_{max}= 3968 molar^{-1}cm^{-1}) and (450 nm =22222cm^{-1} ;ε_{max}= 210 molar^{-1}cm^{-1}) are due to the intra ligand and charge transfer transition respectively. The two peaks at (918 nm =10893 cm^{-1} ;ε_{max}=121 molar^{-1}cm^{-1}) and the second peak at (1037 nm =9643 cm^{-1} ;ε_{max}=123 molar^{-1}cm^{-1}) are assigned to the (d-d) electronic transition type $^3T_1 \rightarrow {}^3T_{1(P)}$ and $^3T_1 \rightarrow {}^3A_2$ respectively ,suggested a distorted tetrahedral structure around the (Ni^{II}) ion [166].

The (UV-Vis) spectrum of [Zn(L^1)(P)] complex ,exhibits three peaks Fig.(3.88) ,the first, second and third peaks at(279 nm=35842cm^{-1};ε_{max}=3998 molar^{-1}cm^{-1}),(304 nm =32894 cm^{-1} ;ε_{max} =3983 molar^{-1}cm^{-1}) and (398nm =25125 cm^{-1} ;ε_{max}= 912 molar^{-1}cm^{-1}) are due to the intra ligand and the charge transfer transition. Since the metal ion of complex belongs to (d^{10}) system, these peaks suggested a tetrahedral structure around (Zn^{II}) ion[167].

The (UV-Vis) spectrum of [Co(L^2)(P)] complex, exhibits three peaks Fig. (3.89), the first and second peaks at (300 nm =33333 cm^{-1} ;ε_{max}=3928 molar^{-1}cm^{-1}) and (366nm =27322 cm^{-1} ;ε_{max}= 2614 molar^{-1}cm^{-1}) are due to the intra ligand and the charge transfer transition respectively, while the third peak at (607nm =16474 cm^{-1} ;ε_{max}=106 molar^{-1}cm^{-1}) is due to the (d-d) electronic transition type $^4A_{2(F)} \rightarrow {}^4T_{1(p)}$ suggested distorted tetrahedral structure around the (Co^{II})ion [173] .

The (UV-Vis) spectrum of [Ni(L^2)(P)] complex, exhibits four peaks Fig. (3.90), the first three peaks at (281 nm =35587 cm^{-1} ;ε_{max}=3872 molar^{-1}cm^{-1}), (353 nm=28328 cm^{-1} ;ε_{max}=3804 molar^{-1}cm^{-1}) and (460 nm =21739 cm^{-1};ε_{max}=998 molar^{-1}cm^{-1}) are due to the intra ligand and the charge transfer transition

respectively, while the fourth peak at (858 nm =11655 cm^{-1} ;ε_{max}= 139 molar^{-1}cm^{-1}) is assigned to the (d-d)electronic transition type $^3T_{1(F)} \rightarrow ^3T_{2(p)}$ suggested distorted tetrahedral structure around the (Ni^{II}) ion[166].

The (UV-Vis) spectrum of [Zn(L^2)(P)] complex, exhibits three peaks Fig. (3.91), the first and second peaks at (238 nm =42016= cm^{-1} ;ε_{max}=1614 molar^{-1}cm^{-1}) and (293nm =34129= cm^{-1} ;ε_{max}=3863 molar^{-1}cm^{-1}) are due to the intra ligand. While the peak at (400 nm =25000 cm^{-1} ;ε_{max}=369 molar^{-1}cm^{-1}) which assigned to the charge transfer transition. Since the metal ion of complex belongs to (d^{10}) system, these peaks suggested distorted tetrahedral structure around (Zn^{II}) ion[167,174].

The (UV-Vis) spectrum of [Co(L^3)(P)] complex ,exhibits five peaks Fig. (3.92) ,the first, second and third peaks at (232nm=43103cm^{-1};ε_{max}=627 molar^{-1}cm^{-1}) ,(305nm=32786 cm^{-1} ;ε_{max}=3622 molar^{-1}cm^{-1}) and (355nm =28129= cm^{-1} ;ε_{max}= 3318 molar^{-1}cm^{-1})are due to the intra ligand transition respectively. The fourth peak at (488 nm =20491 cm^{-1} ;ε_{max}=626 molar^{-1}cm^{-1}) is due to charge transfer transition. The fifth peak at (620 nm =16129 cm^{-1} ;ε_{max}= 452 molar^{-1}cm^{-1}) is due to the (d-d) electronic transition type $^4A_2 \rightarrow ^4T_{1(P)}$, suggested distorted tetrahedral structure around the (Co^{II}) ion [173].

The (U.V-Vis) spectrum of [Ni(L^3)(P)] complex, exhibits four peaks Fig. (3.93),the first, second and third peaks at (226nm =44247cm^{-1};ε_{max}=634 molar^{-1}cm^{-1}),(304 nm =32894 cm^{-1} ;ε_{max}=3628 molar^{-1}cm^{-1}) and (378nm =26455 cm^{-1};ε_{max}=631 molar^{-1}cm^{-1}) are due to intra ligand and charge transfer transition respectively . The fourth peak at (1034 nm=9671 cm^{-1} ;ε_{max}=153 molar^{-1}cm^{-1}) is due to the (d-d) electronic transition type $^3T_{1(F)} \rightarrow ^3A_{2(F)}$ suggested distorted tetrahedral structure around the (Ni^{II}) ion [166].

The (UV-Vis) spectrum of $[Zn(L^3)(P)]$ complex, exhibits three peaks Fig. (3.94), the first and second peaks at (249 nm=40160 cm^{-1} ;ε_{max}=2895 molar^{-1}cm^{-1}) and (292nm =34246 cm^{-1} ;ε_{max}= 3786 molar^{-1}cm^{-1}) are due to the intra ligand, while the third peak at (450nm =22222 cm^{-1} ;ε_{max}=912 molar^{-1}cm^{-1}) is due to the charge transfer transition. Since the metal ion of complex belongs to (d^{10}) system, these peaks suggested distorted tetrahedral structure around (Zn^{II}) ion[167,174].
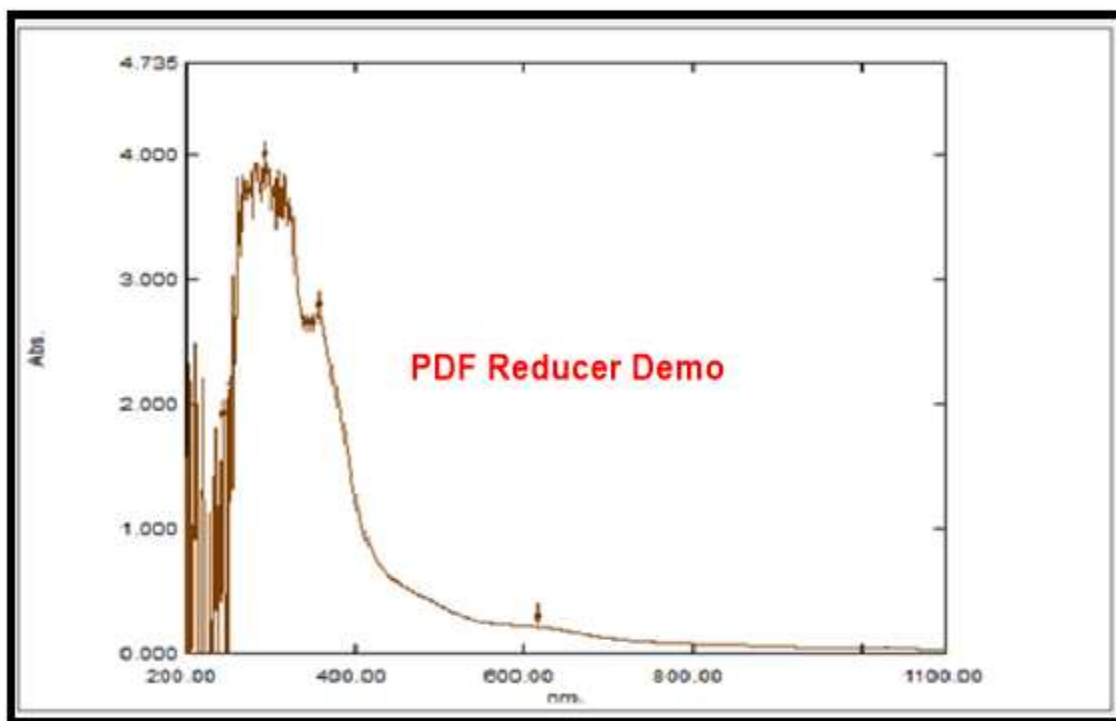
Figure(3.86):Electronic spectrum of[Co(L^1)(P)]complex in DMSO solution.

156
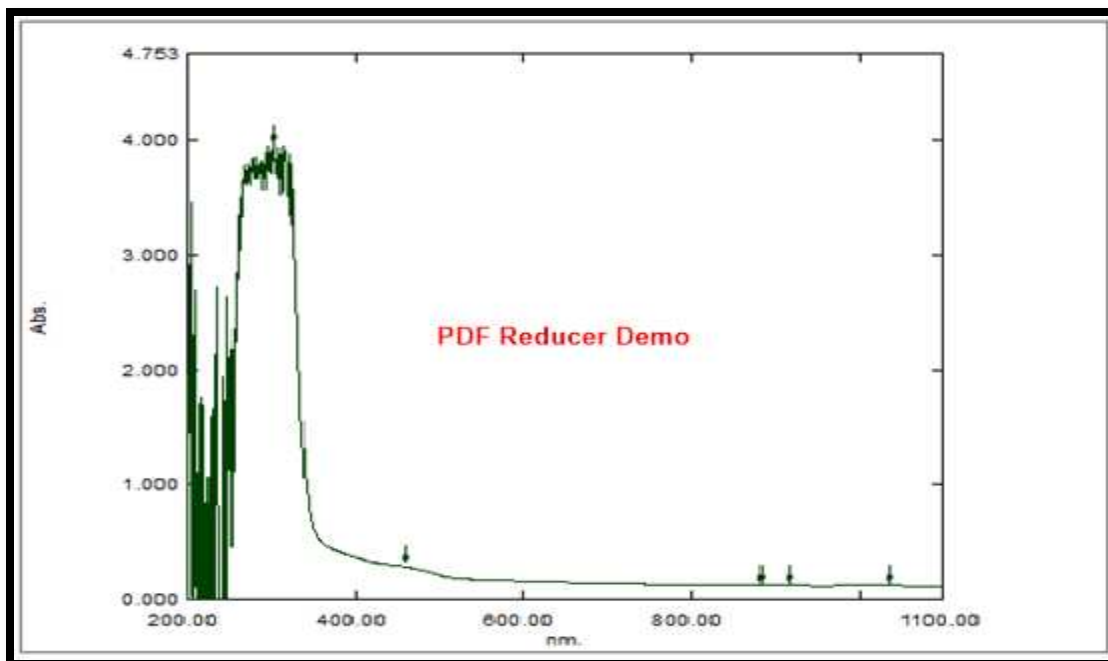
Figure(3.87):Electronic spectrum of[Ni(L^1)(P)]complex in DMSO solution.
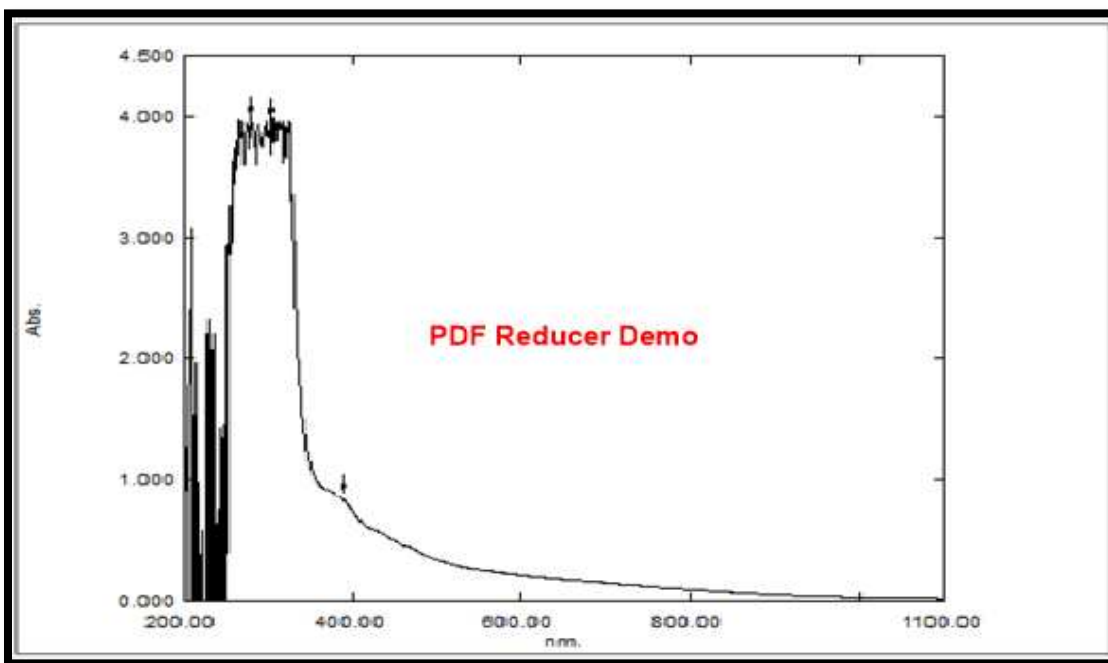
Figure(3.88):Electronic spectrum of[Zn(L^1)(P)]complex in DMSO solution.
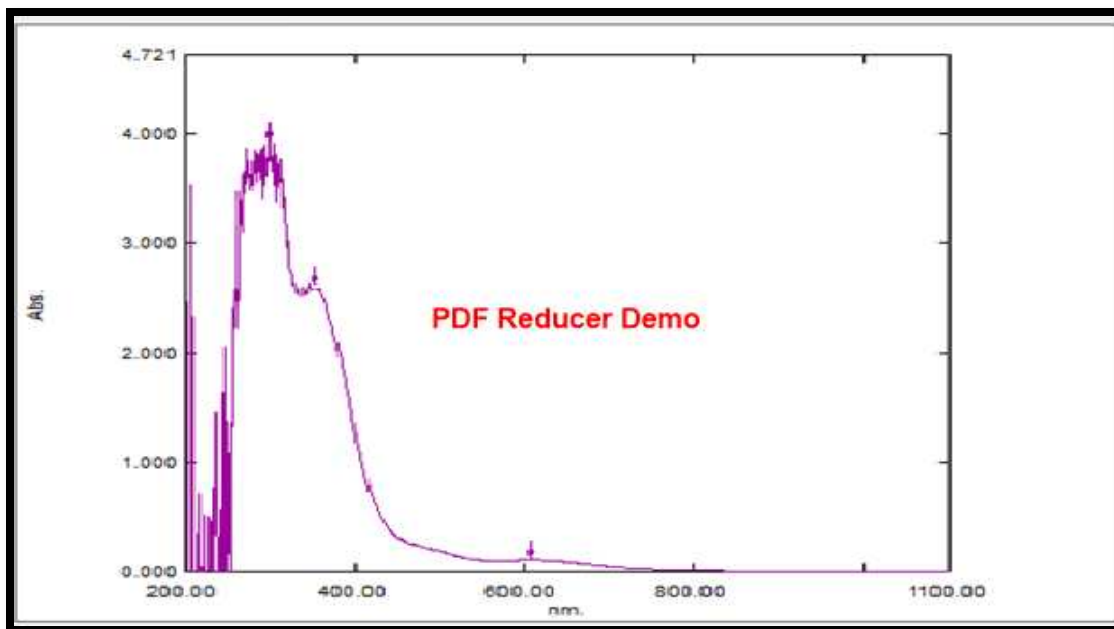
Figure(3.89):Electronic spectrum of[Co(L^2)(P)]complex in DMSO solution.
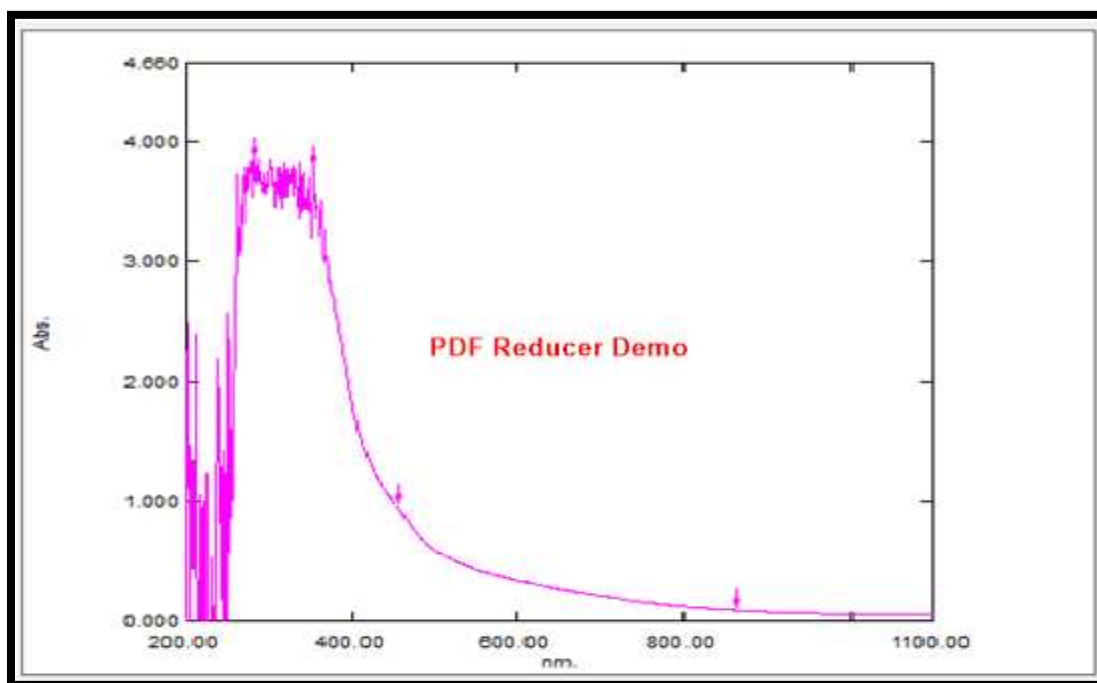
Figure(3.90):Electronic spectrum of[Ni(L^2)(P)]complex in DMSO solution.

158
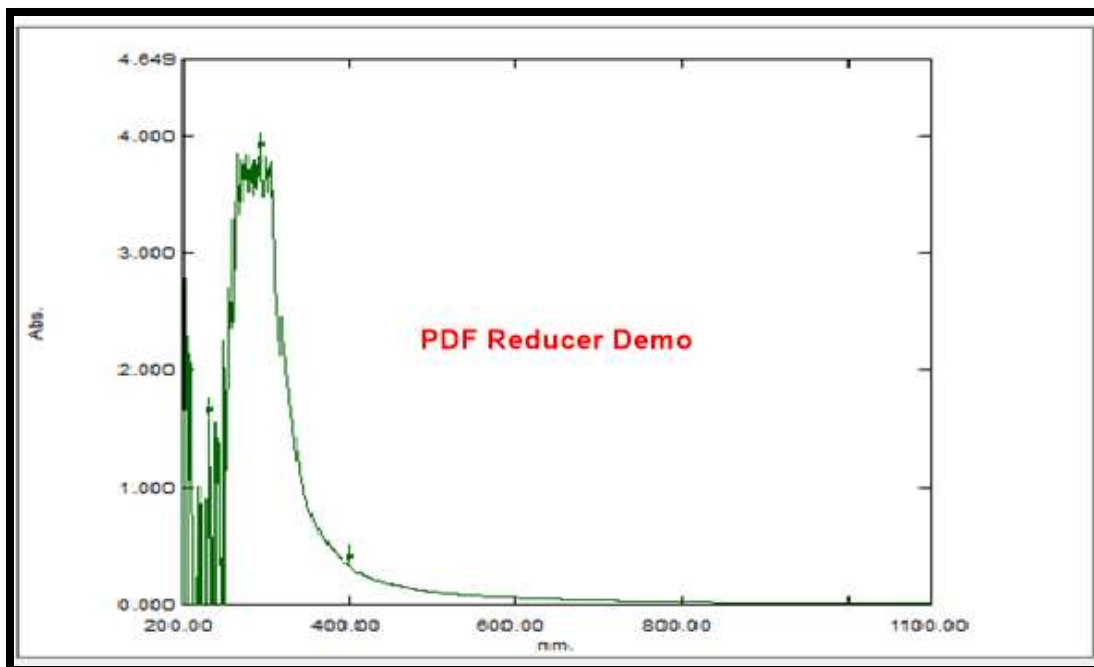
Figure(3.91):Electronic spectrum of[Zn(L^2)(P)]complex in DMSO solution.
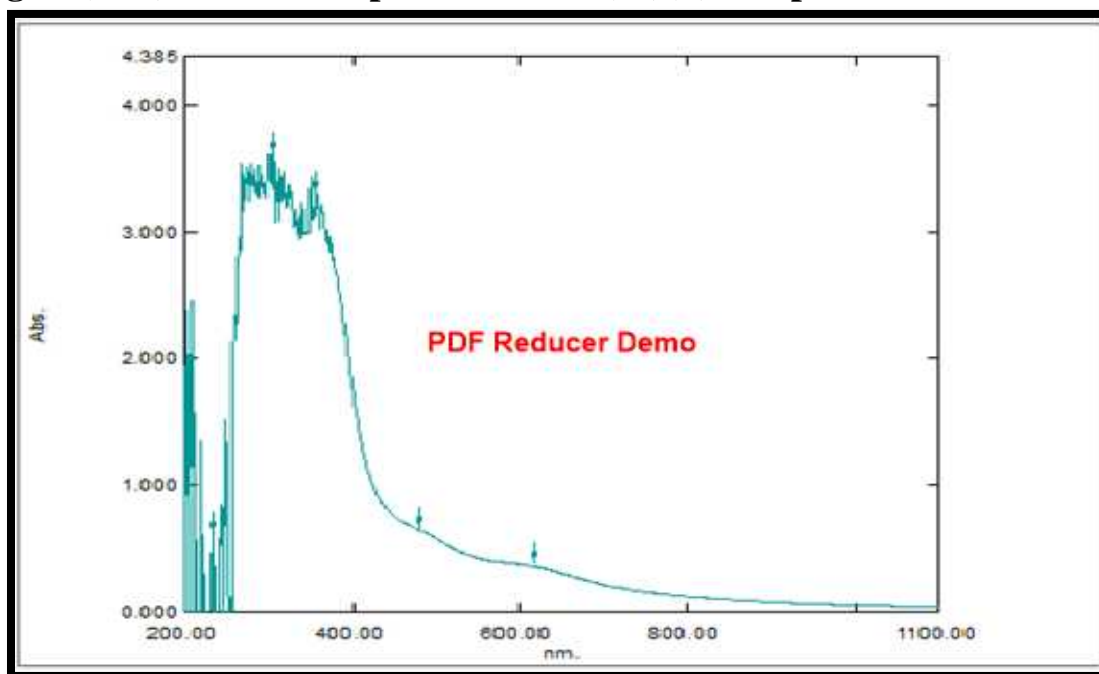
Figure(3.92):Electronic spectrum of[Co(L^3)(P)]complex in DMSO solution.

159
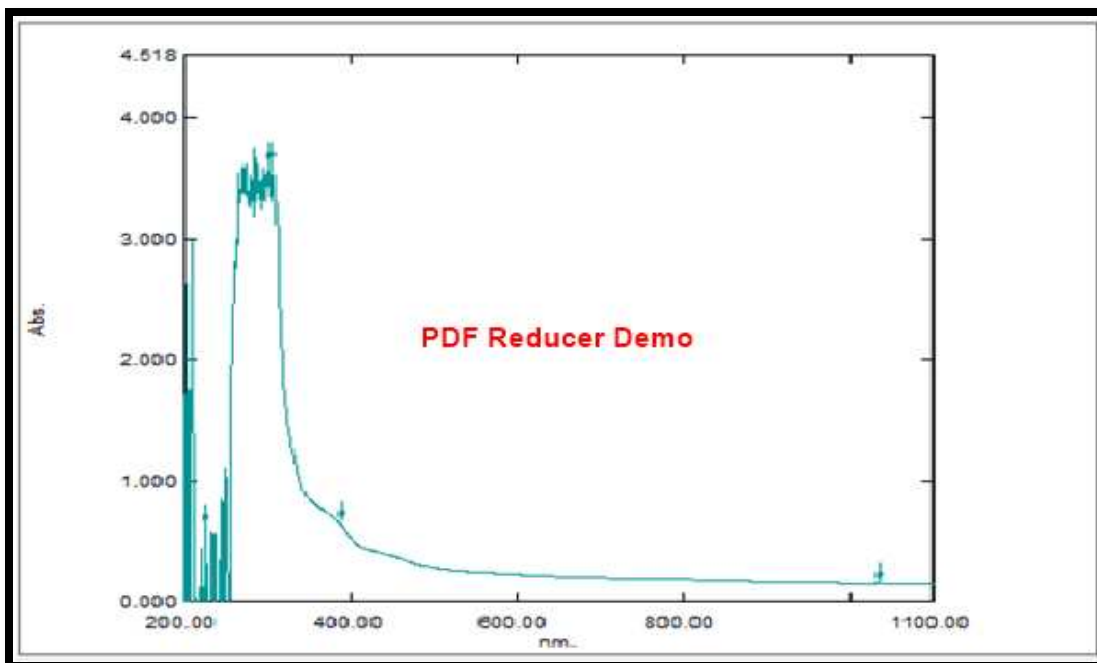
Figure(3.93):Electronic spectrum of[Ni(L^3)(P)]complex in DMSO solution.
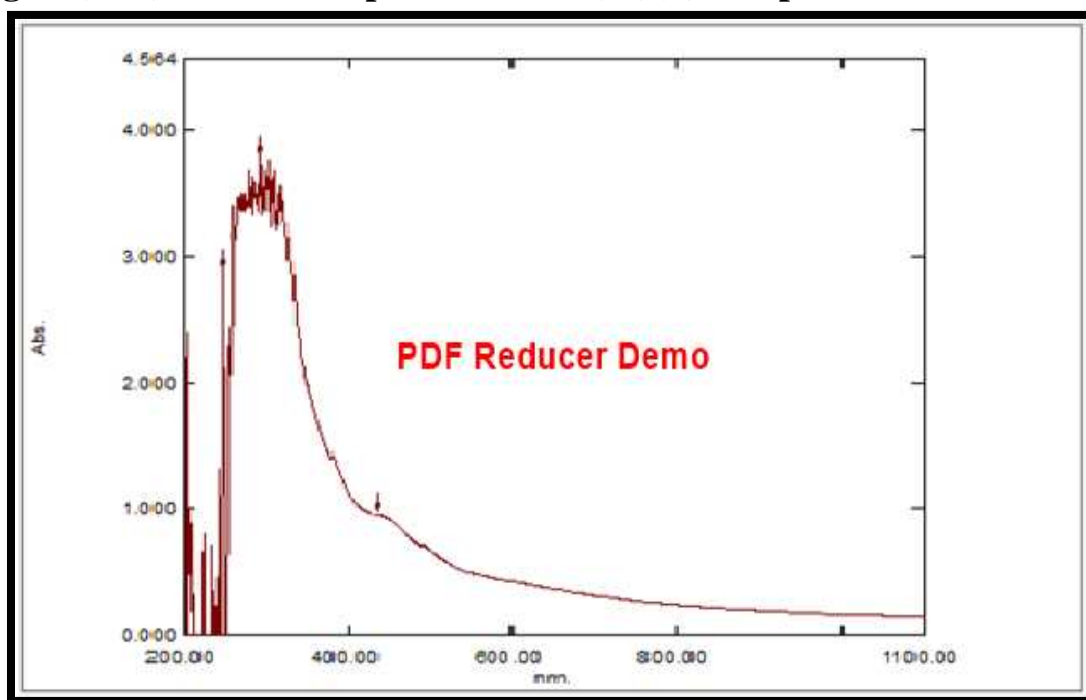
Figure(3.94):Electronic spectrum of[Zn(L^3)(P)]complex in DMSO solution.
(3.3.4.2)(UV-Vis)Spectra of [Co(L^1)(Q)],[Ni(L^1)(Q)],[Zn(L^1)(Q)],

[Co(L^2)(Q)],[Ni(L^2)(Q)],[Zn(L^2)(Q)], [Co(L^3)(Q)], [Ni(L^3)(Q)] and [Zn(L^3)(Q)]

for mixed-ligand complexes.

160

The (UV-Vis) spectrum of $[Co(L^1)(Q)]$ complex , exhibits four peaks Fig.(3.95), the first and second absorption peaks at (301nm =33222cm^{-1} ;ε_{max}=3857 molar^{-1}cm^{-1}) and (378 nm =26455 cm^{-1} ;ε_{max}=3820 molar^{-1}cm^{-1}) are due to the intra ligand and charge transfer transition respectively .The third peak at (599nm =16694cm^{-1} ;ε_{max}=159 molar^{-1}cm^{-1}) is due to the (d-d) electronic transition type $^4A_{2(F)}\rightarrow^4T_{1(P)}$ suggested a distorted tetrahedral structure around the (Co^{II}) ion [173].

The (UV-Vis) spectrum of $[Ni(L^1)(Q)]$ complex, exhibits three peaks Fig. (3.96), the first peak at (305nm =32786cm^{-1} ;ε_{max}= 3979 molar^{-1}cm^{-1}) is due to the intra ligand. The second peak at (401nm =24937cm^{-1} ;ε_{max}=1912 molar^{-1}cm^{-1}) is due to the charge transfer transition, while the third peak at (875nm =11428cm^{-1} ;ε_{max}=197 molar^{-1}cm^{-1}) which can be assigned to the (d-d) electronic transition type $^3T_1\rightarrow^3T_{1(P)}$ suggested a distorted tetrahedral structure around the (Ni^{II}) ion [166].

The (UV-Vis) spectrum of $[Zn(L^1)(Q)]$ complex ,exhibits three peaks Fig.(3.97) , the first two peaks at (218nm =45871cm^{-1} ;ε_{max}=2048 molar^{-1} cm^{-1}) ,(278nm =35971cm^{-1} ;ε_{max}=3876 molar^{-1}cm^{-1}) are due to the intra ligand ,while the third peak at (400nm =25000cm^{-1} ;ε_{max}=2633 molar^{-1}cm^{-1}) is assigned to the charged transfer transition. Since the metal ion of complex belongs to (d^{10}) system, this peak was assigned to charge transfer transitions and suggested distorted tetrahedral structure around (Zn^{II}) ion[167,174].

The (UV-Vis) spectrum of $[Co(L^2)(Q)]$ complex, exhibits three peaks Fig.(3.98), the first and second peaks at (297 nm =33670 cm^{-1} ;ε_{max}=3457 molar^{-1}cm^{-1}) and (407nm =24570 cm^{-1} ;ε_{max}= 3962 molar^{-1}cm^{-1}) are due to the intra ligand and the charge transfer transition respectively, while the third peak at (610nm =16393cm^{-1} ;ε_{max}=440 molar^{-1}cm^{-1}) is assigned to the (d-d) electronic transition

type $^4A_{2(F)} \rightarrow {}^4T_{1(P)}$ suggested distorted tetrahedral structure around the (Co^{II})ion [173] .

The (UV-Vis) spectrum of [Ni(L^2)(Q)] complex, exhibits four peaks Fig. (3.99), the first and second peaks at (290nm =34482 cm^{-1} ;ε_{max}=3911 molar^{-1}cm^{-1}) and (342 nm =29239 cm^{-1} ;ε_{max}=2891 molar^{-1}cm^{-1}) are due to the intra ligand. the third peak at (404 nm =24752 cm^{-1} ;ε_{max}= 2543 molar^{-1}cm^{-1}) is due to the charge transfer transition, while the forth peak at (801)nm =12484 cm^{-1} ;ε_{max}= 51 molar^{-1}cm^{-1}) which assigned to the (d-d)electronic transition type $^3T_{1(F)} \rightarrow {}^3T_{1(P)}$ suggested distorted tetrahedral structure around the (Ni^{II}) ion[166].

The (UV-Vis) spectrum of [Zn(L^2)(Q)] complex, exhibits three peaks Fig.(3.100), the first two peaks at (294nm =34013 cm^{-1} ;ε_{max}=3830 molar^{-1}cm^{-1}) and (339nm =29498 cm^{-1} ;ε_{max}=2539 molar^{-1}cm^{-1}) are due to the intra ligand. While the third peak at (398 nm =25125) cm^{-1} ;ε_{max}=2545 molar^{-1}cm^{-1}) which is assigned to the charge transfer transition. Since the metal ion of complex belongs to (d^{10}) system, these peak was suggested a distorted tetrahedral structure around (Zn^{II}) ion[167,174].

The (UV-Vis) spectrum of [Co(L^3)(Q)] complex ,exhibits three peaks Fig.(3.101) ,the first and second absorption peaks at (321nm =31152cm^{-1} ;ε_{max}=3716 molar^{-1}cm^{-1}) and (429nm =23310 cm^{-1} ;ε_{max}=3870 molar^{-1}cm^{-1}) are due to the intra ligand and charge transfer transition respectively. The third peak at (608 nm =16447 cm^{-1} ;ε_{max}=463 molar^{-1}cm^{-1}) is assigned to the (d-d) electronic transition type $^4A_2 \rightarrow {}^4T_{1(P)}$ suggested distorted tetrahedral structure around the (Co^{II}) ion [173].

The (U.V-Vis) spectrum of [Ni(L^3)(Q)] complex, exhibits four peaks Fig.(3.102),the first and second peaks at (293nm =34129) cm^{-1} ;ε_{max}=3844 molar^{-1}cm^{-1}) and (3421 nm =29239 cm^{-1} ;ε_{max}=2891 molar^{-1}cm^{-1}) due to intra ligand. The

third peak at (407 nm =24570 cm^{-1} ;ε_{max}=3319 molar^{-1}cm^{-1}) is due to the charge transfer transition, while the fourth peak at (800 nm =12500 cm^{-1} ;ε_{max}=16 molar^{-1}cm^{-1}) which assigned to the (d-d) electronic transition type $^{3}T_{1(F)}{\rightarrow}^{3}T_{1(P)}$ suggested distorted tetrahedral structure around the (Ni^{II}) ion [166].

The (UV-Vis) spectrum of [Zn(L^3)(Q)] complex, exhibits three peaks Fig.(3.103), the first two peaks at (274 nm =36496 cm^{-1} ;ε_{max}=3508 molar^{-1}cm^{-1}) and (339nm =2949cm^{-1} ;ε_{max}= 2559 molar^{-1}cm^{-1}) are due to the intra ligand, while the third peak at (399 nm =25062 cm^{-1} ;ε_{max}=2882 molar^{-1}cm^{-1}) is assigned to the charge transfer transition[R] . Since the metal ion of complex belongs to (d^{10}) system, these peak was suggested distorted tetrahedral structure around (Zn^{II}) ion[167,174].
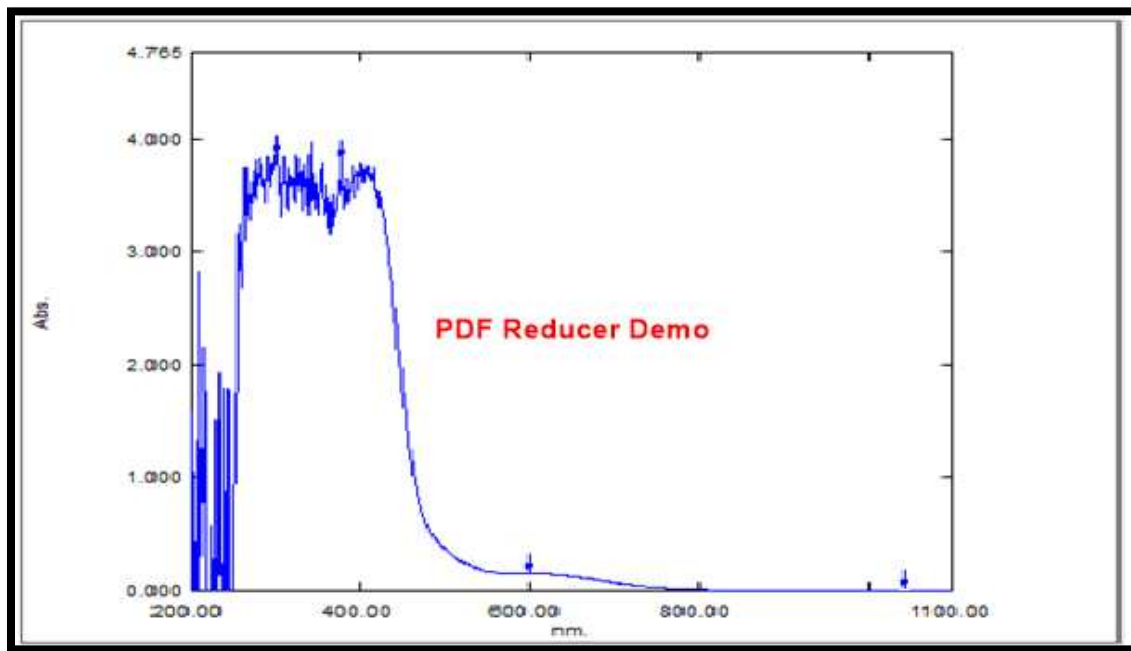
Figure(3.95):Electronic spectrum of[Co(L^1)(Q)]complex in DMSO solution.
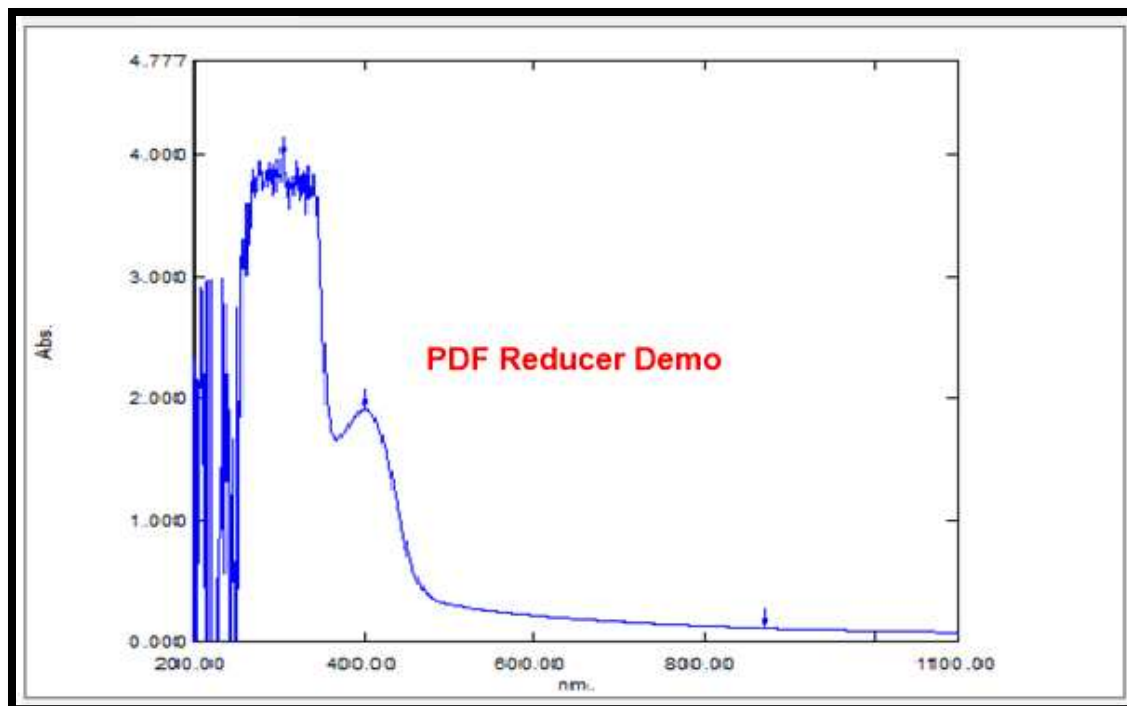
Figure(3.96):Electronic spectrum of[Ni(L^1)(Q)]complex in DMSO solution.
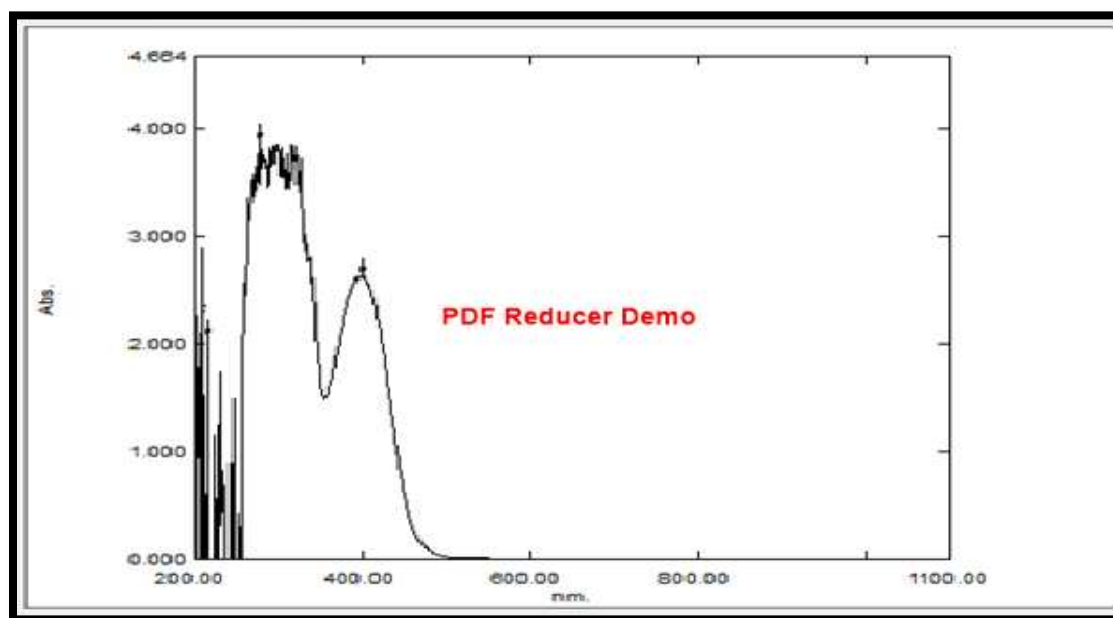
Figure(3.97):Electronic spectrum of[Zn(L^1)(Q)]complex in DMSO solution.

164
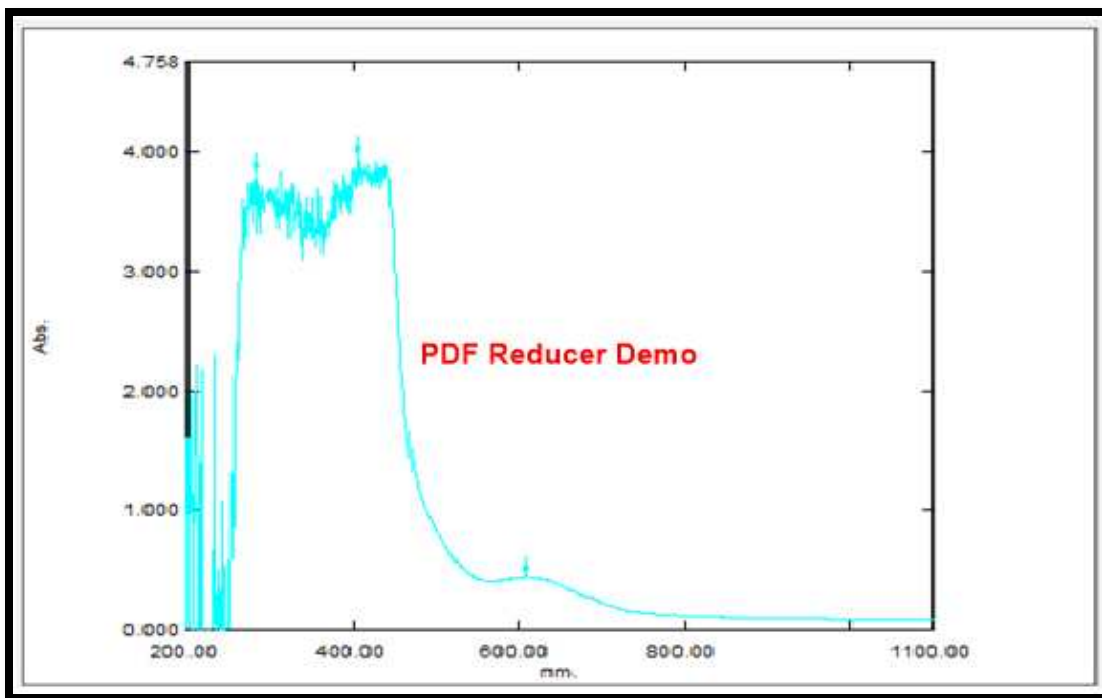
Figure(3.98):Electronic spectrum of[Co(L^2)(Q)]complex in DMSO solution.
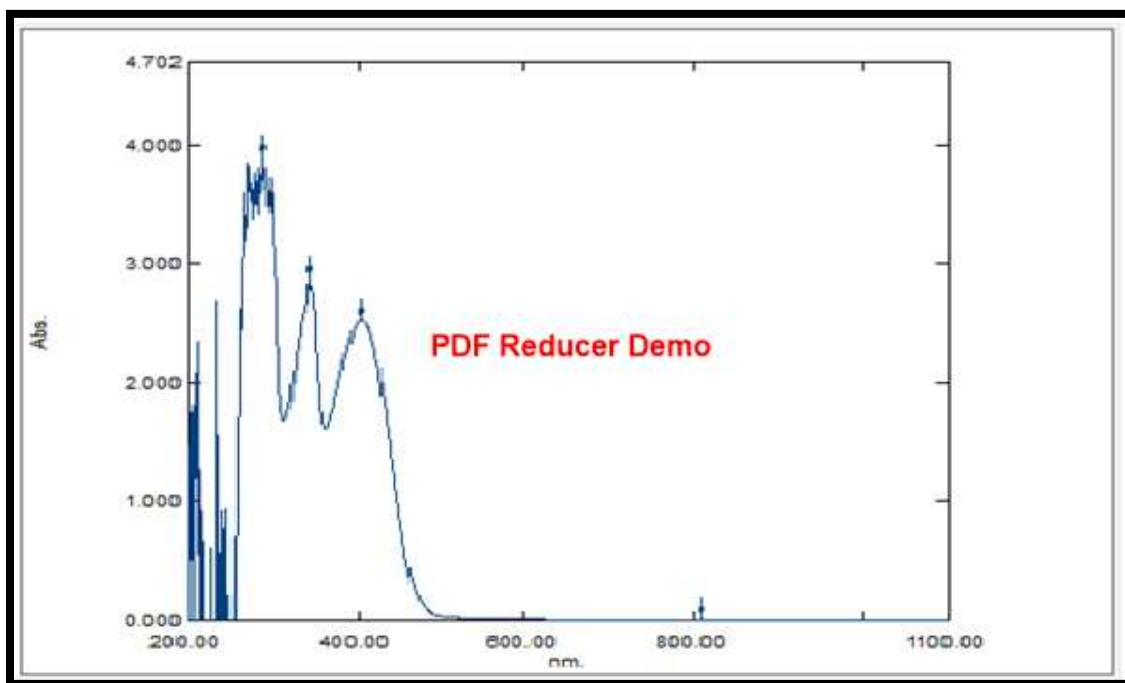
Figure(3.99):Electronic spectrum of[Ni(L^2)(Q)]complex in DMSO solution.

165
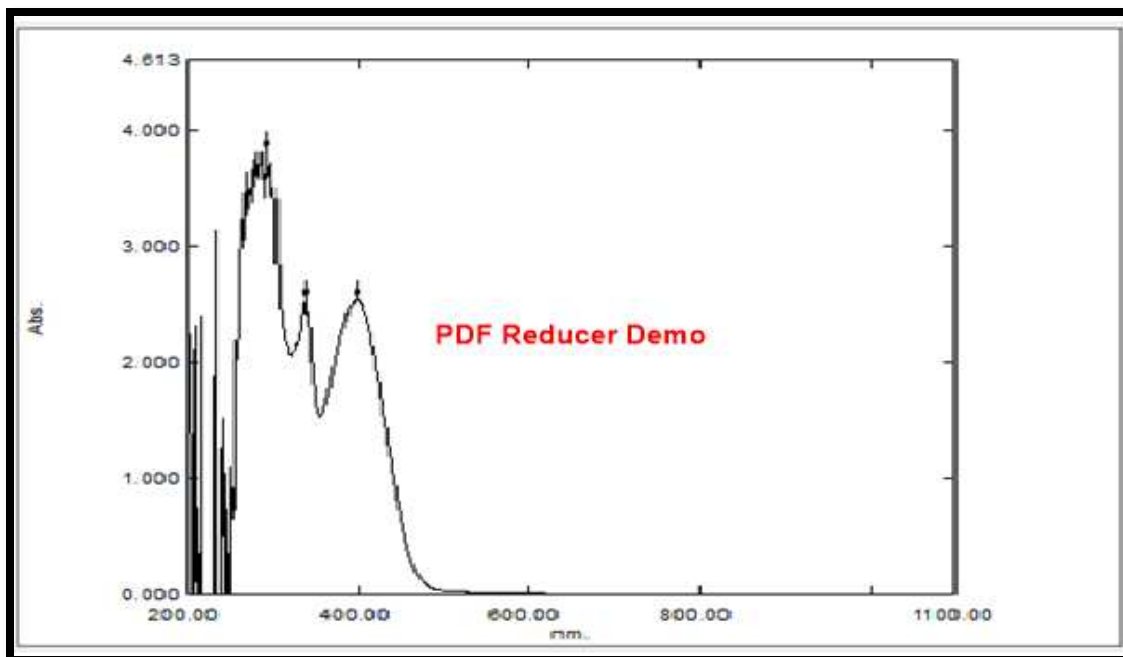
Figure(3.100):Electronic spectrum of[Zn(L^2)(Q)]complex in DMSO solution.
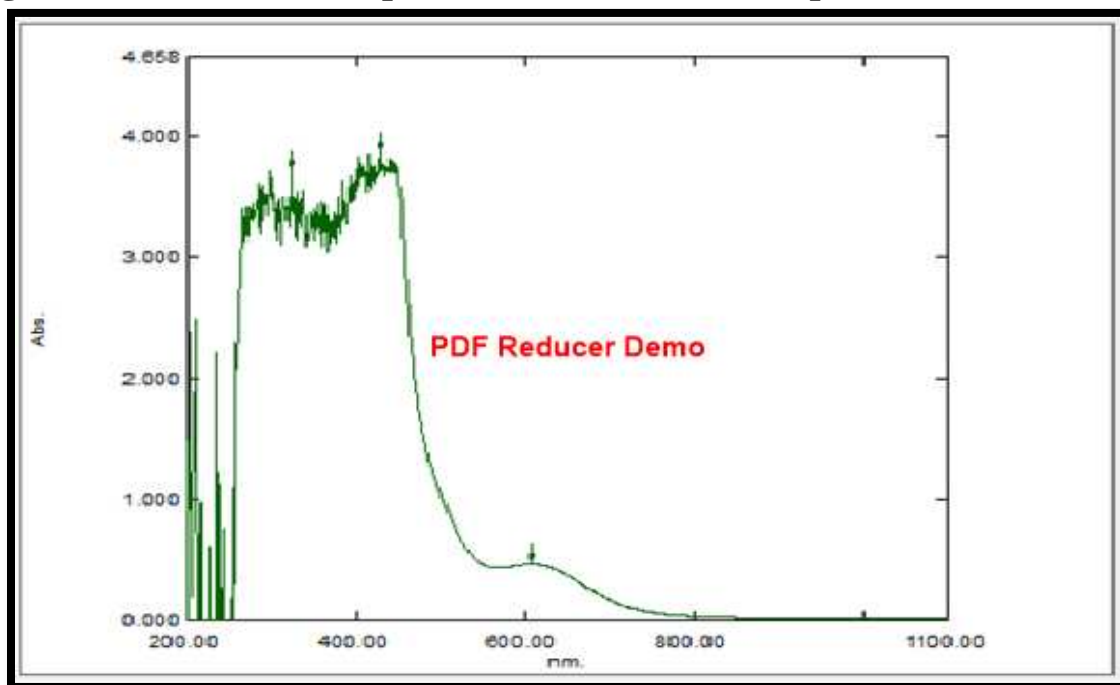
Figure(3.101):Electronic spectrum of[Co(L^3)(Q)]complex in DMSO solution.
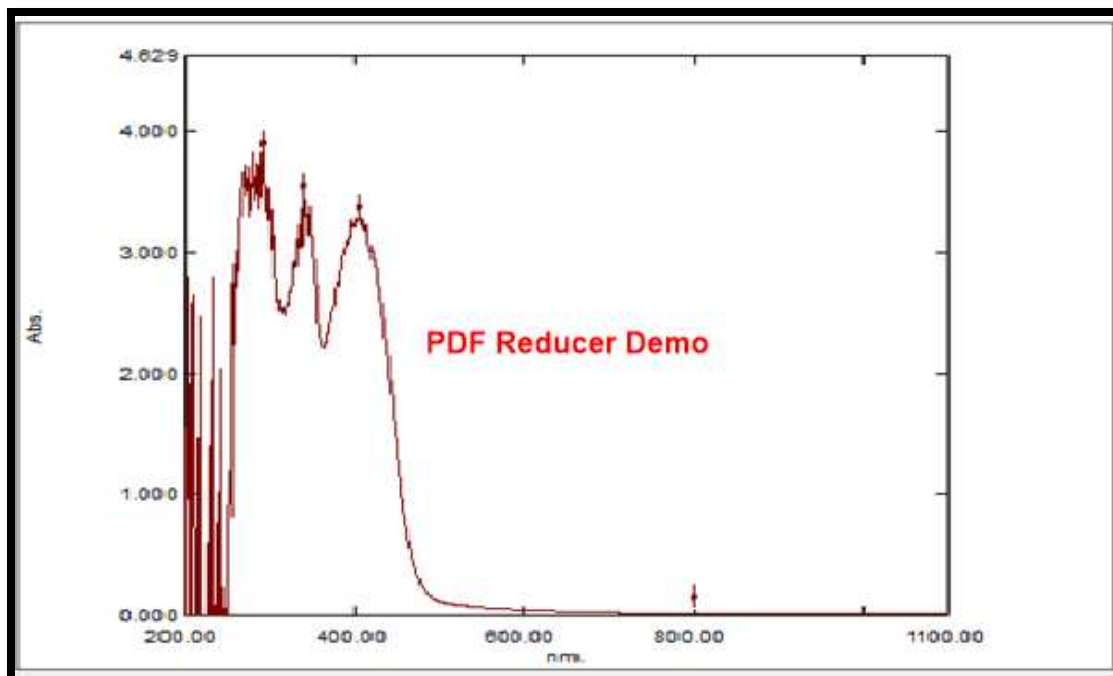
Figure(3.102):Electronic spectrum of[Ni(L^3)(Q)]complex in DMSO solution.
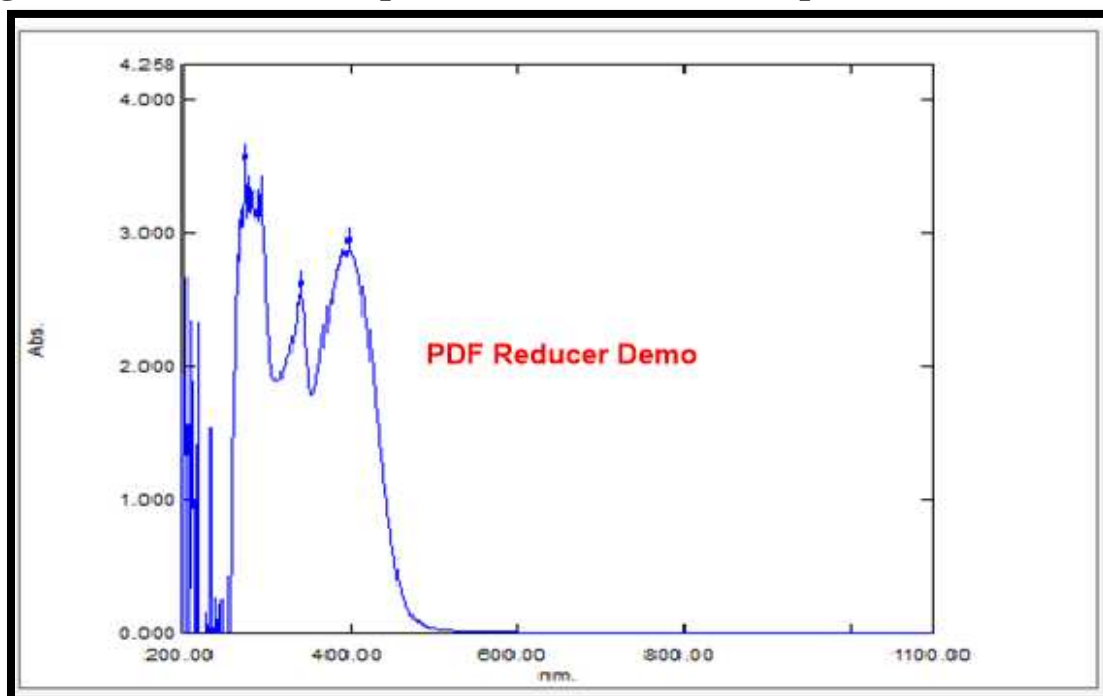
Figure(3.103):Electronic spectrum of[Zn(L^3)(Q)]complex in DMSO solution.

Table (3.37): UV-Vis spectral data of Mix-Ligand complexes in DMSO solutions.

Compound	Wave length λ_{nm}	Wave number (cm^{-1})	ε_{max} $(moler^{-1}.cm^{-1})$	Assignment	Suggested geometry
$[Co(L^1)(P)]$	242	41322	1862	Intra Ligand	Tetrahedral
	295	33898	3941	Intra Ligand	
	358	27932	2740	C.T	
	615	16260	120	$^4A_{2(F)} \rightarrow {}^4T_{1(P)}$	
$[Ni(L^1)(P)]$	303	33003	3968	Intra Ligand	Tetrahedral
	450	22222	210	C.T	
	918	10893	121	$^3T_1 \rightarrow {}^3T_{1(P)}$	
	1037	9643	123	$^3T_1 \rightarrow {}^3A_2$	
$[Zn(L^1)(P)]$	279	35842	3998	Intra Ligand	Tetrahedral
	304	32894	3983	Intra Ligand	
	398	25125	912	C.T	
$[Co(L^2)(P)]$	300	33333	3928	Intra Ligand	Tetrahedral
	366	27322	2614	C.T	
	607	16474	106	$^4A_{2(F)} \rightarrow {}^4T_{1(P)}$	
$[Ni(L^2)(P)]$	281	35587	3872	Intra Ligand	Tetrahedral
	353	28328	3804	Intra Ligand	
	460	21739	998	C.T	
	858	11655	139	$^3T_{1(F)} \rightarrow {}^3T_{1(P)}$	
$[Zn(L^2)(P)]$	238	42016	1614	Intra Ligand	Tetrahedral
	293	34129	3863	Intra Ligand	
	400	25000	369	C.T	
$[Co(L^3)(P)]$	232	43103	627	Intra Ligand	Tetrahedral
	305	32786	3622	Intra Ligand	
	355	28129	3318	Intra Ligand	
	488	20491	626	C.T	
	620	16129	452	$^4A_{2(F)} \rightarrow {}^4T_{1(F)}$	
$[Ni(L^3)(P)]$	226	44247	634	Intra Ligand	Tetrahedral
	304	32894	3628	Intra Ligand	
	378	26455	631	C.T	
	1034	9671	153	$^3T_{1(F)} \rightarrow {}^3A_{2(F)}$	
$[Zn(L^3)(P)]$	249	40160	2895	Intra Ligand	Tetrahedral
	292	34246	3786	Intra Ligand	

	450	22222	912	C.T	
$[Co(L^1)(Q)]$	301	33222	3857	Intra Ligand	Tetrahedral
	378	26455	3820	C.T	
	599	16694	159	$^4A_{2(F)} \rightarrow {}^4T_{1(P)}$	
$[Ni(L^1)(Q)]$	305	32786	3979	Intra Ligand	Tetrahedral
	401	24937	1912	C.T	
	875	11428	197	$^3T_1 \rightarrow {}^3T_{1(P)}$	
$[Zn(L^1)(Q)]$	218	45871	2048	Intra Ligand	Tetrahedral
	278	35971	3876	Intra Ligand	
	400	25000	2633	C.T	
$[Co(L^2)(Q)]$	297	33670	3457	Intra Ligand	Tetrahedral
	407	24570	3962	C.T	
	610	16393	440	$^4A_{2(F)} \rightarrow {}^4T_{1(P)}$	
$[Ni(L^2)(Q)]$	290	34482	3911	Intra Ligand	
	342	29239	2891	Intra Ligand	Tetrahedral
	404	24752	2543	C.T	
	801	12484	51	$^3T_1 \rightarrow {}^3T_{1(P)}$	
$[Zn(L^2)(Q)]$	294	34013	3830	Intra Ligand	Tetrahedral
	339	29498	2539	Intra Ligand	
	398	25125	2545	C.T	
$[Co(L^3)(Q)]$	321	31152	3716	Intra Ligand	Tetrahedral
	429	23310	3870	C.T	
	608	16447	463	$^4A_{2(F)} \rightarrow {}^4T_{1(P)}$	
$[Ni(L^3)(Q)]$	293	34129	3844	Intra Ligand	
	341	29325	3483	Intra Ligand	Tetrahedral
	407	24570	3319	C.T	
	800	12500	16	$^3T_{1(F)} \rightarrow {}^3T_{1(P)}$	
$[Zn(L^3)(Q)]$	274	36496	3508	Intra Ligand	Tetrahedral
	339	29498	2559	Intra Ligand	
	399	25062	2882	C.T	

(3.4) Thermal analysis of ligands and some selective metal complexes.

The thermal properties of prepared compounds were examined by TGA-DSC technique within the temperature range from 25-600 ºC. The heating rate was controlled at 10 ºC .min^{-1} under atmosphere of argon gas. Thermal analysis data for KL^1,KL^2 and some selective metal complexes are summarised in Table(3.38).

(3.4.1) Thermal analysis of ligand (KL[1]).

The thermogram for ligand KL[1] is shown in Fig.(3.104) , revealed that the ligand is stable up to 132ºC, as there was no significal weight loss was observed. The decomposition is a two steps process. The first step occurred within the temperature range of 132-181ºC with a quick mass loss of (5.38 %) on TG curve, which may correspond to loss of (CS_2) fragment. The second step starts at 185-255ºC with mass loss of (2.67%), which may attribute to the lossing of organic part of the ligand KL[1]. The peaks at temperature 132.1 and 221.4ºC indicated by DSC analysis refers to endothermic decomposition process, the endothermic peaks may indicate pyrolysis of organic part of ligand in an argon atmosphere [175,176].
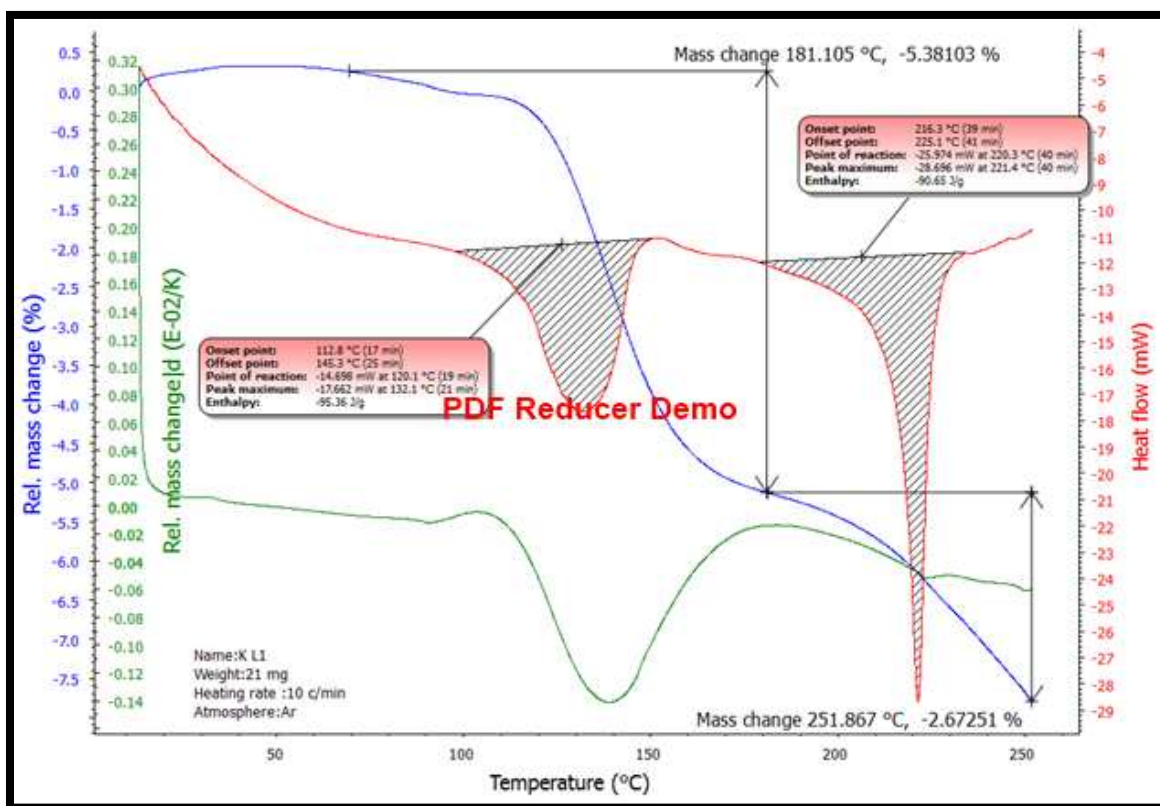
Figure(3.104): TG - DTG curve and DSC thermogram of KL[1] ligand in an argon atmosphere.

170

(3.4.2) Thermal analysis of ligand (KL^2).

The TGA curve for the ligand KL^2 is shown in Fig.(3.105) ,which revealed that the ligand is stable up to 120ºC as there was no significal weight loss was observed. The thermal decomposition of ligand KL^2 essentially taking place in three steps. The first step occurred within the range of 122-192ºC, with lossing weight of (KCS$_2$) (7.47%), and the second step at the range of 125-276.2ºC attributed to the loss of (CO + N=C-S + CH$_3$) fragment ,with lossing weight of (15.42%). The third step within the ring of 280-450ºC is due to the loss of the remaining organic parts of the ligand with lossing weight (10.24%). The peaks at of temperatures 142.3, 225 and 350ºC are indicated by the DSC analysis, the peak at 142.3ºC refers to an endothermic process, while peak at 225ºC refers to an exothermic process, last peak at 350ºC refer to exothermic process. The exothermic and endothermic peaks may indicate pyrolysis of organic ligand in an argon atmosphere. Finally the endothermic beak at temperature 60ºC in DSC thermogram may be due to presence of traces amount of ethanol trapped during the preparation process[175,176].
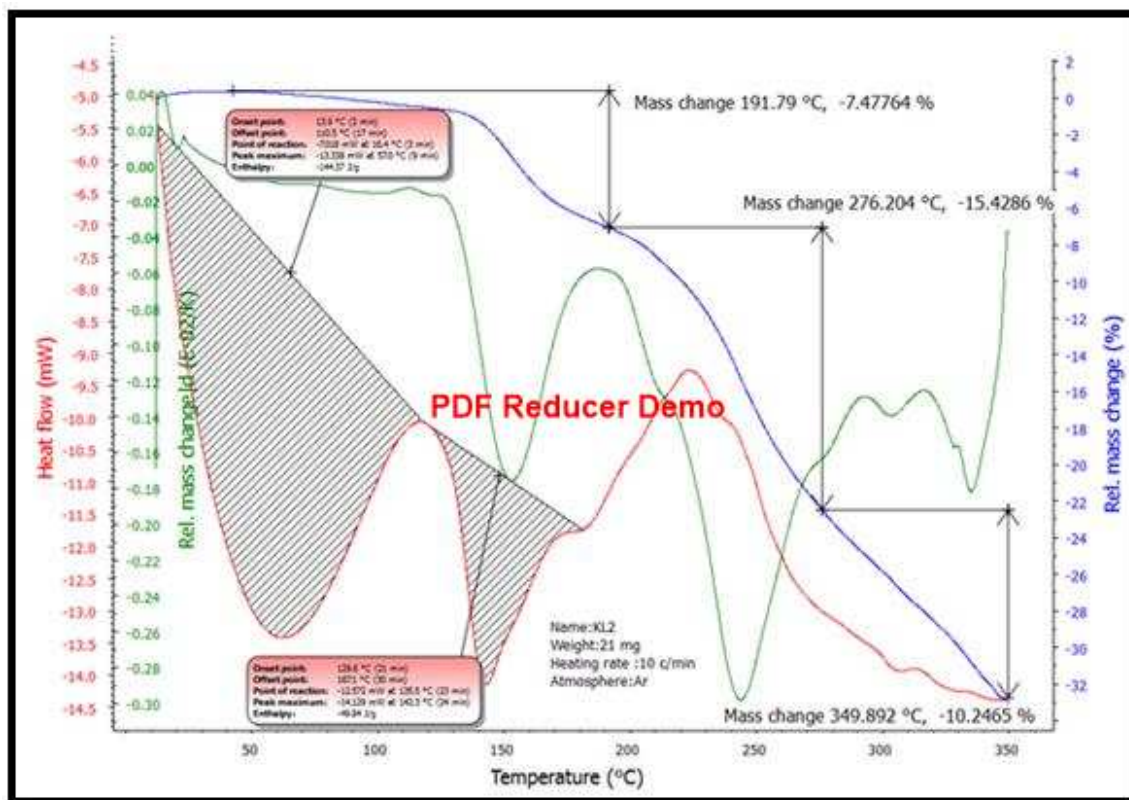
Figure(3.105): TG - DTG curve and DSC thermogram of KL^2 ligand in an argon atmosphere.

(3.4.3) Thermal analysis of [Zn(L^1)$_2$] complex.

Fig.(3.106) showed the thermogram for [Zn(L^1)$_2$] complex, which revealed that [Zn(L^1)$_2$] is stable up to 155ºC. The thermogram peaks observed at 155-594ºC attributed to the loss of (CS$_2$ + CO + 2NO + organic part of the ligand)fragment (48.40%).The differential scanning calorimetry thermogram shows four peaks, an endothermic peak at 155.8ºC and two exothermic peaks at 248.4 and 268.1ºC may refer to decomposition of the organic ligand in an argon atmosphere. The fourth exothermic peak observed at 594.3ºC may signify metal-ligand disband [177,178].

172
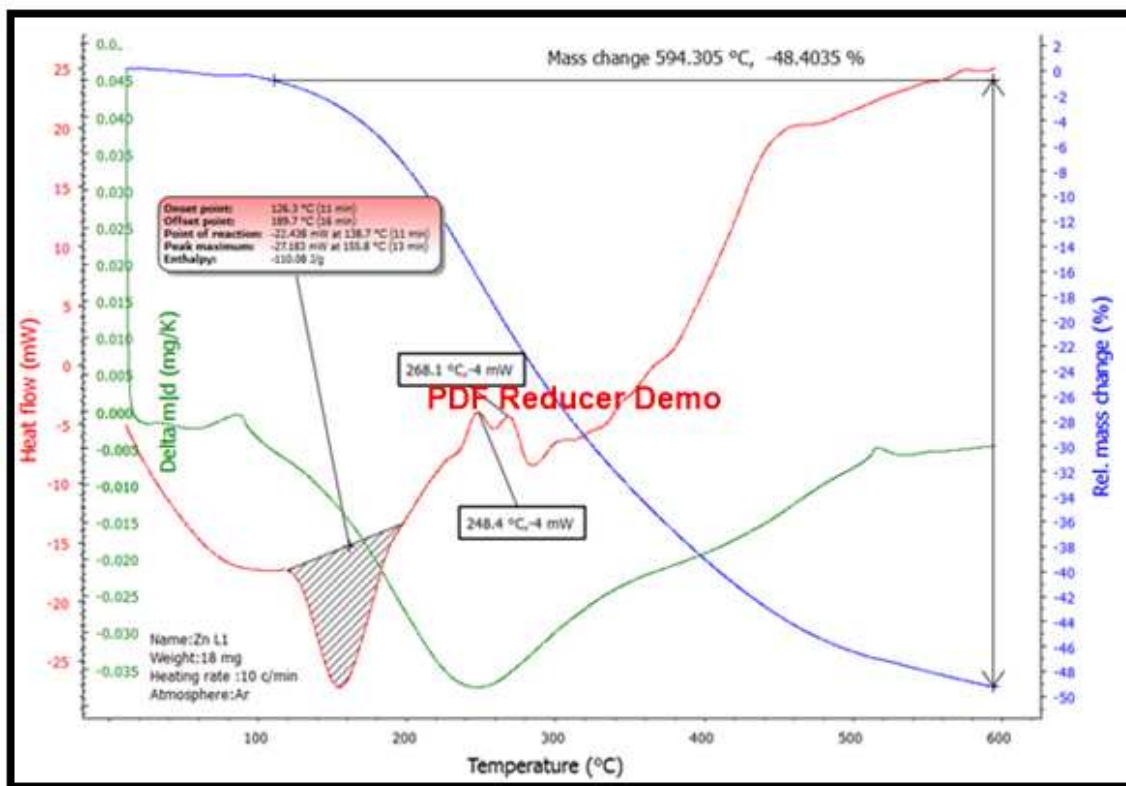
Figure(3.106): TG - DTG curve and DSC thermogram of [Zn(L^1)$_2$] complex in an argon atmosphere.

(3.4.4) Thermal analysis of [Ni(L^2)$_2$] complex.

Fig.(3.107) showed the thermogram of [Ni(L^2)$_2$]complex, which revealed the [Ni(L^2)$_2$] is stable up to 140ºC, this Figure shows two decomposition steps. The first from the range of 140-315ºC with a mass loss of (40.53%) may be due to the valitliazation of the CS$_2$ and some other parts of the ligand. The decomposition resume to about 450ºC at which point virtually of the organic part of the complex have been lost (20.32%). Ni(II) dtc symbolize a class of volatile dtc yielding the corresponding metal sulphide at about 600ºC. DSC shown three an endothermic peaks at 97.3, 149.0 and 182.8ºC may refer to decomposition process of the organic ligand in an argon atmosphere . The last an exothermic peak about may signify metal-ligand disband [179].

173
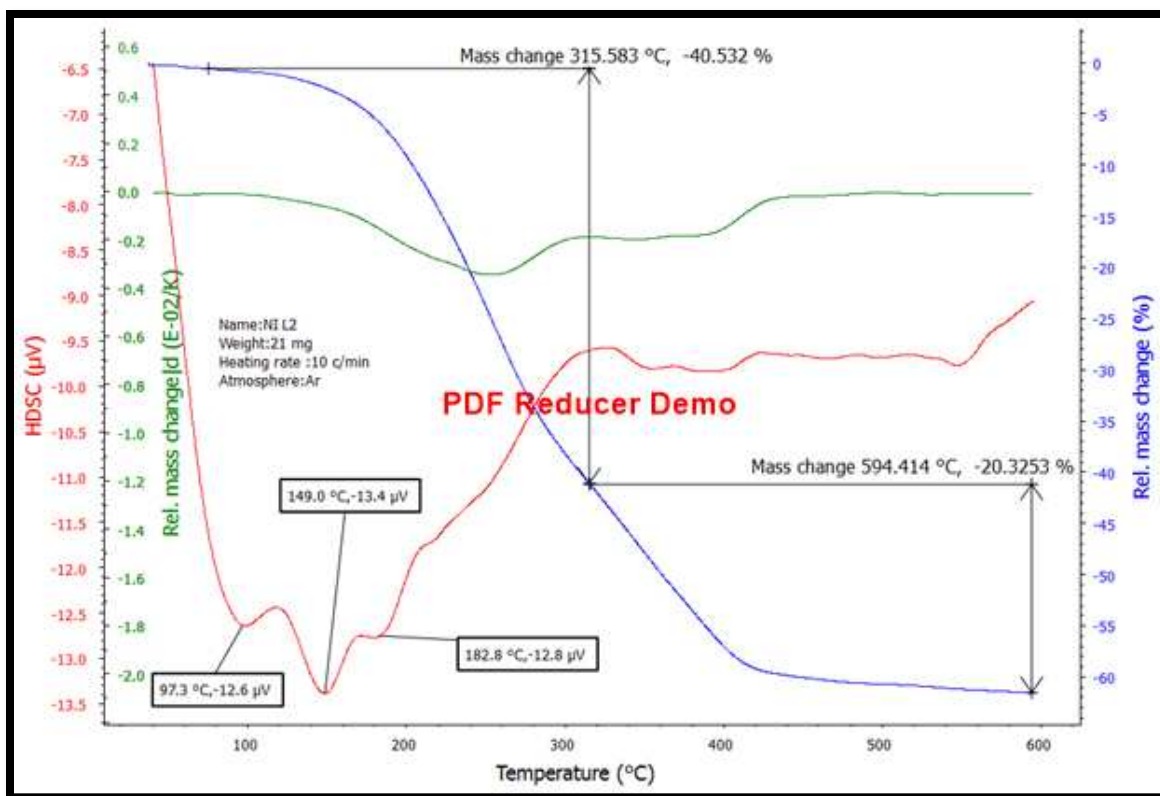
Figure(3.107): TG - DTG curve and DSC thermogram of [Ni(L^2)$_2$] complex in an argon atmosphere.

(3.4.5) Thermal analysis of [Co(L^3)$_2$] complex.

The TGA curve for [Co(L^3)$_2$]complex depicted in Fig.(3.108), revealed that the complex is stable up to 100ºC ,this Figure shows two decomposition steps. The first step occurs at 100-293ºC related to the loss of (CS$_2$ + CO + NH) fragment (24.85%). The second step at 300-595.68ºC attributed to the loss of (NH + organic parts of the ligand) fragment (23.17%).The DSC thermogram indicated an endothermic peaks at 100 and 221ºC may refer to decomposition process of the organic ligand in an organ atmosphere. The endothermic peak observed at 595.68ºC may signify metal-ligand bond breaking [180].

174
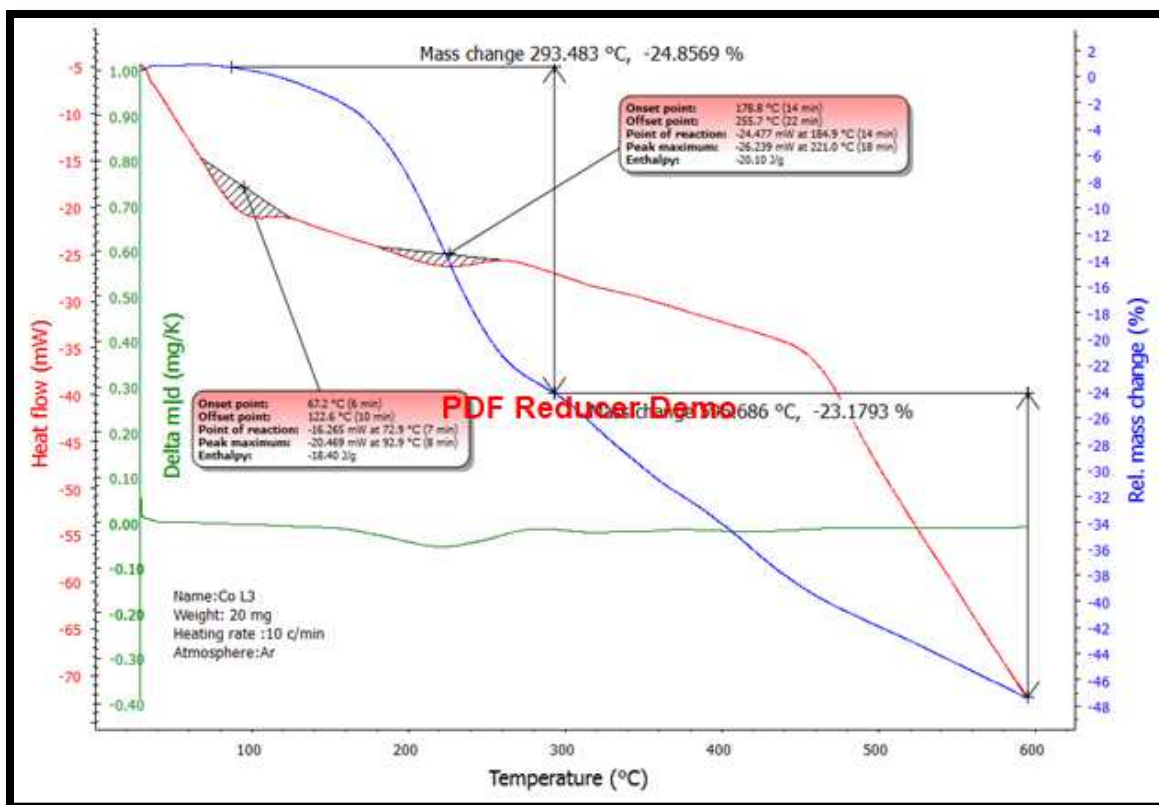
Figure(3.108): TG - DTG curve and DSC thermogram of [Co(L^3)$_2$] complex in an argon atmosphere.

(3.4.6) Thermal analysis of mixed-ligand [Zn(L^1)(P)] complex.

The TGA carve for [Zn(L^1)(P)] complex depicted in Fig.(3.109), revealed that the complex is stable up to 210ºC. peak observed at 210ºC attributed to the loss of (CS$_2$) fragment (17.43%). The other two steps at 338-480ºC and 480-595ºC attributed to the loss of organic mixed-ligand fragment (11.66%).The DSC analysis indicated an endothermic peaks at 165 and 485ºC may refer to decomposition of the organic mixed-ligand in an argon atmosphere, while peak at 261.3ºC refers to an exothermic decomposition process. Finally the exothermic peak at 595.2ºC may signify the metal-ligand bond breaking[177,178].
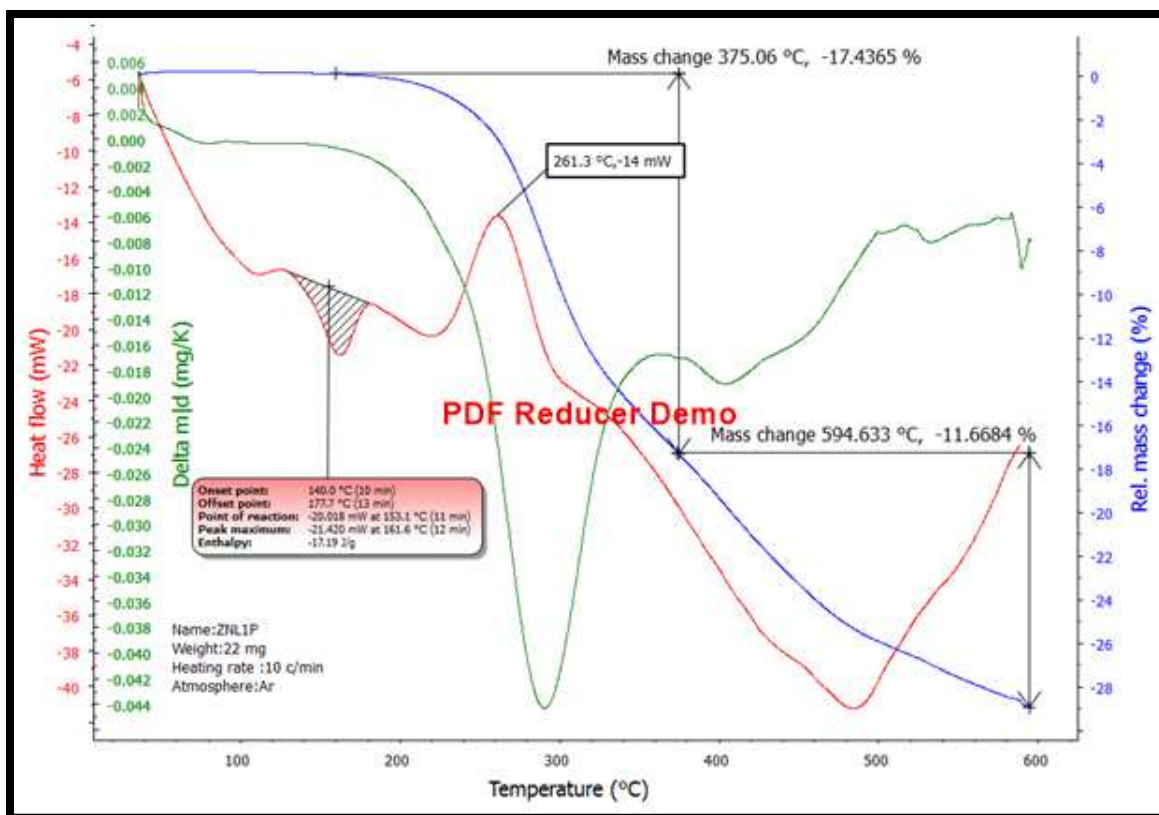
Figure(3.109): TG - DTG curve and DSC thermogram of [ZnL^{1}P] complex in an argon atmosphere.

(3.4.7) Thermal analysis of mixed-ligand [Ni(L^2)(P)] complex.

The TGA curve for [Ni(L^2)(P)] complex depicted in Fig.(3.110), revealed that the complex is stable up to 175ºC. This Figure shows three decomposition peaks in the thermogram. The first one at 290ºC, which has the highest mass loss (19.48%) ,which assigns to the loss of CS_2 fragment. The other two steps at 300-424ºC and 430-595ºC assign to the loss of organic mixed-ligand fragment (12.88% and 10.95%). The DSC analysis point to three an endothermic peaks at 88.7 ,124.0 and 241.4ºC may refer to decomposition of the organic mixed-ligand in an argon atmosphere ,the fourth peak at 595ºC refer to an exothermic decomposition process, which may signify the metal-ligand bond breaking [179].

176
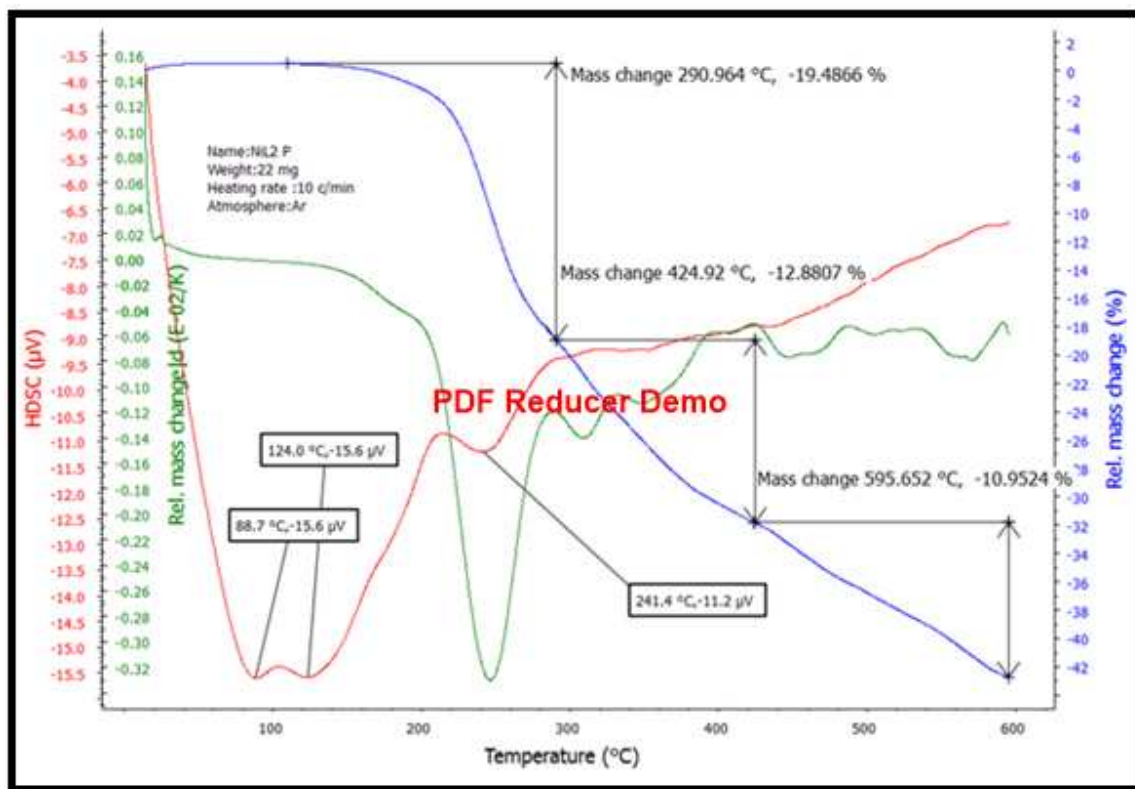
Figure(3.110): TG - DTG curve and DSC thermogram of [NiL^{2}P] complex in an argon atmosphere.

(3.4.8) Thermal analysis of mixed-ligand [Co(L^3)(P)] complex.

The TGA carve for [Co(L^3)(P)] complex is depicted in Fig.(3.111). The thermogram revealed that the complex is stable up to 118ºC. Peak observed at 118-224.2ºC attributed to the loss of (CS_2 + NH_2 +CO) fragment, (11.97%).The second step at 226-303.05ºC attributed to the loss of (phenol + CH_3 + HN-Ph-N) fragment , (17.31%) .The third step occurs at 305-595.3ºC is related to the loss of the remaining organic part of ligand. Peaks at 174 and 250.5ºC are measured by DSC analysis, both of them refer to endothermic decomposition process, while peak at 595.3ºC refers to exothermic decomposition process, this peak may signify the metal-ligand bond breaking, while the endothermic peak may indicate pyrolysis of the organic ligand in an argon atmosphere [179].

177
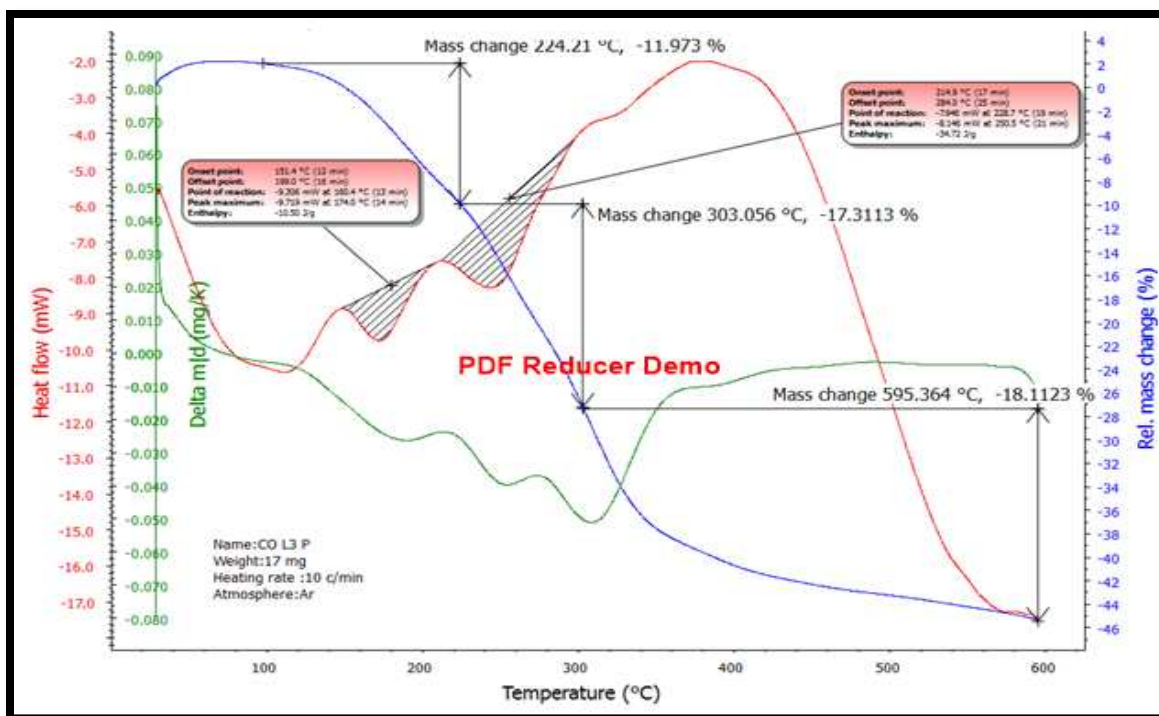
Figure(3.111): TG - DTG curve and DSC thermogram of [CoL^{3}P] complex in an argon atmosphere.

Table(3.38):Temperature values for analysis along with corresponding weight loss values.

Compound	Decomposition range (ºC)	Peak temp. (ºC)	Percentage weight loss %	Mass /mg change (Found)
KL^1	132-265	181.1	5.38	1.13
		251.8	2.67	0.561
KL^2	120-350	191.79	7.477	1.57
		276.20	15.428	3.24
		349.89	10.246	2.15
[Zn(L^1)$_2$]	155-594	594	48.403	8.713
[Ni(L^2)$_2$]	140-594	315.58	40.532	8.512
		594.4	20.325	4.268
[Co(L^3)$_2$]	100-595	293.48	4.856	4.971
		595.68	23.179	4.635

178

[Zn(L^1)(P)]	210-600	375.06	17.436	3.836
		594.63	11.668	2.566
[Ni(L^2)(P)]	175-600	290.96	19.486	4.287
		424.92	12.880	2.834
		595.65	10.952	2.409
[Co(L^3)(P)]	118-600	224.21	11.973	2.035
		303.05	17.311	2.943
		595.36	18.112	3.079

(3.5) Magnetic moment measurements

Magnetic measurements give us important information to elucidate proposed geometry around metal ion in complexes. Also, magnetic moment values for complexes may be used to predict the monomeric and/or their polymeric entity of species. The magnetic susceptibility measurements were determined using a Guoy balance [181,182] .The effective magnetic moment was calculated using equation (3.1):

$$\mu_{eff} = 2.828 \, (\chi_A T)^{1/2} \tag{3.1}$$

Where; χ_A, is the Atomic magnetic susceptibility corrected for diamagnetism of other atoms in the complex using Pascal constants, Table(3.39) and T is the temperature in Kelvin (k)

Table(3.39): Pascal's Constants in $\times 10^{-5}$ /g atom or $\times 10^{-6}$ erg*G^{-2} mol^{-1} [181,182].(3.5.1) Guoy balance susceptibility calculation   The molar

Pascal's Constants							
H	2.93	Te	37.3	N(diamide imide)	2.11	Li	4.2
C	6.00	P	26.3	O(ether alcohole)	4.61	Na	9.2
N(ring)	4.61	As(V)	43.0	O(ketone aldehyde)	⁻1.73	K	18.5
N(open chain)	5.57	As(III)	20.9	O(carboxyl)	3.36	Si	20
N(mono amide)	1.54	Sb(III)	74.0	F	6.3	Pb	46
Cl	20.1	Sb(IV)	30				

magnetic susceptibility, χ_M, can be calculateted from the mass magnetic

susceptibility by multiplying it by the molecular weight of the sample.

$$\chi_{M=} M\chi_g \tag{3.2}$$

$\chi_{M =}$ Molar magnetic susceptibility in (cm^3.mol^{-1})units.

$M =$ Molecular weight of the sample in (g/mol) units.

$\chi_{g =}$ Mass magnetic susceptibility in (cm^3.g^{-1})units.

   Measured molar magnetic susceptibility must have diamagnetic corrections, which aroused from ligand electron pairs, counter ion electron and core paired electrons (metal ion) [183].

$$X_{A =} X_M \text{ -}D \tag{3.3}$$

$X_{A =}$ Atomic magnetic susceptibility

The measured value of μ_{eff} varies slightly from one compound or material to another, as shown in Table(3.40), for transition metals in an tetrahedral geometry.

Table(3.40): Measured magnetic moments, d-configuration, and number of unpaired electrons for transition metal ions with a tetrahedral geometry[184,185].

Metal ion	d configuration	Number unpaired electrons	Magnetic moment
Ti^{4+} ,V^{5+}	d^0	0	0
Cr^{5+}	d^1	1	1.7-1.8
Cr^{4+}	d^2	2	2.6-2.8
Fe^{5+}	d^3	3	3.6-3.7
-	d^4	-	-
Mn^{2+}	d^5	5	5.9-6.2
Fe^{2+}	d^6	4	5.3-5.5
Co^{2+}	d^7	3	4.2-4.8
Ni^{2+}	d^8	2	3.7-4.0
Cu^{2+}	d^9	1	1.7-2.20
Cu^+	d^{10}	0	0

(3.5.1.1) Worked example for the calculation of magnetic moment, μ

$[Cu(L^1)_2]$ complex has been used as an example for KL^1 complexes for the calculation of the magnetic susceptibility and as follows:

$D = [(20 \times C)+(22 \times H)+(1 \times k)+(2 \times (N\text{-ring}))+(1 \times (N\text{-open chain}))+(2 \times O)$
$+ (2 \times S)] \times 10^{-6}$

$[20 \times (6.0)+22 \times (2.93)+1 \times (18.5)+2 \times (4.61)+1 \times (5.57)+2 \times (^-1.73)+2 \times (15)] \times 10^{-6}$

$= -251.21 \times 10^{-6}$ erg* G^{-2} mol^{-1}

$Xg = 35 \times 10^{-7}$ cm^3.g^{-1}

$Xm = Xg.$ M.wt

$= 35 \times 10^{-7}$ cm^3.g$^{-1} \times 439.63$ g.mol^{-1}

$=15387.05 \times 10^{-7}$ cm^3.mol^{-1}

$X_A = Xm - D$

$=15387.05 \times 10^{-7} - (-251.21 \times 10^{-6})$

$=17899.15 \times 10^{-7}$ cm^3.mol^{-1}

$\mu_{eff} = 2.828 \ (X_A.T)^{1/2}$

$= 2.828(17899.15 \times 10^{-7} \times 298)$

$= 2.06$ B.M.

The units are B.M.(Bohr Magnetons),which is a unit of magnetic moment and equal to eh/4πmc $=9.27 \times 10^{-21}$ erg/gauss.

Where e= elementary charge

h= plank constant

m=electron rest mass

c= speed of light

erg= unit of energy and work= 10^{-7} Joules

guesses= unit of measure ment of magnetic flux density= one Maxwell/cm^2

(3.5.2) Calculation of magnetic moment (μ) of [Mn^{II}(L^n)$_2$] ,[Co^{II}(L^n)$_2$], [Ni^{II}(L^n)$_2$] and[Cu^{II}(L^n)$_2$] complexes, where; n=1-3

The magnetic moment measurements of [Mn^{II}(L^n)$_2$] complexes (where; n=1-3) reveal μ_{eff} values in the range 5.93-6.05 B.M., Table(3.41). These values are typical for a high spin Mn(II) ion, which assigned to tetrahedral geometries in Mn(II) complexes, Table(3.40), that formed from coupling interaction through sulfur atoms of the dithiocarbamate moieties. [Co^{II}(L^n)$_2$] complexes (where; n=1-3) gave values in the range (4.13-4.86) B.M**.**, Table(3.41). The μ_{eff} values for these complexes are included at the range of tetrahedral, Table(3.40), which indicates a high spin geometry around Co(II) ion. The magnetic moment measurements for [Ni^{II}(L^n)$_2$] complexes,(where; n=1-3) gave values in the range (3.30-3.93)B.M.,

Table(3.40). The μ_{eff} values for these complexes are included at the range of tetrahedral, Table(3.41), which indicates a high spin geometry around Ni(II) ion. $[Cu^{II}(L^{n})_{2}]$ complexes (where; n=1-3) show values in the range (2.06-2.40) B.M. Which can be attributed to the tetrahedral geometry around Cu (II) ion Table(3.41). Same thing about mixed-ligand$[M(L^{n})(P)]$ and $[(M(L^{n})(Q)]$ complexes, where n=1-3. The values for these complexes are included at the range of tetrahedral, Table(3.42).

Table(3.41): Calculation of magnetic moment measurements for (KL^{1}, KL^{2} and KL^{3}) complexes.

complex	$\chi g*10^{-7}$ $cm^{3}.g^{-1}$	$\chi_{M}*10^{-7}$ $cm^{3}.mol^{-1}$	$X_{A}*10^{-7}$ $cm^{3}.mol^{-1}$	μ_{eff} B.M.	Suggest Structure
$[Mn(L^{1})_{2}]$	330	145077.9	14759.0	5.93	Tetrahedral
$[Co(L^{1})_{2}]$	220	96718.6	99230.7	4.86	Tetrahedral
$[Ni(L^{1})_{2}]$	120	52755.6	55267.7	3.62	Tetrahedral
$[Cu(L^{1})_{2}]$	35	15387.05	17899.15	2.06	Square planer
$[Mn(L^{2})_{2}]$	380	146904.2	149057.8	5.96	Tetrahedral
$[Co(L^{2})_{2}]$	180	69586.2	71739.8	4.13	Tetrahedral
$[Ni(L^{2})_{2}]$	120	46390.8	48544.4	3.30	Tetrahedral
$[Cu(L^{2})_{2}]$	50	19329.5	21483.1	2.26	Square planer
$[Mn(L^{3})_{2}]$	410	151511.4	153590.4	6.05	Tetrahedral
$[Co(L^{3})_{2}]$	250	92385.0	94464.0	4.74	Tetrahedral
$[Ni(L^{3})_{2}]$	170	62821.8	64900.8	3.9	Tetrahedral
$[Cu(L^{3})_{2}]$	60	22172.4	24251.4	2.40	Tetrahedral

Table(3.42): Calculation of magnetic moment measurements for mixed- ligand complexes.

complex	$\chi g *10^{-7}$ $cm^3.g^{-1}$	$\chi_M *10^{-7}$ $cm^3.mol^{-1}$	$X_A *10^{-7}$ $cm^3.mol^{-1}$	μ_{eff} B.M.	Suggest Structure
$[Co(L^1)(P)]$	170	93289.20	96439.7	4.79	Tetrahedral
$[Ni(L^1)(P)]$	118	64753.68	67904.18	4.02	Tetrahedral
$[Co(L^2)(P)]$	155	76836.60	79628.30	4.35	Tetrahedral
$[Ni(L^2)(P)]$	115	57007.80	59799.50	3.77	Tetrahedral
$[Co(L^3)(P)]$	160	76587.20	79304.30	3.34	Tetrahedral
$[Ni(L^3)(P)]$	120	57440.40	60157.50	3.78	Tetrahedral
$[Co(L^1)(Q)]$	136	79531.44	82852.04	4.44	Tetrahedral
$[Ni(L^1)(Q)]$	97	56724.63	60045.23	3.78	Tetrahedral
$[Co(L^2)(Q)]$	132	70191.00	73153.10	4.17	Tetrahedral
$[Ni(L^2)(Q)]$	97	51579.7	54561.85	3.60	Tetrahedral
$[Co(L^3)(Q)]$	138	71028.60	73916.10	4.19	Tetrahedral
$[Ni(L^3)(Q)]$	99	50955.32	53842.80	3.58	Tetrahedral

(3.6) Molar conductance measurements

(3.6.1) Molar Conductivity

Since conductivity is concentration dependent, measured values for different solutions are not easy to compare directly. For this reason, a quantity called the molar conductivity. The molar conductivity is symbolized by Λ, and it is defined as the solution conductivity (κ) normalized by the total ionic concentration (C) [187].

$$\Lambda = \frac{\kappa}{C} \qquad (3.4)$$

Molecular conductivity is used to determine the ionic forms of the coordinate compounds in their various solutions. The molecular conductivity of a compound

solution is directly proportional to the number of ions released from that compound in its solution [188,189].

Table (3.43) shows the molar conductance data for the prepared complexes. Conductance measurement values of KL^1, KL^2 and KL^3 complexes in DMSO dilate in the range 0.20-14.50 $\Omega^{-1}cm^2mol^{-1}$. These values indicate the non- electrolyte behaviour of the complexes [190 ,191] .The conductance of mixed ligand complexes ((P),(Q)),Table(3.44), dilate in the range 9.50-20.90 $\Omega^{-1}cm^2mol^{-1}$ indicating non-electrolyte behaviour too[192].

Table(3.43): Molar conductivity measurements in DMSO for complexes (KL^1, KL^2 and KL^3).

Compound	$\Lambda_M(\Omega^{-1}cm^2mol^{-1})$	Behaviour
$[Mn(L^1)_2]$	3.50	non-electrolyte
$[Co(L^1)_2]$	2.64	non-electrolyte
$[Ni(L^1)_2]$	8.32	non-electrolyte
$[Cu(L^1)_2]$	8.01	non-electrolyte
$[Zn(L^1)_2]$	4.00	non-electrolyte
$[Pd(L^1)_2]$	4.19	non-electrolyte
$[Cd(L^1)_2]$	5.82	non-electrolyte
$[Mn(L^2)_2]$	1.24	non-electrolyte
$[Co(L^2)_2]$	1.18	non-electrolyte
$[Ni(L^2)_2]$	0.75	non-electrolyte
$[Cu(L^2)_2]$	0.72	non-electrolyte
$[Zn(L^2)_2]$	2.07	non-electrolyte
$[Pd(L^2)_2]$	0.20	non-electrolyte
$[Cd(L^2)_2]$	0.58	non-electrolyte
$[Mn(L^3)_2]$	14.50	non-electrolyte
$[Co(L^3)_2]$	13.17	non-electrolyte
$[Ni(L^3)_2]$	10.60	non-electrolyte
$[Cu(L^3)_2]$	8.50	non-electrolyte
$[Zn(L^3)_2]$	11.31	non-electrolyte
$[Pd(L^3)_2]$	14.43	non-electrolyte
$[Cd(L^3)_2]$	11.95	non-electrolyte

Table(3.44): Molar conductivity measurements in DMSO for mixed- ligand complexes .

Compound	$\Lambda_M(\Omega^{-1}cm^2mol^{-1})$	Behaviour
[Co(L^1)(P)]	14.43	non-electrolyte
[Ni(L^1)(P)]	16.12	non-electrolyte
[Zn(L^1)(P)]	19.20	non-electrolyte
[Co(L^2)(P)]	9.50	non-electrolyte
[Ni(L^2)(P)]	11.30	non-electrolyte
[Zn(L^2)(P)]	10.46	non-electrolyte
[Co(L^3)(P)]	19.50	non-electrolyte
[Ni(L^3)(P)]	12.41	non-electrolyte
[Zn(L^3)(P)]	18.16	non-electrolyte
[Co(L^1)(Q)]	20.07	non-electrolyte
[Ni(L^1)(Q)]	17.85	non-electrolyte
[Zn(L^1)(Q)]	20.90	non-electrolyte
[Co(L^2)(Q)]	16.03	non-electrolyte
[Ni(L^2)(Q)]	11.65	non-electrolyte
[Zn(L^2)(Q)]	20.00	non-electrolyte
[Co(L^3)(Q)]	16.21	non-electrolyte
[Ni(L^3)(Q)]	14.62	non-electrolyte
[Zn(L^3)(Q)]	19.00	non-electrolyte

(3.7)Examination of Corrosion

Corrosion is the deterioration of materials by chemical interaction with their environment. Copper and its alloys are used extensively and successfully in many types of chemical equipment including evaporators, pumps, valves, fans and fractionating columns. Large quantities of pipes made out of copper and copper alloys are used to make condensers and heat exchangers, where fresh or salt water is used for cooling. Brass is susceptible to a corrosion process known as dezincification and this tendency increases with increasing zinc content of the brass. During the past decade, many techniques have been used to minimise the dezincification and corrosion of brasses. One of the techniques for minimising corrosion is the use of inhibitors. The effectiveness of the inhibitor varies with its

concentration, the corrosive medium and the surface properties of the alloy. Many inhibitors have been used to minimise the corrosion of brass in different media. Over the years, considerable efforts have been deployed to find suitable corrosion inhibitors of organic origin in various corrosive media. Organic compounds, which can donate electrons to unoccupied d orbital of the metal surface to form coordinate covalent bonds, and can also accept free electrons from the metal surface by using their anti-bonding orbital to form feedback bonds, constitute excellent corrosion inhibitors. A number of heterocyclic compounds containing nitrogen, oxygen, and sulfur either in the aromatic or long chain carbon system have been reported to be effective inhibitors[193,194].

(3.7.1)Potentiostatic Polarization Measurements:

The potentiostatic polarization measurements were carried out with a piece of α-brass, the composition of α-brass has been determined by X-ray as shown in the following Table(3.45), which was cut in the form of a disk [2cm diameter and 0.2cm thickness] having an exposed surface area of 1 cm^2 corrosive medium. The working electrode (α-brass) was abraded mechanically and successively with different grades of emery paper [200, 400, 800, 1200 and 2000] and washed with distilled water. Furthermore the samples were degreased with acetone and thoroughly washed with doubly distilled water then dried in air and kept in a desiccator until use[195].

Table(3.45):The composition of α-brass alloy.

α-brass	Wt %						
	Cu%	**Zn%**	**Fe%**	**Sb%**	**Sn%**	**Al%**	**Pb%**
	61.5	37.5	0.014	0.023	0.803	0.012	0.031
	Si%	**P%**	**Mn%**	**Ni%**	**Co%**	**S%**	
	0.001	0.009	0.0005	0.001	0.001	0.008	

The experiments were performed in the electrolyte solution of 0.6 mol dm^{-3} sodium chloride (sea water) at three different pH values (pH=2, pH=4 and pH=7) in the absence and presence of concentration (10^{-3} mol. dm^{-3}) of the inhibitor (ligands) at 298 K[195].

The resulting data (i_{corr} and E_{corr}) which have been derived from the tests of corrosion were displayed in Table(3.46), and these data show that corrosion current density i_{corr} increases with the decrease of pH (increase of acidity) and nearly corrosion potential E_{corr}. follows similar manner on decreasing of pH values in this study.

Table(3.46): Data of polarization measurement for corrosion of α-brass in 0.6 mol.dm^{-3} NaCl solution at three pH values (2,4 and 7) at 298K.

pH	icorr/ $\mu A.cm^{-2}$	-Ecorr/mV	weight loss/ $g.m^{-2}. day^{-1}$	Penetration loss/mm.year^{-1}
2	6.24	242.6	2.010	0.0691
4	1.96	240.3	0.538	0.0243
7	1.83	254.4	0.413	0.0223

(3.7.2) Corrosion Current Density and Corrosion Potential

The relationship between the α-brass corrosion current densities i_{corr} and pH values at 298 K was shown in Fig.(3.112). It was noticed that all values of i_{corr} increase as the acidity of the medium is increased and this reflects the kinetic behaviour of the corrosion process. The rate of corrosion being higher in more acidic medium, i.e.

$$i_{corr}(pH=2) \rangle i_{corr} (pH=4) \rangle i_{corr} (pH= 7)$$

at the temperature of study which indicates that α-brass alloy has more tendency to corrode in more acidic medium and result is enhanced by the values of weight loss and penetration values which are displayed in Table(3.46).

Fig.(3.113) shows the relationship between corrosion potential E_{corr} of α-brass and pH values at 298 K. E_{corr} value moved to less negative values with the increase of pH , as the medium becomes less acidic. The variation of E_{corr} reflects the heterogeneous reaction on α-brass surface[196].
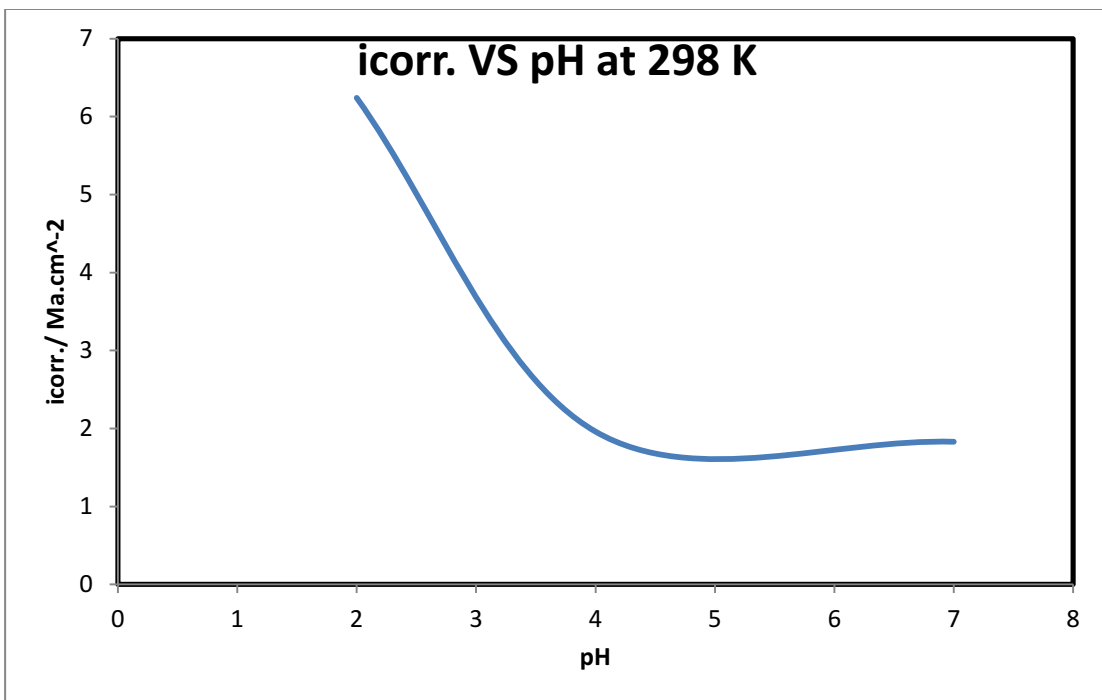
Figure (3.112): Variation of corrosion current densities of α-brass against pH values in 0.6 mol.dm⁻³ NaCl solution at 298K.
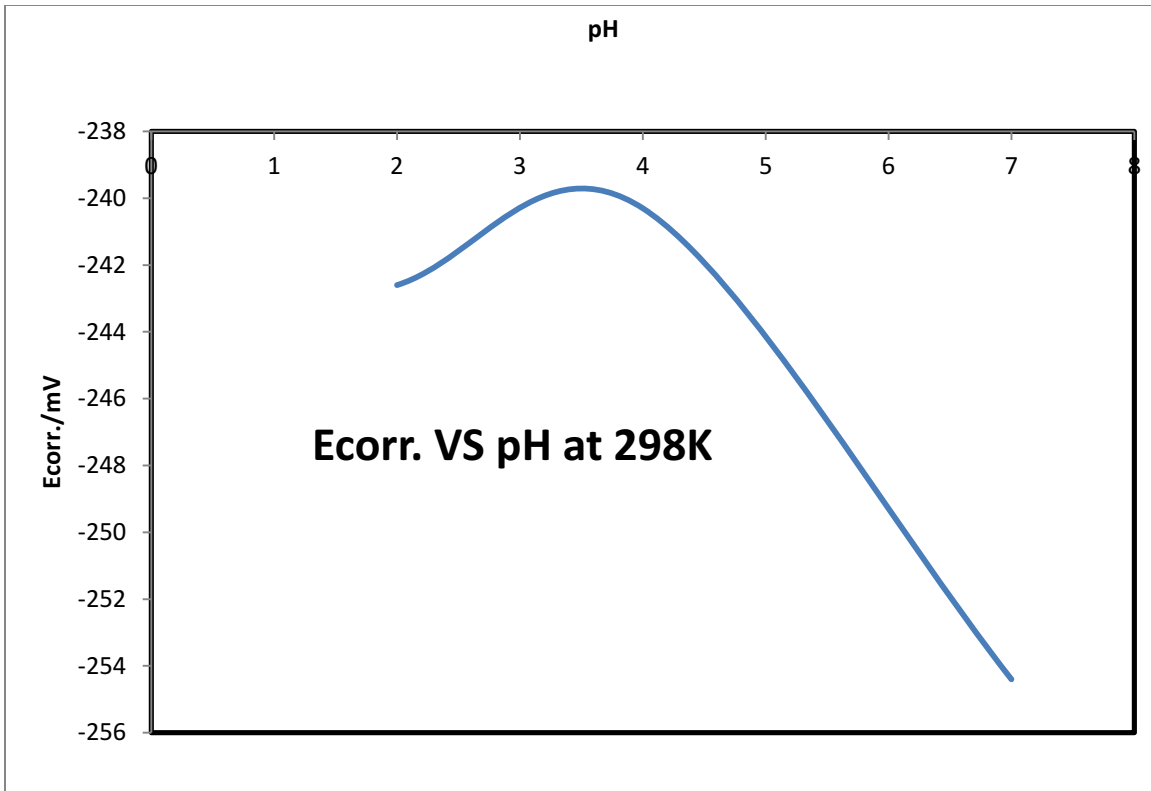
Figure (3.113): Variation of corrosion potentials of α-brass against pH values in 0.6 mol.dm^{-3} NaCl solution at 298K.

Fig.(3.114) shows the variation of weight losses of α-brass corrosion with pH and Table(3.46) presents the values of weight loss. The table shows the weight loss decreased with increase of pH in the range (2-7).

As pH becomes more acidic, ($E_{corr.}$) will become more negative due to the increase in the rate of hydrogen evolution. Subsequently the increase in metal dissolution will result in a larger (i_{corr}), followed by more weight loss as the acidity of the medium increased [197] **.**
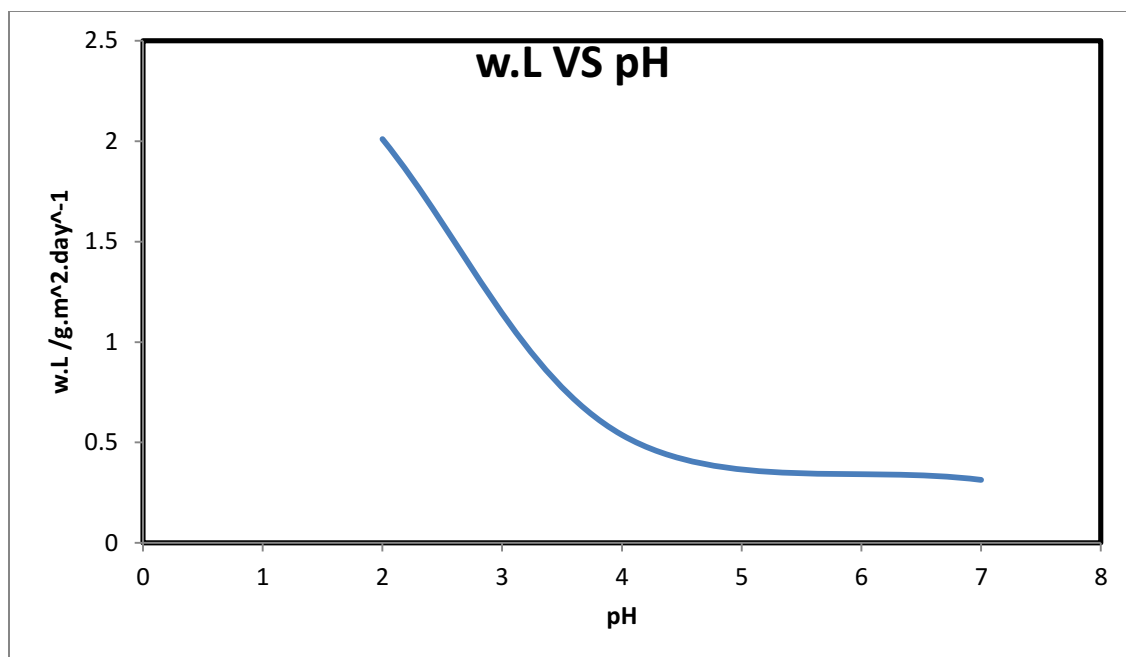
Figure (3.114): Relation between weight loss and pH of α-brass corrosion in 0.6 mol.dm^{-3} NaCl solution at 298k.

(3.7.3) Effect of ligands (KL^1,KL^2 and KL^3) use as inhibitor.

The typical polarization mode for α-brass in 0.6 mol.dm^{-3} NaCl solution in three pH values (2,4 and 7) containing in 10^{-3} mol.dm^{-3} of the ligand at 298 K. Table(3.47) presents the polarization data (the corrosion potential E_{corr} and corrosion current densities i_{corr}). This table presents the influence of ligands concentration on the corrosion current densities, corrosion potential for α-brass at the conditions mentioned above. It is obvious from the data displayed in Table(3.47) that under the experimental conditions, ligands molecule act both as inhibitor and accelerator. ligands caused a decrease in corrosion current densities of α-brass in the two pH values 4 and 7 compared with i_{corr} values in the absence of ligands under the same conditions, that means that ligands inhibit α-brass corrosion, while in (pH=2) it was noticed that the addition of the ligands acts as

accelerator, i.e. i_{corr} increases in the presence of ligands in comparison with i_{corr} value in the absence of ligands.

Table (3.47): Data of Polarization for the corrosion of α-brass in 0.6 mol.dm^{-3} NaCl solution at three pH values (2, 4 and 7) at 298K with (10^{-3} mol.dm^{-3}) concentration value of ligands.

compound	pH	icorr/ $\mu A.cm^{-2}$	-Ecorr/mV	weight loss/ $g.m^{-2}.day^{-1} \times 10^{-1}$	Penetration loss/mm.year$^{-1} \times 10^{-2}$
KL^1	2	6.57	231.10	14.60	7.89
	4	1.25	286.27	3.11	1.29
	7	0.752	294.00	1.15	0.971
KL^2	2	6.77	237.61	13.16	7.11
	4	1.81	271.29	2.91	1.53
	7	0.811	280.17	1.86	1.12
KL^3	2	8.20	229.11	16.14	8.09
	4	1.37	268.55	2.15	1.40
	7	0.885	288.91	1.35	1.00

(3.7.4) Mechanism of inhibition of the ligands KL^1,KL^2 and KL^3.

The choice of inhibitor is based on two considerations. First, it can be synthesized conveniently from relatively cheap raw materials. Second, the presence of an electron cloud on the aromatic ring, the electronegative S,N,O atoms and the relatively long chain compounds to induce greater adsorption on the metal surface promoting effective inhibition[198]. Generally, a strong coordination bond causes higher inhibition efficiency, the inhibition increases in the sequence P>S>N>O [198]. The inhibition of corrosion by ligands (KL^1,KL^2 and KL^3) can be

attributed to coordination through hetro-atoms and π–electrons of aromatic ring. ligands (KL^1,KL^2 and KL^3) ,there are unshared electron pairs on S,N and O capable of forming δ–bond with α–brass, so there are likely to be adsorbed strongly on the alloy surface[199].

At pH= 2 ligands acts as accelerator for the concentrations (10^{-3})mol.dm^{-3} of the inhibitor. This result may attribute to the presence of sulfide ions (which may be produced more in more acidic medium) and these sulfide ions has caused significant increase in the extent of corrosion attack on α–brass. The inhibition effect of inhibitor is markedly reduced in the presence of sulfide ions in the medium. The easy replacement of Cu-inh complex by Cu_2S film on the surface of α–brass is responsible for the inability of ligands to prevent corrosion attack[200].

(3.7.5) Protection Efficiency

Table(3.48) shows the values of protection efficiency (P%) which are calculated using equation (3.5):

$$P\% = 100 \left[1 - \frac{(i_c)_2}{(i_c)_1} \right] \qquad (3.5)$$

PDF Reducer Demo

Where $(i_c)_1$ and $(i_c)_2$ are corrosion current densities of uninhibited an inhibited system respectively [201].

Ligands (KL^1, KL^2 and KL^3) exhibited good performance inhibition efficiency at 298K with ligands concentration of 10^{-3} mol.dm^{-3} in solution of pH=7.

Table(3.48):Values of protection efficiencies calculated from i_{corr}. At pH=7.

compound	P% from i_{corr}
KL^1	58.90
KL^2	55.68
KL^3	51.63

(3.8) Bacterial activity

The synthesised dithiocarbamate ligands and their metal complexes were screened for their antibacterial activity against two bacterial species *[Escherichia coli* (gram negative) and *Staphylococcus aureus* (gram positive)] . This is to assess their potential antimicrobial activity. The role of DMSO in the biological screening was clarified by separate studies carried out with the solutions of DMSO alone, which showed no activity against any bacterial strains   [202]. The measured zones(mm) of inhibition against the growth of different microorganisms are listed in Tables(3.49), (3.50) and (3.51)**.** Fig.((3.115),(3.116)) display the effect of the synthesized compounds on bacterial strains. From the obtained data that shown in the tables, we can conclude two important points;

1- Complexes found to be potentially more active against these bacterial strains, compared with the free ligands, which means complexation increases antibacterial activity. This may be explained by chelation effect in which the partially sharing of the positive charge of the metal in complexes by the donor atoms present in the ligand and there may be π-electron delocalisation over the whole chelate ring that increases the lipophilic character of the metal chelate system. This will favour its permeation through lipid layer of the cell membranes [203,204].

2- The mixed-ligand complexes Fig.(3.116) have the higher antibacterial activity compared with the other complexes. This may be related to the some reason mentioned above. The results are listed in the Table(3.52).

The antibacterial activity of the different compounds against different organisms depends on [205]:

  a- Their impermeability of the microbial cells.

  b- The difference in the ribosome of the microbial cells.

Table(3.49): Bacterial activity of KL^1 and its complexes.

Compounds	*Escherichia coli* (G−)	*Staphylococcus aureus* (G+)
Control (DMSO)	-	-
KL^1	-	-
[Mn(L^1)$_2$]	-	-
[Co(L^1)$_2$]	-	10
[Ni(L^1)$_2$]	3	17
[Cu(L^1)$_2$]	9	12
[Zn(L^1)$_2$]	8	-
[Pd(L^1)$_2$]	-	8
[Cd(L^1)$_2$]	10	9

Table(3.50): Bacterial activity of KL^2 and its complexes.

Compounds	*Escherichia coli* (G−)	*Staphylococcus aureus* (G+)
Control (DMSO)	-	-
KL^2	-	-
[Mn(L^2)$_2$]	-	10
[Co(L^2)$_2$]	-	-
[Ni(L^2)$_2$]	-	8
[Cu(L^2)$_2$]	-	9
[Zn(L^2)$_2$]	9	-
[Pd(L^2)$_2$]	-	-
[Cd(L^2)$_2$]	9	4

Table(3.51): Bacterial activity of KL^3 and its complexes.

Compounds	*Escherichia coli* (G−)	*Staphylococcus aureus* (G+)
Control (DMSO)	-	-
KL^3	-	-
[Mn(L^3)$_2$]	-	-
[Co(L^3)$_2$]	-	6
[Ni(L^3)$_2$]	-	-
[Cu(L^3)$_2$]	-	12
[Zn(L^3)$_2$]	8	-
[Pd(L^3)$_2$]	5	7
[Cd(L^3)$_2$]	9	10

Table(3.52): Bacterial activity of mixed-ligand complexes.

Compounds	*Escherichia coli* (G−)	*Staphylococcus aureus* (G+)
DMSO	-	-
(P)	12	10
(Q)	-	-
[Co(L^1)(P)]	7	9
[Ni(L^1)(P)]	8	9
[Zn(L^1)(P)]	10	7
[Co(L^2)(P)]	5	6
[Ni(L^2)(P)]	7	8
[Zn(L^2)(P)]	9	8
[Co(L^3)(P)]	6	7
[Ni(L^3)(P)]	7	7

[Zn(L^3)(P)]	9	8
[Co(L^1)(Q)]	8	6
[Ni(L^1)(Q)]	7	9
[Zn(L^1)(Q)]	9	9
[Co(L^2)(Q)]	7	10
[Ni(L^2)(Q)]	10	8
[Zn(L^2)(Q)]	11	12
[Co(L^3)(Q)]	9	8
[Ni(L^3)(Q)]	7	6
[Zn(L^3)(Q)]	12	10
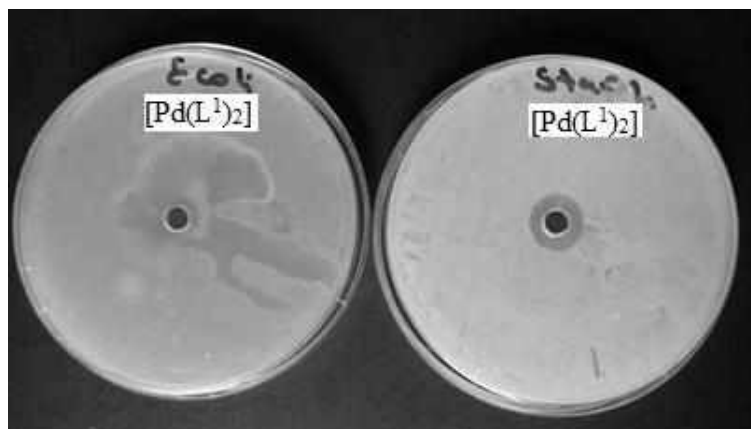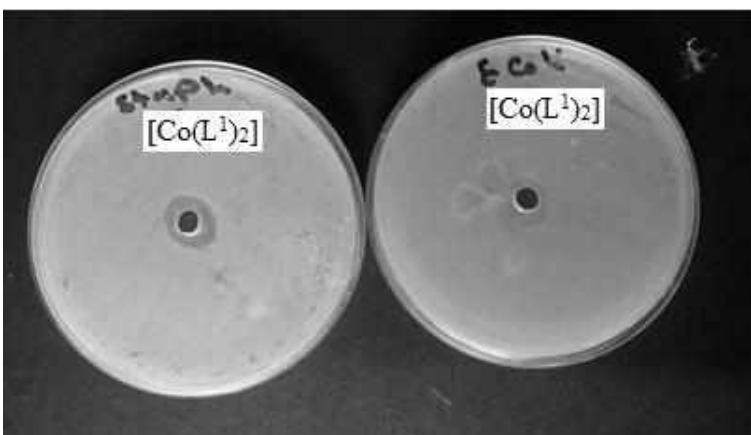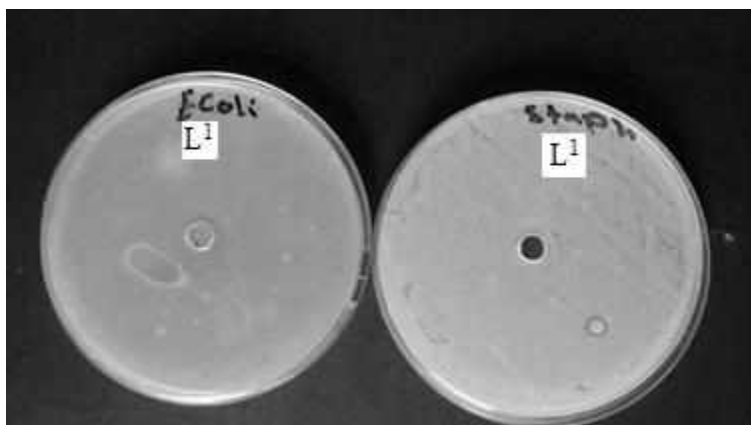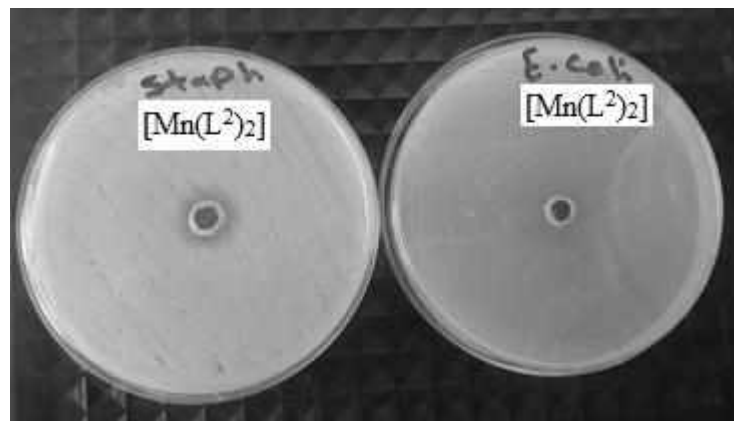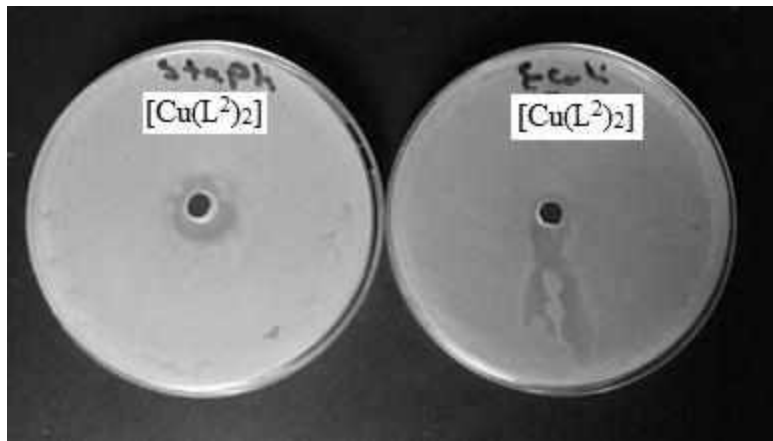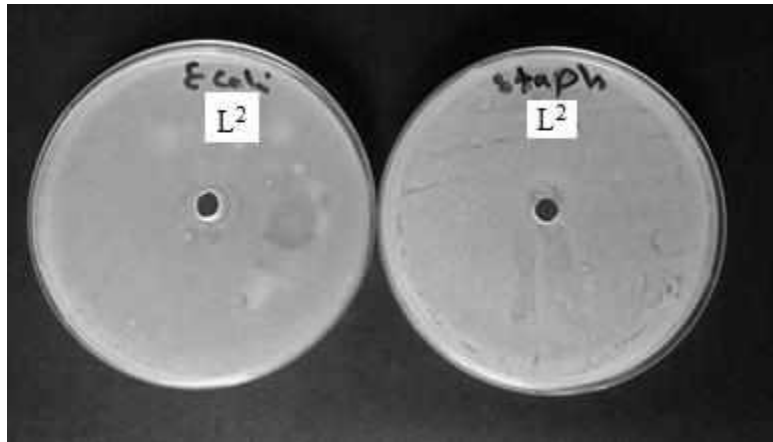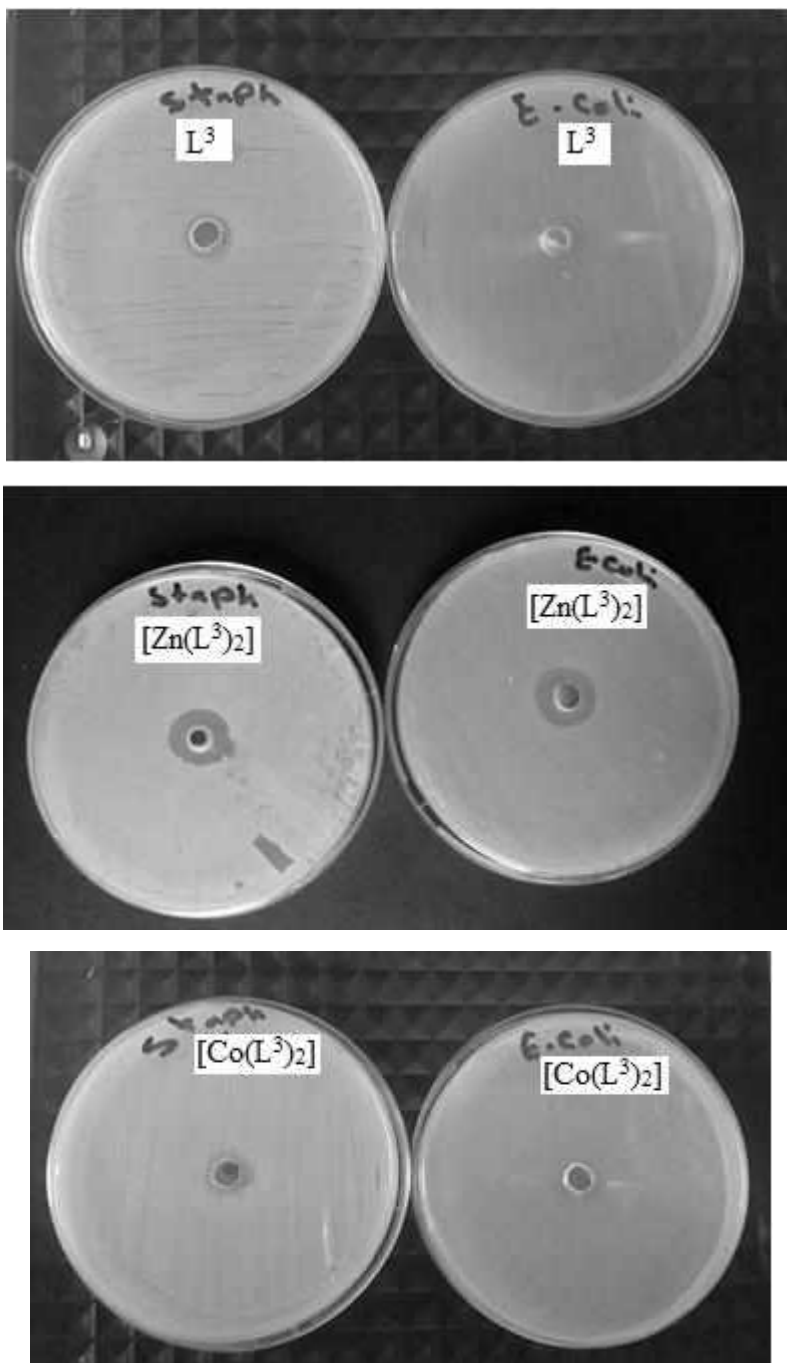
Figure(3.115):The effect of KL^1 , KL^2, KL^3 and its complexes on *Escherichia coli* and *Staphylococcus Aureus*.
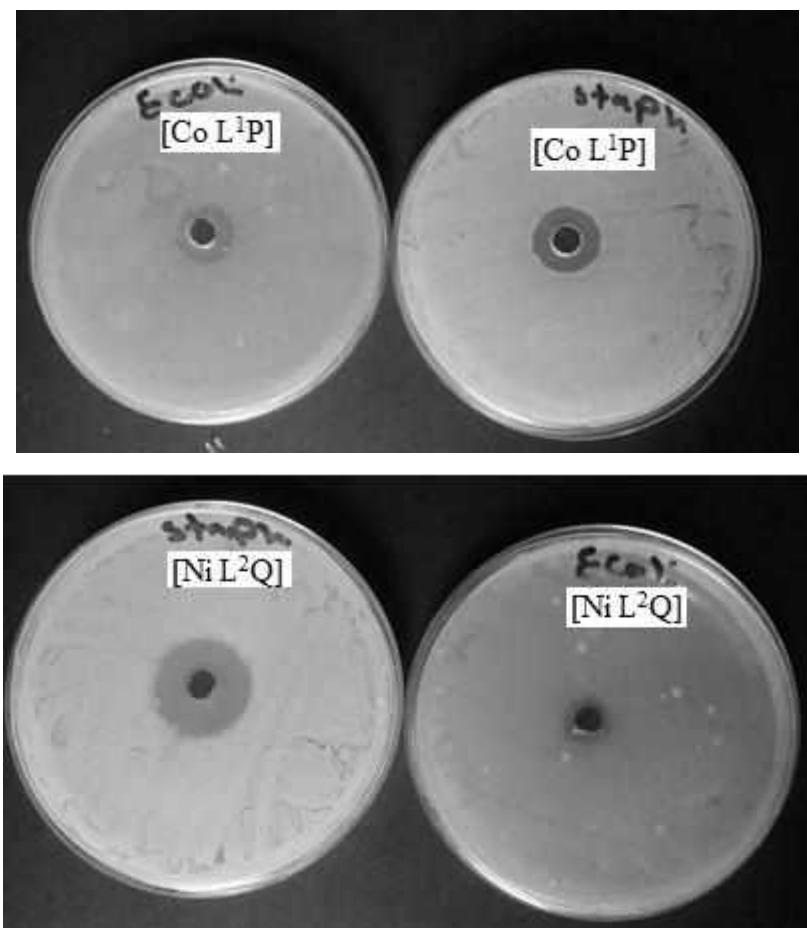
Figure(3.116):The effect of mixed-ligand complexes on *Escherichia coli* and *Staphylococcus Aureus*.
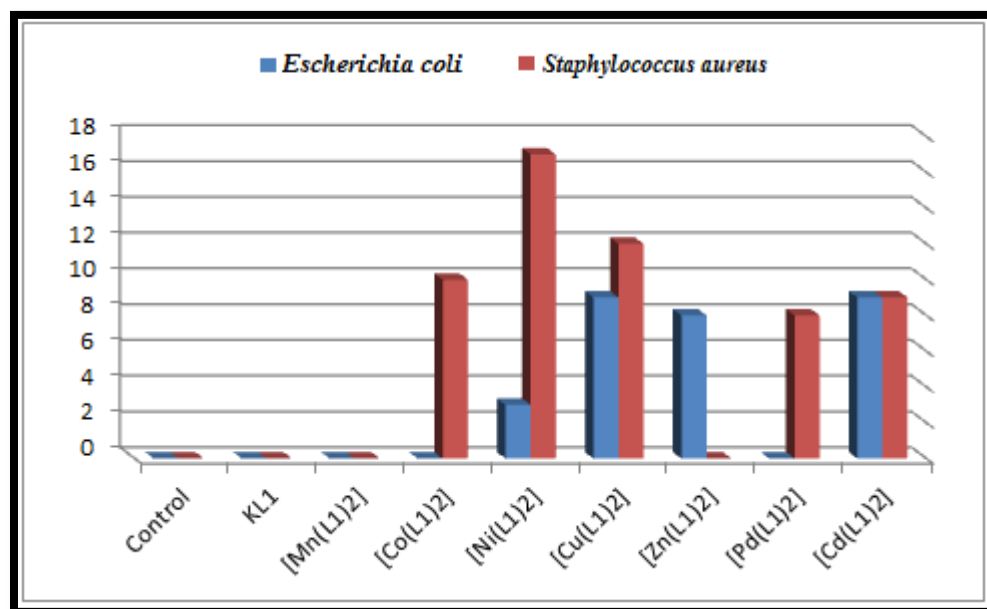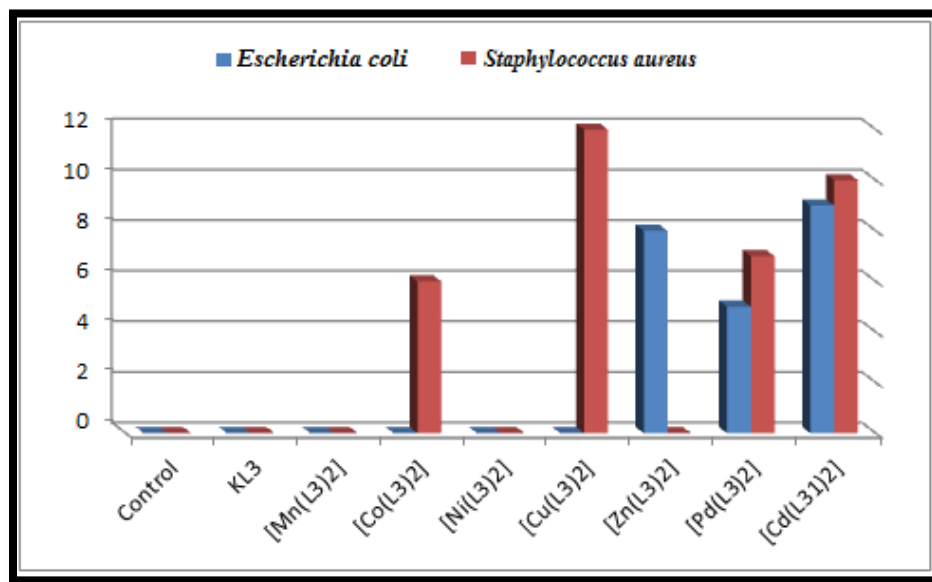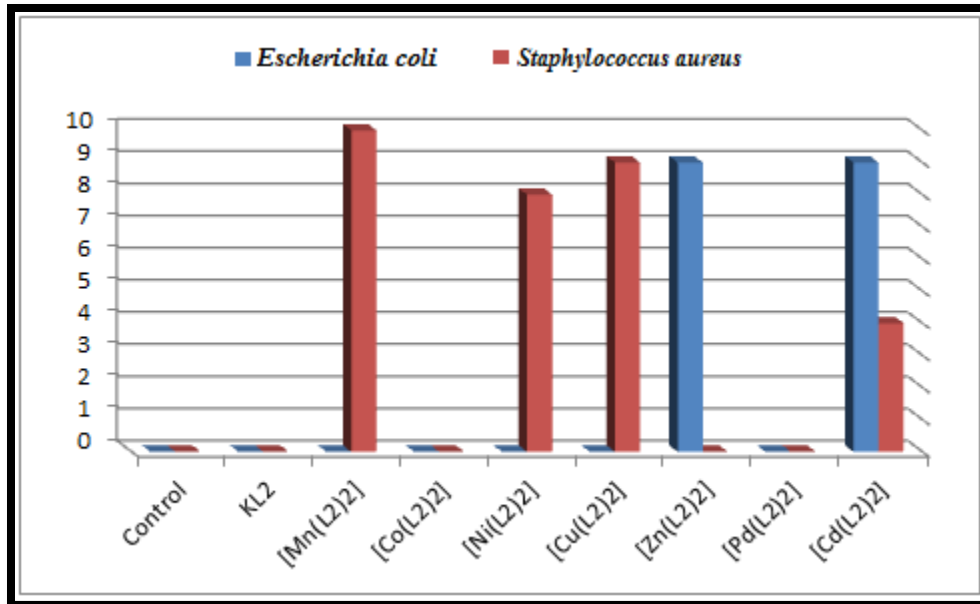
Figure(3.117): Evolution of diameter zone (mm) of inhibition of KL^1, KL^2, KL^3 and its complexes against the growth of *Escherichia coli* and *Staphylococcus Aureus* bacterials.
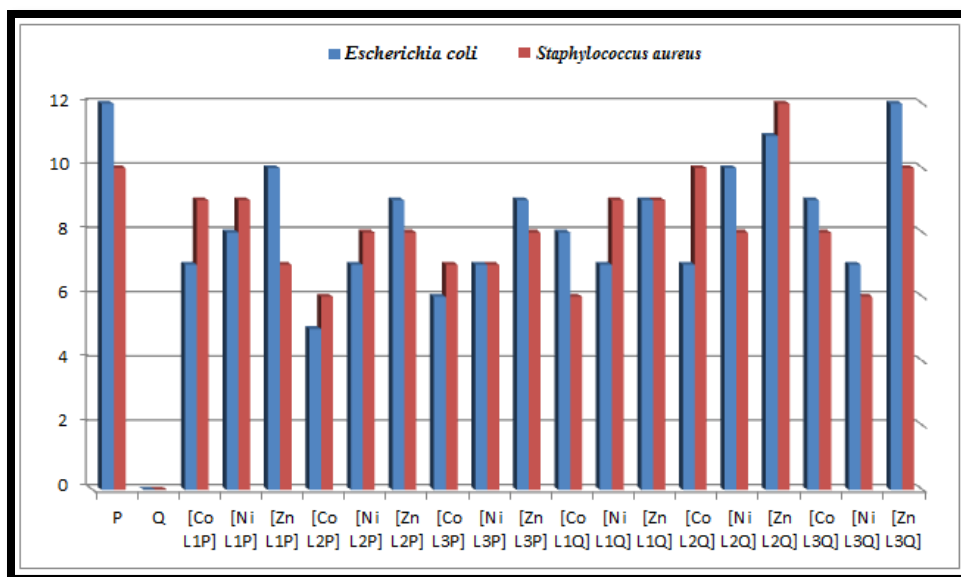
Figure(3.118): Evolution of diameter zone (mm) of inhibition of mixed-ligand complexes against the growth of *Escherichia coli* and *Staphylococcus Aureus* bacterials.

(3.9)Conclusion

According to the characterization data of new three ligands (KL^1) ,(KL^2) and (KL^3) which performed by reaction of dimedone with 4-aminophenazone, 2-aminobenzothiozol and 2-aminobenzoimidazole respectively and carbone disulphide .All prepared complexes identified by FT-IR ,UV-Vis, Flame atomic absorption,^{1}H,^{13}C-NMR, magnetic susceptibility, molar conductivity, elemental microanalysis (C.H.N.S) along and thermal analysis TGA ,we found that:-

1-The new three ligands (KL^1) ,(KL^2) and (KL^3) behave as bidentate ligand through sulphur atoms of carbondithioate group, formation complexes with central metal ions: $M^{(II)}$= Mn ,Co, Ni, Cu, Zn, Pd and Cd. As demonstrated by FT-IR spectra measurements using the vibrational mode of v(M-S).

2-Tetrahedral geometrical structure was suggested for $Mn^{(II)}$,$Co^{(II)}$, $Ni^{(II)}$, $Zn^{(II)}$ and $Cd^{(II)}$ complexes. These data are in agreement with the magnetic moments value μ_{eff} for tetrahedral geometry around $Mn^{(II)}$,$Co^{(II)}$, $Ni^{(II)}$ ions.

3-Square planer geometrical structure was suggested for Cu^{2+} and Pd^{2+} complexes.

4-Preparation of some selective mixed-ligand complexes from mixing liquor solution for ligands alone with 3-aminophenole (P) ,8-hydroxyquinoline (Q) and metal ion in base medium. Tetrahedral geometric structure was suggested for $[M(L^n)(P)]$ and $[M(L^n)(Q)]$ complexes where n= 1-3, $M^{(II)}$= Co, Ni and Zn. These data are in agreement with magnetic moments value μ_{eff} for tetrahedral geometry around Co and Ni ions.

5- The elemental microanalysis (M.C.H.N.S.) results for ligands and complexes are in a good agreement with the calculated values. These data supported the formation of complexes and helped in verifying the suggested formula of the complexes.

6- The ^1H, ^{13}C-NMR spectra of the precursor HDa and the ligands in DMSO -d^6 displayed signals corresponding to the various proton and carbon nuclei consistent with the proposed structural formula are shown in Fig. (3.1-3.8). The chemical shifts of the ^1HNMR spectra of the precursor HDa and the dithiocarbamate ligands are given. Signals related to the $^{13}CNMR$ spectra of dithiocarbamate ligands are given .

7- The mass spectra for ligands (KL^1, KL^2 and KL^3) are reported in Tables (3.21-3.23), and shown in Fig. (3.9, 3.11), where showed several peaks corresponding to successive fragmentations of the parent ion molecule, which indicated the formation of the precursors ligands.

8- This technique was used to show thermal stability and chemical composition of compounds, which helped in the characterisation of ligands and some selective complexes.

9- The molar conductance measurements of complexes in DMSO solutions, indicating their nonelectrolyte behaviour.

10- Some of the prepared complexes showed the ability to inhibition of growth toward *Staphylococcus aureus* and *Escherichia Coli*, at prepared concentration.

11- The new three ligands (KL^1) ,(KL^2) and (KL^3) showed the ability to inhibition of α–brass corrosion in 0.6 mol/dm^{-3} NaCl solution with pH value 4,7, while they have no effect in pH=2.

(3.10) Prospective Studies

1- Synthesis of new dithiocarbamte ligands with different substituents and preparation of their metal complexes.

2- Determination of the stability constants of these ligands with transition metal.

3- Synthesis of new complexes for these ligands with metal ions of second and third series, also metal ions of lanthanides and actinides.

4- Investigation of the selectivity of the ligand toward metal ion under different pH medium.

5- Investigation of the possibility using these ligands in separation of metal ions by column chromatography.

6- Application of these ligands in various fields such as catalysis corrosion, for other types of alloys.

7- Studying the thermodynamic and kinetic of the preparation ligands and their complexes.

8- Studying the biological activity against other microbiological species such as: fungi, etc.

9- Studying the selectivity of the ligands towards metal ions in solution.

References

1. Tiang N., Deng X. and Shan Q., *Synthesis of Novel 7-Substituted-5-phenyl-[1,2,4]triazolo[1,5-a] Pyrimidines with Anticonvulsant Activity.*, J.Iranian of pharmaceutical Research , 2012. 11(3) :p.799-806.

2. Urbaniakm W., Jurek K. , Witt K. and Goraczko A., *Properties and application of diketones and their derivatives*., J. Chemik, 2011. 65(4) :p.273-282.

3. Cullen W. and Wickenheiser E., *Rhodium(I) complexes of β-diketonates and related ligands as hydrosilylation catalysts.* ,J. Organomet. Chem. 1989. 370: p. 141-154.

4. Lewis F., Miller A. and Salvi D. , *Spectroscopy and photochemistry of Nickel (II) , Palladium(II), and Platinum(II) β-diketonates*., Inorg. Chem. 1995. 34 :p. 3173-3181.

5. Semmingsen D., *The crystal and molecular structure of dimedone.*, Acta Chemica Scandinavica ,1974. 28b :p.169-174.

6. George M., Jolocam M. and Mpango B., *New Biologically Active Compounds from 1,3-Diketones.*, Res. J. Chem. Sci., 2011. 1(3) :p. 102-108.

7. Anupama B., Padmaja M. and Gyana C., *Synthesis, Characterization, Biological Activity and DNA Binding Studies of Metal Complexes with 4-Aminoantipyrine Schiff Base Ligand.,* E-Journal of Chemistry , 2012. 9(1) :p. 389-400.

8. Nadiah A., *Synthesis And Characterization of Co(II), Cu(II), Cd(II), Zn(II) and Ni(II) Complexes Of Schiff Base Ligand Derived From S-Benzyldithiocarbazate And 4-aminoantipyrine With Their Biological Activity Studies.*, IOSR Journal of Engineering, 2013. 3 :p.38-50.

9. Mohamed M., *Safety data sheet 4-aminoantipyrine.*, Apollo Scientific limited , (2014).1 :p.1-6.

10. Joydeep C., *Adsorption of 2-aminobenzothiazole on nano-colloidal silver surface: A concentration and time dependent SERS study aided by density functional theory.*, Vibrational Spectroscopy, 2010. 52 :p. 85–92.

11. Akhond M. and Actuators B. ,*A new cerium (III)-selective membrane electrode based on 2-aminobenzothiazole.*, Chemical, 2004. 99(2) :p. 410-415.

12. Ruijun L. and Xijun C., *Multiwalled carbon nanotubes modified with 2-aminobenzothiazole modified for uniquely selective solid-phase extraction and determination of Pb (II) ion in water samples.*, Microchimica Acta ,2011.172(3) :p. 269-276.

13. Alang G., Kaur G. and Tiwari1 R., *Synthesis, Characterization , and Biological Evaluation of certain 6-methyl-2(3H)-benzo-1, 3-thiazolyl-1'-ethylidene-2-(o, p-Substituted Acetophenones) Hydrazine Analogs.*, J. Young Pharm. ,2010 .2(4) :p. 394–398.

14. Danzeisen R., Schwalenstoecker B. and Gillardon F. ,*Targeted antioxidative and neuroprotective properties of the dopamine agonist pramipexole and its nondopaminergic enantiomer [2-amino-4,5,6,7-tetrahydro-6-Lpropylamino-benza thiazole dihydrochloride]* , J.Pharmacol Exp Ther. ,2006. 316 :p. 189–99.

15. Bartolome S., *Al Programmed enzyme-mimic hydrolysis of a choline carbonate by a metal-free 2-aminobenzimidazole-based cavitand.*,Organic letters, 2014. 16(3) :p. 840–843.

16. Ya-Shan H., *One-pot, two-step synthesis of imidazo[1,2-a]benzimidazoles via a multi component[4+1]cycloaddition reaction.*, ACS Comb.Sci., 2013. 15(10) :p. 551–555.

17. Sunita B. and Shinde L., *Synthesis, Characterization Antimicrobial Investigations of Copper (II) Complexes with Some Benzylbenzimidazole Derivatives.*, Research Journal of Pharmaceutical, Biological and Chemical Sciences, 2013. 4(4) :p. 1285-1290.

18. Ruchita A., Sharmila T. and Trupti D., *Microwave Assisted Synthesis, Characterization and Antibacterial Activity of 2- Chloromethyl BenzImidazole*

Derivatives., International Journal of Scientific Research in Science and Technology ,2016. (2)4 :p. 243-249.

19. Boddeti G. and Bhagavathula S ., *A brief review on synthesis & applications of β-enaminone carbonyl compounds.*, Org. Commun. ,2012. 5(3) :p. 105-119.

20. Narsaiah A., Reddy A. and Yadav J., *Synthesis of β-enaminone and their bromination.*, The Open Catalysis Journal, 2011. 4 :p. 43-46.

21. Kaliyan P., Matam S., *A Simple, Efficient Green Protocol for the Synthesis of β-Enaminone and Enamino Ester Derivatives by Using Onion Extract as Green Catalyst.*, Chemistry select , 2017. 2(8) :p. 2363-2372.

22. Dawood F., *Synthesis, Spectroscopic and Adsorption Studies of Cobalt (II) Complex for a ligand β-enaminone Derived from Sulfamethoxazole.*, Ibn Al-Haitham Jour. for Pure & Appl. Sci. ,2016. 29(1) : p.445-458.

23. Mingdong C. ,Shijie L. and Guangpu Y., *Synthesis and Antibacterial Activity of some Heterocyclic β-enaminone Derivatives with 1,2,3-triazole.*, Heterocyclic Communications, 2011. 6(5): p. 421–426.

24. Pramod K. and Ajay J., *An Efficient Synthesis of β-Enaminoketone/Ester Under Grinding Condition Using Calcium Bromide as Solid Support Catalyst*, Der Pharma Chemica, 2017. 9(8): p.55-58.

25. Fei L. ,Lian X. and Lu F., *Copper Catalysis for Nicotinate Synthesis through β-Alkenylation/Cyclization of Saturated Ketones with β-Enamino Esters*, Advanced Synthesis & Catalysis ,2018. 360(3): p.444-448.

26. Ali reza H., Mohsen S., *Silica-supported $LiHSO_4$ as a highly efficient, heterogeneous and reusable catalytic system for the solvent-free synthesis of β-enaminones and β-enamino esters.*, Journal of the Iranian Chemical Society, 2010. 7(1) :p.69-76.

27. Amiya S. and Devendra D., *Zeolite (ZSM-5) as a Highly Efficient and Heterogeneous Catalyst for the Synthesis of β-Enaminones and β-Enamino Esters.*, E-Journal of Chemistry ,2011.8(4) :p. 1632-1637.

28. Ming Z. , Ablimit A. and Chengjian Z., *Efficient Synthesis of β-Enaminones and β-Enaminoesters Catalyzed by Gold(I)/ Silver(I) under Solvent-Free Conditions.*, Molecules, 2012. 17 :p. 2812-2822.

29. Muhammad N. , Ihsan A. and Muhammad R. , *Efficient PPA-SiO$_2$-catalyzed Synthesis of β-enaminones Under Solvent-Free Conditions.*, Molecules ,2013. 18(12) :p.15182-15192.

30. Ramin R. and Mozhdeh S., *A Mild and Efficient Method for Synthesis of β-Enaminones using Melamine-Formaldehyde Resin Supported H$^+$ Under Solvent Free Conditions.*, Asian Journal of Chemistry,2013. 25(13) :p. 7079-7082.

31. Karimi-Jaberi Z. and Takmilifard Z., *Efficient Synthesis of β-enaminones and β-enamino esters using tris(hydrogensulfato)boron or trichloroacetic acid as Catalysts.*, Eur. Chem. Bull., 2013.2(4) :p. 211-213.

32. Cheng-Liang F., Ning-Ning C. and Shu-Guang Z., *Solvent-free synthesis of β-enamino ketones and esters catalysed by recyclable iron(III) triflate.*,   Chemical Papers, 2014. 68(8) :p. 1097–1103.

33. Sunil U. , Vivekanand B. and Shivaji B., *Grinding induced solvent free, catalyst free synthesis of β-enaminones and β-enamino esters.*, Der Chemica Sinica, 2015. 6(1) :p.38-41.

34. Arijit S., Soumen P. and Sohel A., Fabrication of Nano‑CuO and ZnO for the Synthesis of Functionalized β‑Enaminone Derivatives from β‑Nitrostyrenes, Aliphatic/Aromatic Amines and 1,3‑Dicarbonyl/4‑Hydroxy Coumarin., Chemistry select ,2017. 2(24) :p. 7319-7324.

35. Dabon L., Sang M. and Hajime H. , *Gold (I)/Gold(III)-Catalyzed Selective Synthesis of N-Sulfonyl Enaminone Isomers from Sulfonamides and Ynones via Two Distinct Reaction Pathways.*, Organic Letters,2017. 19(18) :p. 734-4737.

36. Nabipour H.,Ghammamy S. and Ashuri S., *Synthesis of a new dithiocarbamate compound and Study of Its biological properties.*, The Journal of Organic Chemistry , 2010. 2 :p.75-80.

37. Emmanuel S., Marc D. and Samuel R., Design, *Synthesis and evaluation of pH-dependent hydrolysable emetine analogs as treatment for prostate cancer.*, Journal of Medicinal Chemistry, 2012. 55(17) :p.450–7459.

38. Maria G. ,Vasquez R. and Viviana R., *Macrocyclic Diorganotin(IV) Bis-dithiocarbamates: Synthesis, Spectroscopic Characterization., DFT Calculations, and Physicochemical Analysis as Anion Receptors*, European Journal of Inorganic Chemistry, 2016. 21: p. 3429-3440.

39. Ajit N., Vinod K., *Synthesis, crystal structures and conducting properties of heteroleptic nickel(II) 1,1-dithiolate-bpy/dppe ligand complexes*, Polyhedron ,2015.101: p. 251-256.

40. Marzano C., Ronconi L., Chiara F., *Gold(III)-dithiocarbamato anticancer agents: activity, toxicology and histopathological studies in rodents.*, International Journal of Cancer, 2011.129(2) :p. 487-496.

41. Amin E., Saboury A. and Mansuri H. ,*Potent inhibitory effects of benzyl and p-xylidine-bis dithiocarbamate sodium salts on activities of mushroom tyrosinase.*, Journal of Enzyme Inhibition and Medicinal Chemistry, 2010. 25(2) :p. 272-281.

42. Hogarth G., *Metal-dithiocarbamate complexes: chemistry and biological activity.*, Journal of Medicinal Chemistry, 2012.12(12) :p.1202-1215.

43. Cvek B. and Dvorak Z., *Targeting of Nuclear Factor-KB and Proteasome by Dithiocarbamate Complexes with Metals.*, J.Curr. Pharm. Des., 2007.13(30) :p. 3155-3167.

44. Awang N. and Baba I., *Diorganotin(IV) Alkylcyclohexyldithiocarbamate Compounds: Synthesis, Characterization and Biological Activities.*, Sains Malaysiana, 2012.41: p.977-982.

45. Awang N., Baba I. and Yamin B., *Synthesis, Characterisation and Antibacterial Activity of New Diorganotin(IV) Bis(2-Methoxyethyl) dithio carbamate Complexes.* , Proceedings of the International Seminar on Chemistry, 2008.2: p. 565-572.

46. Cookson J., Beer P., *Exploiting the dithiocarbamate ligand in metal-directed self-assembly.*, Dalton Trans., 2007.15: p. 1459-1472.

47. Ahamad M., Rao R. and Suresh E., , *Synthesis, characterisation and biological evaluation of noveldithiocarbamate metal complexes.*, J. Chem. Pharm. Res., 2012. 4(3): p. 1601-1605.

48. Mansouri H. and Shahrakib S., *Platinum(II)/palladium(II) complexes with n-propyldithiocarbamate and 2,2'-bipyridine: synthesis, characterization, biological activity and interaction with calf thymus DNA, Complex Metals*, An Open Access Journal , 2014.1(1): p.23-31.

49. Kana A. and Hibbert T., *Organotin unsymmetric dithiocarbamates: synthesis, formation and characterisation of tin(II) sulfide films by atmospheric pressure chemical vapour deposition.* , Polyhedron,2001. 20: p. 2989-2997.

50. Law N., Dietzsch W. and Duffy N., *Spectral, thermal stability and antibacterial studies of copper, nickel and cobalt complexes of N-methyl-Nphenyl dithiocarbamate.*, Polyhedron,2003. 22: p.3423-3432.

51. Ashwaq S. *,Synthesis, Characterization and Antibacterial activities of new dithiocarbamate and its complexes with Co(II), Ni(II), Cu(II) and Zn(II) ions,*

International Journal of Chemical Sciences, 2016.14(2): p.693-703.

52. Bera P., Kim C. and Seok S., *Synthesis of nanocrystalline CdS from cadmium(II) complex of S-benzyldithiocarbazate as a precursor.*, Journal Solid State Sciences., 2010.12(10): p. 1741-1747.

53. Mathew, E., *Studies on some metal complexes of dithio ligands.*, Philosophy Doctor Thesis, Cochin University of Science and Technology., 1990: p. 4-6.

54. Hogarth G., *Transition metal dithiocarbamates: 1978–2003*.Progress in Inorganic Chemistry, 2005. 53: p. 71-74.

55. Hans W., *Rubber, Chemicals and Additives*, in Ullmann's Encyclopedia of Industrial Chemistry., Wiley-VCH., 2007.Weinheim. pub2, p. 23-365.

56. Shkaraputa L., Kononov A. and Polackov A., *Gold Dithiocarbamate Derivatives as Potential Antineoplastic Agents: Design, Spectroscopic Properties, and in Vitro Antitumor Activity.*,Ukrainian Chemistry Journal,1991.9 :p. 979-989.

57. Ghobad M. and Fateme H., *Synthesis, characterization and antibacterial study of cyclometalated rhodium(III) complex containing dithiocarbamate* , Journal of Molecular Structure,2016. 1121: p.128-134   .

58. Onwudiwe D. and Ajibade P. , *Synthesis and Characterization of Metal Complexes of N-alkyl-N-phenyldithiocarbamates.* ,Polyhedron J., 2010.29: p. 1431-1436.

59. Cotton F., Wilkinson G. and Murillo C., *Advanced Inorganic Chemistry*, 6th Ed., John Wiley and Sons, Inc, New York, 1996.

60. Nami S., Ullah I. and Alam M., *Synthesis, characterization, molecular docking and biological studies of self -assembled transition metal dithiocarbamates of substituted Pyrrole-2-Carboxaldehyde.*, Journal of Photochemistry and Photo biology B: Biology, 2016.160: p. 392-399.

61. Siti M. and Siti N., *Crystal structures of (2,2'-bipyridyl -N,N') bis [N,N-bis (2-hydroxyethyl) dithiocarbamato -S,S']zinc dihydrate and (2,2'-bipyridyl-N,N')bis[N-*

(2-hydroxyethyl)-N-isopropyl dithiocarbamato -S,S']zinc, Acta Crystallographica Section E Crystallographic Communications,2016.**72**(2): p.203-214.

62. Al-Fahdawi A., *Formation of Bimetallic Bis(dithiocarbamate) Macrocyclic Complexes.*, philosophy doctor thesis, Babylon University, College of science, 2015: p.1-242.

63. Kanchi S. and Singh P., *Dithiocarbamates as hazardous remediation agent:A critical review on progress in environmental chemistry for inorganic species studies of 20th century.*, Arabian Journal of Chemistry , 2014. 7: p. 11–25.

64. Bai L., Hu H. and Fu W., *Synthesis of a novel silica-supported dithiocarbamate adsorbent and its properties for the removal of heavy metal ions.*, Journal Hazard Mater., 2011.195: p.261-275.

65. Isabella P., Geraldo M., *Study of metal dithiocarbamate complexes, Part V. Metal complexes of $[S_2CN(CH_2CH(OMe)_2]$: A standard dimeric zinc dithio carbamate structural motive, a rare cadmium dithiocarbamate coordination polymer, and a hydrated sodium dithiocarbarmate complex, with a$[Na_2O_2]$ core and chain*)), Inorganica Chimica Acta, 2016. 441: p.137.

66. Narayanaswamy S., Panneerselvam V. and Subbiah T., *Synthesis and spectral studies on NiS_4, NiS_2PN, NiS_2P_2 chromophores: Single-crystal X-ray structure of [Ni(dbpdtc)$_2$].*, Transition Metal Chemistry , 2010. 35(7): p.815–819.

67. Zia R., Niaz M. and Saqib A., *Synthesis, spectroscopic properties, X-ray single crystal analysis and antimicrobial activities of organotin(IV) 4-(4-methoxyphenyl)piperazine-1-carbodithioates.*, Inorganica Chimica Acta , 2011. 376 : p.381–388**.**

68. Damian C. and Peter A. , *Synthesis, Characterization and Thermal Studies of Zn(II), Cd(II) and Hg(II) Complexes of N-Methyl-N-Phenyldithiocarbamate: The Single Crystal Structure of [(C$_6$H$_5$) (CH$_3$) NCS$_2$]$_4$ Hg$_2$.*, International Journal of Molecular Sciences , 2011 .12 (3) : p.1964-1978.

69. Jayaraju A., Moustapha A. and Mallikarjuna R., *Synthesis, characterization and biological evaluation of novel dithiocarbamate metal complexes.*, Der Pharma Chemica, 2012.4(3): p.1191-1194.

70. Musthak M. ,Jayaraju A., Noorjahan T. and Sreeramulu J., *Synthesis, characterization and biological evaluation of novel dithiocarbamate metal complexes.*, Journal of Chemical and Pharmaceutical Research, 2012.4(3): p.1601-1605.

71. Sajad H., Subbiah T. and Sivashanmugam S., *Synthesis, spectral and X-ray structural studies on Hg(II) dithiocarbamate complexes: A new precursor for HgS nanoparticles.*, Polyhedron, 2015. 96: p.16-24.

72. Chauhan H. and Jaswant C., *Synthesis, characterization and single crystal X-ray analysis of chloro bis(N,N-dimethyldithiocarbamato-S,S') antimony (III). ,* Journal of Saudi Chemical Society, 2015.19(4): p.417-422.

73. Ajit N., Vinod K. and Vikram S., *Influence of Functionalities on the Structure and Luminescent Properties of Organotin(IV) Dithiocarbamate Complexes.*, Journal of Organometallic Chemistry, 2015.787: p.65-72.

74. Sathiyaraj E., Thirumaran S. and Samuele C., *Synthesis and spectral studies on Ni(II) complexes involving N-furfuryl-N-substituted benzyldithiocarbamates and PPh₃: Anagostic and C–H¨π interactions in (N-furfuryl-N-(4-fluorobenzyl) dithiocarbamato-S,S')(thiocyanato-N)(triphenylphosphine)nickel(II),*Phosphorus., Sulfur, and Silicon and the Related Elements, 2016.191(7): p. 1042-1050.

75. Reena Y., Manoj T. and Ratna C., *Supramolecular architecture of organotin (IV) 4-hydroxypiperidine dithiocarbamates: crystallographic, computational and Hirshfeld surface analyses.*, Inorganica Chimica Acta, 2016.450: p.57-68.

76. Imadul S., Suvendu B. and Sutapa C. , *Synthesis, Characterization, and Biological Activity of Nickel (II) and Palladium (II) Complex with Pyrrolidine Dithiocarbamate (PDTC).*, Advances in Chemistry ,2016.1: p.1-6.

77. Ye-Hong D., Shou-De X. and Xiang-Hua W., *Synthesis, characterization, and anticancer activity of dithiocarbamate ruthenium(II) complexes.*, Phosphorus, Sulfur, and Silicon and the Related Elements, 2017.192(11): p.1219-1223.

78. Felicia F., Jejenija O. and Damian C. ,*Syntheses and characterization of nickel(II) dithiocarbamate complexes containing NiS₄ and NiS₂PN moieties: Nickel sulphide nanoparticles from a single source precursor.*,Journal of Saudi Chemical Society, 2018. 22(4), : p.381-395.

79. Mrinalinil L. and Manihar K., *Synthesis and Characterization of some biologically active transition metal complexes for a ligand derived from dimedone with mixed ligands.*,Research Journal of Chemical Sciences, 2012. 2(1): p.45-53.

80. Mohammed K. I., *Synthesis, Characterization and Biological Evaluation of New Mixed Ligand Complexes of Dithiocarbamate with Some Metal Ions.*, philosophy doctor. Thesis, University of Anbar, College of Science, 2017, p.1-232.

81. Ashwaq S., *Preparation, Spectral Characterization of New Mixed Ligand Complexes with Dithiocarbamate*., Journal of Kufa for Chemical Science, 2015. 1(10) : p.113-120.

82. Amaal Y., *Synthesis and characterization of Fe(II), Co(II), Ni(II), Cu(II) and Zn(II) complexes with mixed ligands of α-naphthylamine dithiocarbamate and 1,10-phenanthroline*. ,Tikrit Journal of Pure Science ,2009.14(2): p.103-106.

83. Jassim M. and Amira F., *Synthesis and Characterization of Co(II) , Ni(II), Cu(II) Zn(II) and Cd(II) mixed complexes of imidazol dithiocarbamate and 1,10-phenanthroline*., Iraqi National Journal of Chemistry,2012.45 :p.105-116.

84. *Zdenek T. ,Pavel S. and Richard P., Synthesis and X-ray structure of nickel(II) benzylpiperazine-dithiocarbamate complex [Ni(bpdtc)(PPh$_3$)$_2$] ClO$_4$·PPh$_3$., Journal of Molecular Structure, 2013.1049: p.22-26.*

85. Prakasam B., Lahtinen M. and Peuronen A., *Synthesis, NMR spectral and structural studies on mixed ligand complexes of Pd(II) dithiocarbamates: First structural report on palladium(II) dithiocarbamate with SCN_ligand.*, J. Molec. Struct., 2016.1108: p. 195-202.

86. Mitchell S. and Waring H. , *Aminophenols* , Ullmann's Encyclopedia of Industrial Chemistry. Wiley-VCH, 2002, p.170-171

87. Reference Handbook of Fine Chemicals, *Computational Studies on the IR and NMR Spectra of 2-Aminophenol* , Acros Organics Publishers, Fisher Scientific UK, 2007.

88. Filip E., Humelnicu I. and Ghirvu C., *Comparative solution equilibrium studies of anticancer gallium(III) complexes of 8-hydroxyquinoline and hydroxyl (thio) pyrone ligands.*, Acta Chemica Iasi., 2009.17: p.85-96.

89. Shavlev E., Pankratov N. and Shalabay V., *Some Aspects of 8-hydroxy quinoline in Solvents.*, International journal of Quantum Chem., 2006.106: p.876-880.

90. Amati M., Belviso S. and Cristinzano L., *8-Hydroxyquinoline Monomer, Water Adducts, and Dimer. Environmental Influences on Structure, Spectroscopic Properties, and Relative Stability of Cis and Trans Conformers.*, The Journal of Physical Chemistry A, 2007.111: p.13403-13414.

91. Bardez E., Devol I. and Valeur B., *Theoretical Studies on Proton Transfer Reactions of 8-Hydroxy quinoline Monomers and Dimers.*, The Journal of Physical Chemistry B, 1997.101: p.7786-7793.

92. Li S. and Fang H., *Theoretical studies on structures and reactivity of 8-hydroxyquinoline and its one-water complex in the ground and excited states. ,* Chemical Physics Letters, 2003.367: p.637-644.

93. Camargo J., Napolitano B. and Zukerman J., *Theoretical investigation of the intramolecular hydrogen bond formation, non-linear optic properties, and electronic absorption spectra of the 8-hydroxiquinoline.*, Journal of Molecular Structure, 2007.816: p.145-151.

94. Sharma M., *Synthesis and characterization of dithiocarbamate complexes of some 3d metals and their adducts with nitrogen donors. ,* philosophy doctor, thesis , university of Jammu, department of chemistry, 2013. p.1-189.

95. Ghosh P., Katare S. and Patkar P., *Sulfur vulcanization of nutral rubber for benzothiozole accelerated formulation: reaction mechanisms to a rational kinetic model.,* Rubber Chemistry and Technology, 2003. 76(3): p. 592-689.

96. Ali M., Wani W. and Saleem K., *Design and synthesis of thalidomide based dithiocarbamate Cu(II), Ni(II) and Ru(III) complexes as anticancer agents.*, Journal Polyhedron., 2013. 56: p. 134-143.

97. Kanchi S., Saraswathi K. and Venkatasubba N., *The determination of cobalt(II) at DME using catalytic hydrogen current technique in various water.*, Environmental Monitoring and Assessment, 2011.183 : p.531–543.

 98. Dilli S., Tong P., *Liquid chromatography of metal chelates. Chromatographic studies of homologous dialkyldithiocarbamates.*, J. Anal.Chim.Acta., 1999. 395 (1–2): p.101–112.

99. Senkbeil S., Lafleur J. and Jensen T. ,*Gold Nanoparticle-Based Fluorescent Sensor For the Analysis of Dithiocarbamate Pestides in water.*, 16th Inter. Conference on Miniaturized Systems for Chem. and Life Sci.. Okinawa. Japan., 2012: p.1423-1425.

100. Turker A. and Sezer B., *Indirect determination of dithiocarbamate fungicides (zineb and ferbam) in some foodstuffs by flame atomic absorbtion spectroscopy.*, Turkish Journal Of Pharmaceutical Sciences, 2005. 2(1): p. 35-42.

101. Damicone J., *Fungicide Resistance Management., Division of Agricultural Sciences and Natural Resources.*, Oklahoma State Univ., 2016. EPP-7663 : p.1-8.

102. Riadi Y., El haddad M. and Mamouni R., *Determination of kinetics of degradation and mobility of dithiocarbamates fungicides in water and in moroccan soil.*, St. Cerc. St. CICBIA., 2010.11(2): p.289-297.

103. Ashwaq S., *Prepartion, Characterization of new ligands dithiocarbamate and studying their complexes with some transition metal ions and studying bacteria activity.*, Philosophy doctor ,thesis, university of babylion, College of Science, department of chemistry, 2016. p.1-148.

104. Yousif E. I., *New Bis(dithiocarbamate) Ligand Systems for Complex Formation; Synthesis, Spectral Characterisation and Bacterial Activity.*, Philosophy doctor thesis, Baghdad University, College of Education (Ibn Al-Haitham), 2016: p.2-216.

105. *Eman M.*, *Synthesis and Characterization of some biologically active transition metal complexes for a ligand derived from dimedone with mixed ligands.*, thesis, University of Baghdad , College of Education for pure Science-Ibn-Al-Haitham, department of chemistry, 2006. p.1-114.

106. Bannamane N., Kaoua R. and Nedjar-Kolli B., *Synthesis of new amino-1, 5-benzodiazepine and benzotriazole derivatives from dimedone*, Organic Communications, 2008 . 1(3): p.62-68.

107. Silva J., Garden S. and Pinto A., *The Chemistry of isatins a review from 1975 to 1999*, Journal of the Brazilian Chemical Society, 2001. 12(3): p.1-105.

108. Sapkal S., Shelke K. and Shingare M., *NaHSO$_4$/SiO$_2$: An Efficient Catalyst for the Synthesis of β-Enaminones and 2-Methylquinolin-4(1H)-Ones under Solvent -Free Condition.* ,Journal of the Korean Chemical Society, 2010.6: p.723-726.

109. Kelode S., *Synthesis, Characterization, And Thermal Studies Of Co(II), Ni(II), Cu(II), Cr(III), Mn(III), Fe(III), Vo(IV), Zr(IV) And Uo₂(VI) CIomplexes Derived From Thiazole Schiff Base.*,International Journal of ChemTech Research, 2012. 4(4): p.1442-1446.

110. El-Sayed H., Awad L. and El-Sayed L., *Microwave irradiation for accelerating the synthesis of acridine and xanthene derivatives from dimedone.* 2006.ii : p.178-186**.**

111. ShiY., Chu W., Wang Y., Wang S., Du J., Zhang J., Li S.,Zhou G., QinX. and Zhang C., *Synthesis, characterization and cytotoxicity of the Au(III) complexes with cyclicamine-based dithiocarbamate ligands.,* Inorganic Chemistry Communications , 2013. 30: p. 178-181

112. Damian C. and Anthony C. ,*Syntheses, characterization, and antimicrobial properties of nickel(II) dithiocarbamate complexes containing NiS₄ and NiS₂PN moieties.*, Journal of Coordination Chemistry ,2016. 69(16):p.2454-2468.

113. Emily J., Matthew R. and Stuart R., *Coordination polymers of sulphur-donor ligands*, Inorganica Chimica Acta, 2013.403: p.9-24.

114. Edward R*., Perplexing Coordination Behaviour of Potentially Bridging Bipyridyl-Type Ligands in the Coordination Chemistry of Zinc and Cadmium 1,1-Dithiocarbamate Compounds*, Crystals, 2018. 8(1): p.1-29 .

115. Pavel P. and Edward R. ,*Crystal structure of bis[N-(2-hydroxyethyl)-N-methyldithiocarbamato,S,S-](pyridine)zinc(II) pyridine monosolvate and its N-ethyl analogue.*, Acta Cryst. , 2017. E73: p.1246–1251.

116. Cric-Marjanovic G. and Trchova M., *Electrochemical oxidative polymerization of sodium 4-amino-3- hydroxynaphthalene-1-sulfonate and structural characterization of polymeric products*., Reactive & Functional Poly., 2006. 66 :p.1670-1683.

117. Hassan A., *Synthesis, Characterization and Biological Studies of Some New Mixed Nickel(II) Complexes Containing Dithiocarbamate and1,10-phenanthroline Ligands.* , J. Chem. Mat. Res., 2015.7(4): p.9-15.

118. Bhandari H., Choudhary V. and Dhawan S.K., *Influence of self-doped poly(aniline-co-4-amino-3-hydroxy-naphthalene -1-sulfonic acid) on corrosion inhibition behaviour of iron in acidic medium.*, J. Synthetic Metals, 2011.161: p. 753–762.

119. Ámbar Y., Miriam M., *Chloro diphenyl tin(IV) dithiocarbamate complexes as chemodosimeters and host for anions and neutral compounds in solution.*, Polyhedron, 2016.111: p.132-142.

120. Fulmer G., Miller A. and Sherden N., *NMR Chemical shifts of trace impurities: common laboratory solvents, organics, and gases in deuterated solvents relevant to the organometallic chemist.*, Organomet., 2010. 29(9): p. 2176-2179.

121. Ivanov I. and Nikolova S., *Regioselective acylation of β-enaminones of homo veratryl amine*,2007. Xv: p.11-17.

122. Bamanie F., Shehata A. and Mashaly M., *Enaminones in heterocyclic synthesis: part 5: isoniazid-enaminone a new organic synthon and tuberculostatic candidate.*, Nature and Science., 2012.10(6): p.95-98.

123. Braibante H., Braibante M. and Oriques D., *Preparation of b-enamino carbonylic compounds using microwave radiation/K-10.*, J. Braz. Chem. Soc., 2003. 6(14): p.994-997.

124. Ashwaq S., *Synthesis and characterization study of new dithiocarbamate complexes with some of transition metls.* , journal of multifunctional material and photoscience, 2015.6(1): p.21-26.

125. Salman B. K., *Metal Complexes of Multidentate N_2S_2 Heterocyclic Ligands; Formation and Structural Characterisation.*, PH.D. thesis, Baghdad University, College of Education (Ibn Al-Haitham), 2017: p.1-335.

126. Hogarth G., Jewel E. and Brent R., *Functionalised dithiocarbamate complexes: Synthesis and molecular structures of 2-diethylaminoethyl and 3-dimethyl aminopropyl dithiocarbamate complexes[M{S_2CN($CH_2CH_2NEt_2$)$_2$}n] and [M{S_2CN ($CH_2CH_2CH2NMe_2$)$_2$}n] (n= 2, M = Ni, Cu, Zn, Pd; n = 3, M = Co).* , J. Inorganica Chimica Acta, 2009. 362(6): p.2020-2026.

127. Sathiyaraj E., Selvaganapathi P. and Thirumaran S. ‚*Synthesis, spectral, structural and computational studies on NiS4 and NiS2NP chromophores: Anagostic and CeH⋯p (chelate) interactions in [Ni(dtc)(PPh$_3$)(NCS)] (dtc ¼ N-(2-phenylethyl)-N-(4-methoxybenzyl)- dithiocarbamateandN-(2-phenylethyl)-N-(4-chlorobenzyl)dithiocarbam ate).* , J. Molec. Struc., 2016. 1119: p.385-395.

128. Parveen B., Bukhari I. and Shahzadi S., *Synthesis and spectroscopic characterization of mononuclear /binuclear organotin(IV) complexes with1H-1,2,4-triazole -3-thiol: Comparative studies of their antibacterial/antifungal potencies.*, J. Serb. Chem. Soc., 2015. 80(6): p.755–766.

129. Wehrli F., Marchand A. and Wehrli S., *Interpretation of Carbon-13 NMR Spectra.*, Wiley: New York, USA, 1988. p.49-159.

130. Yousif E. and Hasan H., *Formation of macrocyclic complexes with bis(dithiocarbamate) ligand; synthesis, spectral characterisation and bacterial activity.*, J. Der Chemica Sinica, 2016. 7(2): p.53-65.

131. Vogel A., *Vogel's Textbook of Practical Organic Chemistry*, 5th Ed., John Wiley and Sons, Inc., New York, 1989. p.1219.

132. Singh G. and Pheko T., *Spectroscopic Characterization of the 1-Substituted 3,3'-Diphenyl-4-(2'-hydroxyphenyl)azetidine-2-ones: Applic- ation of ^{13}C NMR,*

1H NMR and Mass Spectroscopy., J. Spectrochim. Acta, Part A, 2008. 70 : p.595-600.

133. Tamizmani M., Kankanala R. and Sivasankar C., *Coordinated and uncoordinated anion dictated coordination mode of PN(Me)P ligand in Pd(II) complexes and their catalytic applications.*, J. Organomet. Chem. 2014. 6(12): p. 763-764.

134. John M., Norman V., *Structural characterization and preliminary decomposition study of four unsymmetrically substituted nickel dithiocarbamate complexes*, Journal of Coordination Chemistry, 2016. 69(1): p.90-104.

135. Courtney M. and Isabella K., *Synthesis, characterization and structural comparisons of phosphonium and arsenic dithiocarbamates with alkyl and phenyl substituents*, Polyhedron, 2014. 75(110): p.39-55.

136. Faraglia G., Sitran S. and Montagner D., *Pyrrolidine dithiocarbamates of Pd(II).*, Inorg. Chim. Acta., 2005. 358: p. 971-980.

137. Yin D., Zhai J., Sun Y-Y., Wang D-Q., *Synthesis, characterizations and crystal structures of new antimony (III) complexes with dithiocarbamate ligands.*, Polyhedron., 2008. 27(2): p. 663-670.

138. Sykes A., Wilkinson G. and Gillard R., *Comprehensive Coordination Chemistry.*, Pergamon Press: Oxford, UK., 1987: p.229.

139. Kalia S., Kausha G. and Kumar M., *Physcochemical studies on some 4-methylpiperazine-1-carbodithioate complexes of zinc(II), cadmium(II) and mercury(II).*, Indian J. Chem.A., 2008. 47(9): p.1323-1332.

140. Jamuna P., Thirumaran S. and Ciattini S., *Synthesis and characterization of Ni(II) and Zn(II) complexes of (furan-2-yl)methyl(2-(thiophen-2-yl)ethyl)dithiocarbamate (ftpedtc): X-ray structures of [Zn(ftpedtc)2(py)] and [Zn(ftpedtc)Cl(1,10-phen)].*, Spectrochim Acta A Mol Biomol Spectrosc, 2015. 25(137): p.1164-1173.

141. Johnson B., Al-Obaidi K. and Mecleverty J., *Transition-metal nitrosyl compounds. Part III. (NN-dialkyldithiocarbamato)nitrosyl compounds of molybdenum and tungsten.*, J. Am. Chem. Soc. A., 1969. 19: p.1668-1670.

142. Al-Jeboori M., Al-Jebouri F. and Al-Azzawi M., *Metal complexes of a new class of polydentate Mannich bases: Synthesis and spectroscopic characterisation.*, Inorg. Chim. Acta., 2011. 379(1): p.163-170.

143. Siddiqi K. and Nami S., *Template synthesis of symmetrical transition metal dithiocarbamates.*, J. Braz. Chem. Soc., 2006. 17(1): p.107-112.

144. Kader A. , Eman M., *Synthesis and characterization of new bidentate chalcone ligand type (NO) and its Mn^{II}, Co^{II}, Ni^{II} and Cu^{II} complexes with study of their antibacterial activity. *, Diyala Journal for pure Sciences , 2015.11(3): p.25-42.

145. Osulaja A., Ndahi N. and Adetoro A., *Synthesis, Physico-Chemical and Antimicrobial Properties of Co(II), Ni(II), and Cu(II) Mixed-Ligand Complexes of Dimethylglyoxime.*, Res. J. Appl. Sci. Eng. Technol., 2011. 3(11): p.1233-1238.

146. G. Socrates, *Infrared Characteristic Group frequencies*, Wiley, New York, 1980.

147. G. Varsanyi, *Vibrational Spectra of Benzene Derivatives*, Academic Press, New York, 1969.

148. Silverschtien R. and Morril A., *Spectrophotometers Indentification of Organic Compounds*, Translated by Ali Hussain And Suphi Al-Azawi, 1981.

149. Subburayan S. and Kuppukkannu R. , *Metal dithio carbamate precursors for the preparation of a binary sulfide and a pyrochlore: Synthesis, structure, continuous shape measure and bond valence sum analysis of antimony(III) dithiocarbamates. *, Polyhedron , 2015. 85 : p.598-602.

150. Krstic N., Nikolic R., *Coordination Compounds of M(II) Bio metal Ions with Acid-Type Anti-inflammatory Drugs as Ligands– A Review*, Tropical Journal of Pharmaceutical Research February , 2015. 14(2): p.337-349.

151. Alim A., Kudrat M., Synthesis and Characterization of Some Metal Complexes of Cu(II), Ni(II), Zn(II), Cd(II), Sn(II), Co(II), Sb(III) and Fe(III) Containing Bidentate Schiff Base of Smdtc, Science Journal of Chemistry, 2015. 39: p.33-35.

152. Halli M., Patil. V. and Mallikarjun K., *Synthesis, characterization and biological activity of mixed ligand metal (II) complexes derived from benzofuran-2-carbohydrazide schiff base and 3-aminophenole.*, Dev Pharma Chemica, 2012. 4(6): p.2360-2367.

153. Edward R., *Tin dithiocarbamates: applications and structures*, Applied Organometallic Chemistry, 2008. 22(9): p. 533-550.

154. Nakamoto K., *Infrared and Raman Spectra of Inorganic and Coordination Compounds*, Parts A and B, 5th ed., John Wiley Sons, New York, 1997.

155. Christoph L. and Wolfgang B., *On Ammonium ‑tetrakis (dithiocarbamato) ‑bismuth(III)‑monohydrate and Tris (dithiocarbamato) ‑bismuth(III)* , Zeitschrift for anorganische and allgemeine Chemie,2011. 637(3-4), p.406-414.

156. Hai-Rong Z., Ke-Bin H. and Zhen-Feng C., Cobalt(II) 8-hydroxyquinoline complexes: structure, cytotoxicity and action mechanism., Med. Chem. Commun., 2016. 7: p.806-812.

157. Nakamoto K. and McCathy K., *Spectrascopy and structure of Metal Chelate Compounds*, John Wiley and Sons, New York, 1968. 285: p.217.

158. Srisung S., Suksrichavalit T. and Prachayasittikul S., *Antimicrobial Activity of 8-Hydroxyquinoline and Transition Metal complexes.*, International Journal of Pharmacology, 2013.9(2) :p. 170-175.

159. Saliu A. Sheriff A. and Caroline A., *Iron(III) and copper(II) complexes bearing 8-Hydroxyquinolin with amino-acids mixed ligands: Synthesis, characterization and antibacterial investigation.*,Arabian Journal of Chemistry, 2015. 8(5) :p.742-747.

160. Orescanin V., Mikelic L. and Roje V, *Determination of lanthanides by source excited energy dispersive X-ray fluorescence (EDXRF) method after preconcentration with ammonium pyrrolidine dithiocarbamate (APDC).*, Anal. Chim. Acta., 2006. 570(2): p.277-282.

161. Jowitt R., and Mitchell P., *Complexes of molybdenum(VI) and molybdenum(V) with dithiocarbamate, dithiocarbonate, and phosphoro thiolothionate .*, J. Chem. Soc. part A., 1970 : p.1702-1708.

162. Ronconi L., Giovagnini L. and Marzona C., *Gold dithiocarbamate derivatives as potential antineoplastic agents:Design, spectroscopic properties, and in vitro antitumor activity.*, Inorg. Chem., 2005. 44(6): p.1867-1881.

163. Al-Jeboori M. and Al-Tawel H., *New metal complexes of N_2S_2 tetradentate ligands: Synthesis and spectral studies.,* Inorg. Chim. Acta., 2010. 363(6): p.1301-1305.

164. Slddappa K., Mallikarjun K. and Reddy T., *Synthesis, characterization and antimicrobial studies of N^1-[(1E)-1-(2-Hydroxyphenyl)ethylidene]-2-oxo-2H-chromene-3-carbohydrazide and its metal complexes.,* E-Journal of Chemistry., 2009. 6(3): p.615-624.

165. Mamba S., Mishara A. and Mamba B., *Spectral thermal and in vitro antimicrobial studies of cyclohexylamine-N-dithiocarbamate transition metal complexes.,* Spectrochimica Acta part A., 2010. 77(3): p.579-587.

166. Lever A., "Inorganic Electronic Spectroscopy" 2nd. Ed., New York, 1984.

167. Salim S., *Synthesis,Charaterization and Biological Activity Studies of Some Transtion and Non transition Metalcomplexes with(4 – Dithiocarbamato-N-(5-*

methylisoxazole-3-yle)-ion-ligand ,Ibn Al-Haitham Jour. for Pure & Appl. Sci.,2017. 30(2) : p.266-278.

168. Hazarika T. and Bora T., *Studies on Nickel (II) Complexes of Some Poly(1-pyrazolyl)alkane Ligands* ,Trans. Met. Chem., 1982. 7: p. 210-254.

169. Hasan A. , Enaam I., *Formation of New Macrocyclic Complexes with Bis (Dithiocarbamate) Ligand;Preparation, Structural Characterisation and Bacterial Activity,* Ibn Al-Haitham Jour. for Pure & Appl. Sci.,2016. 29(3) : p.146-166.

170. Pandey P., Mishra A. and Ojha K., Phescochemical studies of menganese(II), cobalt(II), Zinc(II), and copper(II) complexes derived from 2-substituted benzaldehyde thiosemicarbazones., indian J. Sci. Res., 2012. 3(1): p.119-122.

171. Enaam I. and Hasan A. ,*New Bis(dithiocarbamate) Ligand for Complex Formation; Synthesis, Spectral Analysis and Bacterial Activity*, Ibn Al-Haitham Jour. for Pure & Appl. Sci., 2017. 30(1): p.73-87.

172. Ledbetter j., *Spectroscopic Evidence for the Enol Imine-Keto Enamine Tautomerism of N-(o- and p-Hydroxybenzylidene) Anils in Solution*, J. Phys. Chem., 1966. 70: p. 2245-2249.

173. Chauhan H. and Singh U.,*Synthetic, spectral, thermal and antimicrobial studies of bis(N,N-dialkyldithiocarbamato)arsenic(III) and antimony(III) complexes with diphenyldithiophosphate and diphenyldithiophosphinate* , Applied Organometallic Chemistry,2006. 20(6): p.404-410.

174. Chauhan S.,*Synthetic, spectral, thermal and antimicrobial studies on some bis(N,N'-dialkyldithiocarbamato) antimony(III) alkylenedithiophosphates, Applied Organometallic Chemistry*, 2007. 21(10): p.880-889.

175. Qing C., Ming-Hua Z. and Lian-Qiang W., *$[Co^{II}_6O_{12} X]^-$ (X = Cl^- or F^-): Halide Template Effect and Frustrated Magnetism.*, Chem. Mater., 2010 .22 : p. 4328-4334.

176. Hasan H. and Ahmad R., *Formation of macrocyclic complexes with bis(dithiocarbamate) ligand; synthesis, spectral characterisation and bacterial activity*., Der Chemica Sinica, 2016. 7(2): P.53-65.

177. Arumugam M., Kuppukannu R. and Kottamalai K., *Thermal characterization studies on Zinc, Cadmium and Mercury dithiocarbamate complexes*., International Journal of ChemTech Research, 2014. 6(5): p. 2620-2627.

178. Damian C. and Peter A. , *Thermal Studies of Zn(II), Cd(II) and Hg(II) Complexes of Some N-Alkyl-N-Phenyl-Dithiocarbamates*., Int J Mol Sci. ,2012. 13(8): p. 9502–9513.

179. Achut S., Amarnath N., *Synthesis, characterization and thermal study of some transition metal complexes of an asymmetrical tetradentate Schiff base ligand*, J. Serb. Chem. Soc., 2010. 75(3), p.349–359.

180. Sanjay K. and Vinay K. , *Synthesis, electrochemical, fluorescence and antimicrobial studies of 2-chloro-3-amino-1,4-naphthoquinone bearing mononuclear transition metal dithiocarbamate complexes [M{S,S-S_2C–piperazine–$C_2H_4N(H)ClNQ\}_n$]*, RSC Adv.,2015. 5: p.53036-53046.

181. Evans D., *A new type of megnetic balance.*, J. phys. E; Sci. instrum., 1974. 7(4): p. 274.

182. Senqupta O., Gole B. and Mukheriee S., *A series of transition metal–azido extended complexes with various anionic and neutral co-ligands: synthesis, structure and their distinct magnetic behavior.*, Dalton Trans., 2010. 39(32): p. 7451-7465.

183. Bain G. , Berry J., *Diamagnetic corrections and Pascal's constants.*, J. Chemi . Educ., 2008. 85(4) :p.532-546.

184. Housecroft C. and Sharpe A., *Inorganic Chemistry*; Pearson Education Limited: 2008. 3rd Ed.

185. Ahlam J., Al-Karawi A. ,*Synthesis and spectral studies of new N_2S_2 and N_2O_2 Mannich base ligandsand their metal complexes.*, J. Coord. Chem., 2009. 62(16): p.2736-2744.

186. Carlin R. and Duynevacldt J., *Magnetic Properties of Transition Metal Compound* , New York , 1977 : p.353-357.

187. Berezanski P. in *Handbook of Instrumental Techniques for Analytical Chemistry*, Chapter 39, F. Settle, Ed., Prentice-Hall, Upper Saddle River, NJ, 1997: p.749-764.

188. Abhinav K. and Heike M. , *Synthesis, Structure, Conductivity, and Calculated Nonlinear Optical Properties of Two Novel Bis(triphenylphosphane)copper(I) Dithiocarbamates.*, European Journal of Inorganic Chemistry ,2009. 2009(18), p.2720-2725.

189. Adrian T. and Herbert H., *Synthesis, Spectroscopic Characterization, DFT Calculations, and Dynamic Behavior of Mononuclear Macrocyclic Diorganotin(IV) Bis‑Dithiocarbamate Complexes*, Zeitschrift for anorganische and allgemeine Chemie,2012. 638(11): p.1731-1738.

190. Campolat E. and Kaya M., *Spectroscopic Characterization of N,Nbis (2-[(2,2imethyl1,3-Dioxolan-4-yl)Methyl]Amino}Ethyl) N',N'-Dihydroxy ethanedi imidamide and Its Complexes.*, J.Cood.Chem, 2005. 31(7): p.511-515.

191. Geary G., *The use of conductivity measurements in organic solvents for the characterisation of coordination compounds.*, Coord. Chem.Rev,1971 :p.81-122.

192. Kohji K., Kazumasa I. and Shinzi K., *Alkali Metal and Trimethylsilyl Carbamoselenothioates – Synthesis, Structure, and some Reactions*, Zeitschrift for anorganische und allgemeine Chemie,2007. 633(4): p.625-634.

193. Udhayakala P., Rajendiran T., *A theoretical evaluation on benzothiazole derivatives as corrosion inhibitors on mild Steel*, Der Pharma Chemica., 2015. 7(1): p. 92-99 .

194. Ravichandran R., *Corrosion inhibition of brass by benzotriazole derivatives in NaCl solution, Anti-corrosion Methods and Materials*, 2005. 52(4): p. 226-232.

195. Wisal A., Awf A., *Corrosion and Corrosion Inhibition of α-Brass by Thiourea*, Ibn AL- Haitham Journal For Pure and Applied Science, 2014. 27(1) : p. 212-224.

196. Dillard I., *Inorganic Chemistry with the Elements of Physical and Theoretical Chemistry*, New York, John Wiley & Sons, 1988, 2nd ed. : pp 506-508.

197. Conway B., Bokris J. and White R. ,*Modern Aspects of Electrochemistry*, Phenum press, New York, 1989. 19: pp.78-93.

198. Asan A., Kabasakaloglu M., *Corrosion inhibition of brass in presence of terdantate ligands in chloride solution*, Corrosion Science, 2005. 47: p.1534-1544.

199. Fouda A., Diab M. and Hassan A., *Benzothiazole derivatives as corrosion inhibitors for carbon steel in 1 M phosphoric acid (H_3PO_4) solutions*, African Journal of Pure and Applied Chemistry, 2013. 7(2): p. 67-78.

200. Satendra K., Sankara N. and Manimoran A., *Dezincification of Brass in Sulfide Polluted Sodium Chloride Medium*, Int. J. Electrochem. Sci., 2006. 1: p. 456-469.

201. Joseph X. and Rajendran N., *Corrosion Inhibition of Substituted Thiadiazoles on Brass*, Int. J. Electrochem. Sci., 2010. 6: p.348-366.

202. Rahman A., Choudhary M. and Thomsen W., *Bioassay Techniques For Drug Development.*, Harwood Academic, Amsterdam, The Netherlands, 2001.

203. Singh R. V., Dwivedi R. and Joshi S. C., "*Synthetic, magnetic,spectral, antimicrobial and antifertility studies of dioxomolybdenum(VI) unsymmetrical imine complexes having a N ∩ Ndonor system,*" Trans .Met .Chemi , 2004. 29 (1) : p. 70–74.

204. Tweedy B. G., *"Plant extracts with metal ions as potential antimicrobial agents"*, Phytopathology., 1964. 55: p. 910–914

205. Ramesh, R. and Maheswaran S., *Synthesis, spectra, dioxygen affinity and antifungal activity of Ru(III) Schiff base complexes*, J.Inorg .Biochem ., 2003. 96: p. 457–462.

الخلاصة

تضمنت الدراسة تحضير وتشخيص ثلاث مركبات جديدة (HDa وHDb وHDi) وثلاث ليكاندات ثنائي ثايوكارباميت(DTCs) جديدة هي:-

KL^1= potassium (1,5-dimethyl-3-oxo-2-phenyl-2,3-dihydro-1H-pyrazol-4-yl)(5,5-dimethyl-3-oxocyclohex-1-en-1-yl)carbamodithioate.

KL^2= potassium benzo[d]thiazol-2-yl(5,5-dimethyl-3-oxocyclohex-1-en-1-yl) carbamodithioate.

KL^3=potassium(1H-benzo[d]imidazol-2-yl)(5,5-dimethyl-3-oxocyclohex-1-en-1-yl)carbamodithioate.

اشتملت طريقة تحضير الليكاندات على خطوتين من التفاعل حيث تضمنت الخطوة الاولى تحضير وتشخيص المركبات المشتقة (HDa وHDb وHDi) والناتجة من تفاعل ثنائي الكيتون مع الامين الاولي ثم تفاعلها مع ثنائي كبريتيد الكاربون بوجود هيدروكسيد البوتاسيوم كقاعدة للحصول على الليكاندات ثنائي ثايوكارباميت . تم تشخيص الليكاندات المحضرة باستخدام طيف الرنين النووي المغناطيسي للبروتون وللكاربون وطيف الكتلة وطيف الاشعة تحت الحمراء وطيف الاشعة فوق البنفسجية والتحليل الحراري والتحليل الدقيق للعناصر.

تم تفاعل الليكاندات المحضرة (DTCs) مع الايونات الفلزية الثنائية التكافؤ لتحضير المعقدات التي لها الصيغة العامة $[M(L^n)_2]$ في مذيب الايثانول حيث ان:-

n=1,2,3. $M^{(II)}$=(Mn, Co, Ni, Cu, Zn, Pd, Cd)

اما معقدات مزيج الليكاند فحضرت من الليكاندات ثنائي ثايوكارباميت المحضرة مع الليكاند المشارك 8-هيدروكسي كوينولين (Q)و 3-امينو فينول (P) والاملاح الفلزية لتصبح الصيغة العامة للمعقدات كالاتي حيث $[M(L^n)(Q)]$, $[M(L^n)(P)]$

$M^{(II)}$=(Co, Ni, Zn)

شخصت المعقدات المحضرة باستخدام طيف الاشعة تحت الحمراء وطيف الاشعة فوق البنفسجية والتحليل الدقيق للعناصر والتوصيلية المولارية والحساسية المغناطيسية والتحليل الحراري.

قيست التوصيلية المولارية لمحاليل المعقدات الفلزية للليكاندات المحضرة في مذيب ثنائي مثيل سلفوكسايد(DMSO)وبتركيز(1×10^{-3})M عند درجة حرارة المختبر وعند ملاحظة قيم التوصيلية المولارية التي تم الحصول عليها للمعقدات المحضرة تبين انعدام الصفة الالكتروليتية لجميع تلك المعقدات المحضرة وهذا يتفق مع تلك القيم المستحصلة لكثير من المعقدات الفلزية التي لا تمتلك اي سلوك الكتروليتي.

من خلال قياسات المجال المغناطيسي تبين ان قيم العزوم المغناطيسية لجميع المعقدات المحضرة تتفق مع قيمتها في المعقدات رباعية السطوح ماعدا معقدات النحاس مع KL^1 وKL^2, البلاديوم مع الليكاندات الثلاثة ذات الشكل مربع مستوي.

تم تقيم الفعالية الحيوية لبعض الليكاندات والمعقدات المحضرة $[M(L^n)(Q)]$, $[M(L^n)(P)]$ $[M(L^n)_2]$باستخدام طريقة الانتشار diffusion.ولقد اثبتت النتائج ان بعض المعقدات المحضرة تكون اكثر تثبيطا للبكتريا قيد التجربة.

تم دراسة تاثير العامل المثبط لليكاندات الثلاثة المحضرة على تاكل سبيكة الفا ـ براص بتركيز مقداره(10^{-3})مولاري وعند ثلاثة قيم للاس الهيدروجيني(7,4,2) في محلول كلوريد الصوديوم بتركيز(0.6) مولاري وعند درجة حرارة المختبر298 كلفن، حيث اوضحت النتائج ان الليكاندات الثلاثة قامت بعمل التثبيط لتاكل سبيكة الفاـ براص عند قيمتي الاس الهيدروجيني 7,4 في حين كان دورها متمثل بتسريع تفاعل التاكل عند الاس الهيدروجيني 2.

جمهورية العراق

وزارة التعليم العالي والبحث العلمي

جامعة بغداد

كلية التربية للعلوم الصرفة /ابن الهيثم

قسم الكيمياء

تحضير ، تشخيص ،تأكل والفعالية البايولوجية لبعض معقدات مختلطة الليكاند للفلزات الانتقالية وغيرالانتقالية لثنائي ثايوكارباميت مع 3-امينو فينول ،8-هيدروكسي كوينولين

اطروحة مقدمة الى مجلس كلية التربية للعلوم الصرفة /ابن الهيثم/جامعة بغداد وهي جزء من متطلبات نيل درجة دكتوراه فلسفة في الكيمياء اللاعضوية من قبل

عوف عبدالرحمن احمد

بكالوريوس علوم كيمياء (1991) كلية التربية للعلوم الصرفة /ابن الهيثم / جامعة بغداد

ماجستير علوم كيمياء (2014) كلية التربية للعلوم الصرفة /ابن الهيثم / جامعة بغداد

بأشراف

أ.د. أحمد ثابت نعمان

2018 م   **1440 هـ**